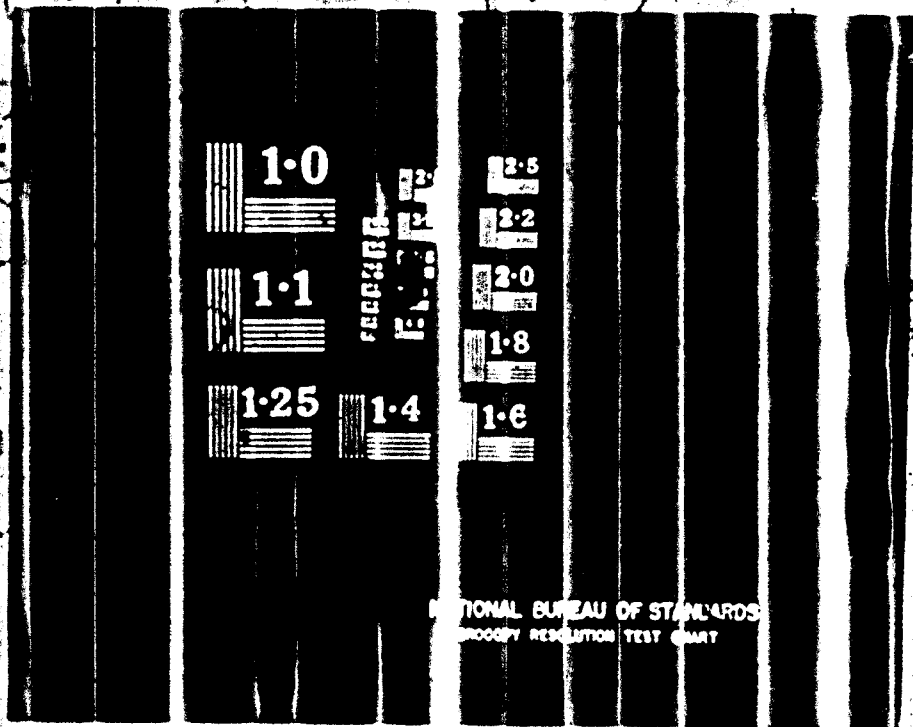


1 OF 1  
AD477679

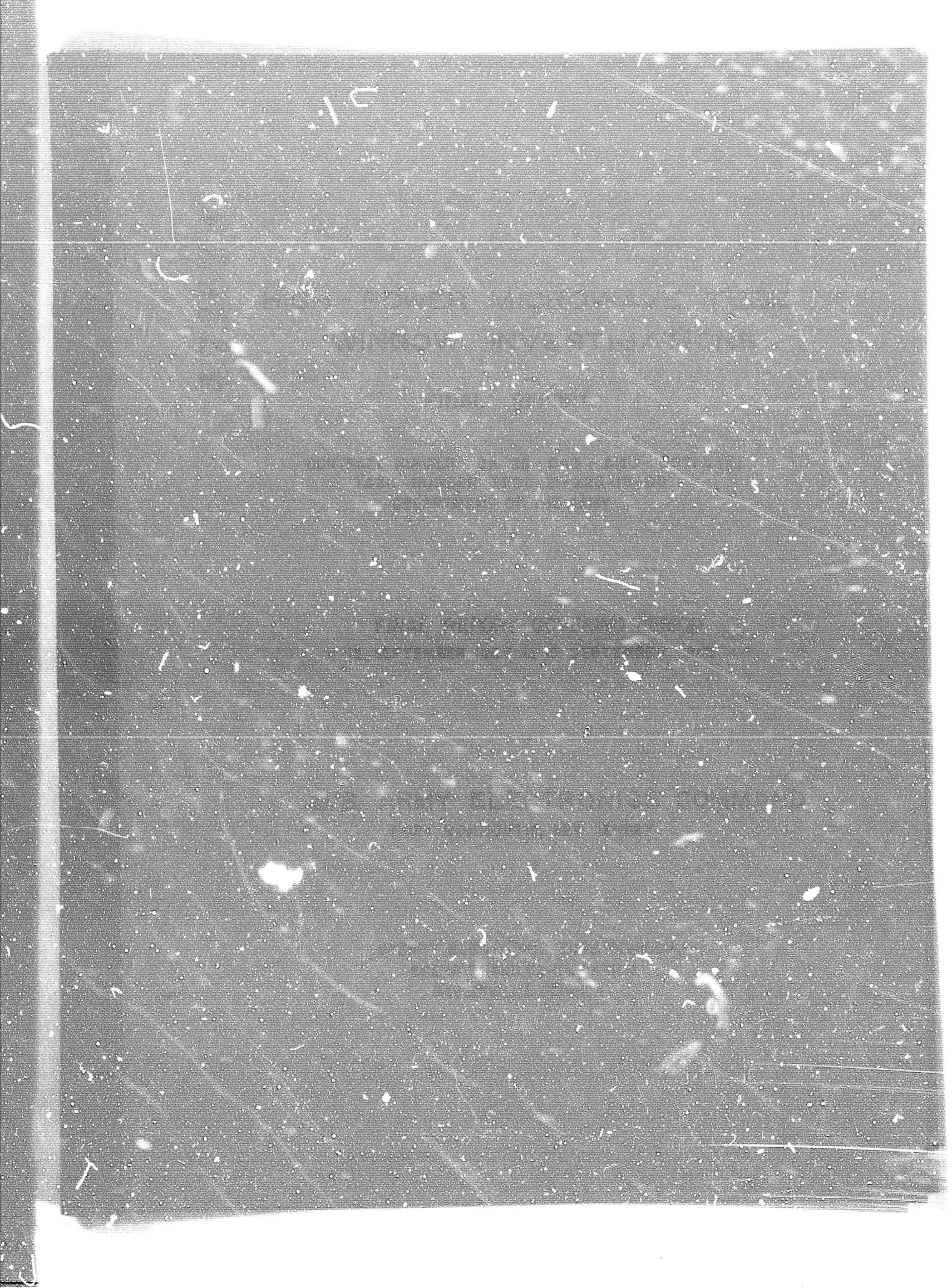


NATIONAL BUREAU OF STANDARDS  
MICROSCOPY RESOLUTION TEST CHART

# DISCLAIMER NOTICE

THIS DOCUMENT IS THE BEST  
QUALITY AVAILABLE.

COPY FURNISHED CONTAINED  
A SIGNIFICANT NUMBER OF  
PAGES WHICH DO NOT  
REPRODUCE LEGIBLY.



HIGH-POWER MICROWAVE TUBE WINDOW  
INVESTIGATIONS

FINAL REPORT

Contract No. DA 28-043-AMC-00373(E)

DEPARTMENT OF THE ARMY  
Task Number 7900-21-223-15-00

Final Report Covering Period

15 September 1964 through 14 September 1965

Object of This Research Program: To study the single-surface multipactor suppression properties of different window coating materials and evaluate the effect of tube processing techniques on these coatings. In addition, to investigate the effect of different metalizing techniques on seal-area breakdown of windows.

Prepared by

A. Saharian  
A. Kiefer  
P. Lally

SETD NO. NJ-2761-0179-12

September 1965

This research is part of "Project DEFENDER" sponsored by the Advanced Research Projects Agency, Department of Defense. The work prepared under this contract was made possible by the support of the Advanced Research Projects Agency under Order No. 318 through the U. S. Army Electronics Command.

## FOREWORD

This Technical Report covers the work performed for Task Number 7900-21-223-15-00, under Contract No. DA-28-043-AMC-00373(E) under which the work of Contract No. DA-36-039 SC-90818 was expanded. This work was performed during the period 15 September 1964 to 14 September 1965.

This contract with the Sperry Electronic Tube Division of the Sperry Rand Corporation, Gainesville, Florida, is entitled, "High-Power Microwave Tube Window Investigations." It was accomplished under the technical direction of Mr. Gunther Wurthmann of the U. S. Army Electronics Command, Fort Monmouth, New Jersey.

The contract was performed under the overall direction of Mr. P. M. Lally, Manager of Research and Advanced Devices of the Sperry Electronic Tube Division. The chief contributors were Messrs. D. B. Churchill (general consulting work and new window design procedures - Appendix B), A. Kiefer (window coatings), C. Trace (gas analysis), A. Saharian (window evaluation) and L. Tentarelli (ceramic-to-metal seals). Chemical aspects of this window investigation program were under the supervision of Mr. J. White, Engineering Manager of the Materials and Process Laboratory.

This research was part of "Project DEFENDER" sponsored by the Advanced Research Projects Agency, Department of Defense. The work prepared under this contract was made possible by the support of the Advanced Research Projects Agency under Order No. 318 through the U. S. Army Electronics Command.

TABLE OF CONTENTS

<u>SECTION</u>		<u>PAGE</u>
I	PURPOSE.....	1
II	ABSTRACT.....	3
III	PUBLICATIONS, LECTURES, REPORTS AND CONFERENCES.....	5
	3.1 PAPERS PRESENTED.....	5
	3.2 CONFERENCES HELD.....	5
IV	DATA.....	8
	4.1 INTRODUCTION.....	8
	4.1.1 A Brief Description of Window Problems.....	8
	4.1.2 Description of Single-Surface Multipactor.....	12
	4.1.3 Window Failures Due to Multi- pactor Related Problems.....	15
	4.1.4 Means of Eliminating Single- Surface Multipactor.....	17
	4.2 PROBLEMS ASSOCIATED WITH THE USE OF COATINGS FOR MULTIPACTOR SUPPRESSION....	21
	4.2.1 Coating Thickness Required for Multipactor Suppression.....	21
	4.2.2 Coating Thickness Required for Uninhibited Transmission of RF Power.....	25

TABLE OF CONTENTS (Continued)

<u>SECTION</u>		<u>PAGE</u>
IV (Cont'd)	4.2.3 Changes in Physical and Chemical Properties of Thin Films..... ..	27
4.3	SPUTTERING EQUIPMENT AND EXPERIMENTAL PROCEDURES..... ..	29
	4.3.1 Choice of Thin Film Deposition Technique..... ..	29
	4.3.2 Description of Sputtering Equipment..... ..	31
	4.3.3 Control of Deposition of Sputtered Coatings..... ..	35
	4.3.4 Sputtering Procedure..... ..	39
	4.3.5 Changes in the Surface Resistivity of Coatings..... ..	45
	4.3.6 Effect of Tube Processing Techniques on Window Coatings....	47
	4.3.7 Identification of Sputtered Coatings..... ..	57
	4.3.8 Uniformity of Sputtered Coatings..... ..	60
4.4	HIGH-POWER TEST EQUIPMENT..... ..	66
	4.4.1 Description of Multipactor Test Cavities..... ..	66
	4.4.2 Multipactor Test Procedure..... ..	70
	4.4.3 Description of High-Power Test Equipment and Procedure.....	78

TABLE OF CONTENTS (Continued)

<u>SECTION</u>		<u>PAGE</u>
IV (Cont'd)	4.5 EXPERIMENTAL RESULTS. ....	87
	4.5.1 Multipactor Test Data Obtained at S-Band.....	87
	4.5.2 Multipactor Test Data Obtained at X-Band.....	105
	4.5.3 Physical and Chemical Changes in Windows Due to Multipactor.....	106
	4.5.4 High-Power Test Data Obtained at S- and X-Bands.....	125
	4.5.5 Extended Tests in the S-Band, TE <sub>111</sub> <sup>0</sup> -Mode Cavity.....	135
	4.6 EVALUATION OF METALIZING TECHNIQUES.....	139
V	CONCLUSIONS.....	147
VI	RECOMMENDATIONS.....	157
VII	IDENTIFICATION OF KEY TECHNICAL PERSONNEL....	161
 <u>APPENDICES</u>		
A	An Estimate of Multipactor Losses on the Surface of an Uncoated Alumina Window.....	162
B	A Geometrical Method for Designing Windows with Mode Transducers.....	167
C	Attenuation of Electromagnetic Waves Through Thin Metallic Films.....	180
D	Calculation of Thickness of Titanium Films of Very High Resistivity.....	187

TABLE OF CONTENTS (Continued)

<u>APPENDICES</u>	<u>PAGE</u>
E     Sketches of the Sputtering Setups Used in This Program.....	186
F     Resistance Between Two Probes on the Surface of a Conductive Sheet.....	192
G     Calculation of RF Electric Field Distribution in the Sputtering Setup.....	196
H     Design Drawings for the S-Band Multipactor Cavity, $TE_{011}^0$ -Mode.....	200
I     Summary of Electric Field and Power Relations of a Dielectrically Loaded $TE_{011}^0$ -Mode Resonator.....	214
J     Design Drawings for the S-Band $TE_{111}^0$ -Mode Test Cavity.....	219
K     Summary of Electric Field and Power Relations for the High Power Test Cavity.....	231
L     Calculation of Transmitted Power in Circular Waveguide Versus Maximum Field Strength.....	234
M     Preparation of Different Metalizing Paints and Application Procedures.....	239
References.....	243
List of Symbols.....	248

LIST OF ILLUSTRATIONS

<u>FIGURE</u>		<u>PAGE</u>
1	Electrostatic Multipactor Suppression Device.....	20
2	Sputtering Apparatus.....	32
3	Overall View of the Sputtering Equipment...	33
4	Block Diagram of the Crystal Oscillator Thin Film Monitor.....	38
5	Beat Frequency Change Versus Time.....	41
6	Beat Frequency Versus Time.....	44
7	Plot of Resistance Change Versus Time and Temperature for a Titanium Coating.....	50
8	Resistance Change Versus Temperature for Vanadium Carbide.....	51
9	Resistance Change Versus Temperature for Titanium Carbide.....	52
10	Resistance Change Versus Temperature for Tantalum Carbide.....	53
11	Resistance Change Versus Temperature for Titanium Nitride.....	54
12	Contour of Sputtered Titanium on 6" Window Based on Resistance Probe Measurement.....	64
13	Cross-Sectional View of the X-Band Demountable $TE_{011}^0$ -Mode Multipactor Test Cavity.....	68

LIST OF ILLUSTRATIONS (Continued)

<u>FIGURE</u>		<u>PAGE</u>
14	Photograph of a Disassembled S-Band Multipactor Test Cavity.....	71
15	Disassembled X-Band Multipactor Test Structure .....	72
16	Block Diagram of the Window Test Facility..	73
17	Cross-Sectional View of the X-Band, Demountable, $TE_{111}^0$ -Mode Test Cavity.....	83
18	Disassembled High-Power S-Band Test Cavity..	85
19	X-Band, High-Power Test Cavity.....	86
20	Arc Damage to the Titanium-Coated Alumina Window During the High-Power Test.....	97
21	Arc Damage to the Vanadium-Coated Alumina Window.....	99
22	Arc Damage to Tantalum Coated Window.....	100
23	Arc Damage to the Sputtered Carbon Coating..	101
24	X-Band Vanadium Carbide Coated Window After Multipactor Test.....	109
25	Gas Pressure Versus Incident Power.....	115
26	Typical Spectra, Blank Corrected .....	116
27	Uncoated Alumina Window After Multipactor Test.....	118
28	Polished Edge of Section of Ceramic Window..	118
29a	As-Polished Edge of Section Where Yellow Coloring Effect Occurred.....	122

LIST OF ILLUSTRATIONS (Continued)

<u>FIGURE</u>		<u>PAGE</u>
29b	As-Polished Edge of Section Where Yellow Coloring Effect Had Been Annealed Back to Uniform Whiteners.....	122
30	Photograph of Multipactor Glow in the S-Band, $TE_{111}^0$ -Mode Cavity Through the Eloxed Viewing Hole.....	127
31	Photograph of a Non-Damaging Surface Arc in the S-Band Test.....	129
32	Seal-Edge Arc Damage in $TE_{111}^0$ -Mode X-Band Cavity.....	132
33	Multipactor Discharge in X-Band $TE_{111}^0$ -Mode Cavity. a) Glow at an Electric Field of 16 kv/cm. b) Glow at 34 kv/cm.....	133
34	Multipactor Glow on Damaged Coating Resulting from Operation of the Window at 105 MW Peak and 52 kw Average Power.....	138
35	Coating Damaged by Operation of the Window at 105 MW Peak and 52 kw Average Power.....	140
36	Pictorial Representation of a Cross-Sectioned Seal.....	143
37	Photographs Showing Cross-Sections of 99.5% Alumina Samples Using Five Different Metalizing Techniques.....	144
38	Typical X-Band Window Assembly.....	146
A1	Plot of VSWR Versus Incident Power in the Input Line with Uncoated Alumina as the Window.....	163

LIST OF ILLUSTRATIONS (Continued)

<u>FIGURE</u>		<u>PAGE</u>
B1	Cross-Section, Output Half of Window, Showing Reference Planes and Variable Dimensions.....	171
B2	Reflection Coefficient at Plane 1 Over Frequency Range $f_1$ to $f_2$ .....	171
B3	The "g", or Darboux, Transformation.....	171
B4	Transformed Reflection Coefficients on the Circles $C_1$ and $C_2$ .....	171
B5	Semi-Ellipses $C_1'$ and $C_2'$ , and Their Prototype Semicircles.....	172
B6	Construction for Transforming Points $\bar{a}$ and $\bar{c}$ to Points $\bar{a}'$ and $\bar{c}'$ .....	172
B7	Construction for Transforming Point $\bar{b}$ to $\bar{b}'$ .....	172
B8	Construction Showing a Solution Yielding a Compatible Set of Dimensions s and d.....	173
C1	A TEM Wave Incident on a Thin Metallic Plane.....	181
C2	Change in Incident Wave VSWR Versus Surface Resistivity of Thin Film. ....	188
E1	Sketch of Sputtering Apparatus Used For Coating All Unmounted Windows.....	189
E2	Sketch of Sputtering Setup Used For Coating Brazed $TE_{11}^0$ -Mode, S-Band Window Assemblies	190
E3	Sketch of Sputtering Setup Used For Coating Brazed $TE_{11}^0$ -Mode, X-Band Window Assemblies.	191
F1	Two Parallel Conducting Cylinders.....	193

LIST OF ILLUSTRATIONS (Continued)

<u>FIGURE</u>		<u>PAGE</u>
G1	A Cross-Sectional View of the RF Coil in the Sputtering Apparatus.....	197
I1	Schematic of Test Cavity with an Off- Center Dielectric Disc.....	215
L1	Plot of Equivalent Transmitted Power Versus Maximum Field Strength in a Circular S- Band Waveguide at 2856 Mc.....	236
L2	Plot of Equivalent Transmitted Power Versus Maximum Field Strength in a Circular X- Band Waveguide at 8900 Mc.....	238

CONFIDENTIAL

SECRET

SECRET

LIST OF TABLES

<u>TABLE</u>		<u>PAGE NO.</u>
I	Summary of Multipactor Results Obtained at S-Band with Uncoated Windows.....	88
II	Summary of Multipactor Results Obtained at S-Band with Coated Windows. Sputtering Atmosphere was Argon Unless Stated Differently. The Substrate was Ground Alumina Window.....	91
III	Summary of All Multipactor Results Obtained at X-Band.....	106
IV	Summary of High Power Results Obtained with Coated and Uncoated Windows at S- and X-Bands.....	126
MI	Metalizing Data on 99.5% Alumina.....	242

## SECTION I

### PURPOSE

#### 1.1 PURPOSE OF THE PROGRAM

This final report summarizes the work carried out in the High-Power Microwave Tube Window Investigations Program during the period 15 September 1964 through 14 September 1965. This work was performed for the U. S. Army Electronics Command by the Sperry Electronic Tube Division of the Sperry Rand Corporation, Gainesville, Florida, under Contract No. DA 28-043-AMC-00373(E), in accordance with the Electron Tube Division (USAECOM) Technical Guidelines No. MW-16, dated 30 March 1965. This is the final report for this contract, under which the work of Contract No. DA 36-039 SC-90818 was continued and expanded.

The objectives of this research program were to investigate microwave-tube window phenomena occurring at high levels of rf power. In particular, these objectives included a study of the single-surface multipactor suppression properties of different window coating materials and an evaluation of the effect of conventional tube processing techniques on the stability of these

coatings. An analysis was to be made of factors which cause breakdown (arcing) in dielectrics and surrounding seal areas.

The need for improved microwave windows stems from the successful development of high-power microwave generators. Tube technology has progressed to the point where the waveguide window is one of the few remaining factors that seriously limit the power generating capability of high-power tubes. The waveguide window is the port through which the rf power leaves the vacuum envelope of the tube. Although mechanically an integral part of the tube, the window is sufficiently isolated electrically that it can be treated as a separate tube component for developmental purposes.

It was the intention of this program to assemble technical information and design criteria on high-power microwave windows to provide tube engineers with guidance on the selection of proper window configurations for required peak and average power handling capabilities. Guiding principles on the selection of proper dielectric materials and window coatings as well as fabrication and processing techniques were to be supplied. A step-by-step description of the preferred window coating and mounting techniques (which includes metalizing and brazing techniques) were to be furnished.

## SECTION II

### ABSTRACT

This report gives a brief description of high-power microwave tube window problems. The emphasis in the discussion is placed on problems associated with the single-surface multipactor phenomenon. Window coating criteria and means of eliminating multipactor and multipactor-related problems are presented.

Sputtering equipment and new coating and control procedures developed in this program are described in greater detail. Problems associated with the changes in the resistivities of coatings, including the effects of tube processing techniques, are discussed. Work performed on coating identification and problems associated with producing a uniform coating are described.

A wide variety of coating materials were evaluated in specially-designed  $TE_{011}^0$  cavities at S-band and X-band. The most promising coatings were evaluated at S- and X-band in  $TE_{111}^0$  cavities. The geometry of these cavities was such as to closely simulate practical high-power window configurations. This report includes

a description of all of these cavities and the procedures followed in the test work.

Results of some thirty-seven experiments performed in this program are presented. Physical changes in window materials arising from multipactor are described. In the  $TE_{11}^0$ -mode experiments, windows have been tested at S-band up to 120 MW with no multipactor or seal area arcing. At X-band a power level of 13 MW has been obtained without multipactor or arcing.

Finally, a new, improved metalizing-window-brazing technique, which produces a strong metal-to-dielectric bond with thin metalizing layer and a minimum of penetration of metalizing constituents into the dielectric, is given, and pertinent fabrication procedures described.

### SECTION III

#### PUBLICATIONS, LECTURES, REPORTS AND CONFERENCES

##### 3.1 PAPERS PRESENTED

On 29 September 1964 a paper entitled, "Problems Associated with Waveguide Pressure Windows for Microwave Tubes" was presented by Mr. D. B. Churchill at the Seventh National Conference on Tube Techniques in New York City, New York. The conference was sponsored by the Advisory Group on Electron Devices.

##### 3.2 CONFERENCES HELD

On 14 October 1964 at U. S. Army Electronics Command, Fort Monmouth, New Jersey. Present were Messrs. Irving Reingold, Gunther Wurthmann, Bernard Smith and Stanley Leefe, all from USAECOM. Sperry was represented by Messrs. D. B. Churchill, F. Tyndall, P. M. Lally, R. Petticrew and A. Saharian. Work already in progress and detailed plans of future work were discussed.

On 10 November 1964 at U. S. Army Electronics Command, Fort

Monmouth, New Jersey. Present were Messrs. Irving Reingold, Gunther Wurthmann and Bernard Smith from USAECOM. Sperry was represented by Messrs. J. Whitford, F. Tyndall and J. M. White. The general status and future plans of the High-Power Microwave Tube Window Investigations Program were discussed.

On 13 and 14 January 1965 Messrs. Gunther Wurthmann and Stanley Leefe of USAECOM visited Sperry Electronic Tube Division, Gainesville, Florida. Mr. D. B. Churchill of Sperry Gyroscope Company, Great Neck, New York, was also present. The progress of the program and plans for the future were reviewed. Equipment in operation was inspected.

On 27 and 28 April 1965, Mr. Gunther Wurthmann of USAECOM visited Sperry Electronic Tube Division, Gainesville, Florida. Mr. D. B. Churchill of Sperry Gyroscope Company, Great Neck, New York, was also present. The progress of the program and plans for the future were discussed. Equipment in operation was observed.

On 6 May 1965, Dr B. B. Brown of Sperry visited the U. S. Army Electronics Command, Fort Monmouth, New Jersey. At a meeting with Messrs. I. Reingold and G. Wurthmann, both from USAECOM, progress of the Window Program and future plans were reviewed.

On 14 June 1965 work accomplished to date and plans for future work were discussed at the U. S. Army Electronics Command, Fort Monmouth, New Jersey. Present were Messrs. Irving Reingold and Gunther Wurthmann from USAECOM. Sperry was represented by P. M. Lally, F. Tyndall and A. Saharian.

On 15 June 1965, at the Pentagon, Washington, D. C. Present were Col. B. I. Hill of ARPA, Messrs. L. Kaplan, I. Reingold, G. Wurthmann and Miss Barbara Malley of USAECOM. Sperry was represented by Messrs. P. M. Lally and A. Saharian. Present also were Messrs. L. Resd and W. Wade of Bitel-McCullough and Mr. L. Feinstein of the Stanford Research Institute. The purpose of the conference was a review of ARPA-sponsored research programs on high-power windows.

On October 13, 14 and 15 at Sperry Electronic Tube Division. Mr. G. Wurthmann was present on October 13 and 14, and Mr. B. Smith was present on October 13, 14 and 15. The purpose of the visit was to review the results of the program. Mr. Smith also spent some time reviewing plans and progress on a USAECOM-sponsored program on the metalizing and brazing of ferrites.

## SECTION IV

### DATA

#### 4.1 INTRODUCTION

Waveguide windows are gas-tight dielectric bulkheads that are wholly-enclosed in two port waveguide sections and more or less freely transmit microwave power over a specified band of frequencies. The principal use of windows is in microwave tubes. As the port through which rf power leaves the tube, the window constitutes a part of the tube envelope, and is subjected to bakeout and processing conditions as well as to high-level rf fields. From the standpoint of manufacturing the window, the criteria of interest are reproducibility and low cost. From an operational standpoint, the principal criteria are electrical efficiency and physical stability.

##### 4.1.1 A Brief Description of Window Problems

Rapid advances in tube technology in the past decade have brought forth a number of problems concerning windows. First came the problem of providing adequate window bandwidth. Because

of their low dielectric constant, glass windows could be broadbanded without too much difficulty. However, at higher power levels, the temperature-sensitive loss factors of the available glasses made them subject to run-away heating; consequently, tube designers sought more stable dielectric materials for high-power windows.

The most readily available material with the required electrical and mechanical properties was alumina - a sintered aluminum oxide ceramic that could be formed in various sizes and shapes at reasonable cost. Produced in varying degrees of purity and density by a number of companies, alumina rapidly became the most widely accepted window material. The dielectric constant of alumina, however, is about twice that of glass; consequently, the reflective loss at the interface is appreciably higher. In a properly-designed window structure, the reflections from the dielectric element are matched out so that at the midband frequency the structure as a whole is essentially reflectionless. Nevertheless, the bandwidth over which the matching is effective becomes narrower as the dielectric constant of the window element is increased. The problem of broadbanding alumina windows was a difficult one, and led to some novel design concepts.<sup>1,2,3</sup>

At higher power levels, window heating became a serious problem. Many instances of window failure due to thermally-induced stresses have been recorded. Also, window heating was found to be closely related to the window-puncture problem. It was noticed that in certain applications window-punctures were associated with waveguide arcing at or near the window seal, while in others the arcing was confined to isolated spots on the dielectric surface. After prolonged operation, the vacuum-side surface often was eroded and marked with numerous small craters. In such cases, the body of the window element usually was honey-combed with small tunnels, some of which constituted gas leakage paths.

From the available experimental data, it was observed that windows which have failed exhibited either puncture or rupture, or both, depending on conditions of operation and their configuration. At high-peak powers and low-duty cycles, the windows were prone to puncture. At high-average powers on the other hand, overheating usually caused the window to rupture before the surface was noticeably eroded. It was also observed that, at high-peak powers at least, the window heating was greater than could be accounted for by dielectric losses alone. Many windows ruptured, presumably in consequence of thermally-induced strains.

Use of the purest and most dense alumina bodies reduced, but did not eliminate this problem. This extra heating, which also served to increase dielectric losses of window material, is now recognized to be the result of an electronic discharge on the vacuum side of the window commonly referred to as single-surface multipactor.

Less serious, but nevertheless important, window problems are losses due to spurious ("ghost") mode resonances, metalizing losses in the seal, and occlusions (particularly gas-filled voids) in the dielectric element. Contamination and residual gas are contributory factors in window punctures with the electronic discharge providing the underlying failure mechanism.<sup>4</sup>

In view of the scope of high-power tube applications and the seriousness of window problems, government agencies moved to establish a number of window study programs that were rather independent of the existing tube-development programs.<sup>5</sup> As a result of these investigations, several successful methods have been devised to improve bandwidths of windows (Reference 4, paragraph 4.2 gives a detailed review on this subject). Furthermore, the single-surface multipactor discharge on the vacuum side of a high-power window has been identified as a serious window

problem. It was found to be the cause, or at least a contributing factor, of most window failures, particularly at very high levels of peak rf power. The problem of seal-edge arcing near the metal-dielectric vacuum joint has also been established. This latter problem is primarily due to improper metalizing and brazing techniques used for assembly of windows, which produce brazing fillets and overlaps near or on the active side of the window.

#### 4.1.2 Description of Single-Surface Multipactor

The nature of the multipactor discharge has been previously described in the literature,<sup>6,7</sup> and for this reason, only a brief explanation of this phenomenon will be given here. If the discharge region is at a pressure of  $10^{-6}$  torr or less, and is free of static magnetic fields, the mechanism can be described approximately as follows:

A cloud of electrons oscillates in synchronism with the applied rf field, moving on the average through the same trajectory on each successive cycle. At one point of the trajectory, electrons strike the surface of the window producing more secondary electrons for each incident primary. Typical window dielectrics have a fairly high secondary emission ratio over a wide primary electron energy range. The background radiation usually is

sufficient to provide initiating electrons. Under the influence of the rf field, most of the secondaries join the electron cloud, replacing the electrons lost by collision, diffusion or other depletion mechanisms. The released secondary electrons leave the non-conducting window positively charged. The positive charge on the window in turn provides the restoring force for the discharge to continue. Certain factors tend to force a state of equilibrium in which the average number of electrons in motion remains constant at a given level of the rf field intensity. The magnitude of the space-charge cloud is probably one of these limiting factors. The limiting mechanism in this case can be described as follows. When the window becomes charged sufficiently positive, the secondary electrons make only a small excursion in front of the multipactoring window and are drawn back to the window by the space-charge forces before they gain sufficient energy from the rf field to cause more secondaries.

The kinetic energy of motion, of course, is derived from the rf field and is dissipated upon impact as heat. The amount of rf power which flows into the multipactor discharge can be significant. In Appendix A, calculations based on experimental data show that at 5 MW of equivalent transmitted power through an S-band alumina window, the energy delivered by the multipactor

discharge to the window exceeds dielectric heating by about three times. The amount of power dissipated in the multipactor discharge of uncoated windows is usually a function of surface conditions and the type of window material used. Both of these factors determine the effective secondary emission ratio of the window surface. At times multipactor losses can be quite large, and a ten-fold increase in the cavity losses by the electronic discharge has been measured.<sup>8</sup> The added heating of the window by the multipactor reduces the power handling capability of the window, especially at high-average levels of high-peak power.

Even though multipactor has been an important contributing factor in many window failures, there is no evidence of any chemical changes in ceramics due to multipactor. The only physical change directly attributable to multipactor has been yellowing of ceramic due to X-ray bombardment. There is evidence which shows that the presence of multipactor greatly increases the probability of arcing. This is likely due both to local outgassing and the copious supply of electrons. Arcing can cause severe damage to ceramics, i.e., local melting, pitting, cracking, etc. The heat dissipated by multipactor can cause thermally-induced cracks in ceramic. Multipactor probably contributes to the transfer of materials on the window surface and adjacent metal

parts. The copious electron supply will cause some ionization even without arcing, and the ions, accelerated by the rf field, can cause sputtering.

#### 4.1.3 Window Failures Due to Multipactor-Related Problems

In certain window configurations, the intensity of the multipactor discharge on the surface of the window is not entirely dependent on the properties of the window material used. An improperly designed window assembly, particularly one where there is a normal component of electric field on the surface of the window, can be a contributing factor in the early initiation of the single-surface multipactor discharge. In fact, in isolated cases, an improperly designed window assembly can produce window failures by multipactor discharges of the double-surface type. For example, canted windows (including conical windows) are prone to electric field breakdowns and multipactor discharges at higher levels of rf power. The axially symmetric conical windows can support both types of multipactor discharge, single and double surface.

The problem of canted windows arises from the fact that they are elongated in the axial direction, and present a distributed, rather than abrupt, discontinuity to the propagating wave. Many of these windows, for this reason, have very high bandwidths -

up to 25 percent. But they also have two significant drawbacks. First, being elongated in axial direction, they form regions where spurious modes come into resonance at frequencies within or near the operating band. Second, having surfaces normal to the dominant mode of the propagating electric field, the canted windows are subject to intense electronic discharges and breakdowns at high levels of rf power. These drawbacks were sufficient to limit the value of canted-surface windows and eventually led to the development of transverse dielectric windows.

In a transverse rectangular window, the dielectric element fills the waveguide cross-section and has purely tangential electric field at the surfaces. In a transverse-circular window, the electric field is tangential to the dielectric only if the rectangular-to-circular transitions are sufficiently far away from the dielectric element of the window assembly. When these conditions are satisfied, no higher order modes are produced near the window.

As part of a continuing effort devoted to the development of improved methods of window design, a new design procedure has been studied as part of this program. The procedure, given in Appendix B, applies particularly to the design of windows using

plane, transverse dielectric discs in uniform cylindrical sections greater than one-half wavelength long. (Using relatively long sections of circular guide will preclude normal electric fields on the window, and thus reduce both multipactor and surface arcing.) This new technique promises to reduce the experimental work involved in achieving an acceptable window design.

#### 4.1.4 Means of Eliminating Single-Surface Multipactor

The multipactor discharge on the surface of the ceramic can be eliminated or at least partially suppressed by coating of the window with some low secondary emission film. This fact has been known for some time, and titanium metal (which is reported to have a maximum secondary emission ratio of less than one<sup>9</sup>) was the first material to be used for the suppression of multipactor.<sup>10</sup>

In the case of window coatings with the secondary emission ratio less than one for all energy ranges of primary electrons, the mechanism of multipactor suppression is not difficult to understand. In this case, the copious supply of secondary electrons from the dielectric surface has been almost completely eliminated. Under these conditions, no buildup of multipactor can result regardless of the number and the energy range of incident electrons.

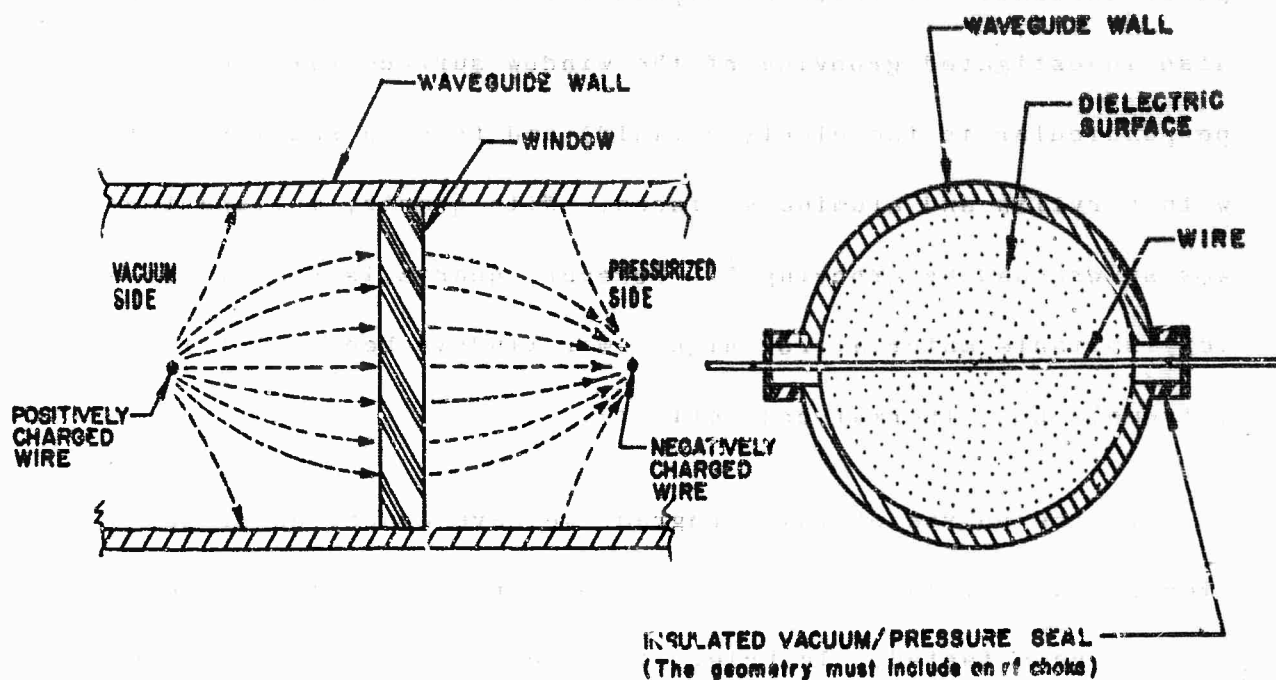
Very often, however, even with a secondary emission reducing coating, the secondary emission ratio is greater than one over some small range of primary electron energy. In this case, it is not uncommon that some weak multipactor discharge does take place on the surface of the window. Usually, the operation of the window with a partially effective coating produces initially a rise in multipactor discharge with increasing power, followed by a reduction in multipactor glow at higher values of the applied electric field. The maximum multipactor discharge on any one area of the window, of course, will occur when the mean, effective energy of the incident electrons falls into that range of the secondary emission curve for which the secondary emission ratio exceeds unity. Nevertheless, the reduction of the overall magnitude of the secondary emission ratio of such a window surface is usually very significant. This fact, together with the reduction in the energy range of primary electrons for which the secondary emission ratio exceeds unity, results in a reduction in the total amount of dissipated power at the window. From this point of view, a window coating which permits a multipactor discharge does not necessarily represent a complete failure.

The other possibilities for elimination or reduction of single-surface multipactor include magnetic, geometric and

electrostatic means. Eitel-McCullough found that a static magnetic field of any orientation tended generally to lower the power threshold at which multipactor began.<sup>11</sup> Eitel-McCullough also investigated grooving of the window surface (grooves perpendicular to the electric field) and found a small reduction with beryllia and alumina surfaces. With quartz, multipactor was suppressed by grooving.<sup>12</sup> However, quartz is really not a very suitable material for high-power windows because of its extremely poor thermal conductivity.

In the course of this program, we have conceived of an electrostatic means for multipactor suppression. The concept has not been tested. In brief, the idea consists of providing a dc electric field at the vacuum surface of a window, in order to draw electrons away, and thus prevent buildup of the multipactor discharge.

Figure 1 shows a sketch of one embodiment of the idea. Wires are stretched across the guide on either side of the window, normal to the rf electric field. Such wires will result in a negligible rf discontinuity. The wire on the vacuum side is maintained positive with respect to the waveguide walls and the wire on the pressurized side negative with respect to the waveguide walls.



Dashed lines show approximate electrostatic field

**FIGURE -1 ELECTROSTATIC MULTIPACTOR SUPPRESSION DEVICE**

In operation, electrons resulting from ionizing radiation, will be drawn away from the window, and collected on the wire. Any secondaries emitted by the wire will be drawn back to the wire. If the electric field is sufficiently strong, the secondaries will be collected without gaining much energy from the rf field.

#### 4.2 PROBLEMS ASSOCIATED WITH THE USE OF COATINGS FOR MULTIPACTOR SUPPRESSION

##### 4.2.1 Coating Thickness Required for Multipactor Suppression

Window coatings are used to make the window surface appear to incident electrons as a surface with the secondary emission characteristics of the coating material. The thickness of deposited films required depends on the incidence angle of primary electrons and their energy level. The maximum energy of multipactoring electrons, in electron volts, at the moment of impact is given by:<sup>13</sup>

$$V_{\max} = \frac{2\eta E_0^2}{\omega^2} \text{ volts} \quad (1)$$

where  $\eta$  is the electronic charge-to-mass ratio,  $\omega$  is the radian frequency of the applied rf field, and  $E_0$  is the maximum

amplitude of the field. For an electric field of 50 kv/cm,\*

$V_{max}$  is equal to 24.8 kv at 3000 Mc and 2.75 kv at 9000 Mc.

The available information on penetration of electrons into thin films is rather limited, but it is known, for example, that the transmission of electrons through an aluminum foil of 3.5 microns is almost nil if the energy level of incident electrons does not exceed 20 kv.<sup>59</sup> This fact implies that an aluminum coating of 3.5 microns on the surface of the window would certainly be sufficient to provide all the characteristics of an aluminum film, even for the multipactor electrons of 100 MW, S-band wave.

The requirement of providing enough coating material (like 3.5 microns of aluminum), in itself, is not difficult to accomplish. The difficulty in coating of windows with rather highly conductive materials such as aluminum or titanium, arises from the fact that the dielectric window must remain transparent for transmission of rf power. This latter requirement, which is discussed subsequently in greater detail, implies that the thickness of the metallic film

---

\*The value of electric field of 50 kv/cm corresponds roughly to the maximum electric field of a 100 MW electromagnetic wave propagating through a round S-band window with a diameter of 3.800 inches. This diameter is equal to the diagonal dimension of WR-340 waveguide. At X-band, 50 kv/cm corresponds to about 10 MW through a 1.226-inch window; a diameter equal to diagonal of WR-112 waveguide. These diameters are a logical choice for high-power window designs at S- and X-band. For further information, see Appendix L.

on the surface of the window must be significantly less than the skin depth of the deposited material, which, in the case of an aluminum film, by itself is less than one micron.

Fortunately, there are several arguments that can be advanced to justify the use of a very thin coating. First, from statistical considerations, the majority of primary electrons produced by the multipactor discharge will have energies corresponding to much less than 20 kv, even in the case of a 100 MW S-band electromagnetic wave. Second, the secondary emission ratio of all materials drops off at higher energy levels of incident primary electrons. Therefore, greater attention should be given to that range of the secondary emission curve for which the secondary emission ratio is highest. Usually, this maximum value occurs near the energy level of 1000 electron volts, so that much thinner coatings can be used than the hypothetical 3.5 micron thick aluminum coating previously discussed. Third, the angle made by incident electrons with the window surface is very small. Primary electrons with grazing incidence produce a rather shallow penetration into the bombarded surface.

From the above discussion, it appears that some reduction in the thickness of the window coating can be tolerated. However,

it is questionable if on these arguments alone the coating thickness could be reduced to a value very much less than the skin depth of the coating material. Nevertheless, the experimental data indicates that films of only a few hundred angstroms are sufficient to alter completely the secondary emission ratio of the substrate material.<sup>14</sup> The argument that appears to explain the secondary electron suppression action of thin films is this: Consider a very thin coating (with a relatively good secondary emission characteristic) on the surface of a dielectric window which has a high secondary emission value. An incident electron on such a surface will do one of two things. It will either dissipate its kinetic energy entirely in the thickness of the film alone - in which case the secondary emission will be a function of the coating material only. If the primary electron penetrates the thin layer of film and enters the substrate material, the majority of the secondaries will probably be produced in the window material itself. A small number of fast secondaries will not be stopped by the coating and probably will be lost on the waveguide walls through diffusion. However, since the greatest number of secondaries produced in the substrate will be slow ones with energies less than a few hundred volts,<sup>15</sup> even a very thin coating will prevent these slow electrons from

leaving the surface of the window. For example, it is reported that a gold film 130 angstroms thick is capable of stopping electrons of 1,000 electron volts,<sup>10</sup> and a significantly thinner coating will stop electrons of a few hundred volts. This argument appears to be a reasonable explanation for the fact that very thin coatings have been effective.

From the above discussion, it appears that the minimum thickness of the coating that is still effective as a multiplier suppressor should be in the general neighborhood of 100 angstroms. This value of minimum thickness cannot be given with greater precision for it is a function of the coating material, its density (both of these factors control the secondary emission ratio of the material) and the energy distribution of incident electrons.

#### 4.2.2 Coating Thickness Required for Uninhibited Transmission of rf Power

In Appendix C, the attenuation of electromagnetic waves through thin conductive films has been calculated. The results show, for example, that in order to have a VSWR of 1.025 in the incident wave, the surface resistivity of the film should not be less than 2.5 megohms/square. For a VSWR of 1.05, the surface resistivity should not be less than .63 megohms/square. The

incident VSWR was found to be a function of surface resistivity only. The results of Appendix C are in general agreement with the available experimental data. For example, it is known that conductive films of about .40 megohms/square begin to affect the loaded Q of a test cavity.<sup>17</sup>

It is interesting to calculate the thickness of thin titanium films of  $10^6$  ohms/square surface resistivity. In Appendix D, this thickness has been computed, and the results show that the film must be about three orders of magnitude smaller than one atomic layer. Such calculations are inapplicable when they predict a thickness of less than a few atomic layers. However, the calculation leads us to think that the typical thin film of titanium is either of less than theoretical density, or is discontinuous on the surface, or is not all titanium (some material oxidized, for example). It is likely that all three conditions exist.

Experimental data show that typical titanium coatings of  $10^6$  ohms/square are in the range of about 20 to 200 angstroms in thickness (depending on conditions during the film deposition).<sup>18</sup>

Using the results of Appendix D, it can be shown that a film of pure titanium 200 angstroms thick, of the density of

bulk material, should have had a surface resistivity of only 25 ohms/square. These observations support our contentions about the nature of the coatings.

It may be concluded that films of sufficient thickness to greatly reduce the secondary emission coefficient of a window surface can readily be of high enough resistance to cause negligible rf effects, even though the coating material is a highly conductive metal. In the case of titanium, the experimental data supports this argument very well. It is not intended here to minimize the difficulties which are encountered in the preparation of such films.

Materials of intrinsically high resistivity that also have low secondary emission ratios are obviously advantageous from the viewpoint of film deposition; control of thickness, etc., need not be as precise. However, there are other criteria. For example, carbon has good secondary emission properties and fairly high resistivity, but experiments conducted in this program show that surface arcing removes it very readily.

#### 4.2.3 Changes in Physical and Chemical Properties of Thin Films

With such thin coatings, rather serious control problems

arise in coating windows for multipactor suppression. The main difficulty comes from susceptibility of many of the coatings to oxidation and reduction. With the coating being only a few tens of atomic layers thick and being porous in nature, chemical changes can happen readily, even in good vacuum atmospheres where the partial pressure of residual gases is small. The changes in the chemical composition of the coating due to the variation in the ambient conditions can be easily observed by monitoring changes in the surface resistance of the coating. For some coatings these resistance fluctuations can be several orders of magnitude.

Changes in chemical and physical composition of coatings, which take place during the deposition process, make the control of the film deposit extremely difficult, and affect the reproducibility of coatings. For example, experimental data show that for the same surface resistivity obtained under slightly different conditions, the thickness of the coating of deposited titanium films varied by one order of magnitude.<sup>18</sup>

Some changes in coatings have also been observed during high-power operation of windows. The term that is usually used here is "conditioning". That is, on first applying rf power,

multipactor might appear, but, after a period of time, ranging from a few seconds to as much as an hour, the multipactor discharge would disappear. Some chemical or physical change in the coating, which affects its effective secondary emission ratio, must be taking place under the multipactor discharge, at least during its initial stages. A more detailed analysis of problems associated with thin coatings is given in Sections 4.3.5, 4.3.6 and 4.3.7.

#### 4.3 SPUTTERING EQUIPMENT AND EXPERIMENTAL PROCEDURES

##### 4.3.1 Choice of Thin Film Deposition Technique

Prior to this program, two window coating procedures had been utilized extensively. Evaporation was used to obtain titanium films and sputtering was used to obtain coatings from a titanium monoxide cathode.<sup>19</sup> The sputtering technique is particularly useful for window coating application of refractory compounds, and for certain materials it appears as the only means of thin film deposition because of disassociation of these compounds upon heating. Also, it is believed that sputtered coatings provide a bond between the coating and the surface of the substrate which is better than the bond obtained by evaporation. The greater strength of the bond is derived from the higher

velocity of sputtered particles.

Among other potential coating techniques, chemical vapor deposition shows some promise, and it is known that stable carbon films can be formed using pyrolytic deposition. Plasma-torch coatings do not appear suitable for window coating because of the non-uniformity of the spray, and because of the particle size a coating of about .001 inches is necessary to obtain coverage.<sup>20</sup> Such thick coatings, most likely, will have a too low surface resistivity to be of any use. In any case, the size of deposited particles will probably reduce the arcing threshold of the window surface by creating points of locally high electric field between the individually protruding particles. Most likely, there are other suitable techniques of creating thin films on the surface of a window, for example, by a chemical solution deposition followed by a drying or a firing process, by ion plating, or diffusion.

Of all of these thin film deposition techniques, evaporation and sputtering were the most known and widely used. The other techniques entailed many unknown factors and would have required extensive preliminary investigations. For this reason, and because coatings of carbides and nitrides had to be studied in

this program, sputtering was finally chosen as the film deposition technique to be used in this program.

#### 4.3.2 Description of Sputtering Equipment

The sputtering apparatus, especially designed for use with a six-inch cathode, is shown in Figure 2. The chamber itself consists of a 6-1/2 inch diameter pyrex cylinder mounted on the base plate of a pumping station, with a top plate consisting of a water-cooled cathode mount, anodic shield and an argon leak. The anodic shield was used to prevent sputtering from the back of the cathode and the cathode lead. This was accomplished by positioning the shield close to the cathode to prevent maintenance of a glow discharge. Both the cathode block and the anodic shield are removable to allow the installation of different size cathodes. The lower base plate, which mounts on the vacuum station, consists of a movable anode-substrate holder with a heater, thermocouple, crystal holders and various feedthroughs. The vacuum station is a liquid-nitrogen-trapped, oil-diffusion pump system. Twenty-seven Mc rf excitation of the discharge is permitted by an rf coil located outside the bell jar. This prevents sputtering of coil material. Figure 3 shows the overall view of the sputtering setup. The rf equipment is to the right of the sputtering chamber. All coatings sputtered in this program were done using

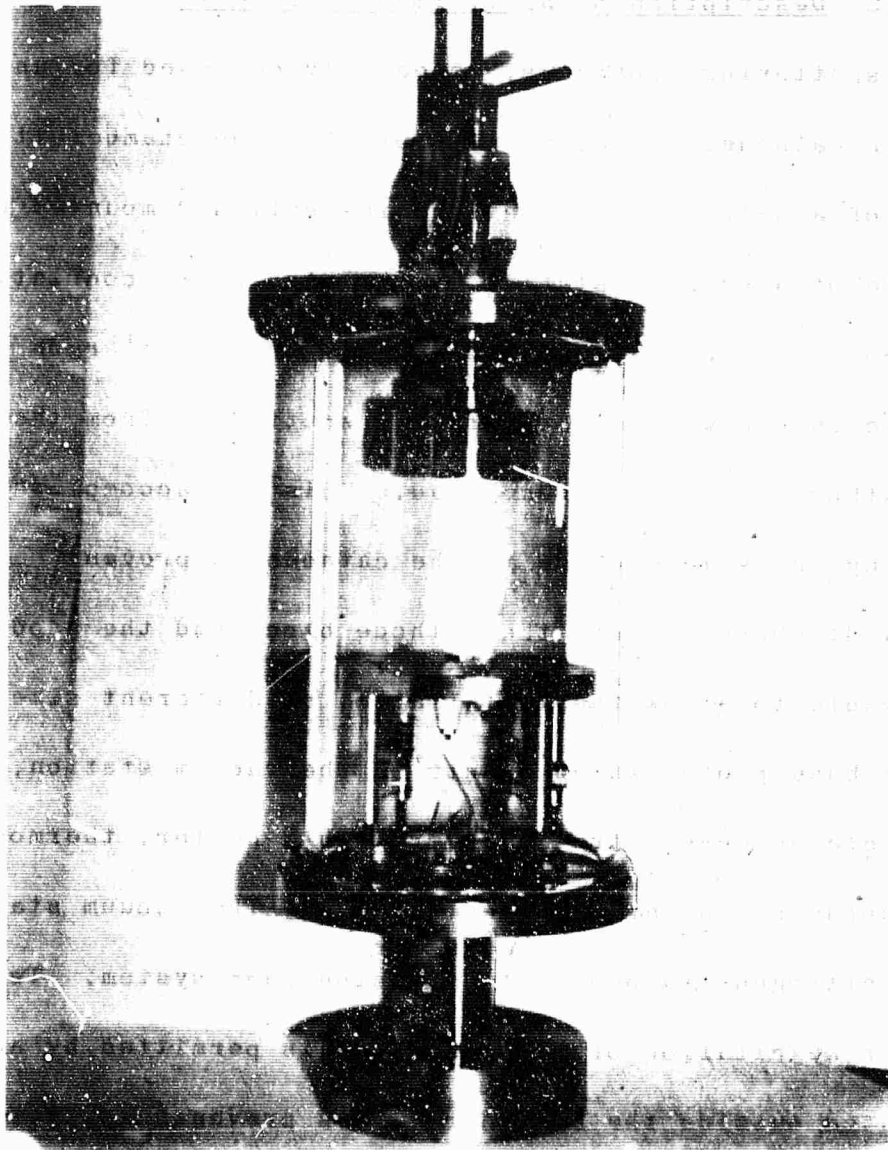


**FIGURE 2 SPUTTERING APPARATUS**



**FIGURE 3** OVERALL VIEW OF THE  
SPUTTERING EQUIPMENT

the 27 Mc rf source. The use of rf is desirable when the gas density is not high enough to maintain an adequate discharge with dc current alone.<sup>21</sup> Also, it was found that more uniform coatings could be obtained using rf.

About half-way through the program a modification of the sputtering equipment of Figure 3 was necessary. This change in the equipment consisted in turning the sputtering chamber of Figure 2 upside down, and was necessitated by the fact that the carbide and nitride materials, in forms useful for cathodes from which windows could be coated, were either unavailable or not available in reasonable purities, and sputtering had to be done from powders.\* Since the original sputtering chamber (Figure 2) was built with the cathode suspended from the top of the pyrex cylinder and the anode-substrate holder below, it was necessary to upend the sputtering chamber. Only a new exhaust tubulation and a new window-holding mechanism had to be provided.

Fabrication of the powder-cathode was accomplished by suspending the powder of the material to be sputtered in

---

\* No pressed or sintered discs could be made by outside vendors without a 2 - 3% nickel content or similar metal added as a binder. Two different attempts of making solid cathodes from powder at Sperry have also failed.<sup>22</sup>

methanol, and coating a six-inch aluminum disc by settling and evaporation. This cake was then dried thoroughly and heated in vacuum. The cathodes, obtained in this fashion, did not break up in vacuum, but did require additional time for outgassing. All carbide and nitride coatings on this program were obtained from such cathodes.

#### 4.3.3 Control of Deposition of Sputtered Coatings

Very early in the program it was determined that control of the obvious variables of the sputtering process, like dc voltage and current, atmosphere, pressure, time, etc., was not accurate enough to provide good regulation for coating deposition. The resistance measurement technique was found to be unreliable to control reproducibility of coatings and almost useless for monitoring of deposits of non-metallic compounds, which tend to produce very high resistance coatings. Problems associated with changes in the resistivity of coatings are discussed later. It was, therefore, decided to use a crystal oscillator thin film monitor for control of the amount of material deposited.

The block diagram of the monitor is shown in Figure 4. Oscillator #1 is connected to the crystal that is to be exposed to the material being deposited in the system. Oscillator #2

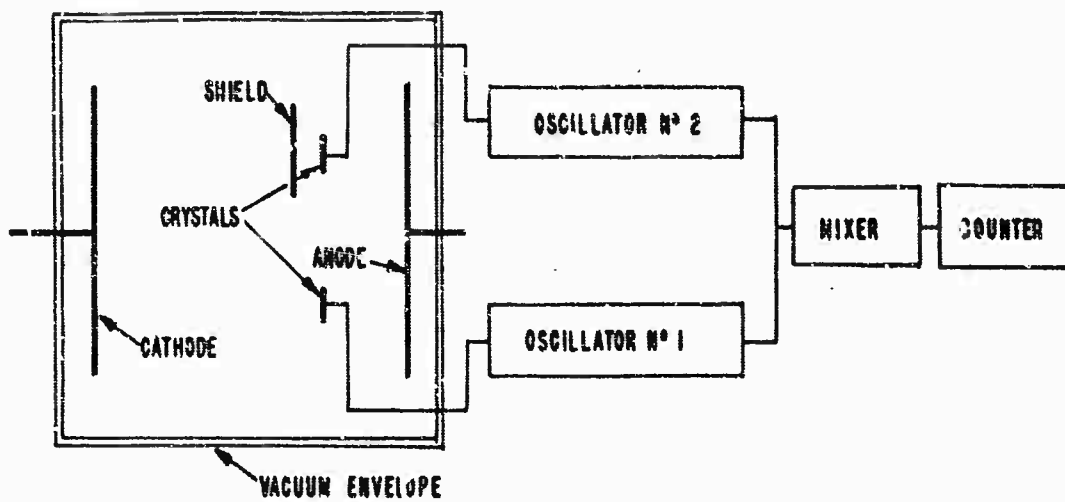


FIGURE - 4 BLOCK DIAGRAM OF THE CRYSTAL OSCILLATOR THIN FILM MONITOR

is connected to an identical crystal which is shielded from the deposit, but exposed to the same thermal environment in the chamber as the sensor crystal. In operation, the resonant frequency of the crystal exposed to the deposition changes linearly with the mass of material deposited on it. The amount of material deposited is monitored by observing the change in beat frequency between the two oscillators.

The monitor was calibrated using a method described by Hall.<sup>23</sup> The procedure was to mount four 4.5 megacycle crystals about 1 cm in diameter in a vacuum chamber. Three of the crystals were exposed to gold evaporated from a pure gold wire wrapped around a heated tungsten wire three inches above the crystals. The fourth crystal was shielded from the gold by a thin sheet of mica. Before evaporating the gold, the beat frequency for each of the unshielded crystals with respect to the shielded crystal was read at three-minute intervals over a period of thirty minutes. The beat frequency was found to vary less than  $\pm 2$  cycles per second during this period.

After this period, gold was evaporated into the crystals until the observed changes in beat frequencies were large enough to ensure a mass change great enough for accurate weighing. The

pressure in the chamber during the evaporated period was about  $5 \times 10^{-8}$  torr. After the evaporation was completed, the apparatus was allowed to cool until the beat frequencies had stabilized, which took about 10 to 15 minutes. Final values of the three beat frequencies were measured. The apparatus was then let down to air and the crystals removed for weighing.

The values obtained from the three crystals were sufficiently alike,<sup>24</sup> so that reasonable accuracy was to be expected in calculating the amount of material deposited in a given sputtering or evaporation experiment. It should be noted that frequency shift of a quartz crystal depends only on the mass deposited and not on the material deposited. The area of the crystals exposed to the gold was 1.76 sqcm, and the surface density sensitivity was 18.0 micrograms/square cm/kc.

During sputtering of windows with high-resistivity materials, it was found that uniform results were obtained in using the thin film monitor if the system was pumped and the 27-megacycle rf source was turned on without any applied dc voltage until the crystal count became stable and good vacuum was maintained. This is termed rf clean-up. It was observed that if no rf clean-up was performed, an error in the reading of the beat frequency was obtained. The crystal

count in this case would first decrease then increase as the coating was built up. On the other hand, if the rf was applied and the count allowed to decrease until a repeatable beat frequency was obtained before dc voltage was applied, the digital counter immediately showed an increase in count consistent with the expected rise from application of the coating. The reading of the crystal was made when the glow discharge in the sputtering chamber was out. This crystal oscillator thin film monitor technique was used to control coating deposits throughout the program.

#### 4.3.4 Sputtering Procedure

The sputtering procedure used throughout the program was essentially the same. The following description of a specific sputtering experiment is illustrative of the technique used. In this experiment, an attempt was made to correlate the crystal-oscillator monitor with surface resistivity measurements using titanium as the deposited metal. In each test, a ceramic slide 7 cms long and 2 cms wide was metalized and plated on both ends leaving a square in the center 2 cms on a side. Crystal oscillator measurements were made simultaneously by mounting a crystal at the same distance from the center of the anode as the resistance square. The anode was a circular aluminum disc 6 inches in

diameter. The cathode was a 6-inch diameter disc of titanium. The measuring devices were both mounted 1 inch from the center of the anode in a plane 1.75 inches from the cathode and .25 inches above the anode. Sketches of sputtering setups used in this program are given in Appendix E. The trapped system was pumped down to  $2$  to  $4 \times 10^{-7}$  torr, then flushed with dried argon and pumped back to the same pressure. This process was repeated three times. The argon pressure was then regulated and argon allowed to flow through for ten minutes before sputtering. Sputtering runs were made at various argon pressures from 32 to 50 microns and at dc voltages of 3 to 4.5 kv. The sputtering runs were of 30-second and one-minute duration with resistance and beat frequency measurements performed after each period. In addition, runs under the same conditions were performed in which the equipment was operated continuously for the same total time as accumulated in the short duration runs. Duplicate runs were made in a number of cases. Figure 5 shows a plot of change in beat frequency of the thin film monitor in cycles per second versus sputtering time for three different values of argon pressure. It can be seen that slight changes in argon pressure produced relatively large changes in the sputtering rate. For this reason, the control of the amount of the material deposited by attempting

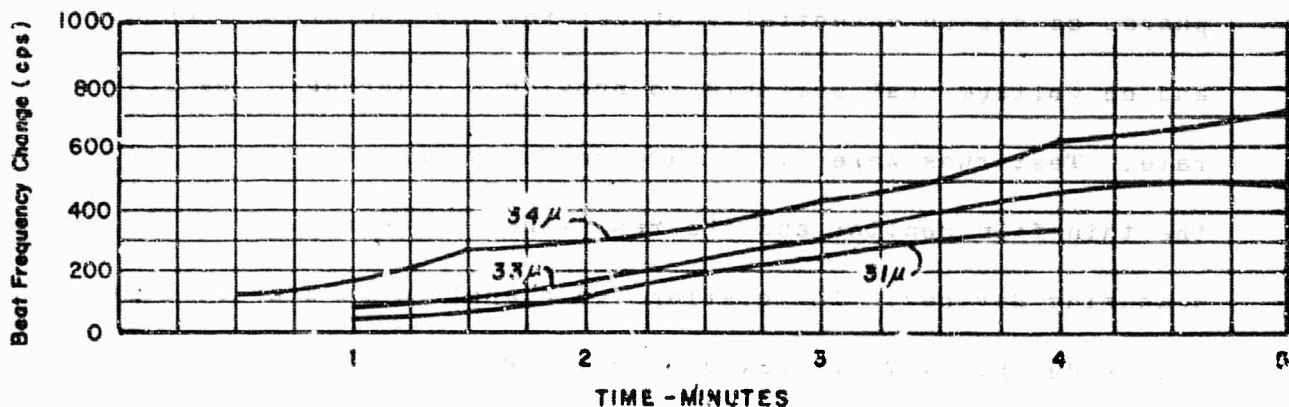


**FIGURE-5 BEAT FREQUENCY CHANGE V<sub>a</sub> TIME**

**TI SPUTTERED AT 31,33,34 μ ARGON 3 KV DC 27 MC RF**

to operate at a given pressure, voltages and anode-to-cathode spacing for a given time appeared impractical.

The technique for sputtering in argon and nitrogen atmospheres consisted essentially of determining the argon pressure and dc voltage most suitable to provide a reasonable coating rate. Test runs were first made on dummy ceramics using both the thin film monitor and the resistance slide monitor as measuring devices. The coatings were applied at 3 kv dc voltage and using the 27 Mc rf power source. Pressures during coating in argon were kept in the range of 35 - 45 microns while those in nitrogen (see last paragraph) were held at 85 - 90 microns. The spacing of the objects was as reported in the previous paragraph.

After having first determined the approximate rate of deposition of a particular coating under given operating conditions, the coating was then applied to an actual window. By keeping track of the elapsed time, the approximate amount of sputtered coating was thus known. As the amount of the coating deposited began to approach its predetermined value, the sputtering process was stopped and the actual amount of the material deposited was determined by measuring the shift in the beat frequency. The

results of this measurement were then used to determine if the sputtering should be continued and for how long. Often, several checks of the heat frequency had to be performed during the same run indicating a change in the sputtering rate between the trial run and the actual run.

In addition to experiments with sputtering titanium metal in an argon atmosphere, experiments have been conducted on the sputtering of titanium in a nitrogen atmosphere (these were the only two atmospheres investigated in this program). The object of sputtering titanium in nitrogen was to achieve a coating of titanium nitride.<sup>25</sup> The technique used here was identical to the one just described for experiments in argon atmosphere. The nitrogen was maintained at a pressure of 80 to 85 microns. The coating process was controlled using both the thin film monitor and the resistance slide monitor. Figure 8 shows the beat frequency of the thin film monitor versus sputtering time for two values of dc voltage. It can be seen that an increase in the sputtering voltage of only 30 percent produced a five-fold increase in the sputtering rate. Assuming a linear dependence between the sputtering rate and the applied voltage, a doubling of the sputtering rate can be produced by an approximate 10 percent increase in the applied dc voltage, indicating a rather

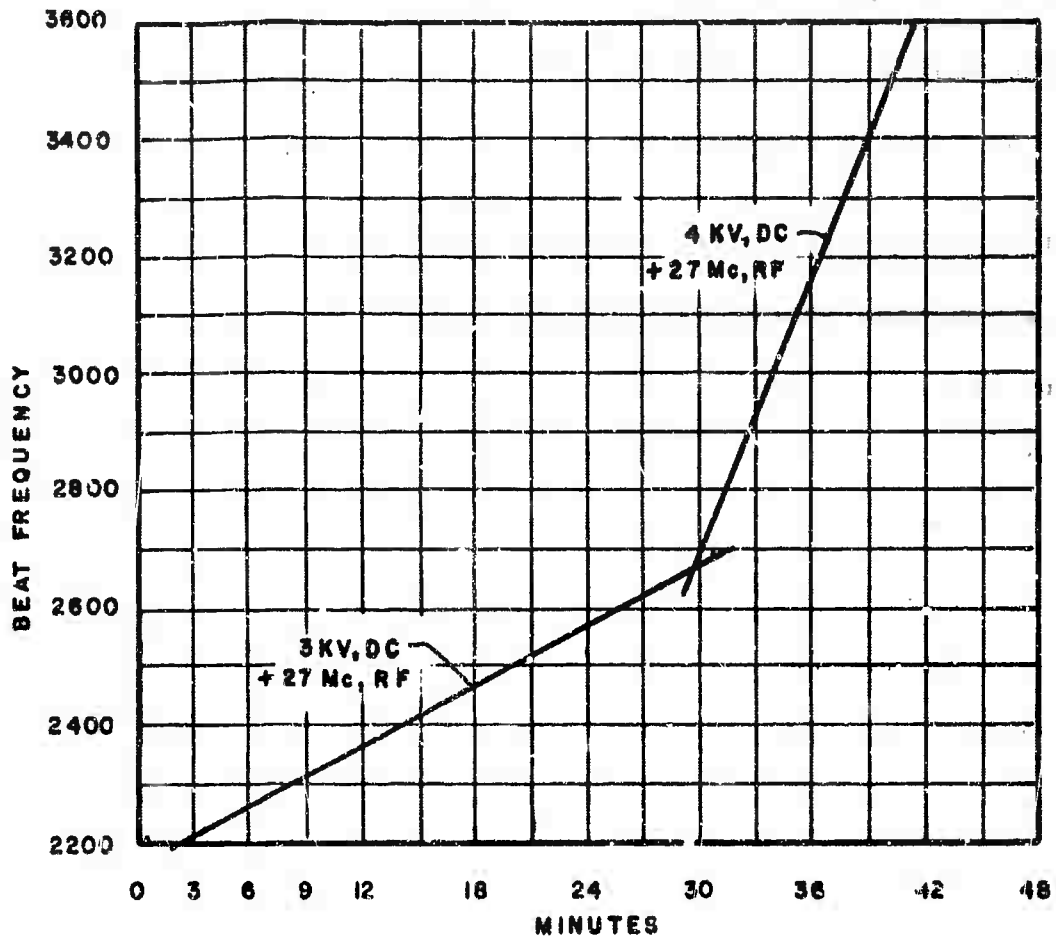


FIGURE-6 BEAT FREQUENCY Vs TIME

TI SPUTTERED AT 85 MICRONS  $H_2$

critical control requirement for the dc voltage.

#### 4.3.5 Changes in the Surface Resistivity of Coatings

In the calibration experiment described in Section 4.3.4, the two leads of the resistance slide were connected to a General Radio Type 544-B megohm bridge, and changes in the resistance of the slide were measured. It was observed in between sputtering periods, and at the end of each particular sputtering run, that the resistance of the titanium coating changed with time even though the argon atmosphere was maintained at about constant value. During the same interval, the beat frequency change of the oscillator was very small, indicating that not the quantity of material, but its resistivity, were changing. It is suspected that this resistance change was due to partial oxidation of the titanium coating by small amounts of oxygen inevitably present in the system. A similar observation was made previously by Eimac.<sup>26</sup> The change in the resistivity of the coating made direct comparison between resistance and beat frequency measurements impractical. Other changes in the resistance of coatings are described in Section 4.3.6.

In the experiments in which titanium was sputtered in a nitrogen atmosphere (in an attempt to deposit titanium nitride),

the resistivity of the coatings deposited remained very high although the thin film monitor indicated that fairly heavy films were being deposited. This was to be expected since titanium nitride is an insulator. The fact that the coatings had a finite, but high, resistivity is indicative of some titanium metal in the coating. Upon admission of air to the sputtering apparatus, the resistivity increased due to oxidation of the free metal. The coatings obtained in these runs had the characteristic yellow color of titanium nitride. (As reported in Section 4.3.7, the resultant films were largely titanium dioxide).

In almost all sputtering experiments, both resistance slide and crystal oscillator measurements were made.\* Nearly always, the thin film monitor was found to be a more reliable and practical device for monitoring the amount of material deposited. However, resistance measurements have been found useful and at times very important, like in determining the uniformity of sputtered coatings. This subject is discussed in Section 4.3.8 in greater

---

\*Crystal oscillators and the resistance slide were always positioned close to the anode-substrate. For larger windows, the coating was usually deposited to two different thicknesses, so that each time there was at least one-half of the 6-inch window that was blocked off from sputtering. The control devices were then located in this area of the window.

detail.

#### 4.3.6 Effect of Tube Processing Techniques on Window Coatings

All window coatings must go through the bakeout process. The actual temperature at which the window is baked in vacuum is generally in the 400° - 600°C range, and the window coating must survive this bakeout without a serious loss of its mechanical and electrical properties. The majority of coatings evaluated in this program were baked at about 400°C. In almost all cases, the change in loaded Q of the test cavities before and after the bakeout was small and usually within the range of the error of the cold-test equipment.

In one case a very significant change was observed in the resistivity of the coating. In this instance, chromium metal was sputtered on a test ceramic slide to a surface resistivity of .7 megohms/square, as measured in argon atmosphere at the end of the sputtering cycle. On exposure to air, the resistance rose to a value in excess of 30,000 megohms/square. Upon heating in vacuum to 600°C, the resistance dropped very sharply to less than 10,000 ohms/square. On cooling to room temperature, but still in vacuum, the resistance rose to 50,000 ohms, and did not change much on admission to air. The resistance of the chromium-coated

ceramic slide after wet hydrogen firing was found to be so high that it could not be measured with the available equipment.

At about the same time this test was being performed, an alumina window was coated with chromium for evaluation in the multipactor test cavity. After bakeout of the cavity, the resistance of the coating was so low that the cavity resonance had completely disappeared and testing was impossible.

In many instances, however, it would be desirable to coat the window before brazing it into a window assembly. Such a coating would then have to survive the brazing process, usually a hydrogen firing. In order to study the effect of tube processing atmospheres and temperatures on window coatings, several ceramic slides were coated. In all tests the slides were first fired at  $1100^{\circ}\text{C}$  in a wet hydrogen atmosphere to simulate brazing of a window into its frame. It was not possible to measure any of the properties of the coatings during the firing process, but the resistance was conveniently measured before and after. Typically, the resistivity of slides increased several orders of magnitude as a result of this firing.

The samples were then subjected to a  $900^{\circ}\text{C}$  firing in wet hydrogen to simulate brazing of the window and its frame to the

tube or to a waveguide run. This firing increased resistance of the slides some more, but this time only by a factor of 2 or 3. Finally, 10 samples were mounted in vacuum and the temperature gradually increased to 600°C, held for a short period, and then allowed to return to room temperature. The object of this cycle was to simulate vacuum bakeout of the tube.

It was discovered that the resistance of the slides dropped from the very high values, observed at the end of the hydrogen firing cycle, after the samples were subjected to vacuum atmosphere. As the temperature of the samples went up, the resistance continued to drop and reached a minimum value at the highest temperature. As the slides were cooled, the resistance rose again and reached a relatively high value at room temperature. Upon opening of the bell jar to air, the resistance climbed even more. Figures 7, 8, 9, 10 and 11 give resistance changes versus temperature for five most important coating materials tested in this program.

The results obtained with the titanium coating of Figure 7 suggest that for titanium, normal tube assembly brazing operations in wet hydrogen oxidize metallic titanium, but that the reaction is reversible. The oxide, at least partially, reverts to metal

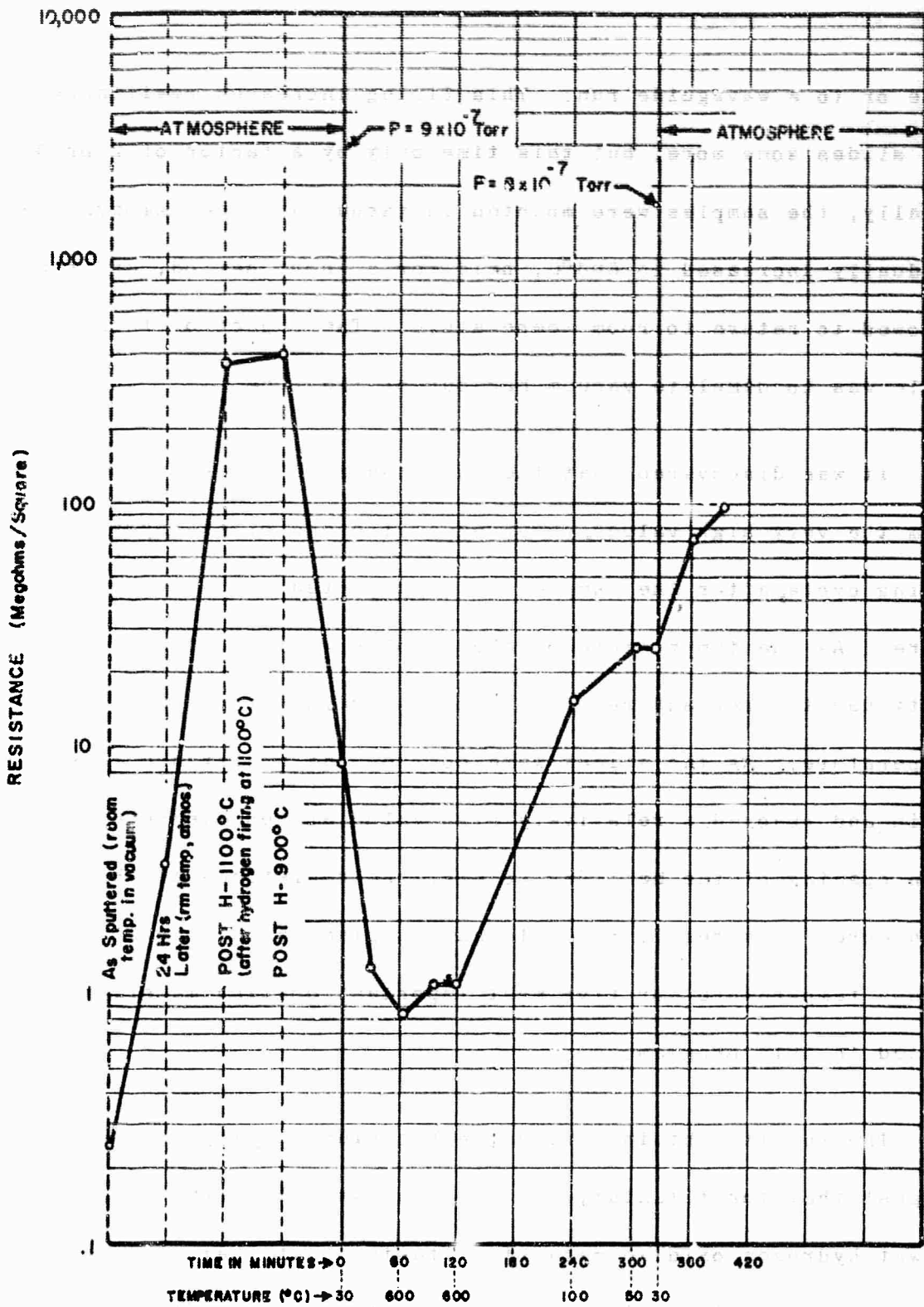


FIGURE - 7 PLOT OF RESISTANCE CHANGE VS TIME AND TEMPERATURE FOR A TITANIUM COATING

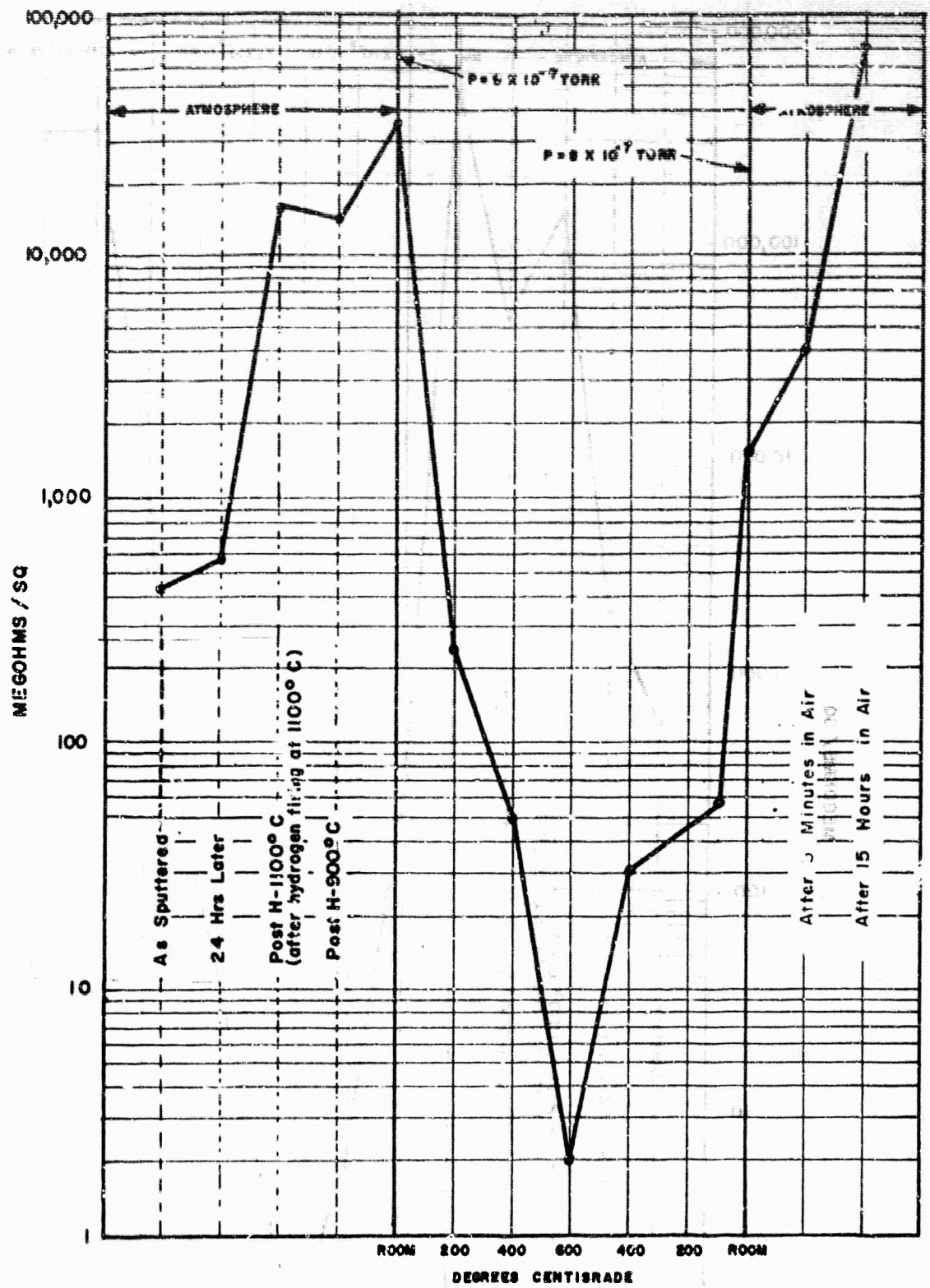


FIGURE-8 RESISTANCE CHANGE VS TEMPERATURE FOR VANADIUM CARBIDE

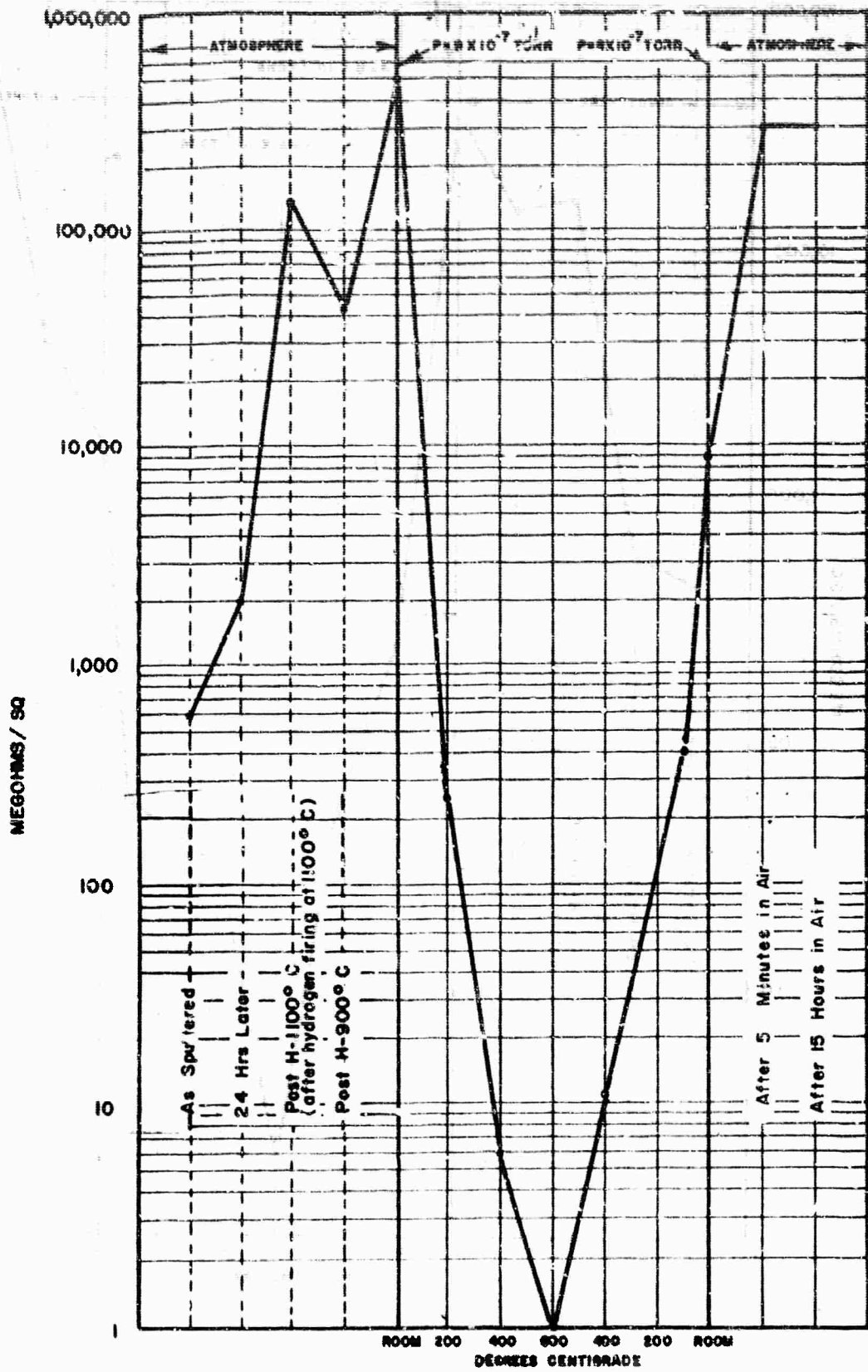


FIGURE - 9 RESISTANCE CHANGE VS TEMPERATURE FOR TITANIUM CARBIDE

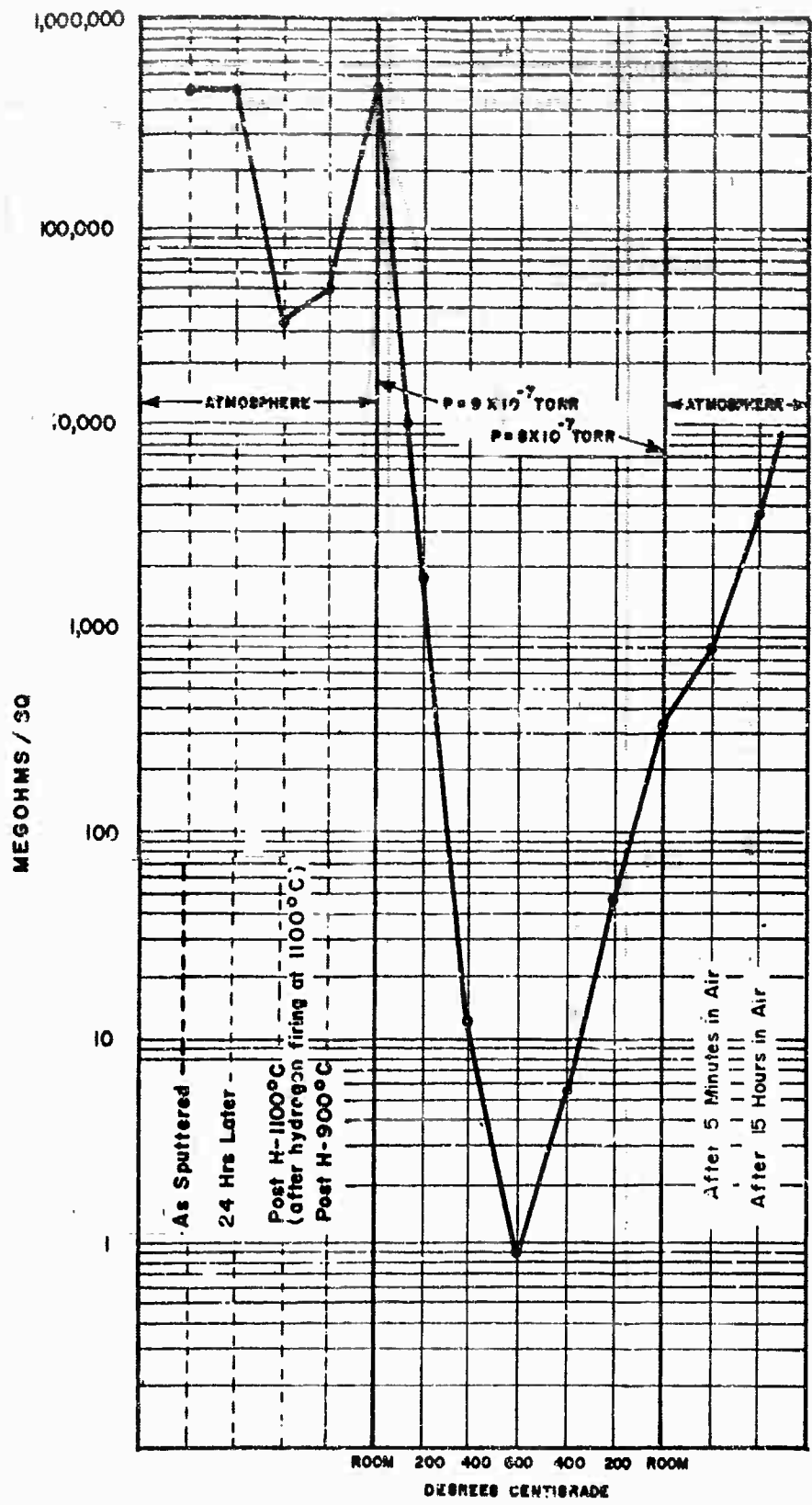


FIGURE -10 RESISTANCE CHANGE VS TEMPERATURE FOR TANTALUM CARBIDE

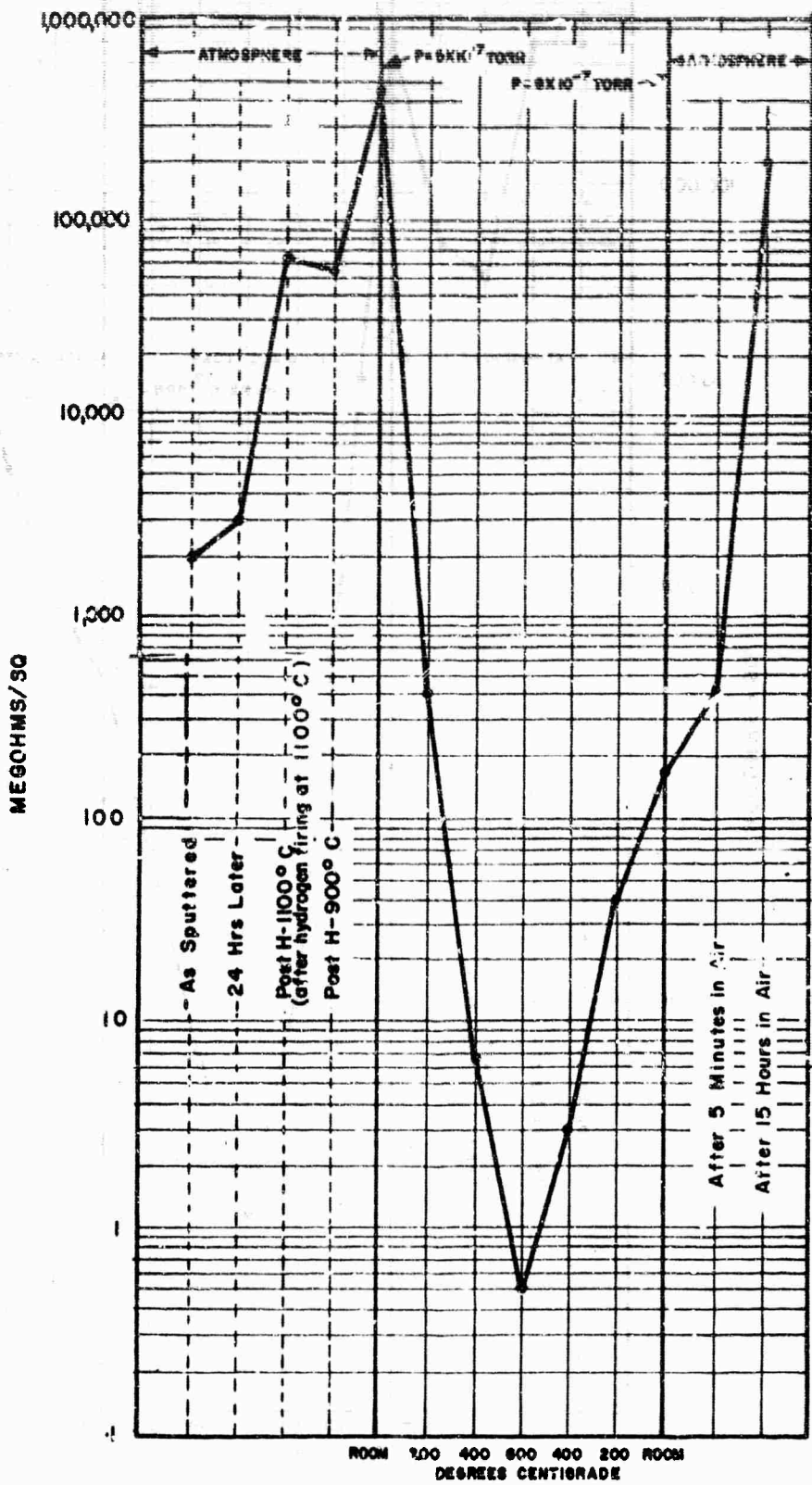


FIGURE -11 RESISTANCE CHANGE VS TEMPERATURE FOR TITANIUM NITRIDE

upon heating in vacuum and the surface resistivity of the coating approaches the value it had at the end of the sputtering cycle in the argon atmosphere. The coating then reoxidizes with the reduction in temperature.

The results obtained with other coatings are similar to those just described with titanium, except that resistance fluctuations were found to be much greater than experienced with titanium coating. In all cases shown, the resistance of coatings at 600°C in vacuum was much lower than the value of the resistance at the end of the sputtering cycle as measured in argon. Oxidation-reduction reactions, similar to those observed with titanium films, appear to be taking place here also.

Section 4.5.1.3 describes multipactor test data obtained with a vanadium carbide coated window fired in wet hydrogen at 1100°C. Since the results obtained with this coating were found to be poor (Experiment #19, Table II, p. 24), it was decided to see if a change from a wet to a dry atmosphere would produce any significant changes in the behavior of the coating.

A total of thirteen tests were performed with dry hydrogen fired vanadium carbide coated resistance slides and windows. The dewpoint of the hydrogen furnace was less than -40°F. The

mass density of deposited coatings ranged between 1.9 and 4.3 micrograms/cm<sup>2</sup>. In all cases, the resistance of the coating went down after dry hydrogen firing.\* The reduction in the resistance was either small (typically from about 20,000 megohms/square to about 18,000 megohms/square) or very large (typically from about 20,000 megohms/square to about 3,000 ohms/square).

An attempt to obtain a dry hydrogen fired vanadium carbide coating of about 1 - 10 megohms/square resistivity was unsuccessful. A total of four six-inch diameter windows were coated in this attempt. The two closest values achieved were a surface resistivity of about 2,500 ohms/square and a surface resistance of 6,000 megohms/square. No doubt, chemical and physical properties of very thin coatings (discussed in Section 4.2.2 and 4.2.3) must be responsible for this behavior. The window with the coating of 2,500 ohms/square completely eliminated the resonance response of the multipactor cavity, whereas the window with the 6,000 megohms/square coating was a poor multipactor suppressor (Experiment #21, Table II, p. 95).

A similar investigation was performed with window coatings

---

\* Note that wet hydrogen firing produced an increase in the surface resistance of a coating sputtered from a vanadium carbide cathode (Figure 8).

sputtered from a vanadium carbide cathode and fired in a 900°C wet hydrogen atmosphere. This firing was to simulate brazing of a window into its frame using a low-temperature, silver-copper eutectic. The 900°C wet hydrogen firing produced a reduction in the surface resistivity of coatings as did dry hydrogen firing at 1100°C. Wet hydrogen firing of vanadium carbide coatings caused very large increases in surface resistivity. From the five coatings investigated, the resistivity of the coating after 900°C firing was at least one order of magnitude smaller than its value measured in air before firing. The inconsistency in the resistance changes between the 900°C and 1100°C wet hydrogen firing is unexplained. The experimental data obtained with a vanadium carbide coated six-inch window fired at 900°C in a wet hydrogen atmosphere is given in Table II (Experiment #20, p. 95). No attempt was made to simulate brazing windows in a vacuum atmosphere. Vacuum brazing of window assemblies is not a suitable assembly method, since evaporation of the brazing alloy onto the window surface is almost inevitable.

#### 4.3.7 Identification of Sputtered Coatings

Coatings of sputtered titanium metal show a substantial increase in resistivity on exposure to air as shown in Figure 7, and it has been generally assumed that these coatings oxidize. A

similar observation was made at Eimac.<sup>26</sup> In this program, a sample of sputtered titanium on an alumina substrate was exposed to air for a period of about two weeks, but protected from dust and abrasion. It was then analyzed at the Sperry Rand Research Center, Sudbury, Massachusetts, using electron diffraction techniques.

The results of this analysis indicated that the coating was either titanium monoxide, titanium nitride or titanium carbide. All of these compounds have virtually the same lattice constant and cannot be distinguished from one another by electron diffraction. There was no evidence of titanium metal, or of titanium dioxide or titanium sesquioxide.

The formation of titanium nitride and titanium carbide is extremely unlikely, since the coating was sputtered in an argon atmosphere, and it is very unlikely that these compounds would be formed subsequently by exposure to the atmosphere at ordinary temperatures. Therefore, it has been concluded that the coating was titanium monoxide. Since coated windows must almost inevitably be exposed to air after coating before mounting in a tube, this work strongly suggests that sputtering with titanium monoxide will produce the same results as sputtering with titanium metal.

The above results show that a sputtered titanium coating, upon sufficiently long exposure to air, transforms completely to titanium monoxide. Figure 7 also shows that this transformation is at least partially reversible in vacuum at elevated temperatures.

A sputtered coating produced from a titanium cathode in a nitrogen atmosphere, as described in Section 4.3.4, was also sent to the Research Center for identification. The coating was exposed to air for at least a week before identification was attempted. The electron diffraction technique identified the coating material as titanium dioxide. It is not clear why the dioxide was deposited rather than the nitride or the monoxide. As a result of this identification, it was decided that nitride coatings could best be made by sputtering directly from nitride in an argon atmosphere. It was also decided that carbide coatings would be deposited by sputtering the carbide in an inert (argon) atmosphere.

It is possible that reactive sputtering (sputtering a metal in a chemically active atmosphere, in order to deposit a compound of that element) could have been successfully applied with further effort. It is also possible that a combination of reactive and non-reactive sputtering might have been advantageous. For

example, titanium nitride could have been sputtered in a nitrogen atmosphere. This might result in depositing more nearly pure titanium nitride; at least some of the nitride disassociated by the sputtering process might have recombined with the nitrogen atmosphere.

No other electron diffraction tests of coatings were made.

The results of Figure 8 and 9 show that the resistance of sputtered carbide coatings increases on exposure to air. The fact that a simple exposure to air causes an increase in the resistance of the coating indicates probable deposition of some metal together with the carbide. The exact nature and composition of the as-deposited coatings is not known. Some chemical spot tests were made on coatings sputtered from vanadium carbide cathodes. Partial solubility in sulfuric acid indicate that indeed some decomposition of the compound during the sputtering process must be taking place. Resistance fluctuations due to hydrogen firing and bakeout (oxidation-reduction reactions), are also indicative of presence of metal in sputtered coatings of all carbides and even titanium nitride.

#### 4.3.8 Uniformity of Sputtered Coatings

In the evaporation process, the amount of material deposited

on the surface is proportional to the inverse of the square of the distance between the evaporating source and the substrate surface. Therefore, as long as this spacing is large as compared to the diameter of the flat window, evaporated coatings exhibit good uniformity, and the degree of uniformity is not affected, if, for example, the window to be coated is placed at the bottom of a metallic cylinder.

In the sputtering process, coating uniformity is much more difficult to obtain. It is very seriously affected by the anode-to-cathode spacing and the dimensions of the anode and cathode.<sup>27</sup> Also, all the metallic objects placed in the space between the cathode and the anode affect the uniformity of the sputtered film. For this reason, the uniformity of sputtered coatings was extensively studied in this program.

After most coatings have been at atmospheric pressure for some time, their resistance stabilizes, and it is usually possible to measure the uniformity of the coating by resistance measurements. The surface resistance, in ohms per square, is conveniently measured by measuring the resistance between two probes maintained a short distance apart. In Appendix F it is shown that the resistance so measured is directly proportional

to the surface resistivity. The measured resistance is numerically equal to the surface resistance for a particular ratio of probe diameter to spacing. The surface resistivity in ohms/square can be measured fairly accurately as long as the separation between the probes is small compared to the dimensions of the coating, and small compared to the distance from the point of measurement to the edge of the coating.

Making use of this technique, the variation in the surface resistivity of several six-inch diameter alumina windows sputtered from a six-inch cathode was measured. The sputtering procedure in these tests was as described in Section 4.3.4. It was found that some control over deposition of a coating could be achieved by the variation of the cathode-to-anode distance. With a large anode-cathode spacing, the coating was heaviest at the center. As the anode-to-cathode distance was decreased, the applied film became more uniform until the dark space (in front of the cathode) was approached closely. When the dark region was penetrated, the pattern of the sputtered film reversed and the film became a doughnut-shaped ring with the substrate nearly bare both at the edge and in the center.

It was found that even the best coatings produced by this

technique exhibited a resistance variation with radius, and that the variation in the resistance of the film was greater when the 27 Mc rf source was not used. With simplifying assumptions (for example, neglecting space charge), the variation in the magnitude of the rf electric field was computed; the calculation is shown in Appendix G. It was found that the rf electric field is directly proportional to frequency and the radius, being zero at the center of the disc. Since the rf electric field contributes to the ionization of the gas, a relative improvement in the surface resistivity of the sputtered film with application of rf is understandable. Since the rf electric field is also proportional to the rf current in the sputtering coil, a measure of control over radial variation in deposition of material can be exercised.

By the use of these techniques, plus partial shielding of the cathode, reasonably uniform coatings could be achieved. Figure 12 shows a typical plot of surface resistance of a six-inch alumina disc as a function of radius. The resistance variation shown is about 3 to 1. For this particular coating, the film is thicker at the center of the disc. A sketch of the sputtering apparatus used to obtain this coating is shown in Figure E1 of Appendix E.

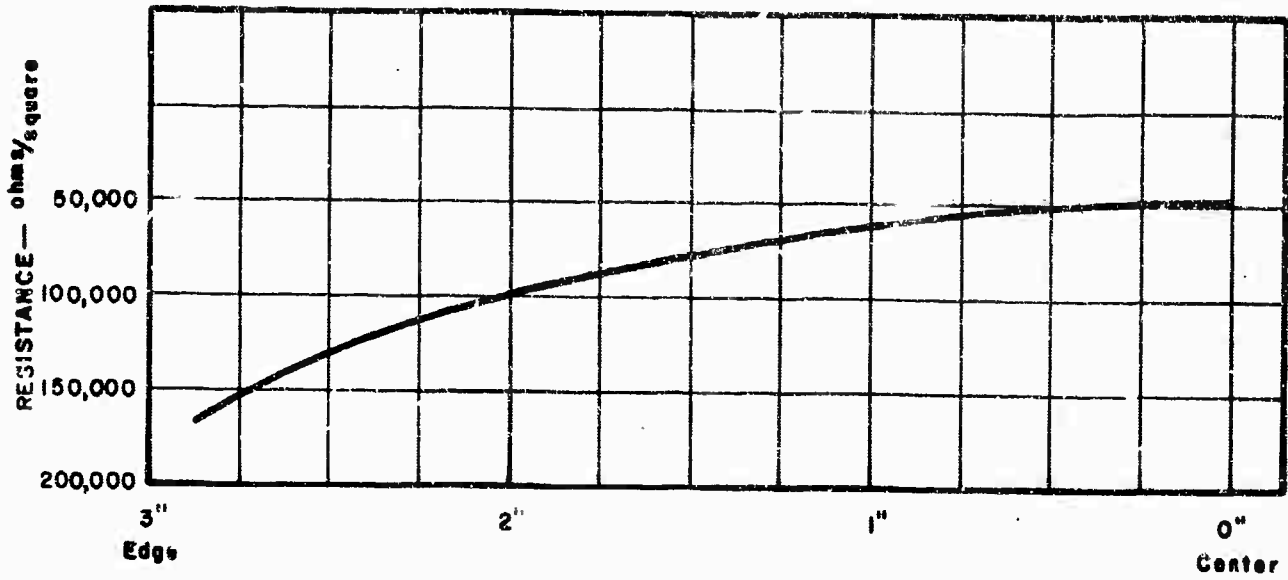


**FIGURE-12 CONTOUR OF SPUTTERED TI ON 6" WINDOW.  
BASED ON RESISTANCE PROBE MEASUREMENT**

Multipactor test results obtained with hydrogen fired vanadium carbide coated windows have shown that the firing process degrades the multipactor suppression properties of these coatings. For this reason, it was decided to coat the windows for high-power tests in the  $TE_{11}^0$ -mode cavities after the windows had been brazed into position. In this way, high temperature firing of the coated window could be avoided. Both S-band and X-band windows were coated in this fashion. The modified sputtering equipment used for coating of windows at S-band is shown in Figure E2 of Appendix E. This sputtering procedure did not produce very uniform coatings. In one window sputtered from a vanadium carbide cathode, the resistivity of the coating in the center of the window was measured to be 100 megohms/square, increasing to about 2000 megohms/square at the window edges. Several other positions of the cathode with respect to the windows were tried, but the coating uniformity could not be improved. An attempt at coating an S-band window subassembly of Figure E2 in the manner used for sputtering the X-band  $TE_{11}^0$ -mode window (Figure E3) produced even greater variations in the surface resistivity of the coating.

A method which might improve the uniformity of coatings sputtered onto windows previously brazed into cylinders was

conceived but not tried. This method involves using an aluminum mesh as the anode. The mesh can be either in front of the cylindrical sleeve, or positioned within the sleeve. This would confine the glow discharge to the cathode-mesh region. Since the sputtered particles are mostly uncharged, a large portion of them would pass through the mesh. Aluminum was chosen for the mesh material to avoid contamination. If any aluminum were sputtered or evaporated, it would almost certainly be oxidized to  $Al_2O_3$ , the material of the window. It would be important to limit current to the mesh so that the amount of evaporation would be negligible.

Coating of windows for high-power X-band tests was performed using the sputtering setup shown in Figure E3. Again, the uniformity of coatings was not exceptionally good, but the resulting variation in the surface resistivity of coated X-band windows was better than of those at S-band. Typically, variation in the resistivity of X-band coatings was 4 to 1.

#### 4.4 HIGH-POWER TEST EQUIPMENT

##### 4.4.1 Description of Multipactor Test Cavities

An important feature of the high-power multipactor evaluation part of this program was a method by which multipactor could be

studied without seal-area arcing. This was accomplished by means of specially designed, demountable multipactor test cavities. A cross-sectional view of the test cavity used for evaluation of coatings at X-band is shown in Figure 13. The S-band version had a similar cross-section. Design drawings for the S-band cavity are given in Appendix H. The internal dimensions of the X-band cavity can be scaled from these drawings.

Figure 13 shows that in the multipactor test structure, the dielectric to be tested is placed near one end of the cavity. The dielectric constants of all of the materials of interest (alumina, beryllia, sapphire, etc.) are so high that a relatively short length of dielectric is equivalent to a fairly long distance in vacuum. The electric field strength in the cavity is zero at either end, and is maximum at the surface of the dielectric which faces the viewing hole. The position of the viewing hole is the area of almost zero circumferential electric wall current. The back side of the dielectric window is exposed to an electric field of only one-fifth of its maximum value on the other side of the disc, so that no coatings on this side of the window are required.

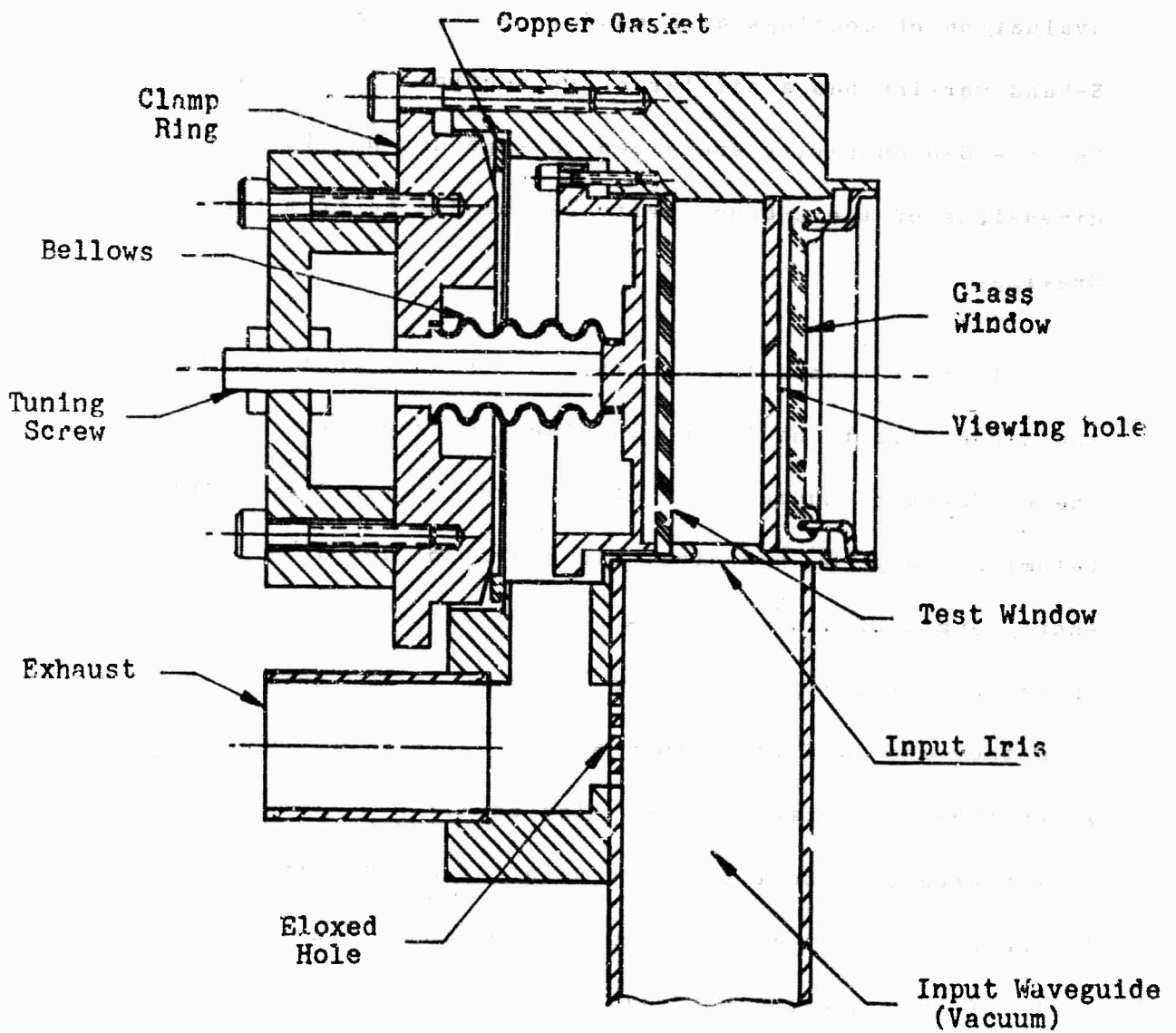


Fig. 12  
 CROSS SECTION VIEW OF THE DEMOUNTABLE  
 TE<sub>011</sub> CIRCULAR MODIFIED MULTIPACTOR TEST  
 CAVITY

The dielectric sample is simply clamped in place. The plate behind the dielectric can be distorted by the tuning screw to tune the cavity. The clamp ring behind that plate forms the vacuum closure and compresses a copper gasket. It is quite easy to replace the dielectric sample. The glass viewing window closes the vacuum at the viewing port, and a conventional waveguide window makes up the vacuum wall in the waveguide.

The cavity is resonant in the  $TE_{011}$ -mode, so that the electric field lines in the cavity are concentric circles. There is zero field on the axis and zero field on the cylindrical wall of the cavity. Hence, there is no electric field normal to any metal surface, and no seal-edge arcing can ever take place in such a cavity. No metal-dielectric seals are required so that the cavity is entirely demountable. The region of the maximum electric field is on a circumference roughly midway between the axis and the cavity wall.

The electric field distribution inside the cavity is determined by the mode. Measurements of the cavity can give the loaded  $Q$  and the external  $Q$ . With these quantities all known, the maximum electric field tangential to the window can be calculated as a function of the power dissipated in the cavity.

which also can be measured. The pertinent mathematical expressions for the maximum electric field in the cavity, the input power and the cavity Q have been derived previously and are summarized in Appendix I. Using these expressions, the field strength at which multipactor starts can thus be determined.

Figure 14 shows a disassembled S-band cavity. Two of these cavities were used for evaluation of coatings at S-band. Figure 15 shows a disassembled X-band multipactor test cavity.

#### 4.4.2 Multipactor Test Procedure

The multipactor test procedure began with clamping of a coated or an uncoated window into one of the multipactor test cavities. After the cavity was made vacuum tight, the loaded Q and the resonant frequency of the cavity were measured and recorded. After the bakeout, normally performed at about 400°C, the measurement of Q and frequency were repeated and compared to corresponding values before the bakeout. Usually, these measurements were found to be within the experimental error of the cold-test equipment. The multipactor test cavity with the attached vacuum station was then connected to the high-power test facility. The block diagram of the experimental test setup used for evaluation of coatings at X- and S-band is shown in Figure 16.

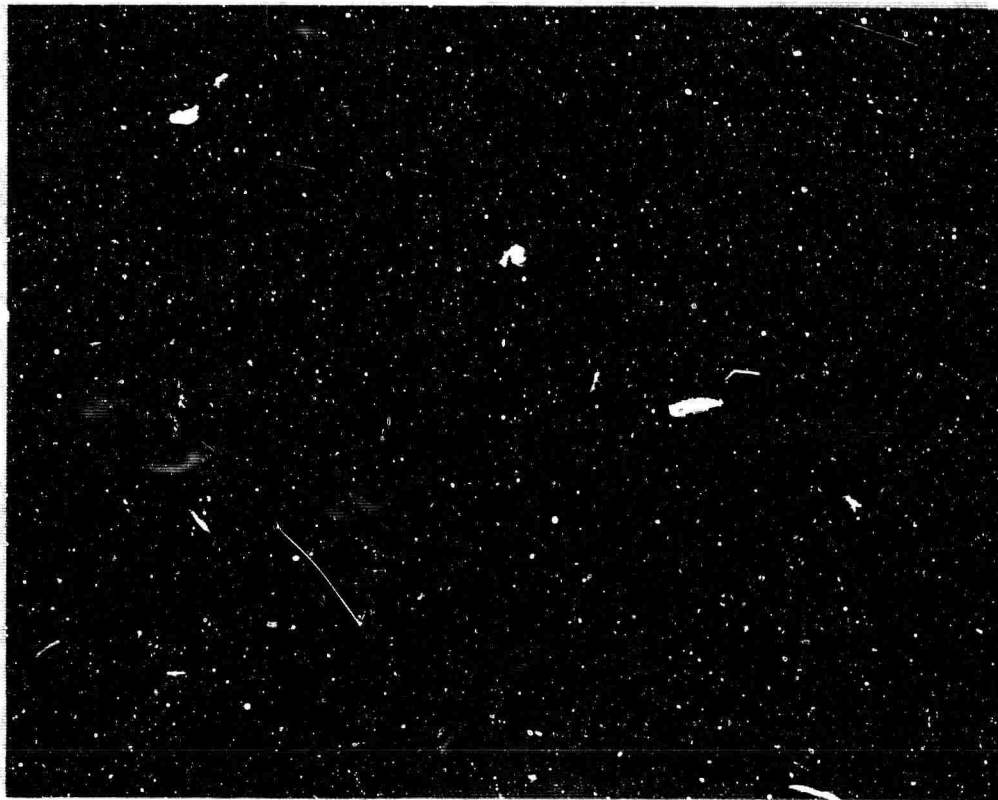


FIGURE 14 PHOTOGRAPH OF A DISASSEMBLED 8-BAND  
MULTIPACTOR TEST CAVITY.



**FIGURE 15 DISASSEMBLED X-BAND MULTI-  
FACTOR TEST STRUCTURE**

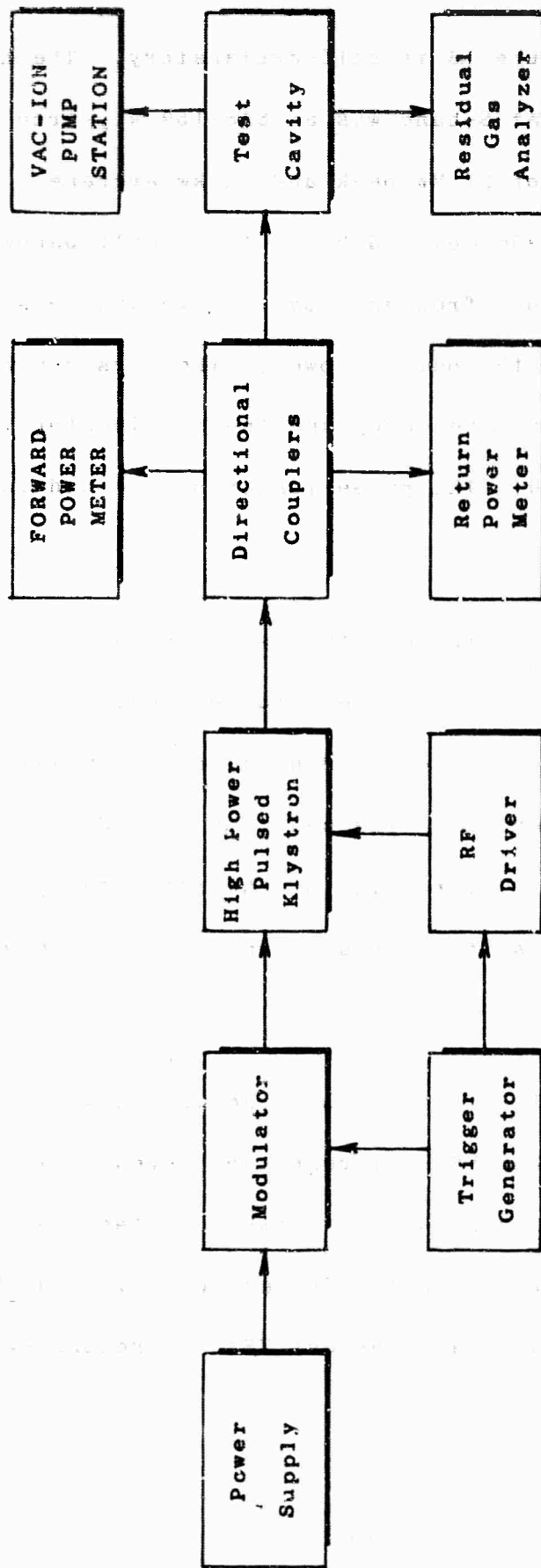


FIGURE 16 BLOCK DIAGRAM OF THE WINDOW TEST FACILITY

The diagram of Figure 16 is self-explanatory. The high-power driver tube used at S-band was an SAS-159 klystron with a nominal power output of 21 MW peak and 20 kw average. It is a fixed frequency tube (2856 Mc) and has only a small bandwidth, but variation of the input frequency over  $\pm 6$  Mc was possible with a moderate reduction of the output power. The klystron was usually operated at fixed frequency and the multipactor test cavity tuned as required. The pulse length of the modulator was fixed at 2.5  $\mu$ sec.

The incident power to the cavity was measured using a calibrated cross-guide coupler. The cold-test calibration of the coupler (50.46 db) was checked by a precision water load at 2856 Mc. The returned power was measured by a coupler-attenuator combination. The reading of the reflected power meter was adjusted against the incident meter using the attenuator and a short in the line.

During experimental evaluation of windows, it was observed that the best value of hot VSWR at resonance (even in the absence of multipactor) was always higher than its cold-test value obtained before or after the test. For example, in a  $TE_{111}^0$ -mode cavity test at X-band, a cold-test VSWR at resonance was

measured to be 1.5 to 1. During the high-power run, the measured VSWR in the input line was always 1.9 to 1. In this test, described in Section 4.5.4.2, no multipactor was observed in the cavity during the whole experiment. Similar observations were made at S-band, where in one particular test with a  $TE_{111}^0$ -mode cavity no multipactor discharge was observed (Section 4.5.5). In this experiment, the hot VSWR at resonance was found to be always 2.1 to 1 against its cold test value of 1.2 to 1.

The reason for the discrepancy in the two values of VSWR is due to the difference in the frequency spectrum between the high-power and cold-test rf sources. In the cold-test setup, a chopped CW signal is used to measure VSWR at resonance. Essentially all of the incident energy is at one frequency. In the high-power setups, on the other hand, an appreciable amount of incident rf energy can be of a slightly different frequency than the resonant frequency of the test cavity. The band spread is produced by the phase modulation in the high-power klystron. In such a case, a part of the incident rf energy is reflected by the relatively narrow bandwidth of the test cavity, producing an incorrect value of VSWR at resonance. An investigation of the rf output pulses of S- and X-band stations has shown that the frequency spread of the S-band station was greater than that of

the X-band station. This fact explains the larger difference between the two values of VSWR measured at S-band.

In all the data given in this report, the value of VSWR calculated from directional coupler readings was used to obtain the maximum electric field in the two test cavities (Eq. I10, Appendix I and Eq. K8, Appendix K). Since the value of  $E_{\max}$  in the cavity is inversely proportional to one plus the value of VSWR at resonance (for an undercoupled cavity), the true value of  $E_{\max}$  would have been higher than calculated. For example, if in the S-band test just described, the hot VSWR was not 2.1 to 1 but closer to 1.2 to 1 (i.e., its cold-test value), then the maximum value of the electric field would have been about 1.5 times higher.

The difference in the two different values of VSWR was observed very early in the program, and a specially-designed, high-power slotted line was incorporated in the S-band input line. The VSWR readings obtained from the slotted line were found to be smaller than the values obtained by using directional couplers,<sup>28</sup> but not accurate enough to make calibration possible. The slotted line was later removed from the circuit in order to pressurize the wavoguide.

The X-band source was an SAX-101 klystron, which has a nominal power output of 1.25 MW peak and 6 kw average. It has a wide electronic bandwidth and was used with a 5  $\mu$ sec pulse length. Frequency adjustments on the X-band multipactor cavity were made again by flexing the back wall of the cavity. The test equipment was very similar to that described for the S-band setup.

Multipactor was detected by viewing the ceramic window in the cavity through the viewing port. A multipactor discharge produces a glow on the surface of the dielectric, which is due to fluorescence under electron bombardment, and can be easily detected. Unfortunately, the initiation point at which the glow is first visible may differ between readings depending on the degree of dark adaptation of the eye. In each test of a coating, the power to the cavity was raised in small steps of 1/2 to 2 db, depending on the incident power. At higher levels of power, the steps were finer than at lower levels. The increase in power was occasionally interrupted to check the coating for conditioning. All visual observations and meter readings made during the run were recorded. A failure of the window normally terminated the experiment.

#### 4.4.3 Description of High-Power Test Equipment and Procedure

The multipactor test cavities described in Section 4.4.1 were particularly suitable for evaluating the properties of a coating surface for multipactor and arcing without the added problem of arcs originating on the metal walls and at metal-to-ceramic seal areas. However, since one purpose of the program was to evaluate the seal-area-arc problem, it was desirable to test windows in a geometry and mode which was a good simulation of actual operation as part of the vacuum enclosure of a high-power tube.

At the outset of the program, it was intended to test X-band windows in resonant cavities operating in the appropriate waveguide modes ( $TE_{11}$  in circular guide;  $TE_{10}$  in rectangular guide) with the dielectric positioned so that one face was at the plane of maximum electric field. These windows were to be brazed in place, and the cavities evacuated.

At S-Band it was intended to use a ring resonator so as to subject the window to a simple traveling wave. In this case two window sections, very much like window sections for high-power tubes, are brazed together. The space between them is evacuated. Such assemblies are called "windowtrons" and are essentially

reflectionless at the frequency of interest. The windowtron is inserted in the resonant ring, which is usually pressurized.

At the outset of the program, design work on the S-band ring was initiated. In view of the required high-power handling capability of the primary directional coupler, a rather detailed theoretical analysis of directional couplers was performed. A new technique which involves the staggering of binomial arrays has been developed for this purpose.<sup>29</sup> It was found that a nine-hole directional coupler consisting of seven staggered three-hole binomial couplers would give the desired coupling coefficient and directivity.

In order to check the theoretical values of the coupling coefficient equation,<sup>30</sup> four two-hole and one six-hole couplers were designed and built. The experimental data obtained with these couplers, i.e., measured values of the coupling coefficient and the required spacing of holes for maximum directivity, has been previously reported.<sup>31</sup> The design of the rest of the ring, including the monitor coupler and the H-plane bends with viewing holes, was straightforward.

The design of the windowtron followed a procedure developed at Sperry.<sup>32</sup> It consisted of two identical transverse dielectric

elements, spaced apart by some specified distance and mounted normal to the axis of a uniform, round waveguide. Two identical, negative-susceptance obstacles (rectangular-to-circular waveguide transitions) were mounted at equal distances at either side of the dielectric elements. The structure was symmetric with respect to its midplane.

The most important electric property of this windowtron was that the voltage reflection coefficient and its first derivative were zero at the design frequency. The "maximum flatness" response was a desirable feature and gave a reasonable working bandwidth. The experimental data for the final design of the windowtron was taken using a procedure developed by D. E. Churchill for this particular application.<sup>33</sup>

After the ring resonator design had been completed, we became aware of an S-band ring rated at 100 megawatts peak and 1 megawatt average which was government property and located at Lincoln Laboratories. Arrangements were made to deliver this ring to Sperry for use in this program.

When the ring was assembled, many leaks at the flanges, at monitor couplers, at bolted-on sections, etc., were found. Quite a bit of work went into making the ring pressure tight.

Many solder joints in the monitor couplers were broken, and it was necessary to repair these joints and recalibrate each coupler.

The ring was first operated with pressurized air, and it arced at about 15 MW peak circulating power. The ring was then pressurized to 25 lbs. gauge with Freon C 318. This gas is reputed to be substantially better in breakdown strength than sulfur hexafluoride.<sup>34</sup> Once again arcing occurred, this time at about 19 MW. Since the ring was so massive in construction that it was impossible to determine where the arcs were by listening, the ring was allowed to arc for some time in order to leave visible tracks.

It was found that arcing was occurring at the face of each moving short, across small dielectric spacers mounted at the four corners.\* This was suspected since the power-handling ability of the ring did not improve much when a better gas, Freon, was used. At this point, it was concluded that further work on the ring was undesirable, and it was decided to test windows in cavities at S-band as well as at X-band.

---

\*The ring incorporated a pair of short slot hybrid junctions back to back which could be moved individually or together. They were used to change the length of the ring and to introduce a reflection of arbitrary amplitude and phase.

A cross-sectional view of the demountable  $TE_{11}^0$ -mode X-band cavity is shown in Figure 17. Design drawings for the S-band test cavity are given in Appendix J. Electrically, the X-band cavity is essentially a scaled-down version of the S-band cavity, but being small in size (test window dimensions: diameter - 1.250 inches; thickness - .050 inches), it has no frequency tuning provision. In both cavity designs, the test window is brazed into its frame, and the metal-dielectric seal must be vacuum tight. The frame is bolted to the viewing section of the test cavity using a vacuum-tight crush seal. An annealed copper gasket provides the vacuum seal and assures good electrical conductivity between the window frame and the cavity wall with the viewing hole. The other side of the window frame is pressed against the cavity wall containing the input waveguide. Again, a soft copper gasket provides a good electrical path between the two parts. The viewing hole in both cavity designs is composed of many small apertures, manufactured by the spark-erosion process, filling an area 1-3/16 inches in diameter. This means that in the X-band design, the viewing hole is almost as large as the test window, so that photographs of the whole window could be taken.

The internal design of the cavities was essentially the

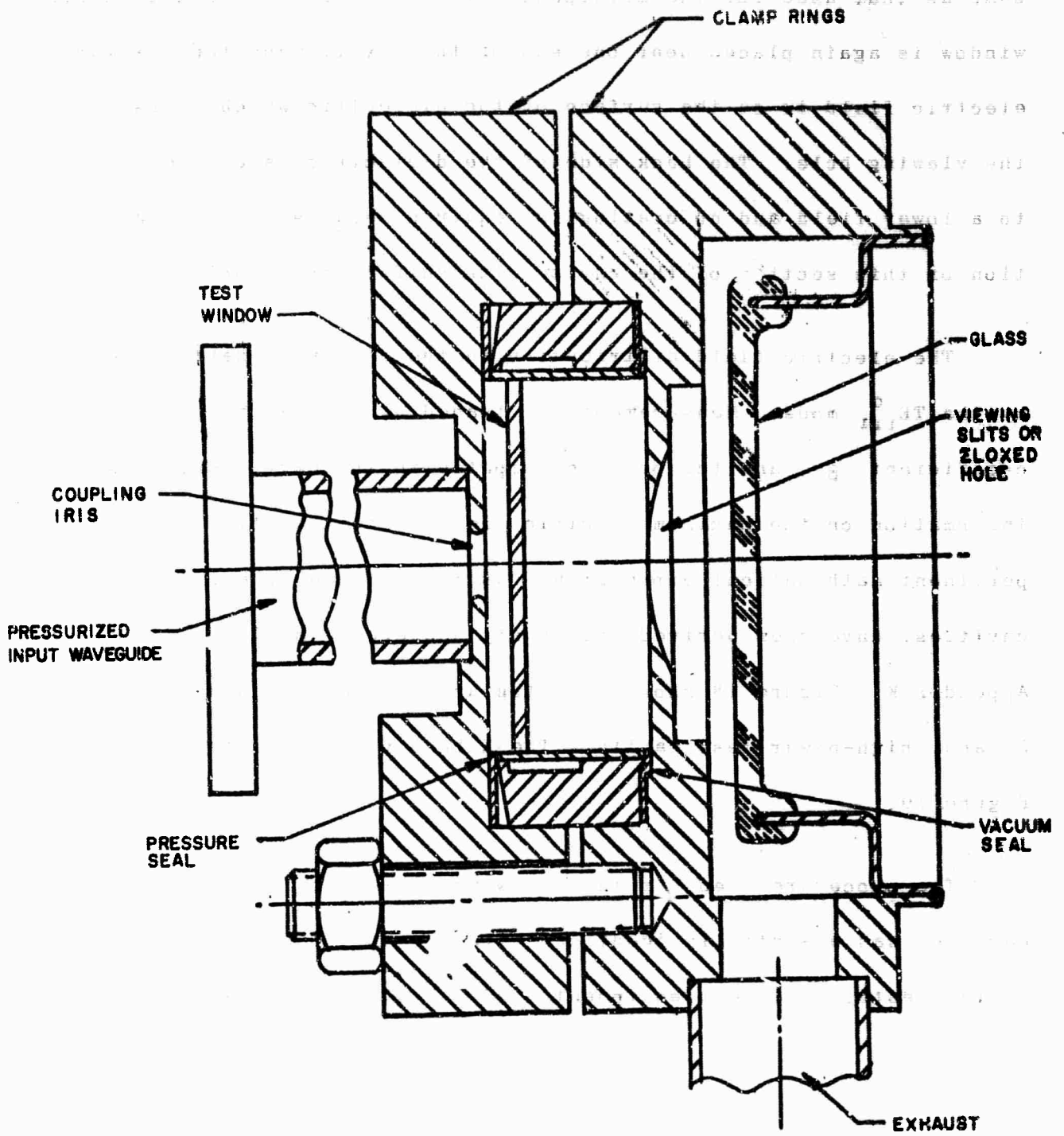


FIGURE-17 CROSS SECTION VIEW OF X-BAND DEMOUNTABLE  
 $TE_{111}$  CIRCULAR MODE TEST CAVITY

same as that used for the multipactor test cavities. The dielectric window is again placed near one end of the cavity, and the maximum electric field is on the surface of the dielectric which faces the viewing hole. The back side of the dielectric is exposed to a lower field and no coating is required because of pressurization of this section of the cavity with sulfur hexafluoride.

The electric field distribution in the cavity is determined by the  $TE_{111}^0$ -mode. Measurements of loaded Q, the cavity coupling coefficient  $\beta$ , and the power dissipated in the cavity provides information on the maximum electric field in the cavity. The pertinent mathematical expressions, as in the case of multipactor cavities, have been derived previously and are summarized in Appendix K. Figure 18 shows a photograph of the disassembled S-band, high-power test cavity. The X-band version is shown in Figure 19.

The procedure used for testing windows in the  $TE_{111}^0$ -mode cavities was essentially identical with the one used for multipactor tests. The test equipment used was also identical.



**FIGURE 18 DISASSEMBLED HIGH-POWER,  
S-BAND TEST CAVITY**

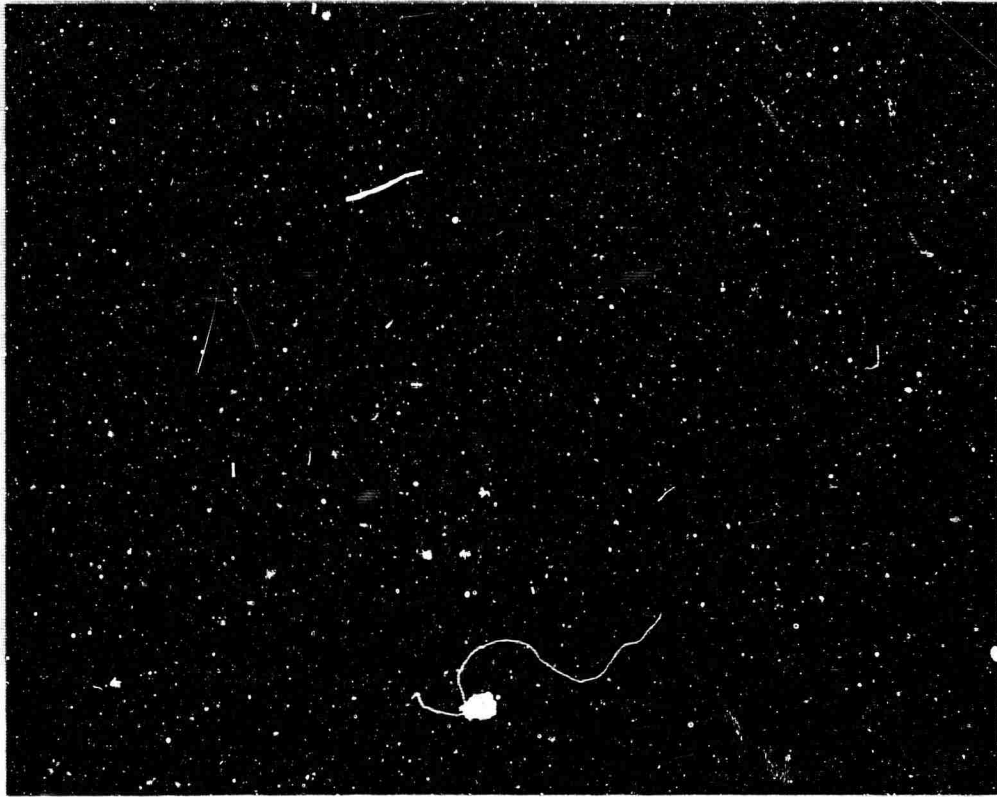


FIGURE 19 X-BAND, HIGH-POWER TEST CAVITY

## 4.5 EXPERIMENTAL RESULTS

### 4.5.1 Multipactor Test Data Obtained at S-Band

#### 4.5.1.1 Results Obtained with Uncoated Windows - Table I

gives a summary of all the tests performed at S-band with uncoated windows. In the first two experiments, a ground alumina window was tested for multipactor. In both cases multipactor increased with input power. The multipactor glow in the cavity was roughly proportional to the electric field of the  $E_{01}^0$ -mode, with the maximum glow occurring at the point of maximum electric field - about half-way between the center of the disc and the cavity wall. The color of the observed glow was blue.

In the first experiment, outgassing of the cavity was quite strong (because of inadequate bakeout). As the pressure rose, the color of the glow changed to light purple, and the glow extended over the whole volume of the cavity. This was, of course, an rf glow discharge. In all other experiments (except Experiment #1, Table II, p. 91), no such outgassing was observed.

In the second experiment, arcing at the window surface was observed at 56 kv/cm, corresponding to an equivalent

TABLE I

## SUMMARY OF MULTIPACTOR RESULTS OBTAINED AT S-BAND WITH UNCOATED WINDOWS

EX-PERIMENT NO.	WINDOW MATERIAL	SURFACE FINISH	INITIAL MULTI-PACTOR AT	MULTIPACTOR ACTIVITY WITH INCREASED POWER	MAXIMUM FIELD AND POWER TRANSMITTED AT	WINDOW FLASH-ARCING AT	APPEARANCE OF WINDOW AFTER TEST
1	AL-995 Alumina	Ground	3 kv/cm	Multipactor Increasing. Cavity Very Gassy.	26 kv/cm (25 MW)	--	Undamaged
2	AL-995 Alumina	Ground	2 kv/cm	Multipactor Increasing with Power.	56 kv/cm (112 MW)	56 kv/cm (112 MW)	Damage Due to Arcing and X-rays
3	AL-995 Alumina	Lapped	No Experiment	Performed with This Window. During Bakeout.			Surface Contaminated
4	AL-995 Alumina	Lapped	3 kv/cm	Multipactor Increasing with Power.	50 kv/cm (90 MW)	50 kv/cm (90 MW)	Arc Tracks Near Input Iris, X-Ray Damage
5	AL-995 Alumina	Lapped	2 kv/cm	Multipactor Increasing with Power.	47 kv/cm (78 MW)	47 kv/cm (78 MW)	Arc Tracks Near Input Iris, X-Ray Damage
6	Quartz	Lapped	2 kv/cm	Multipactor Increasing with Power.	76 kv/cm (210 MW)	--	No Visible Damage

transmitted power of 112 MW\* and the experiment was terminated. The change in VSWR with the input power for this experiment is shown in Figure A1 of Appendix A. Appendix I gives a relationship between the maximum electric field and the input power as a function of the multipactor cavity parameters. In this appendix, a numerical calculation of the maximum electric field reached during this test is given as a sample calculation.

When the cavity was disassembled after the experiment, it was observed that the ceramic had become yellowed due to X-ray bombardment. The yellowing across the surface of the ceramic and in depth of penetration was proportional to the observed multipactor glow intensity, which in turn was a function of the mode pattern of the  $TE_{01}^0$ -mode.

In the next three experiments, lapped, uncoated AL-995 alumina windows were evaluated for multipactor. The purpose of

---

\*The equivalent transmitted power mentioned in discussion of these and other S-band multipactor test cavity experiments (and in Tables I and II) corresponds to the peak power that would be transmitted in the  $TE_{11}$ -mode through a circular window of 3.80 inches in diameter (the diagonal of WR-340 waveguide, a logical choice for high power at S-band) if the maximum electric field at the surface of that window were equal to the electric field reached at the surface of the dielectric in the multipactor test cavity. Appendix L gives details on the calculation of the equivalent power.

These experiments was to determine whether or not a lapped surface had a greater resistance to arcing than a ground surface. The general behavior of the lapped window was the same as that of a ground window. Arcing near the input iris prevented the establishment of the arcing threshold of a lapped window. X-ray damage to the ceramic was clearly visible on the lapped surfaces.

In the last experiment, a lapped quartz surface was studied for multipactor. Severe detuning and loading of the cavity was observed. The glow was pale blue. At the electric field of 76 kv/cm, an X-ray intensity of 250 mr/hour was measured near the viewing hole, but the window showed no damage or discoloration.

4.5.1.2 Results Obtained with Coated Windows - Table II gives a summary of multipactor results obtained at S-band with coated windows. In the first three experiments, coatings were sputtered from a titanium metal cathode to various resistivities.\* Note that in Experiment #3 alone four different resistivities were used. The suppression of multipactor in these tests was not complete, although some improvement in the initiation level

---

\* All the resistivity values given in this Section are as measured in the argon atmosphere at the completion of sputtering unless specifically stated to the contrary.

TABLE II

SUMMARY OF MULTIPACTOR RESULTS OBTAINED AT S-BAND WITH COATED WINDOWS. SPUTTERING ATMOSPHERE WAS ARGON UNLESS STATED DIFFERENTLY. THE SUBSTRATE WAS GROUND ALUMINA WINDOW.

EX-PERIMENT NO.	SPUTTERED MATERIAL	COATING DENSITY OF COATING	RESISTIVITY	INITIAL MULTI-PACTOR AT	MULTIPACTOR ACTIVITY WITH INCREASED POWER	MAXIMUM FIELD AND POWER TRANSMITTED AT	APPEARANCE OF WINDOW FLASHING AFTER TEST
1	Titanium	8.4 $\mu\text{gms/cm}^2$	1.9 megohms/square		Cavity was gassy. Observation of multipactor was hindered by the presence of a gas discharge.		
2	Titanium	6.5 $\mu\text{gms/cm}^2$	.3 megohms/square	16 kv/cm (9 MW)	Slight Glow $\rightarrow$ Increased $\rightarrow$ Decreased $\rightarrow$ No Glow in the Region of Max. E - Field	34 kv/cm (41.5 MW)	No Visual Damage
3	Titanium	7.2 $\mu\text{gms/cm}^2$	.02 megohms/square	17 kv/cm (10 MW)	Slight Glow $\rightarrow$ Increased $\rightarrow$ Decreased $\rightarrow$ No Glow in the Region of Max. E - Field	38 kv/cm (52 MW)	Window Cracked
4	Vanadium	11.0 $\mu\text{gms/cm}^2$	.03 megohms/square	52 kv/cm (96 MW)	No Glow Until "Jumping Arcs" Then Glow Until Final Arcing	72 kv/cm (186 MW)	Damaged Coating (186 MW) "Jumping Arcs" Small Crack

TABLE II - CONTINUED

EX- PERI- MENT NO	SPUTTERED MATERIAL	MASS DENSITY OF COATING	COATING RESIS- TIVITY	INITIAL MULTI- PACTOR AT	MULTIPLIER ACTIVITY WITH INCREASED POWER	MAXIMUM FIELD AND POWER		APPEAR- ANCE OF WINDOW AFTER TEST
						TRANS- MITTED	FLU- ENCING	
5	Vanadium	7.3 μgms/cm <sup>2</sup>	.6 megohms/ square	44 kv/cm (70 MW)	No Glow Until "Jumping Arc Glow Until Final Arcing	57 kv/cm (116 MW)	54 kv/cm (104 MW)	57 Ceramic Damaged (116 Slightly MW) By Arcs
6	Chromium	8.0 5.4 μgms/cm <sup>2</sup>	-- --	The loaded Q of the cavity after bakeout was so low that it was impossible to measure.				
7	Chromium	1.7 1.4 μgms/cm <sup>2</sup>	500 .25 megohms/ square	34 kv/cm (41 MW)	Mod. rate Glow Persis- ted Until End of Test	46 kv/cm (75 MW)	---	-- No Visual Damage
8	Tantalum	7.3 4.6 μgms/cm <sup>2</sup>	-- --	56 kv/cm (112 MW)	No Multipactor	56 kv/cm (112 MW)	--	56 Arc kv/cm Damage (112 MW)
9	Carbor.	5.4 4.0 μgms/cm <sup>2</sup>	-- >30,000 megohms/ square	46 kv/cm (74 MW)	No Multipactor	46 kv/cm (74 MW)	--	46 Arc kv/cm Damage (74 MW)
10	Titanium In Nitrogen	9.3 4.8 μgms/cm <sup>2</sup>	>30,000 >30,000 megohms/ square	4 kv/cm (1 MW)	Light Glow → No Glow → Light Glow	59 kv/cm (126 MW)	59 kv/cm (126 MW)	-- No Visual Damage (126 MW)

1921

TABLE II - CONTINUED

EX- PERI- MENT NO.	SPUTTERED MATERIAL	MASS DENSITY OF COATING	RESIS- TIVITY	COATING	INITIAL MULTI- FACTOR	MULTIPLIER ACTIVITY WITH INCREASED POWER	MAXIMUM FIELD AND POWER TRANS- MITTED	WINDOW FLASHING ARCING AFTER TEST	APPEAR- ANCE OF WINDOW	
11	Vanadium In Nitrogen	1.4 .5 μgms/cm <sup>2</sup>	1.0 2,000 megohms/ square		16 kv/cm (9 MW)	Light Glow → No Glow Until Flashing	47 kv/cm (79 MW)	42 kv/cm (63 MW)	47 kv/cm (79 MW)	No Visual Damage
12	Tantalum In Nitrogen	8.8 2.0 μgms/cm <sup>2</sup>	>30,000 >30,000 megohms/ square		Cavity developed a leak during bakeout at 400°C. Experi- ment discontinued.					
13	Titanium Nitride	3.6 2.4 μgms/cm <sup>2</sup>	.35 2,000 megohms/ square		14 kv/cm (7 MW)	Moderate Glow → Increasing → De- creasing. Very Faint Glow at Highest Levels of RF Power	78 kv/cm (215 MW)	71 kv/cm (179 MW)	78 kv/cm (215 MW)	Small Crack
14	Tantalum Carbide	8.0 3.6 μgms/cm <sup>2</sup>	>30,000 >30,000 megohms/ square		5 kv/cm (1 MW)	Light Glow → Moderate Glow → No Glow	46 kv/cm (85 MW)	--	49 kv/cm (85 MW)	Small Crack
15	Titanium Carbide	6.3 3.9 μgms/cm <sup>2</sup>	40 600 megohms/ square		18 kv/cm (12 MW)	Moderate Glow → Increasing → Almost No Glow Except For Points of Low Field	69 kv/cm (281 MW)	79 kv/cm (224 MW)	89 kv/cm (281 MW)	Small Crack

TABLE II - CONTINUED

EX- PERI- MENT NO.	SPUTTERED MATERIAL	DENSITY OF COATING	WASL DENSITY OF COATING	RESIS- TIVITY	INITIAL MULTI- FACTOR AT	MULTIPLIER ACTIVITY WITH INCREASED POWER	MAXIMUM FIELD AND POWER		APPEAR- ANCE OF WINDOW	
							TRANS- MITTED	FLASHING AT		
16	Vanadium Carbide	2.2	3,000		26	Moderate Glow →	69	59	69	Arcing
		1.4	490		kv/cm	Very Light Glow	kv/cm (171 MW)	kv/cm (125 MW)	kv/cm (171 At Iris Near Iris MW)	69 Arcing Tracks
17	Vanadium Carbide	5.6	>30,000		12	Light Glow →	58	58	58	Thicker
		4.8	200		kv/cm	Increasing →	kv/cm	kv/cm	kv/cm	Coating
		4.1	200		(5 MW)	Flashing and Arcing	(118 MW)	(118 MW)	(118 MW)	Damaged
		2.4	52							(MW)
			μgms/cm <sup>2</sup>	megohms/ square						
18	Vanadium Carbide	8.8	.1		10	Light Glow → Flashing	80	18	61	Damage
		5.3	.64		kv/cm	Across Coating Over-	kv/cm	kv/cm	kv/cm	To
		μgms/cm <sup>2</sup>	megohms/ square	(4 MW)	lap → No Multi- plier Except For Point of Low Field	(229 MW)	(12 MW)	(133 MW)	(133 MW)	Ceramic and Coating
19	Vanadium Carbide Fired In Wet Hydrogen at 1100°C	8.4	.06		4	Moderate Glow In-	53	--	53	No
		6.0	.02		kv/cm	creasing with Power	kv/cm	kv/cm	kv/cm	Damage
					(1 MW)	→ Some Reduction at Highest Power Level	(101 MW)		(101 MW)	Except to Arcing Tracks Near the Iris

1041

TABLE II - CONTINUED

EX- PERI- MENT NO.	SPUTTERED MATERIAL	MASS DENSITY OF COATING	COATING RESIS- TIVITY	INITIAL MULTI- PACTOR AT	MULTIPACTOR ACTIVITY WITH INCREASED POWER	MAXIMUM FIELD AND POWER TRANS- MITTED	WINDOW FLASHING AT	WINDOW ARCING AT	APPEAR- ANCE OF WINDOW AFTER TEST
20	Vanadium Carbide Fired in Wet Hydro- gen at 900°C	9.2 2.8	.003 1,500 μgms/cm <sup>2</sup> square	26 kv/cm (24 MW)	Light Glow → In- creasing → Decreas- ing → No Glow	66 kv/cm (155 MW)	40 kv/cm (58 MW)	66 kv/cm (155 MW)	Damage To Coating and Arcing Tracks Near The Iris
21	Vanadium Carbide Fired In Dry Hydrogen at 1100°C	--	6,000 After H <sub>2</sub> Firing	7 kv/cm (2 MW)	Light → Moderate → Very Light	56 kv/cm (111 MW)	40 kv/cm (58 MW)	56 kv/cm (111 MW)	Small Crack

of the multipactor discharge has been obtained. At lower levels of electric field, the intensity of multipactor glow was proportional to the electric field strength of the  $TE_{01}^c$ -mode. At higher levels of rf power, the intensity of the glow at the point of maximum electric field began to diminish and continued to do so until at the highest levels of rf there was no glow at the point of  $E_{max}$ . The ceramic window was still glowing at lower values of electric field (at both sides of the area of maximum field) forming two concentric rings.\* In the third experiment a sustained surface arc cracked the ceramic. Figure 20 shows the cracked alumina window. Damage from the sustained arc can be seen.

In the next two experiments, coatings of sputtered vanadium were evaluated for the suppression of multipactor. No multipactor

---

\*Very often, even with a secondary emission reducing coating, the secondary emission ratio is greater than one over some small range of primary electron energy. In this case, a weak multipactor discharge can take place at the window surface. Nevertheless, the reduction of the overall magnitude of the secondary emission ratio of such a window surface is usually very significant. This fact, together with the reduction in the energy range of primary electrons for which the secondary emission ratio exceeds unity, results in a reduction in the total amount of power dissipated at the window. From this point of view, a window coating which permits a multipactor discharge does not necessarily represent a failure. It is a question of degree.

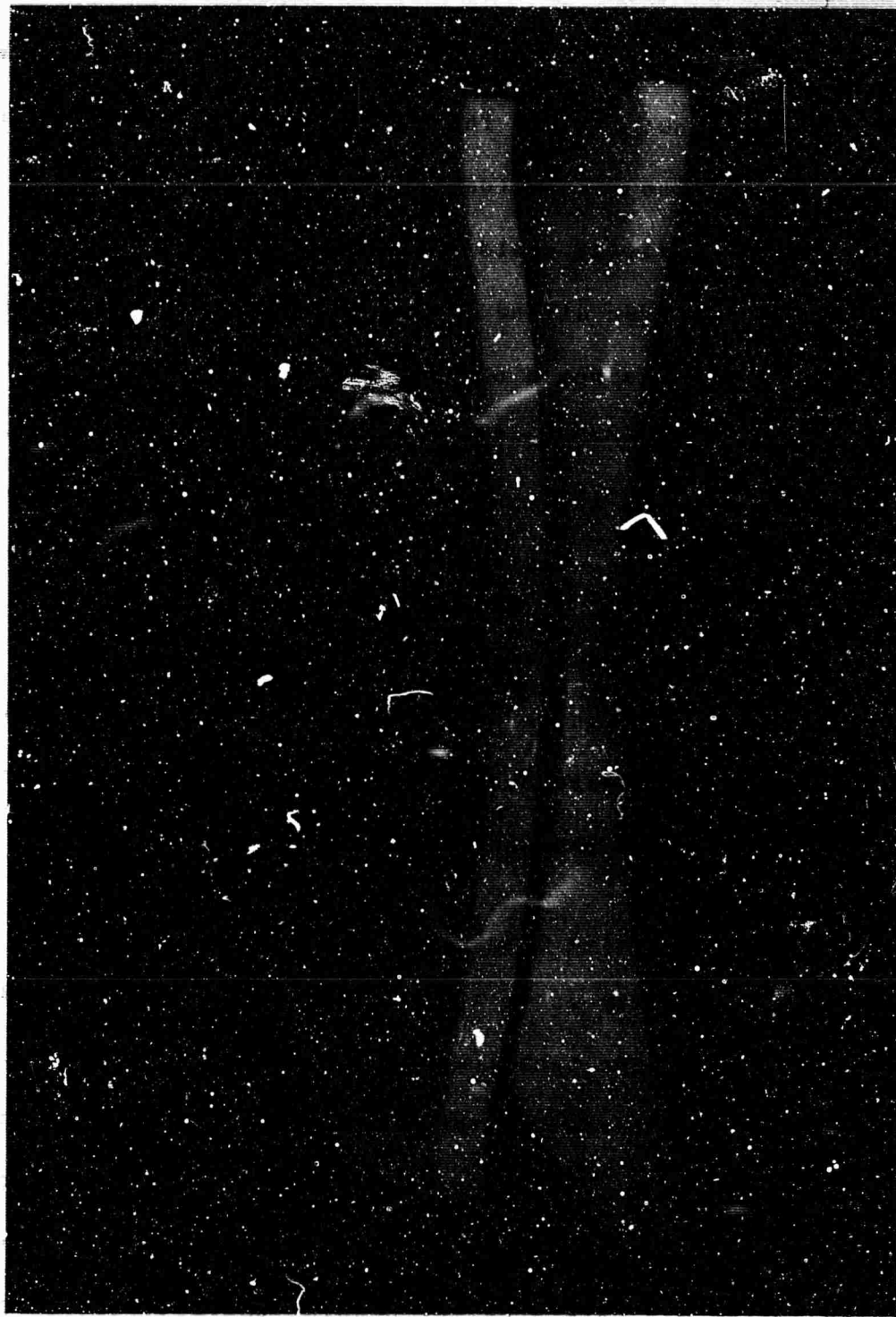


**FIGURE 20 ABC DAMAGE TO THE TITANIUM-COATED  
ALUMINA WINDOW DURING THE HIGH-  
POWER TEST**

was observed until arcing began. First arcing on both windows was observed at about 53 MW. The arcs appeared to move around on the surface of the window (dancing arcs). After a little while the arcing activity would subside and very light multipactor glow would then be seen at the window coating damaged by arcing. These series of events would occur each time the input power level was increased. Figure 21 shows arc damage to the coating after high-power tests in Experiment #4. The heavier of the two coatings appears to have suffered greater damage.

In the next two experiments, coatings sputtered from a chromium cathode in argon were used. The results of Experiment #6 with chromium coating were described in Section 4.3.6; the results of Experiment #7 are summarized in Table II.

Coatings of tantalum and carbon completely suppressed multipactor all the way up to the point of arcing. Figure 22 shows arc damage to the tantalum coated window, whereas Figure 23 shows damage to the carbon coated window. It can be seen that in the vicinity of the arc the carbon coating has been thoroughly removed. A pyrolytically deposited carbon coating (rather than sputtered) which may have a better bonding characteristic has not been tried.

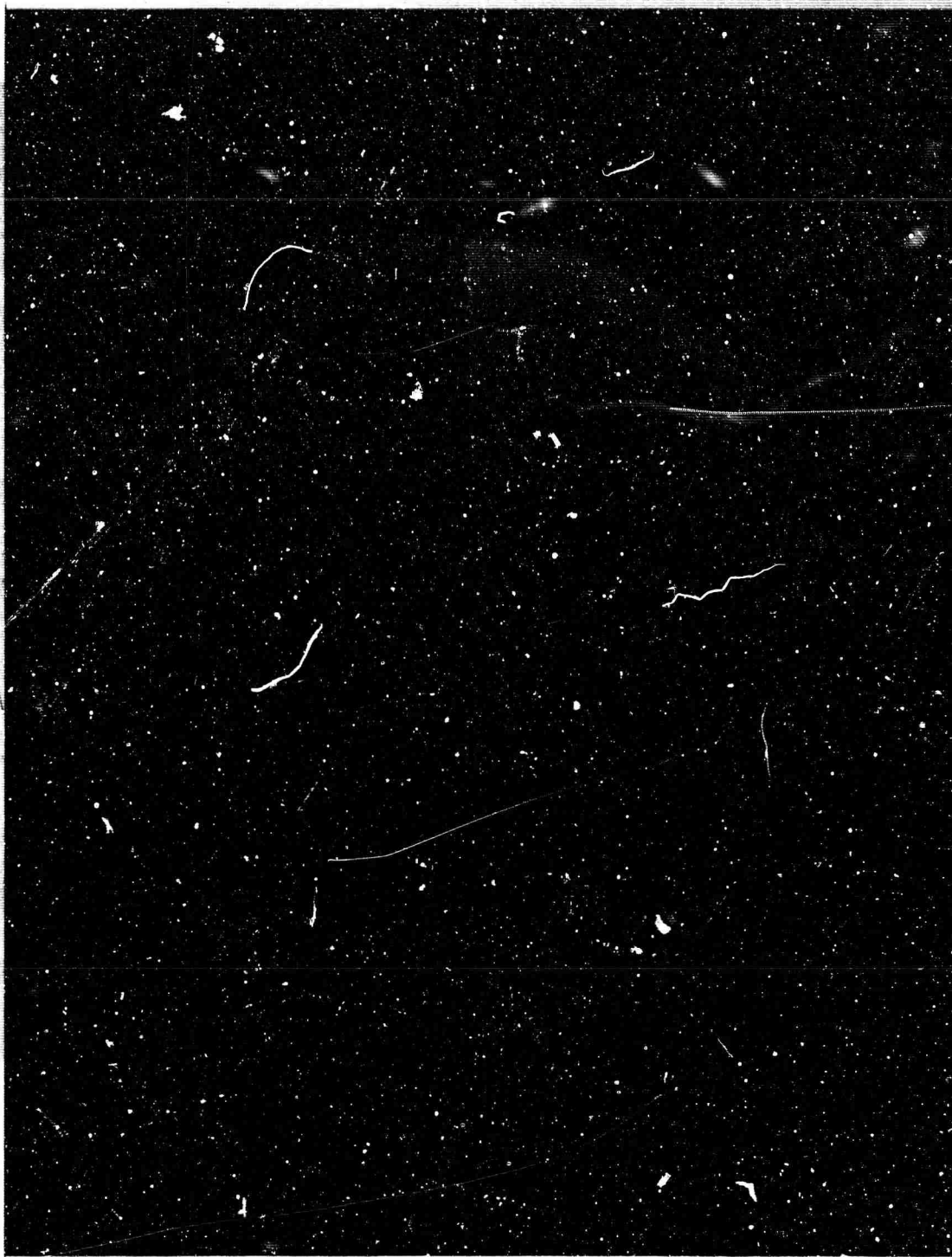


**FIGURE 21 ABC DAMAGE TO THE VANADIUM-  
COATED ALUMINA WINDOW**

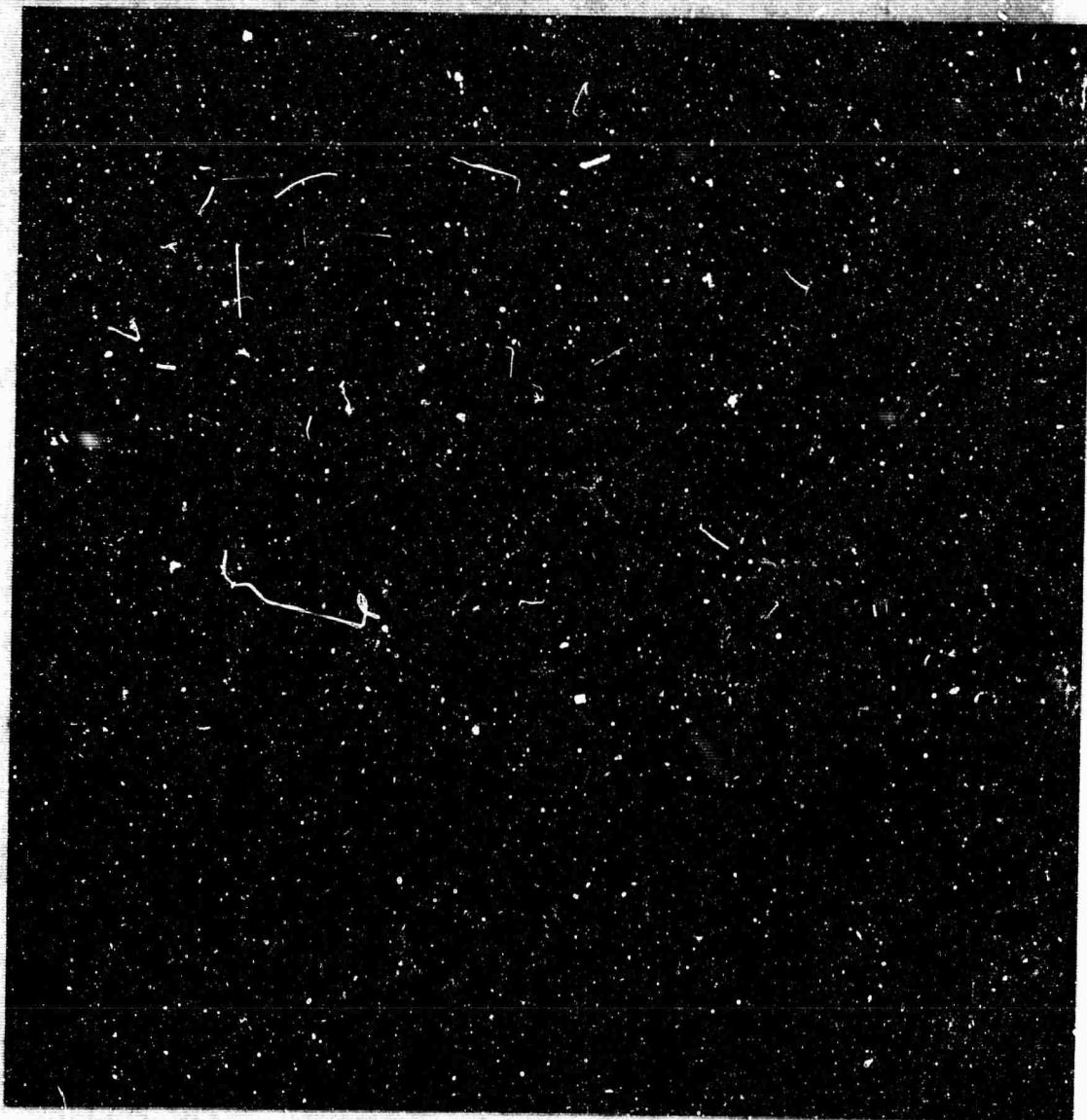
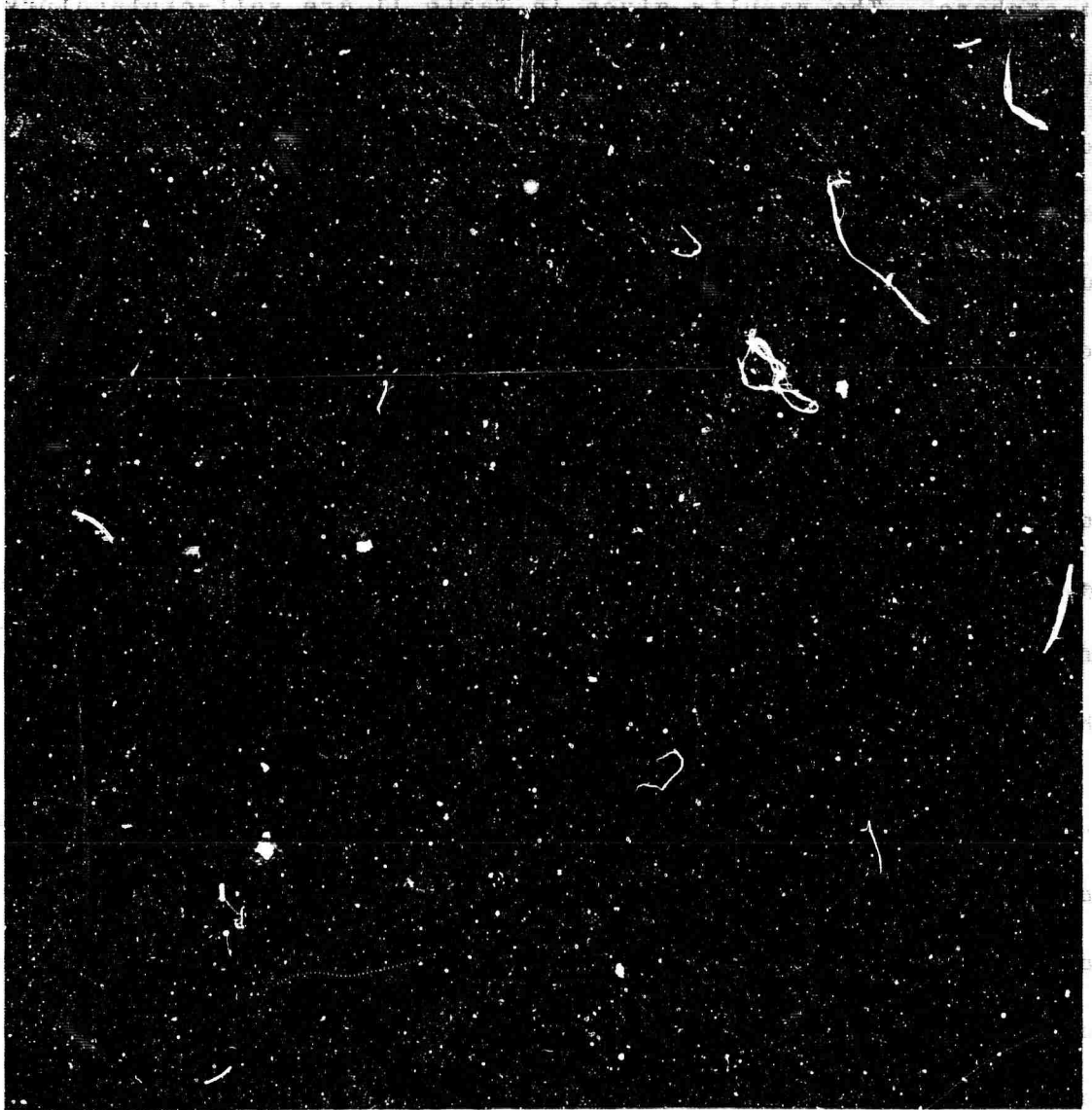


FIGURE 22 ARC DAMAGE TO THE VANADIUM-  
FIGURE 21 ARC DAMAGE TO TANTALUM  
COATED ALUMINA WINDOW  
COATED WINDOW



**FIGURE 23 ARC DAMAGE TO SPUTTERED CARBON COATING**

In the next three experiments, three different metals, titanium, vanadium and tantalum, were sputtered in a nitrogen atmosphere. The results given in Table II are self-explanatory. In the next experiment, titanium nitride in powder form was used to obtain a window coating. Two different coating densities were used on two halves of the ceramic window. Again, the results summarized in Table II under Experiment #13 require no added comment.

In the next two experiments, tantalum and titanium carbide coatings were studied for suppression of multipactor. The results obtained with titanium carbide looked good. Conditioning of the coating, attempted during this test, increased multipactor threshold of the titanium carbide coating from 18 to 34 kv/cm.

In Experiment #16, a vanadium carbide coating was evaluated for the suppression of multipactor. The overall behavior of this coating looked somewhat better than that of the titanium carbide coating, in spite of the fact that the vanadium carbide coating in the end broke down at a lower power level. Since flashing and finally arcing occurred near the input iris of the cavity loaded with the vanadium carbide coated window, it was expected that ultimately a higher-power level on the ceramic surface could

be obtained. Two more experiments with vanadium carbide coatings were then performed. The results of these tests are summarized in Table II.

4.5.1.3 Results Obtained with Vanadium Carbide Coated Windows Fired in Hydrogen - The last three experiments performed at S-band with coated windows were used to study the effects of window brazing techniques on multipactor suppression properties of vanadium carbide coatings. In Experiment #19, a vanadium carbide coating was fired in a wet hydrogen atmosphere at 1100°C. This firing of the window was to simulate brazing of the window into its frame. The results of this test, summarized in Table II, were somewhat disappointing. The multipactor suppression of the fired coating was noticeably poor.

One interesting observation was made in this test. At a power level of 85 MW (49 kv/cm), when the intensity of the discharge began to diminish, it was noticed that the color of the characteristic multipactor glow would change from blue to slightly reddish in appearance. The shape of the glow of either color was always proportional to the electric field intensity of the  $TE_{01}^0$ -mode. The reddish glow was not a gas discharge such as observed previously during the early multipactor experiments in this

program (Section 4.3.1.1). The gas pressure was  $10^{-6}$  torr. A fact which argues against the gas discharge was the reversible nature of the glow - that is, the change of color from blue to reddish and then back from reddish to blue in a rather rapid succession. As the power to the cavity was increased, the color changes of the glow continued until an arc near the input iris terminated the experiment.

In Experiment #20, a vanadium carbide coating was fired at  $900^{\circ}\text{C}$  in a wet hydrogen atmosphere. This firing of the window was to simulate a low-temperature, silver-copper eutectic braze of the window into its assembly. The evaluation of this window showed that the behavior of the fired window was very much like, although not as good as, that of an identically coated but unfired window. The behavior of the  $900^{\circ}\text{C}$  fired window was noticeably better than that of an identically coated window, but fired in  $1100^{\circ}\text{C}$ , also in wet hydrogen. A comparison between the two cases can be made from the summary of results of Table II.

In the final test, a vanadium carbide coating was fired in a dry hydrogen atmosphere at  $1100^{\circ}\text{C}$ . The multipactor suppression property of this window was somewhere between the two previously discussed cases (Experiments #19 and #20 of Table II). The

resistivity of the coating after 1100°C dry hydrogen firing was 12,000 megohms (see Section 4.3.6 for details).

#### 4.3.2 Multipactor Test Data Obtained at X-Band

Table III gives a summary of all multipactor results obtained at X-band. Four uncoated dielectric materials were evaluated. The general behavior of these experiments was the same as the one described for uncoated windows at S-band. In all cases, the intensity of the multipactor glow was proportional to the magnitude of the electric field of the  $TE_{01}^0$ -mode. The color of the multipactor glow was blue - except for quartz where the color was light blue, and for sapphire where the color was purple, but acquired some blue coloring at higher levels of rf power.

The maximum value of the electric field, as in the case of S-band tests, was determined using expressions derived in Appendix I. The equivalent transmitted power is calculated from the electric field as it was done at S-band. In this case the power is computed for a  $TE_{11}^0$ -mode window 1.226 inches in diameter, which is the diagonal of WR-112 waveguide. Appendix L gives the details.

Experiment #3 and #4 utilized materials not tested at S-band, i.e., sapphire and boron nitride. The results with sapphire were not unexpected, since sapphire is a monocrystalline form of

TABLE III

SUMMARY OF ALL MULTIPLICATOR RESULTS OBTAINED AT X-BAND

EX- PERI- MENT NO.	WINDOW MATERIAL	SURFACE FINISH	INITIAL MULTI- PLICATOR AT	MULTIPLICATOR ACTIVITY WITH INCREASED POWER	MAXIMUM FIELD AND POWER TRANSMITTED	WINDOW FLASH- ING AT	WINDOW ARCING AT	APPEAR- ANCE OF WINDOW AFTER TEST
1	AL-995 Alumina	Ground	8.0 kv/cm (.24 MW)	Multipactor Increased with Power	33 kv/cm (4.2 MW)	--	--	Slight X-Ray Damage
2	Quartz	Ground	7.5 kv/cm (.21 MW)	Multipactor Increased with Power	38 kv/cm (5.5 MW)	--	--	No Visual Damage
3	Sapphire	Lapped	3.0 kv/cm (.03 MW)	Multipactor Increased with power	34 kv/cm (4.4 MW)	--	--	No Visual Damage
4	Boron Nitride (Hot- Pressed Type)	Ground	6.0 kv/cm (.14 MW)	Multipactor Increased with Power	38 kv/cm (5.5 MW)	--	--	No Visual Damage
5	Ground AL-995 Alumina. Sputtered with vanadium car- bide in argon to a mass density of 4.3 $\mu\text{gms/cm}^2$ and 510 megohms resistivity.		12 kv/cm (.57 MW)	Very Light $\rightarrow$ Slight Increase $\rightarrow$ Decreasing at $E_{\text{max}}$ $\rightarrow$ Almost No Glow at $E_{\text{max}}$	50 kv/cm (9.6 MW)	--	50 kv/cm (9.6 MW) Arcing near the Input Iris	Evidence of Arcing near the Input Iris

alumina. There was some reason to believe that boron nitride might not support multipactor; other nitrides suppress multipactor, and boron carbide is a moderately effective suppressor of electron emission. Boron nitride has other desirable properties; it can be machined, its loss tangent is low and its thermal conductivity is high. One potential difficulty in using it for windows is that there is no established procedure for metalizing it. However, a high temperature glass which wets boron nitride had been developed at Sperry Electronic Tube Division, and it is likely that this glass could be used for sealing.

The boron nitride sample tested was of the "hot-pressed" rather than pyrolytic variety, and as such was more contaminated with impurities, especially unreacted boric acid and water vapor. There is no reason to suppose that the results obtained in this test would be characteristic of the pyrolytic form.

Subsequent to this test, a representative of the Carbon Products Division, Union Carbide Corporation, informed us that in tests conducted at Stanford University, pyrolytic boron nitride apparently suppressed multipactor.<sup>35</sup> Union Carbide Corporation also has developed a technique for metalizing this material.<sup>35</sup>

Experiment #5 was performed with a vanadium carbide coated

window. The multipactor suppression property of this coating at X-band was similar to the behavior of an identical coating at S-band. Figure 24 shows a photograph of this window. Evidence of arcing to both sides of the input iris can be seen. At S-band, whenever arcing occurred, it was always at the iris; that is, between the two arc stains of Figure 24. A summary of results obtained in this experiment is given in Table III.

#### 4.5.3 Physical and Chemical Changes in Windows Due to Multipactor

##### 4.5.3.1 Conditioning of Window Coatings to Multipactor -

Very early in the program, some conditioning of window coatings to multipactor was observed. Conditioning has been defined as an increase in the threshold level of multipactor observed after multipactor has persisted for some period of time. This was found to be true of nearly all the coatings investigated for multipactor conditioning. A similar observation was made at Eimac, where it was observed that after a period of operation of the window with multipactor glow, the threshold power at which the multipactor glow begins would increase sometimes by a factor of 2 or 3.<sup>36</sup>

In most experiments performed in this program, no concentrated effort on the study of the effect of conditioning of window coatings

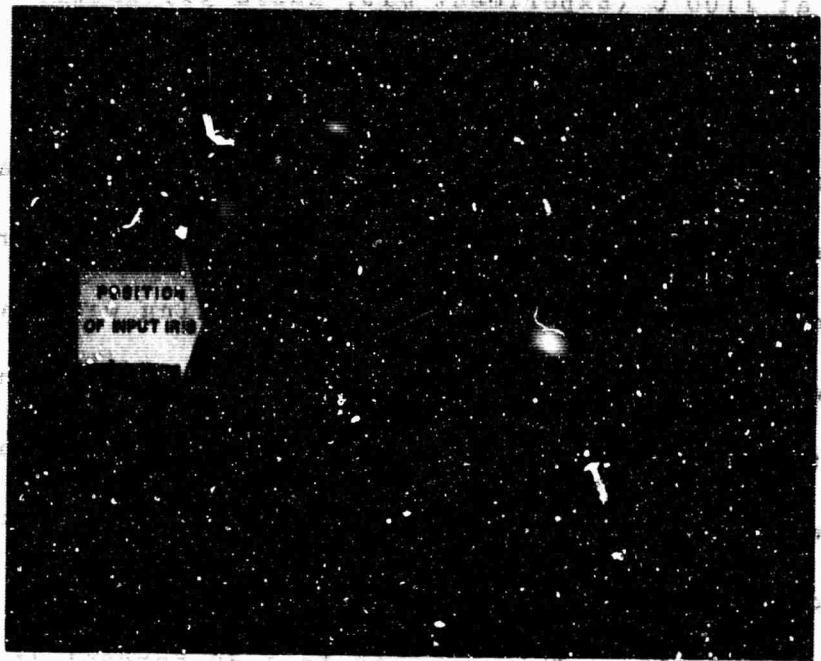


**FIGURE 24 X-BAND, VANADIUM CARBIDE COATED WINDOW AFTER MULTIPACTOR TEST.**

to multipactor was made. In general, the observed conditioning was small. In isolated cases, no conditioning could be observed at all. For example, the vanadium carbide coated window fired in wet hydrogen at 1100°C (Experiment #19, Table II) showed no sign of conditioning.

The procedure used for studying conditioning is characteristically described in the following experiment. In Experiment #18, Table II, conditioning of vanadium carbide coating was investigated. Multipactor was first observed at 9.6 kv/cm. After operation of the window at the maximum electric field of 24.2 kv/cm for a few minutes (at which time some reduction in the multipactor activity could be observed) the multipactor threshold was found to have increased to 13.4 kv/cm. This amounts to a 60 percent increase in the magnitude of the initial electric field. After further operation of the window at a maximum electric field of 46.2 kv/cm (at this power level multipactor glow had completely disappeared from the points of maximum electric field), the multipactor threshold was found to be 20.5 kv/cm. This corresponds approximately to a 130 percent increase in the electric field with respect to its initial value (or a four-fold increase in the level of power).

Conditioning was again tried by operation of the window at approximately 133 MW of equivalent transmitted power corresponding to a maximum electric field of 61 kv/cm for a period of a few minutes. After this run, the multipactor glow was first observed at an electric field of 23.7 kv/cm; this represents only a 15 percent increase in the electric field over its previous value. Conditioning of the coating was tried for the last time after operation of the window surface at an electric field of 79 kv/cm. This time the multipactor threshold was found to be at 22.4 kv/cm.

The results of this study show that major improvement in the multipactor threshold appears to be taking place during the early stages of multipactor activity. For example, it can be seen that no significant conditioning of the vanadium carbide coating could be observed after operation of the window at 46.2 kv/cm electric field level. It is interesting to note that the value of the electric field at which multipactor glow was first observed in Experiment #16, Table II, was 23 kv/cm, or approximately the same threshold field finally reached in Experiment #18.

Only in one case a complete conditioning of the window coating to multipactor was observed. The results of this experiment

are described in Sections 4.5.4.1 and 4.5.5 in greater detail.

In this test, the coating was sputtered vanadium carbide, and conditioning was observed after about one hour of operation of the window at a 48.1 kv/cm electric field level. As pointed out earlier, the time interval used to study conditioning in all other experiments was never greater than a few minutes, and it is possible that better conditioning results could have been obtained if coatings were exposed to multipactor discharge for longer periods of time.

There is no conclusive evidence as to what happens physically during conditioning. During multipactor, the window is certainly bombarded with electrons, and probably with ions. These conditions might lead to cleaning the surface, to chemical changes in the coating (though there is no evidence for this) and in the case of a non-uniform coating, to a redistribution of the coating material.

4.5.3.2 Analysis of Gases Evolved During Multipactor - A multipactor discharge on the ceramic surface, coated or uncoated, produces an increase in the gas pressure in the test cavity. The rise in pressure is probably due to outgassing of the window surface under the influence of electron bombardment.<sup>37</sup> The gas spectrum resembles that of typical outgassing of surfaces of

electron tubes when subjected to electron bombardment.<sup>38</sup>

The analysis of gases evolved during multipactor was made on several coated and uncoated windows in this program. The equipment consisted of a General Electric Mass Spectrometer Tube attached to an S-band multipactor test cavity. In one experiment, an uncoated AL-995 alumina window was investigated. The pressure in the test cavity after bakeout was in the  $10^{-8}$  torr range. The pump system connected to the multipactor test cavity was an 8L/sec ion pump. Also connected to the system was a nitrogen sorbtion pump.

The gas spectrum prior to applying rf power to the cavity was composed mainly of hydrogen and carbon monoxide along with minor peaks indicative of methane fragments. As the power was applied, the system pressure rose to  $3 \times 10^{-7}$  torr. With the onset of multipactor glow, the partial pressure of hydrogen increased by a factor of three while the partial pressure of carbon monoxide increased by a factor of seven. The partial pressures of the mass ranges twelve through sixteen ( $\text{CH}_4$ ) increased roughly proportionally to overall system pressure.

The system pressure and the partial pressures of the main constituents increased with each rise in incident power and then

slowly returned to the previous level or a value slightly above, depending on the recovery time allowed. The evolution of hydrogen during multipactor at the higher incident power was more pronounced than that of the carbon monoxide up to about 750 kw. From this power level up to the point at which window arcing occurred, the two partial pressures were about equal.

Figure 25 shows the partial pressures of hydrogen and carbon monoxide as a function of incident power. Figure 26 shows two typical spectra; one at about 100 kw input with a multipactor discharge at the window, and the other at the point of window arcing (5.6 MW).

All of the above tests were performed with the ion pump on. The spectra all display a series of peaks from mass 12 to mass 16. This has been identified as methane. Since no mass 32 peak was observed, no oxygen is present, and consequently the mass 16 peak cannot be attributed to  $O^+$  or  $O_2^{++}$  ion species. The mass 12 peak is higher than one would expect from methane alone. This is no doubt due to  $C^+$  both from the methane cracking pattern (relative abundance 2%) and the carbon monoxide cracking pattern (relative abundance 8%).

A series of experimental runs with the ion pump on and off

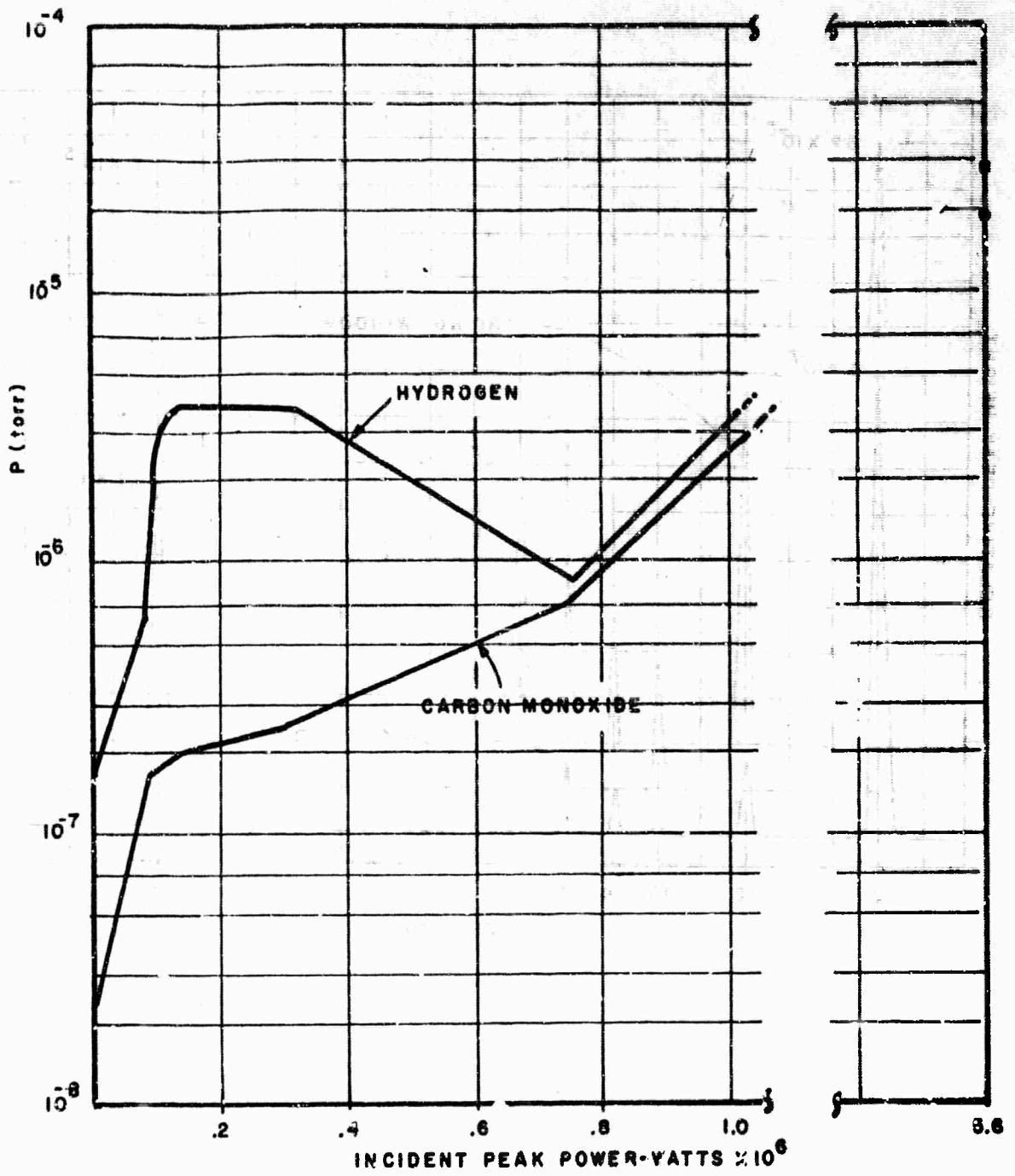


FIGURE-25 GAS PRESSURE Vs INCIDENT POWER

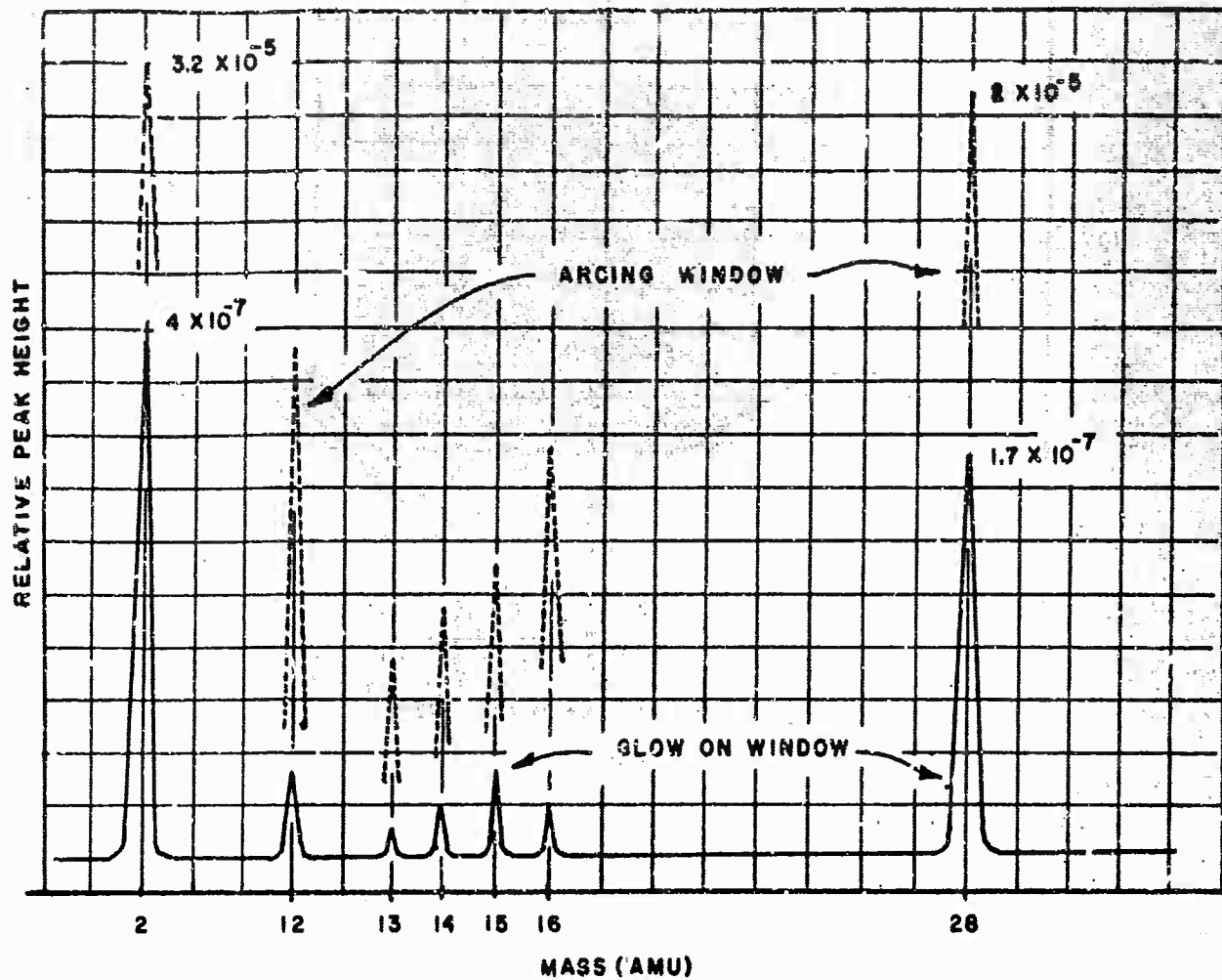


FIGURE-26. TYPICAL SPECTRA, BLANK CORRECTED

show that the methane fraction is due to methane formation by the "turned off" ion pump. During these runs all other peaks increased by only a factor of 1.5 to 2. The methane spectrum increased by at least one order of magnitude. This phenomenon has been reported in the literature by several investigators.<sup>39</sup> Consequently, the methane spectrum is attributed to the ion pump system, and not to the multipactor discharge. Similar observations were made with coated windows. At no time was there any evidence of disassociation of coating or substrate material.

4.5.3.3 X-Ray Damage to Ceramic Windows - After completion of an experiment with an uncoated alumina window (Experiment #2, Table I, p. 88), a light tan to yellow discoloration on the surface of the ceramic was observed. This discoloration displayed a toroidal shape typical of the  $TE_{01}^3$ -mode. Figure 27 shows the multipactor side of the window. Slight radial changes in shading of the surface due to discoloration can be observed. The position of the crack at the point of maximum electric field can also be seen. This crack was relatively shallow, as were several others obtained in this program.

Yellowing of the ceramic of microwave windows due to electron bombardment has been reported previously.<sup>40</sup> Nevertheless, an

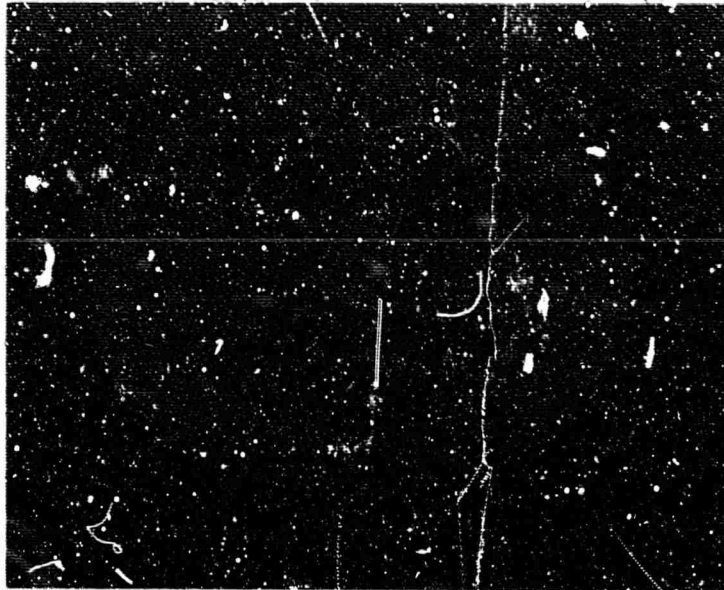


FIGURE 27 UNCOATED ALUMINA WINDOW AFTER MULTI-  
PACTOR TEST. THE CRACK FROM ARCING IS  
ON THE RIGHT.

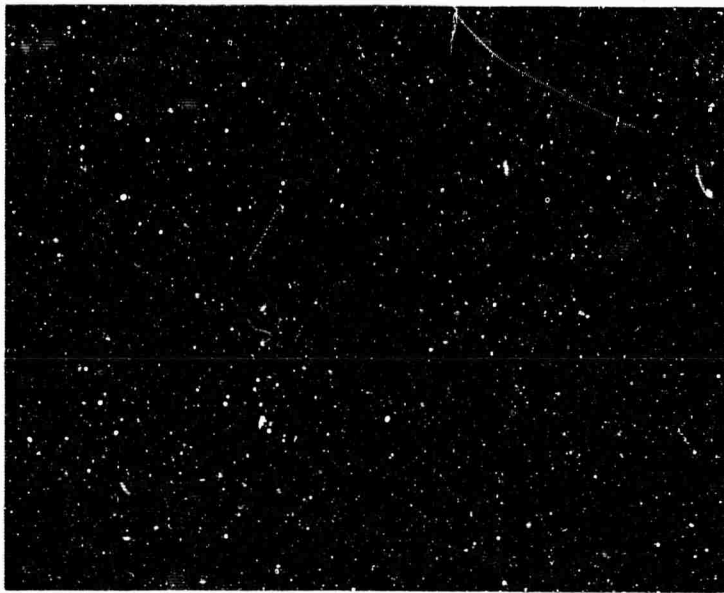


FIGURE 28 POLISHED EDGE OF SECTION OF CERAMIC  
WINDOW. THIS EDGE WAS NOT EXPOSED  
TO MULTIPACTOR. MAGNIFICATION 250X,  
NO ETCH.

effort was made to positively identify discoloration. Standard acid solubility tests were performed. The discoloration was not affected by nitric, sulfuric, hydrochloric and hydrofluoric acids, and various mixtures of these, including aqua regia. Emission spectrographs of stained and unstained areas were identical. It was clear that the discoloration was not a coating but a change of color of the ceramic itself. These discolorations have been observed with various ceramic materials when subjected to Beta or Gamma radiation and to electron bombardment.<sup>41</sup> Firing in air or wet or dry hydrogen removed the yellow color. This is also characteristic of X-ray discoloration.

It is generally believed that electrons stripped from atoms become trapped at dislocations (or other defects) and form color centers. These color centers are regions of altered optical absorption characteristics that are distinguished by discoloration of the material.

The radiation intensity during Experiment #2 (Table I, p. 88, was monitored, and at an electric field of 36.6 kv/cm a radiation level of 2.5 mr/hour was measured. After this point, the multipactor cavity was lead shielded and no further measurements were made. No doubt the radiation went up with increased power, and

the hardness of the released X-rays certainly increased.

Since the maximum electric field intensity reached during this test was 56 kv/cm, the maximum energy of the incident electron can be computed using Eq. 1.  $V_{\max}$  for this case was about 33,000 electron volts. It can be shown<sup>42</sup> that X-rays produced by 33 kev electrons will penetrate to the depth of the tan-to-yellow discoloration observed on the cross-sectional cut of the ceramic, which was about .030 inches at the deepest point.

In view of the severity of X-ray damage, the investigation of the condition of the ceramic surface was continued. The ceramic was sectioned and observations of the cross-section showed the following:

A. Discoloration was deepest at the point of maximum electric field. The color centers were visible only as dots at 1200X magnification. Only one or two were visible in the field at this magnification at each focus level below the surface. Looking at many fields gave the impression that those near the surface, at least, appeared to be in the glassy phase between the alumina crystallites.

B. Figure 28 shows a polished cross-section of the potted

ceramic surface untouched by multipactor. Figures 29a and 29b show the cross-sections of the ceramic surface exposed to multipactor (which produced yellow-tan discoloration). All figures are at 250X magnification. Figure 29a is the appearance of ceramic edge before and Figure 29b after annealing in air. Samples annealed in dry or wet hydrogen produced similar structures.

C. The centers could not be seen in polished cross-sections. However, the edges of these cross-sections showed surprising weakness as opposed to edges of cross-sections not exposed to multipactor. Polished in the same way, potted together in the same specimen mount, the edge of the area broke down much faster and more deeply than did unexposed areas (Figure 28 versus Figure 29a). Attempts to hold the edge for examination by coating, facing with other ceramic samples in the specimen mount, etc., were unsuccessful. It would appear that the glassy phase was so severely weakened that it could not hold the crystallites in place during polishing.

D. A ceramic section that had been annealed and consequently returned to a white color (Figure 29b) showed the same sort of edge breakdown under polishing as occurred on the unannealed exposed section (Figure 29a).

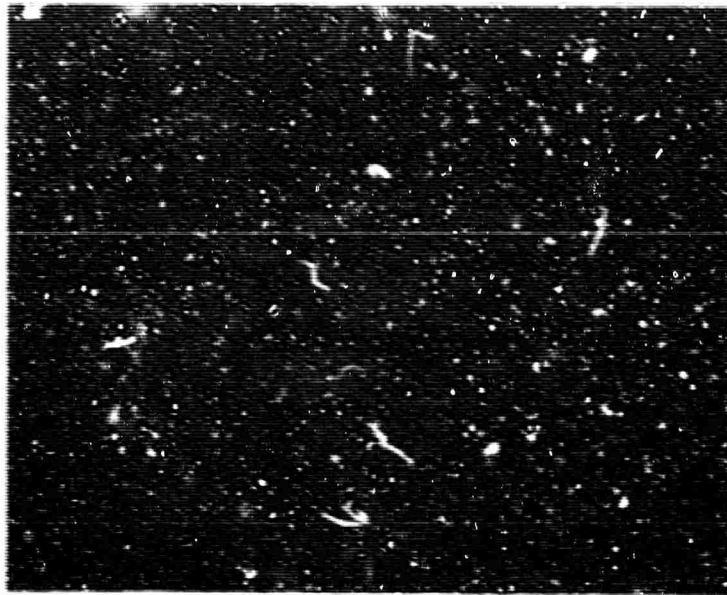
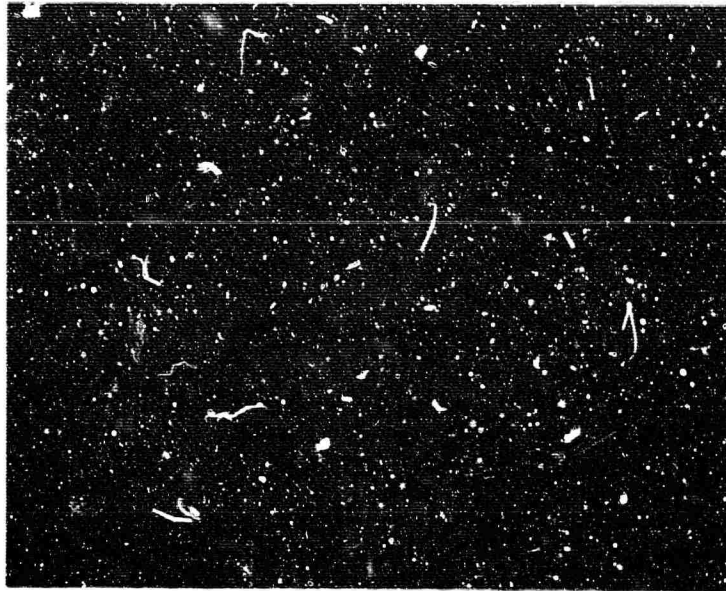


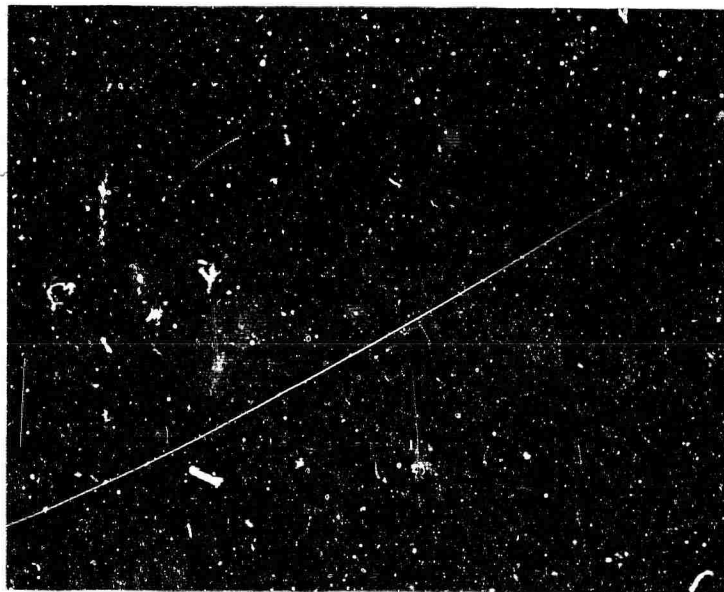
FIGURE 29a AS-POLISHED EDGE OF SECTION WHERE YELLOW COLORING EFFECT OCCURRED. ALL ATTEMPTS TO REDUCE THIS EDGE BREAKDOWN UNDER POLISHING FAILED. MAGNIFICATION 250X, NO ETCH.



FIGURE 29b AS-POLISHED EDGE OF SECTION WHERE YELLOW COLORING EFFECT HAD BEEN ANNEALED BACK TO UNIFORM WHITENERS. EDGE EXHIBITS THE SAME IRREGULAR BREAKDOWN AS OCCURRED BEFORE SPECIMEN WAS ANNEALED. MAGNIFICATION 250X, NO ETCH.



**FIGURE 29a** AS-POLISHED EDGE OF SECTION WHERE YELLOW COLORING EFFECT OCCURRED. ALL ATTEMPTS TO REDUCE THIS EDGE BREAKDOWN UNDER POLISHING FAILED. MAGNIFICATION 250X, NO STCH.



**FIGURE 29b** AS-POLISHED EDGE OF SECTION WHERE YELLOW COLORING EFFECT HAD BEEN ANNEALED BACK TO UNIFORM WHITENERS. EDGE EXHIBITS THE SAME IRREGULAR BREAKDOWN AS OCCURRED BEFORE SPECIMEN WAS ANNEALED. MAGNIFICATION 250X, NO ETCH.

From this and from some experiments with a Vickers indenter on a Kentron microhardness tester, it appeared that the glassy phase of the ceramic was damaged more severely by multipactor than mere production of color centers would indicate. With a 5 kg load on the indenter, the surface of the unexposed part of the ceramic broke some distance from the perimeter of the indentation in jagged crystalline irregularities. With the same indenter load, the yellowed surface powdered and did not visibly crack far beyond the indentation perimeter. Since the surfaces could not be polished for this experiment, details of the different impressions could not be brought to single focus for a picture but could be seen by changing focus depth while observing. These effects lead to the conclusion that the glassy phase and perhaps the crystallites are severely micro-cracked by the X-rays produced by multipactor, and that the degree of cracking is proportional to the yellowing observed which in turn is proportional to the amount of multipactor effect induced on a particular area of the window.

The degree of weakening of the ceramic surface strongly suggests that window assemblies should be replaced on any device that is to be reworked, especially after long operation of the device, particularly if there is any evidence of discoloration since it is likely that the resistance of the ceramic to arcing

is greatly reduced by the phase transformation.

4.5.3.4 Material Transfer Due to Multipactor - The Eimac experiments with half-coated windows and with windows coated in the form of dots strongly suggests that some material transfer along the surface of the window can take place during a multipactor discharge. The mechanism for transfer could be sputtering by the ions that are inevitably present in a cloud of energetic electrons.

No direct evidence for material transfer was obtained in this program. In the S-band  $TE_{111}^c$ -mode experiment described in Sections 4.5.4.1 and 4.5.5, the conditioning observed could have been partly due to transfer of the vanadium carbide coating. Upon disassembly of this cavity, the surface resistivity of the coating was checked, and it was found to be essentially the same as before the experiment. However, the resistances measured both before and after the experiment were very high, and possibly a poor guide to the density of material.

The areas which displayed vigorous multipactor at the end of the experiment were visibly clean of any coating when the cavity was disassembled. Multipactor did not cause the initiation of coating removal in these areas, but the size of the areas of glow

was observed to grow while multipactor continued. As for the initiation of the multipactor, it is likely that a surface arc occurred which initially caused removal of the coating from the areas which subsequently multipacted, but this is speculation.

#### 4.5.4 High-Power Test Data Obtained at S- and X-Bands

4.5.4.1 S-Band Tests - Table IV summarizes the results of all high-power ( $TE_{11}^0$ -mode) tests, both S-band and X-band. The equivalent transmitted peak powers quoted in the Table and in the text are the powers that would have been transmitted by a window of the size used with an electric field equal to the field calculated to exist at the surface of the dielectric.

In the first experiment, an uncoated AD-94 alumina window was evaluated for multipactor in a  $TE_{11}^0$ -mode cavity. First multipactor glow was noticed at an electric field of 4.7 kv/cm. This value is slightly higher than normally observed in the S-band multipactor cavity. The glow was blue in the center, but slightly yellow at points of lower electric field. The yellow tinge in the glow may be due to a different type of ceramic body used in this test - AD-94. In all previous multipactor tests, a purer ceramic body (AL-995) was used. Figure 30 is a photograph of multipactor glow on the middle section of the 3.14-inch

TABLE IV

## SUMMARY OF HIGH POWER RESULTS OBTAINED WITH COATED AND UNCOATED WINDOWS AT S- AND X-BANDS

EX- PERI- MENT NO.	WINDOW AND COATING MATERIAL, SURFACE FINISH	INITIAL MULTI- PACTOR AT	MULTIPACTOR ACTIVITY WITH INCREASED POWER	MAXIMUM FIELD AND POWER TRANSMITTED	WINDOW FLASH- ING AT	WINDOW ARCING AT	APPEAR- ANCE OF WINDOW AFTER TEST
1	AD-94 Ground Alumina, No Coating, S-Band	4.7 kv/cm (0.8 MW)	Multipactor Increased with Input Power	56 kv/cm (112 MW)	40 kv/cm (58 MW)	56 kv/cm (112 MW)	Ceramic Cracked in the Center
2	S-Band, AD-94 Ground Alumina Coated with Vanadium Carbide To About 100 Meg- ohm Resistivity	11 kv/cm (4.0 MW)	Glow Increased with Power, But Conditioning Eliminated Multi- pactor Altogether	63 kv/cm (119 MW)	34 kv/cm (41 MW)	--	Coating Damaged in the Center
3	AD-94 Ground Alumina, No Coating, X-Band	8.6 kv/cm (.27 MW)	At Slightly Higher Power Level, an Arc Near the Damaged Seal was Formed and Experiment Terminated.				
4	AD-94 Ground Alumina, No Coating, X-Band	7.2 kv/cm (.20 MW)	Multipactor Increased with Input Power	45 kv/cm (7.7 MW)	34 kv/cm (4.3 MW)	45 kv/cm (7.7 MW)	Evidence of Arcing Near Metal-Dielec- tric Seal
5	AD-94 Ground Alumina Coated with Vanadium Car- bide to 250 Megohms/ Square and 5.7 $\mu$ gms/ cm <sup>2</sup> Mass Density, X- Band	--	No Multipactor	59 kv/cm (13 MW)	--	59 kv/cm (13 MW)	Evidence of Arcing Near Metal- Dielectric Seal

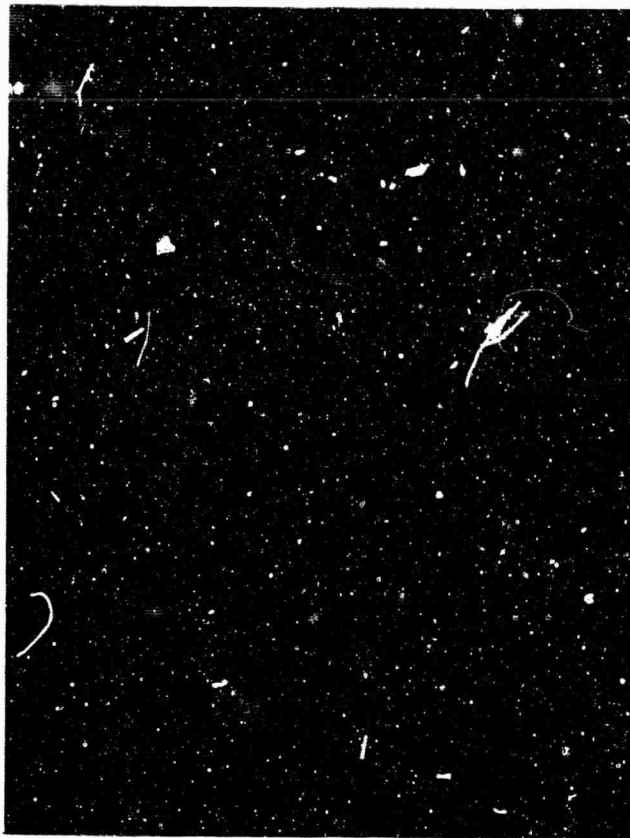


FIGURE 30 PHOTOGRAPH OF MULTIPACTOR GLOW  
IN THE S-BAND,  $TE_{1,1}^0$ -MODE CAVITY  
THROUGH THE ELOXED VIEWING HOLE.  
2.8X ACTUAL SIZE.

diameter window through a 1-3/16-inch diameter viewing port.

At an electric field of 39.7 kv/cm, flashing arcs, in the general vicinity of maximum electric field, were observed. With the power held at a constant level, arcing would normally subside, showing some kind of conditioning of the window surface. This series of events would occur each time the input power level was increased, and at each new power level the location of the arc would move to a different spot. Figure 31 shows a photograph of one of these arcs. Notice the poorly-defined boundary of the glow discharge near the ends of the arc, a characteristic of non-damaging surface arcs. At an electric field of 56.3 kv/cm, a persistent arc was formed along a crack in the ceramic. The arc was too long to be photographed through the viewing port, but was confined entirely to the surface of the ceramic. No arc across the metal-dielectric seal could be seen, and the subsequent examination of the ceramic surface showed no damage to this area of the window.

In the second S-band experiment, a ground AD-94 alumina window sputtered with vanadium carbide was studied for multipactor. As a result of the study performed with hydrogen-fired coatings (Section 4.3.0), the sputtering of this window was done



**FIGURE 31 PHOTOGRAPH OF A NON-DAMAGING SURFACE  
ARC IN THE S-BAND TEST. 2.8X ACTUAL  
SIZE.**

in the modified sputtering setup shown in Figure E2 of Appendix E. A varying surface resistivity (as measured in air after sputtering) was obtained. The surface resistivity at the center of the window was about 100 megohms/square increasing to about 2000 at the window edges.

The first multipactor glow was observed at an electric field of 11 kv/cm. At an electric field intensity of 33.6 kv/cm (40.5 MW), a few flashing arcs were observed in the general vicinity of  $E_{\max}$ . After a little while, arcing disappeared, and power could be raised again. After about an hour of operation at 48.1 kv/cm (83 MW), the window surface was completely dark. A subsequent search for multipactor at lower levels of rf power produced no multipactor discharge. This window was later operated for several hours at various peak and average power levels. These experiments and results are fully described in Section 4.5.5.

4.5.4.2 X-Band Tests - An uncoated AD-94 alumina window was evaluated for multipactor at X-band in a  $TE_{111}^0$ -mode cavity (Experiment #3 of Table IV). The first multipactor glow was observed at 8.0 kv/cm, or at about the same electric field level as in the multipactor cavity. At a slightly higher field, an arc near the metal-dielectric seal was formed. An examination of the window

assembly showed that a very small amount of Gevac,\* which had been used to stop a leak developed during the bakeout of the cavity, had been sucked into the vacuum side of the test cavity. It produced a small dielectric discontinuity at the seal edge. Since the leak was at the point of maximum electric field, arcing occurred at a relatively low power. As the power to the cavity was increased, the seal-edge arcing spread out over the bottom section of the window, but did not subside. Figure 32 shows a photograph of this window assembly. Penetration of Gevac into the vacuum side of the cavity and evidence of arcing can be seen. The arrow drawn on the window shows the direction of electric field during the test.

The experiment with an uncoated AD-94 window was repeated (Experiment #4, Table IV). First multipactor was observed at an electric field of 7.2 kv/cm. Figure 33a shows multipactor glow at 16.4 kv/cm and Figure 33b shows it at an electric field level of 33.5 kv/cm. The intensity of the glow is roughly proportional to the magnitude of the electric field of  $TE_{11}^0$ -mode.

At an electric field of 44.6 kv/cm (7.7 MW), a persistent arc was finally formed near the metal-dielectric seal, and the

---

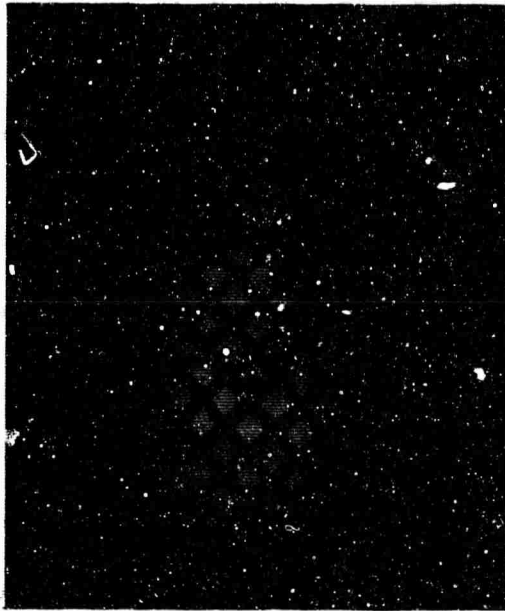
\* General Electric Trade Name.



FIGURE 32 SEAL-EDGE ARC DAMAGE IN  $TE_{111}^o$ -MODE  
X-BAND CAVITY. ARROW SHOWS DIRECTION  
OF ELECTRIC FIELD.



33a



33b

FIGURE 33 MULTIPACTOR DISCHARGE IN X-BAND,  $TE_{111}^0$ -  
MODE CAVITY. a) GLOW AT AN ELECTRIC  
FIELD OF 16 KV/CM. b) GLOW AT 34 KV/CM.  
2.3X ACTUAL SIZE.

experiment was terminated. During this experiment, the VSWR in the output line increased due to multipactor loading from 1.9 at the point of multipactor initiation to 8.7 shortly before arcing occurred. VSWE during window arcing at times was as high as 18 to 1.

One vanadium carbide coated window was studied for multipactor behavior at X-band in the  $TE_{111}^0$ -mode cavity (Experiment #5, Table IV). The sputtering procedure used to obtain a coating is shown in Figure E3 of Appendix E. Although the metallic shoulder of the X-band fixture was relatively short compared to the window diameter, the resulting coating was not very uniform. Its resistivity varied from 250 megohms/square at the center to about 1,100 megohms/square on the outer edges of the window. A crystal monitor next to the window showed a mass deposit of 5.7 micrograms/cm<sup>2</sup>.

No multipactor could be observed with this window until an electric field level of 58.7 kv/cm (13 MW) was reached. At this point an arc across the metal-dielectric seal was formed. The arcing at the seal in turn produced a multipactor discharge as shown in Figure 33b, although not as bright. When the arc extinguished itself, multipactor glow disappeared. This series of events repeated itself a number of times, and in each case,

when arcing stopped, the multipactor discharge would subside. A sustained arc was finally formed and experiment was terminated. The VSWR at resonance in the input line remained constant through the whole experiment. Its value (1.9 to 2) was slightly higher than the cold-test value of 1.5 to 1. This is a rather small discrepancy, normally observed during the high-power test of all windows in X- and S-band cavities, and is probably due to imperfections in the energy spectrum of the rf pulse. The examination of the window showed evidence of arcing near the seal. The brazing fillet near the point of arcing measured .0046 inches, a rather large value as compared to a 1.250-inch diameter of the window.

#### 4.5.5 Extended Tests in the S-Band, $TE_{111}^0$ -Mode Cavity

In the last experiment performed in this program, the vanadium-carbide coated,  $TE_{111}^0$ -mode, S-band window, described in Section 4.5.4.1, was subjected to rf power over extended periods of time. As reported in Section 4.5.4.1, after a period of conditioning, the window displayed no multipactor at power levels as high as 83 MW. This window was then tested for a total of 15-1/2 hours at 80 MW peak and 20 kilowatts average, with no evidence of deterioration. At this point, the duty cycle was doubled, and the window operated for 10-1/2 hours at 40 kilowatts average power and 80 MW peak. Again, there was no evidence of any

deterioration during this period.

In the next run, the repetition rate of the modulator was reduced to 100, and the value of the maximum electric field in the cavity increased to 57.7 kv/cm (119 MW). Numerous surface arcs were observed in the process of increasing the input power. However, none of these arcs were serious enough to damage the window or the coating. The station was left to run at an electric field of 57 kv/cm (116 MW) for a total of seven hours. The equivalent, average transmitted power at this level was 29 kw. It was observed that intermittent surface arcing at this power level persisted and that after seven hours of operation one arc in 10 to 20 minutes could be observed.

As the next step, the maximum electric field in the cavity was reduced to 54 kv/cm (105 MW), and the average power to 26 kw (.00025 duty). No arcing or multipactor could be observed at this level of operation of the window. After one hour, the repetition rate of the modulator was increased from 100 to 200. The window was now subjected to a maximum electric field of 54 kv/cm and a peak equivalent transmitted power of 105 MW corresponding to 52 kw of average power at .0005 duty. After one and one-half hours of operation at this level, a fairly large frequency detuning was

observed. Inspection of the window surface showed a glow of a peculiar-looking shape right at the point of maximum electric field. The glow consisted of two 3/32-inch diameter spots separated in the plane of the electric field by a distance of about 3/8 inch. The two glowing spots were connected by a glowing rod, and the whole picture resembled a dumbbell. As the input power to the cavity was sustained, the size of the spots kept increasing, showing a deterioration of the coating. The color of the glow was a characteristic blue of an uncoated alumina window during multipactor. It is possible that a surface arc might have damaged the coating and initiated a multipactor discharge.

The station was shut off and the cavity retuned. When rf power was again applied, the first glow was observed at an electric field of 4.5 kv/cm, a value corresponding to an uncoated alumina window. The glow had the same shape as observed previously. Figure 34 shows a photograph of the glow on the dark background of the alumina window through the eloxed viewing hole. It could be seen that the size of the spots by that time had increased to about 3/8 inch. At this relatively low electric field level (4.5 kv/cm), corresponding to 700 kw of peak transmitted power (equivalent average transmitted power was only 175 watts), the pressure in the cavity was  $10^{-7}$  torr. On the other hand, at

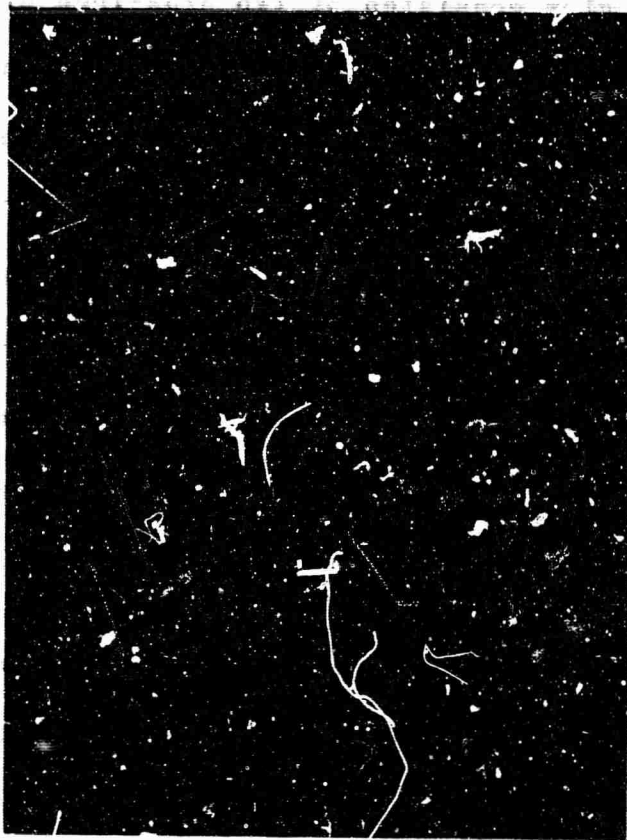


FIGURE 34 MULTIPACTOR GLOW ON DAMAGED COATING  
RESULTING FROM OPERATION OF THE  
WINDOW AT 105 MW PEAK AND 52 KW  
AVERAGE POWER. 1.9X ACTUAL SIZE.

52 kw of equivalent average transmitted power (but in absence of the glow) the cavity pressure was always less than  $2 \times 10^{-8}$  torr.

A photograph of the test window is shown in Figure 35. The damage to coating can be readily seen. The pattern of the damage corresponds to the shape of the observed glow shown in Figure 34. Except for the removal of the coating, no other damage to the surface of the window could be seen. A check of surface resistivity of the window coating detected no change in the surface resistance from its value measured before the test.

#### 4.6 EVALUATION OF METALIZING TECHNIQUES

As part of this window-study program a search for better window assembly techniques was conducted early in this program. Special attention was given to new metalizing techniques that would produce a minimum penetration into the ceramic body and a minimum thickness of metalizing. The developed technique was to be compatible with the use of a minimum fillet consistent with a vacuum-tight joint and minimum disruption of the properties of the ceramic in the immediate vicinity of the seal. The active surface of the ceramic was to be made completely free from metalizing overlaps.



FIGURE 35 COATING DAMAGED BY OPERATION OF THE WINDOW AT 105 MW PEAK AND 52 KW AVERAGE POWER. WINDOW DIAMETER IS 3.14 INCHES.

A series of metalizing experiments were performed. The objective of these tests was to evaluate several metalizing techniques on different alumina bodies. Criteria for evaluation were thickness of metalizing layer, width of the seal area, tensile strength of the seal (which is a measure of quality of the seal), and the depth of penetration of the metalizing constituents. The thickness of the metalized layers was obtained by direct measurement method;<sup>43</sup> seal tensile strength was obtained by using the standard ASTM test specimen. Penetration of metalizing constituents was obtained by optical methods using micrographic techniques.

The five metalizing techniques investigated were:

- A. Conventional Mo-Mn (80:20) metalizing at 1475°C.
- B. MoO<sub>3</sub>-MnO<sub>2</sub> metalizing at 1475°C.
- C. MoO<sub>3</sub>-MnO<sub>2</sub> metalizing at 1100°C.
- D. Solution metalizing at 1475°C.
- E. Solution metalizing at 1100°C.

Preparations of the above metalizing paints and their application techniques are given in Appendix M.

A total of thirty-five test assemblies were built and one test assembly, representing each of the five metalizing groups,

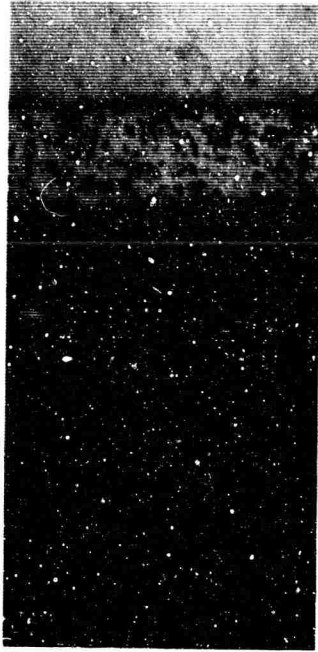
was selected for metallographic inspection. Figure 36 is a pictorial representation of a cross-sectioned seal. Using this as a guide, one can better interpret the photomicrographs of the seals in Figure 37. Only metalizing technique A shows a slight penetration of the metal constituents into the ceramic body. In all others, penetration is not visible. Metalizing thickness in Figures 37C, D and E must be in the order of  $<0.0001$  inch. Metalizing thickness of the conventional Mo-Mn (Figure 37A) is approximately 0.001 inch while that of  $\text{MoO}_3\text{-MnO}_2$  (Figure 37B) fired at  $1475^\circ\text{C}$  is 0.0002 inch. The specimens (Figures 36B to 36E) coated with nickel oxide resulted in wide variations of nickel thickness. A metalizing thickness of 0.0002 inch would permit one to be able to nickel-plate since the deterioration due to activation bath prior to plating would not be sufficient to create bare spots on the metalized ceramic. The average tensile strength obtained in technique B was about 40 percent higher than those obtained using other techniques in this experiment (Appendix M gives data on the five metalizing experiments).\*

Metalizing technique B ( $\text{MoO}_3\text{-MnO}_2$  fired at  $1475^\circ\text{C}$ ) appeared to be the most promising technique for fabrication of window

---

\* All of this metal-ceramic seal work drew very heavily upon work done by Sperry for the U. S. Army Electronics Command.<sup>44</sup>

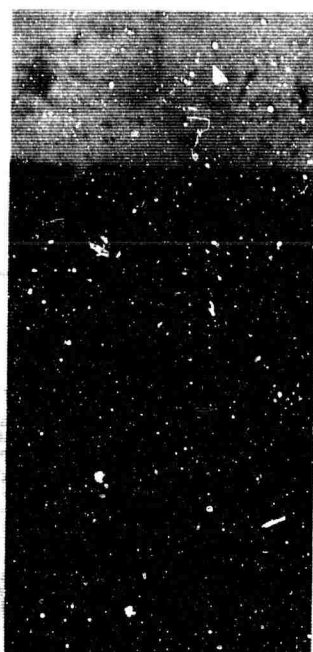




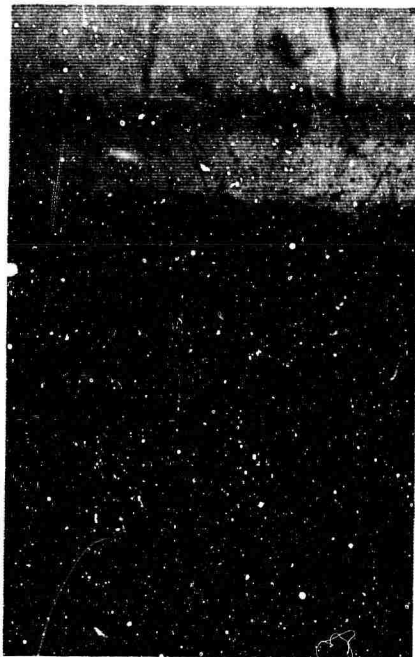
(A)



(B)



(C)



(D)



(E)

FIGURE 37 PHOTOMICROGRAPHS SHOWING CROSS-SECTIONS OF 99.5% ALUMINA SAMPLES USING FIVE DIFFERENT METALIZING TECHNIQUES, A TO E.

assemblies. With a thin and uniform nickel plating and a minimum of metalizing thickness, vacuum-tight window assemblies of high-tensile strength appeared to be possible. This technique was utilized in this program for fabrication of high-power,  $TE_{111}^0$ -mode window assemblies. The windows were usually contained in a kovar sleeve during the brazing operation by four turns of 0.020 inch molybdenum wire around the kovar shell. The 0.001 inch copper plate served as the solder material. Figure 38 shows a typical X-band window assembly. Microscopic examination at 10X revealed a uniform braze fillet  $<.001$  inch.

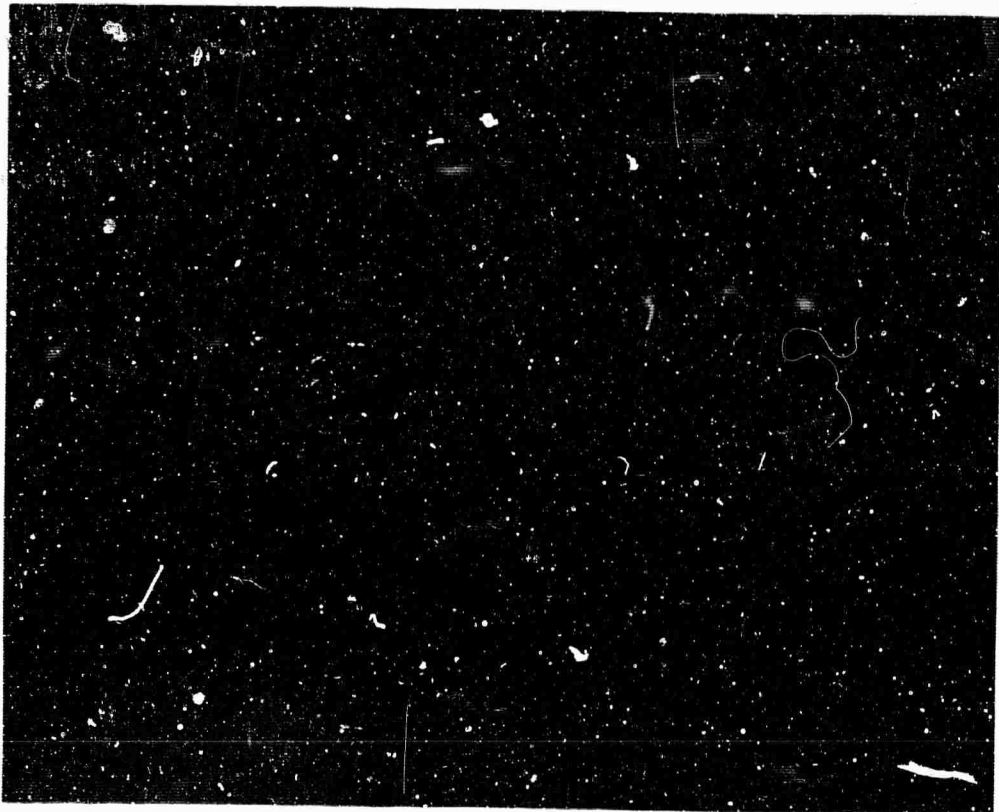


**FIGURE 38 TYPICAL WINDOW ASSEMBLY**

## SECTION V

### CONCLUSIONS

All dielectric materials suitable for high-power windows tested in this program are subject to multipactor. (Pyrolytic boron nitride has been reported to suppress multipactor,<sup>35</sup>) The multipactor phenomenon is a common occurrence at higher power levels at nearly all frequencies. Since the energy of incident electrons is inversely proportional to the square of the frequency, the electric field at which multipactor starts is higher for higher operating frequencies.

When a dielectric window is subjected to a multipactor discharge, the amount of rf power dissipated at the window as heat can be significant. In this program, a three-to-four-fold increase in the test cavity dissipation due to multipactor has been measured. Other investigators have seen a ten-fold increase in the dissipated power in the cavity.<sup>8</sup> From the point of view of efficient operation of the tube and the window power handling capability, the multipactor discharge at the window must be eliminated, or at least reduced to tolerable levels. Coating of

windows with various materials produces the desired reduction in the intensity of the glow, and at times a complete elimination of the single-surface multipactor was observed. The use of grooved surfaces on quartz has also been successful in multipactor elimination.<sup>12</sup>

The question of which is the best dielectric material for microwave windows cannot be answered in a simple way. The choice of the dielectric material is primarily determined by the mode of operation of the window (high peak power or high average power), and the operating frequency of the tube, which determines the size of the window. Although grooved quartz has shown multipactor suppression, it is basically a poor dielectric material. Its thermal conductivity is low (less than 1/10 that of alumina), which renders it unsuitable even for moderately high average power applications. Its extremely low coefficient of expansion makes it difficult to seal. Sapphire is a reasonably good window material. It has a lower loss tangent and higher flexural strength than alumina, but is quite expensive, particularly at low frequencies where large size windows are required.

At the present time, alumina and beryllia appear to be the optimum window materials. Beryllia with its very high thermal

conductivity appears to be uniquely advantageous for high average power use, although it is expensive and toxic. The toxicity of beryllia makes simple tube processing operations like sandblasting extremely difficult. High-grade alumina windows should be used at all power levels where the thermal conductivity of alumina is adequate.

The use of an isotropic boron nitride (of the pyrolytic type) for microwave window applications looks very promising because of its high thermal conductivity and low loss tangent. The problem of metalizing boron nitride windows appears to have been solved.<sup>35</sup> The use of compression seals without any metalizing is another alternative of making vacuum-tight window assemblies.

The question of the best window design is also a function of the mode of operation of the window. From discussion of Section 4.1.3, it is clear that window designs which have cross-sections elongated in the axial direction (for example, all canted windows) are not suitable for high-power applications. In transverse windows, the tangential electric field of the dominant mode is always parallel to the surface of the window, so that they are not subject to a double-surface multipactor discharge. Of course, the uniformity of the dominant mode near the dielectric surface is

guaranteed only if all transitions or irises are sufficiently far away from the window. The spacing of the rectangular-to-circular waveguide transition should be about one-half wavelength away from the window. In Appendix B, a new design procedure for such a window geometry is given. In window designs with transitions too close to the window (for example, in a pill-box window) a certain amount of normal component of electric field on the window surface is inevitable.

For high peak power applications, the use of a round window is more desirable. With this type of window, the maximum electric field intensity at the window, in general, is smaller than at a rectangular window with comparative diagonal dimensions. Also, the maximum field intensity in a round window occurs at its center so that the metal-dielectric seal (a potential window arcing area) is subjected to a relatively lower field intensity. The enormous advantage of sealing a round window over a rectangular window is obvious.

In high average power applications, it is desirable to have all areas of the window close to the outside surfaces which can be cooled. A rectangular window meets these requirements better than a round window, and in those applications where the peak rf

power transmission is not a limiting factor, a rectangular window can be safely used. But the difficulty of making vacuum-tight seals with rectangular windows, and the tendency of windows to crack under high power in the plane of the narrow guide dimension, are the major restraining factors for its use.

The question of window thickness is not a serious one. Thin window designs tend to provide greater bandwidths and less trouble from undesirable modes. Temperature gradients created in windows of the same cross-sectional dimensions by the bulk losses of the dielectric material are independent of the window thickness. On the other hand, a thicker window has a larger cross-sectional area for radial conduction of losses due to multipactor discharge, and for this reason it is generally preferred in high average power applications. But a thin window has a greater flexural advantage which makes up for a smaller radial conduction cross-section.

All windows operating above a certain power level should be coated. The threshold point at which the multipactor discharge is initiated is determined when the energy level of incident electrons (given by Eq. 1) reaches the first cross-over point on the secondary emission curve of the window material. For the same coating material the threshold is a function of the electric field strength and the

operating rf frequency.

All of the coating materials used for the suppression of multipactor in this program were able to reduce the intensity of the multipactor discharge. In isolated cases, the multipactor suppression was a complete one. From coatings obtained from metallic cathodes by sputtering, vanadium showed better multipactor suppression characteristics than titanium. Sputtered tantalum and carbon showed no multipactor discharge up to the point of surface arcing. From non-metallic materials, titanium nitride, and titanium and vanadium carbides showed the best overall multipactor performance of all coatings. The results of these tests are summarized in Table II, p. 91. In one experiment with a sputtered titanium carbide coating, a maximum electric field intensity of 79 kv/cm (224 MW) was reached before surface arcing could be observed. The window failed at an electric field of 89 kv/cm, corresponding to an equivalent transmitted power of 281 MW. No significant differences between the S-band and X-band multipactor results (except for different multipactor thresholds) were observed.

All coatings in this program were applied by the sputtering technique. Sputtering is particularly suitable for a thin film

deposition of refractory materials. The control of coating deposition was obtained using calibrated thin film crystal monitors. The use of control variables of the sputtering process for the control of deposited coatings was found to be entirely unsatisfactory, as was the use of surface resistivity. Resistance changes in between the sputtering runs and within the same run made this measuring procedure unreliable.

Wet hydrogen firings and bakeouts performed on different coatings showed large fluctuations in the value of the surface resistance. The bakeout process by itself (except for sputtered chromium coating) did not appear to affect the chemical properties of the coatings. The 900°C wet hydrogen firing, the 1100°C dry hydrogen firing and the 1100°C wet hydrogen firing affected the multipactor suppression properties of sputtered vanadium carbide coatings with increasing intensity in the above given order. The vanadium carbide coating fired at 1100°C in a wet hydrogen atmosphere nearly completely destroyed the secondary suppression property of the coating. Even though this window behaved as if it were completely uncoated, a gray metallic film was visible on its surface after firing. There is very strong evidence, therefore, that coatings should not be fired in a wet hydrogen atmosphere at temperatures higher than 900°C. Even at this temperature, a

damage to the properties of the coating may result.

The coating thickness required for multipactor suppression was not studied in this program, but the results of other investigators have shown that coatings of the same surface resistivity but of a ten-fold thickness variation (20 - 200 angstroms for evaporated titanium) can suppress multipactor equally well.<sup>45</sup> On the other hand, a theoretical investigation of attenuation of electromagnetic waves through thin conductive films (Appendix C), has shown that the incident VSWR in a propagating wave will exceed 1.05 to 1 if the surface resistivity of the coating is made less than .7 megohms/square. Assuming uniform conductivity (a reasonable assumption for thin coatings), the incident VSWR was found to be independent of film thickness and only a function of the effective surface resistivity.

Materials of high conductivity which deposit on the window surface in their pure state require a thickness of less than one atomic layer to produce a surface resistivity of 1 megohm/square. In fact, an islanding of the coating is required to produce such high surface resistivity. Coatings of this type are probably poor multipactor suppressors. On the basis of the above discussion, it can be seen that only those materials

which produce fairly thick coatings (greater than 20 angstroms) of high resistivity (greater than 1 megohm/square) are suitable window coating materials.

The electron diffraction analysis of a sputtered titanium coating has shown that this coating (after exposure to air) is titanium monoxide. This suggests that coating of the windows with titanium and titanium monoxide will produce the same results. Partial oxidation of titanium metal probably accounts for the high resistances observed.

Oxidation-reduction reactions taking place with sputtered coatings (Figures 7 - 11) indicate that a partial decomposition of carbide and nitride during the sputtering process must be taking place. Partial solubility tests in sulfuric acid were performed on sputtered vanadium carbide coatings. These tests have also shown a presence of some metal in the coating together with some carbide.

Surface arcing independent of seal-area breakdowns was experienced in this program. It can be concluded, therefore, that there will always be arcing problems, even if all arcs traceable to seals were eliminated. But improper sealing procedures can reduce power handling capabilities of the window. A new metalizing

and window sealing technique described in this report produces a strong metal-dielectric seal with a thin metalizing thickness and a minimum of penetration of the metalizing constituents into the ceramic. In one test at S-band, a maximum electric field in the cavity of 63 kv/cm was reached without any voltage breakdown at the seal.

The investigation of coatings and window materials for changes under a multipactor discharge has shown that coatings are subject to conditioning. The chemical process involved here is not well understood, but apparently has something to do with outgassing of the coating.<sup>46</sup> The analysis of gases evolved during the multipactor does not show any chemical decomposition of the coating or window material due to multipactor. Furthermore, the experimental data shows that an excessive multipactor activity on the surface of a ceramic produces changes in the crystal structure of the alumina, but no adverse effects of X-rays on quartz could be observed. Finally, there is some evidence of coating material transfer.

## SECTION VI

### RECOMMENDATIONS

It has been shown in this program that there are many metallic and non-metallic materials which can be used as multipactor suppressor coatings on high-power windows. Tests have shown that coated alumina windows can tolerate higher electric field than uncoated windows. But no matter how good a coating, there was always a limiting value of electric field at which time surface arcing resulted. This arcing limit was established independent of the seal-area breakdowns. From all coating materials tested, titanium carbide and nitride as well as vanadium carbide exhibited the best resistance to surface arcing. Other accomplishments of this window-study program were development of sputtering techniques for new coating materials, devising of better sputtering control procedures, and establishment of new, improved metalizing and window brazing techniques.

However, in spite of the advances made in the control of the single-surface multipactor problem, certain questions related to this problem remain unanswered. The principal area which

requires additional investigation is concerned with control of the coating materials. It has been shown in this program that window coatings change their properties (sometimes irreversibly) not only during the hydrogen firing process (used to simulate window brazing), but also during the bakeout and even during the coating deposition process.

A logical approach for continued investigation at this point would be to select one or two materials and to work on them in a much more intensive fashion. The materials to be investigated can be chosen from either titanium nitride, titanium carbide or vanadium carbide. The work should then begin with film deposition techniques. Using a given material, systematic variations in all the parameters of the method of application should be made so that limits on the variables can be established.

Chemical or electron diffraction techniques of coating identification should be used on the obtained films to determine their composition. Surface resistivity and optical measurements (to determine thickness) should be made for each coating, and several samples of each variation should be made in order to permit statistical evaluation of the data. At the conclusion of this investigation, it should be possible to produce a coating of

desired thickness and composition at will.

With the completion of this phase, multipactor evaluation of coatings in a test cavity should begin. A number of samples of several different thicknesses should be tested. The object of this investigation would be to determine the most suitable range of thicknesses for multipactor suppression and surface arcing. Naturally, all surfaces to be tested in the cavities would be subjected to vacuum bakeout. Chemical and physical analysis of coatings after the bakeout (and preferably after the high-power test) would be highly desirable in order to observe changes which may occur.

Other processes, like hydrogen firing in wet or dry hydrogen atmosphere should be investigated next. Physical and chemical changes during the firing process should be observed and evaluated using sufficient number of samples to get the reliable statistical data. Of course, hydrogen firing of the coating to simulate brazing of the window into a window assembly would not be necessary if the coating of the window were done after the window brazing process was completed. However, in such a case, an investigation of coatings of windows in their brazed subassemblies, especially with respect to their uniformity, must be performed.

The above described investigation procedure would place at least one coating technique on a well-founded engineering base and provide the necessary tools of good window coating control. An extensive life-test program to determine if coating properties degrade with time and average power should also be conducted.

SECTION VII

IDENTIFICATION OF KEY TECHNICAL PERSONNEL

7.1 APPROXIMATE NUMBER OF MAN-HOURS

The following key technical personnel contributed to the High-Power Microwave Tube Window Investigations Program during the period 15 September 1964 through 14 September 1965.

	<u>MAN-HOURS</u>
D. Bell	41
D. Churchill	285
R. Harter	126
A. Kiefer	424
W. Kolb	22
P. Lally	205
K. Reichert	17
A. Saharian	1856
A. Sanders	183
L. Tentacelli	67
C. Trace	36
J. White	265
B. Winters	1222

## APPENDIX A

### AN ESTIMATE OF MULTIPACTOR LOSSES ON THE SURFACE OF AN UNCOATED ALUMINA WINDOW

When the rf power is applied to a cavity incorporating an uncoated alumina window, a multipactor discharge commences as soon as the threshold value for the initiation of multipactor is exceeded. At S-band, this threshold value of the electric field is about 3 kv/cm. As the power to the cavity is increased beyond this critical value, the intensity of the discharge on the surface of the window also increases. If the dielectrically-loaded cavity was originally slightly undercoupled, then a rise in the multipactor intensity will produce an added loading in the cavity observed by an increase in VSWR of the input line. A small frequency detuning will also be produced.

Figure A1 shows a plot of VSWR at resonance ( $r_0$ ) versus the incident power of a dielectrically-loaded cavity. This data was obtained in Experiment #2 of Table I. The plot shows a variation in VSWR up to an incident power of 40 kw. It can be seen that the change in VSWR is rather rapid for the values

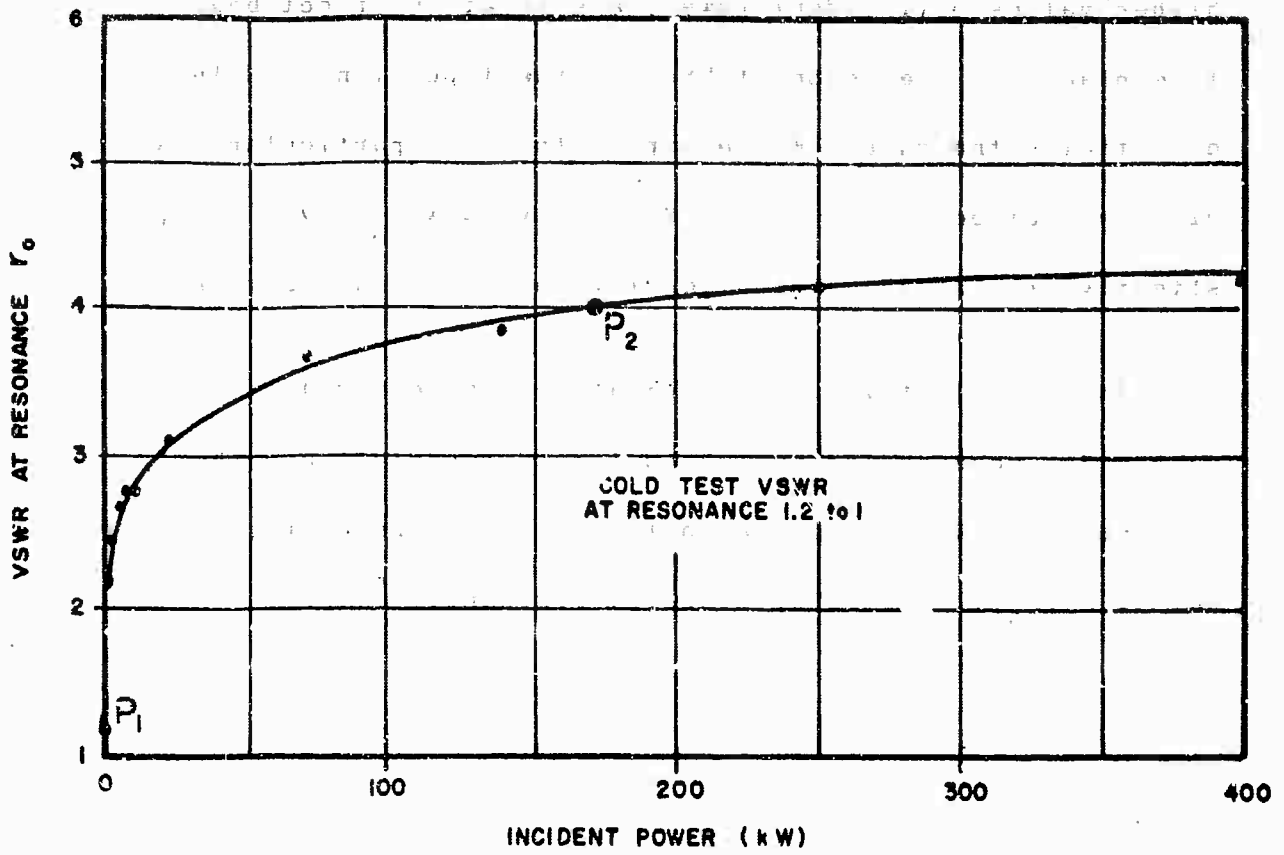


FIGURE-A1 PLOT OF VSWR vs INCIDENT POWER IN THE INPUT LINE WITH UNCOATED ALUMINA AS THE WINDOW.

of incident power slightly exceeding the threshold value. At higher values of incident power, a saturation effect begins to take place and the resonant VSWR of the input line remains essentially the same. For example, for this particular test, with an incident power of 5.6 MW, the VSWR was only 5 to 1, or slightly greater than the highest value shown in Figure A1.

The cold-test value of VSWR at resonance ( $r_0$ ) for this cavity was measured to be 1.2 to 1, undercoupled, and the internal Q ( $Q_0$ ) after bakeout was 1890. Therefore, the external Q ( $Q_{ext}$ ) was 2270, since at resonance:<sup>47</sup>

$$Q_{ext} = Q_0/\beta \quad (A1)$$

and

$$\beta = 1/r_0 \quad (A2)$$

where  $\beta$  is the cavity coupling coefficient defined in Equation A2 for an undercoupled cavity. Using this data, the lower limit of the power dissipated on the surface of an uncoated alumina window due to the multipactor discharge can now be estimated.

From Eq. A1 it follows that

$$\frac{Q_{01}}{\beta_1} = \frac{Q_{02}}{\beta_2} \quad (A3)$$

where subscript one and two refer to two different driving conditions in the cavity. In the derivation of Eq. A3, the use was made of the fact that the external Q of the cavity is independent of cavity loading and remains essentially constant for all driving conditions of Figure A1.<sup>48</sup> By letting the subscript one in Eq. A3 refer to the initial cold-test values of the cavity ( $P_1$ ) and the subscript two, for example, to point  $P_2$  on the VSWR curve of Figure A1, one obtains using numerical values for  $Q_0$ ,  $\beta_1$  and  $\beta_2$ :

$$\frac{1890}{.834} = \frac{Q_{02}}{.25} \quad (A4)$$

It follows that at point  $P_2$ , that is for an incident power of 170 kw, the internal Q was equal to 566.\* The equivalent series resistance of the cavity has, therefore, increased by a factor of 3.3.<sup>48</sup>

The actual added power dissipation in the cavity due to the multipactor discharge can be obtained from the definition of the internal Q of the cavity, which is:<sup>49</sup>

---

\*At the point  $P_2$ , 170 kw of incident power corresponds to an equivalent transmitted power through the window of about 5 MW. The maximum electric field produced at the window is 12 kv/cm (Appendices I and L).

$$Q_0 = \omega \frac{\text{energy stored in cavity}}{\text{power dissipated in cavity}} \quad (\text{A5})$$

Now, the relative amplitudes of electromagnetic fields in the cavity must be the same for an equal amount of rf power transmitted through the window. This fact is true regardless if the multipactor discharge is present or not. Equal field amplitudes, in turn, imply equal energy storage in the cavity for an equal power transfer through the window. The reactive loading of the cavity due to the multipactor discharge can be neglected.

Using Eq. A5 and the two values of  $Q_0$ , it follows that at point  $P_2$ , the dissipated power in the cavity with the multipactor discharge is about 3.3 times higher than it would have been with no multipactor loading. The power dissipated on the surface of the alumina window in the presence of the electronic discharge is actually higher than 2.3 times the power dissipated in the cavity due to bulk dielectric heating and wall losses. The power dissipated by the multipactor discharge was greater than 2.3 times the dielectric losses alone.

## APPENDIX B

### A GEOMETRICAL METHOD FOR DESIGNING WINDOWS WITH MODE TRANSDUCERS

The new window design procedure described in this Appendix is particularly suitable for the design of windows using plane, transverse dielectric discs in uniform cylindrical sections greater than one-half wavelength long, intended to establish purely tangential surface fields for the purpose of minimizing multipactor and surface arcing. It promises to reduce the experimental work involved in achieving an acceptable design.

For most high peak power applications, the circular dielectric disc has come to be accepted as the preferred type of window. Except in special cases involving higher-order mode transmission systems, the window assembly includes transducers to convert the energy of the  $TE_{10}^{\square}$  rectangular mode to that of the  $TE_{11}^{\circ}$  circular mode, and vice versa. A well-matched transducer is several wavelengths long; consequently, practical-sized window assemblies use short, partially-reflecting transducers, and are adjusted for cancellation of the reflections at specified frequencies. The design

problem is similar to that of waveguide bandpass filters, except that mode transducers do not have the simple, predictable reflectance (voltage reflection coefficient) functions that conventional filter components have. There is no known method of synthesizing a short mode transducer to meet a prescribed reflectance function; nor, in general, can the reflectance function of a mode transducer be derived by analytical methods.<sup>50</sup>

Conventionally, window assemblies using mode transducers are designed by "cut-and-try" methods. Owing to the fact that there are several dimensional variables, this procedure is tedious and costly. The proposed new method narrows the area of experimental machining principally to one transducer, and replaces most of the assembly testing by a graphical analysis. It is not necessary to fabricate the other components, or even to make the final choice of the type of dielectric window material, until an acceptable "on-paper" design has been completed.

The principal steps of the new method are summarized as follows:

1. Tentative general specifications are established on the basis of the electrical and mechanical requirements. These include frequency range, waveguide sizes, number of resonant sections, etc.

The data taken on various types of windows in other window study programs can serve as a guide.

2. Tentative contours for the  $TE_{10}^{\square} - TE_{11}^{\circ}$  mode transducer are selected, and a test model is fabricated.

3. The complex voltage reflection coefficient at the terminal plane of the transducer, seen from the circular side with a matched load on the rectangular side, is measured over the frequency band of interest and plotted in polar form. The measurement actually is made on the rectangular side, using an adjustable short circuit in the circular section, following any of several well-known procedures.<sup>51</sup>

4. By translation and projection, the loci of the measured data are transformed to the domain of the dielectric-filled region. The conditions for zero insertion loss at the bandedge frequencies are imposed. A set of compatible dimensions (if it exists) is found by a graphical selection procedure that converges rapidly.

5. If no compatible set of dimensions can be found, the contours of the transducer are modified, and the entire procedure is repeated. At any stage, the insertion loss at other frequencies in the band can be derived.

Theoretically, the method is not restricted to any range of the variable dimensions. However, as a practical matter, certain initial restrictions can be made to reduce the labor involved. Without much loss of generality, the ratio of the circular and rectangular waveguide cross-sections can be held fixed. The impedance ratios then are functions only of the frequency and the dielectric constant. Further, the lengths of the resonant sections can be restricted to one-half wavelength or less. This eliminates higher-order longitudinal resonances. If it is to be regarded as a coupling element, rather than a resonant section, the dielectric disc can be restricted to thicknesses of less than one-quarter wavelength. Appreciable simplification of the graphical analysis results.

A sample design illustrating the method is shown in Figure B1 - B8. The specifications of this design call for a thin-disc window comprised of two resonant sections, matched at frequencies  $f_1$  and  $f_2$  which differ by about ten percent, and having short, tapered transitions joining the circular section whose impedance is roughly equal to that of the rectangular waveguide.\* Figure B1

---

\*The wave impedances of the  $TE_{10}^{\square}$  mode and the  $TE_{11}^{\circ}$  mode (in vacuum) are exactly equal when the ratio of the diameter of the circular section to the width of the rectangular section is  $3.682/\pi$ . However, there is no reason to hold exactly to this ratio, and for mechanical reasons it is expedient to choose the diameter equal to the diagonal of the rectangular section. This choice avoids steps at the junction corners.

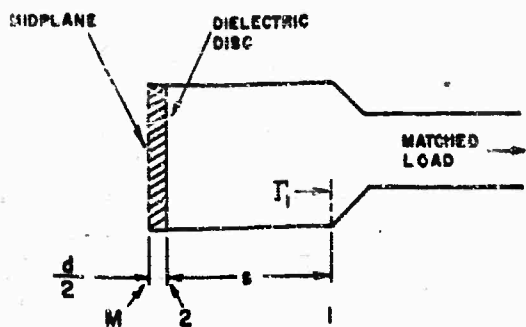


FIGURE-B1 CROSS SECTION, OUTPUT HALF OF WINDOW, SHOWING REFERENCE PLANE AND VARIABLE DIMENSIONS

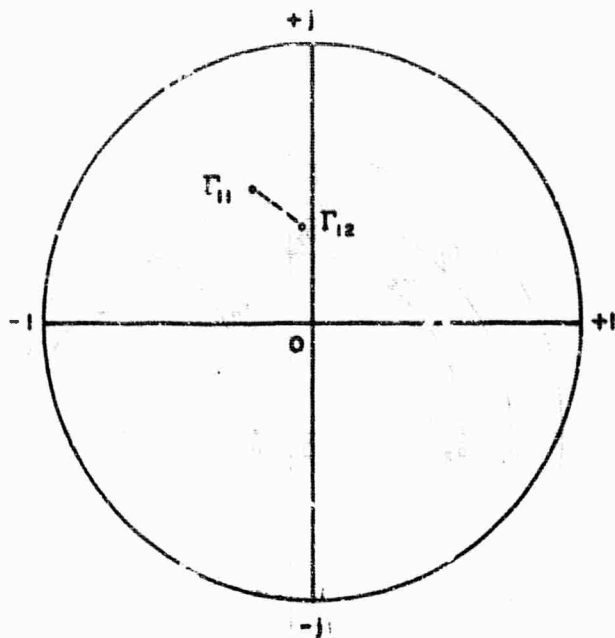


FIGURE-B2 REFLECTION COEFFICIENT AT PLANE 1 OVER FREQUENCY RANGE  $f_1$  TO  $f_2$

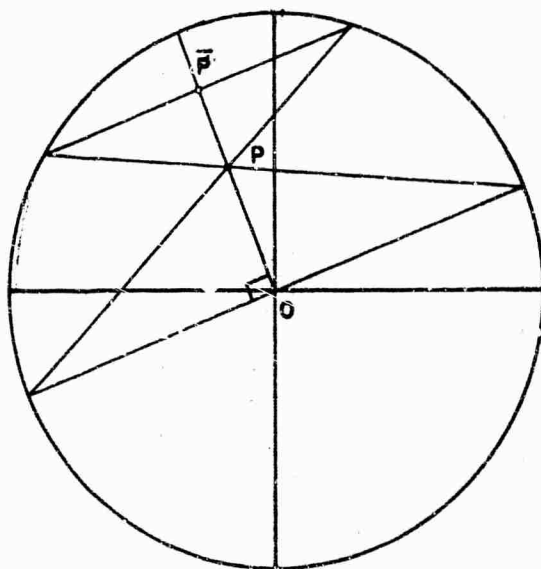


FIGURE-B3 THE  $\beta'$ , OR DARBoux TRANSFORMATION

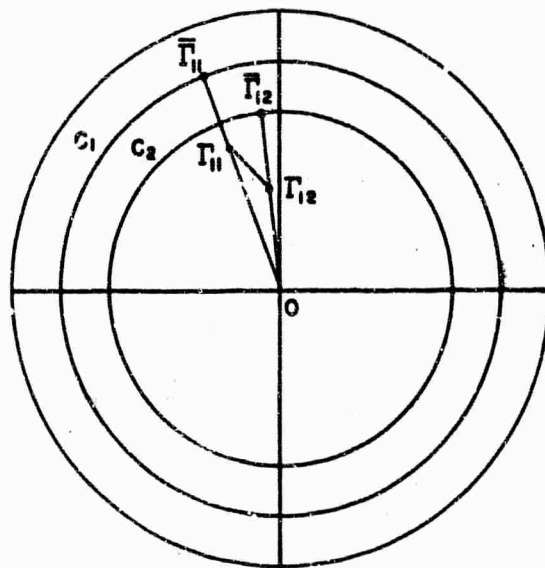


FIGURE-B4 TRANSFORMED REFLECTION COEFFICIENTS ON THE CIRCLES  $C_1$  AND  $C_2$

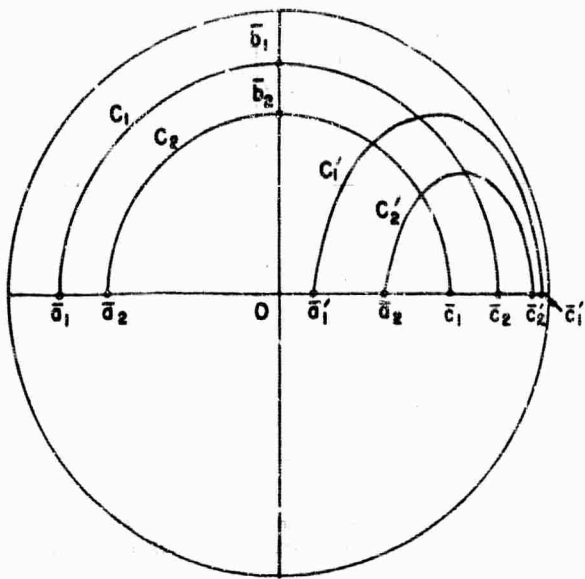


FIGURE-65 SEMI-ELLIPSES  $C_1$  &  $C_2$   
AND THEIR PROTOTYPE SEMICIRCLES

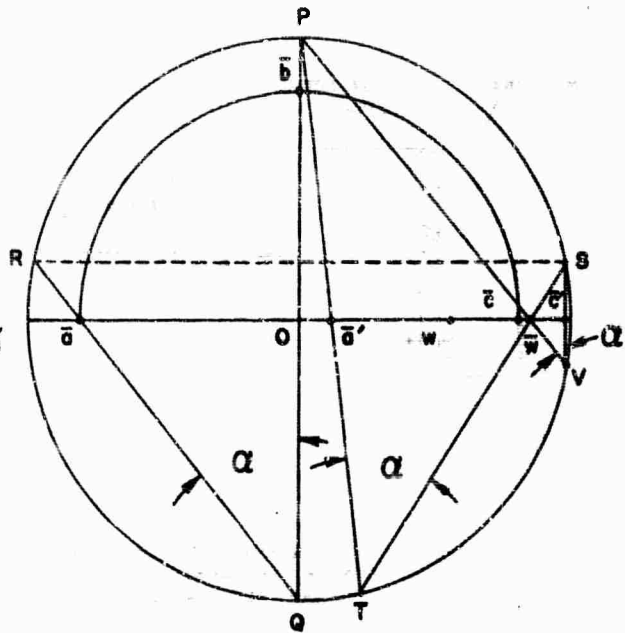


FIGURE-66 CONSTRUCTION FOR TRANSFORMING POINTS  
 $z$  &  $\bar{z}$  TO POINTS  $z'$  &  $\bar{z}'$

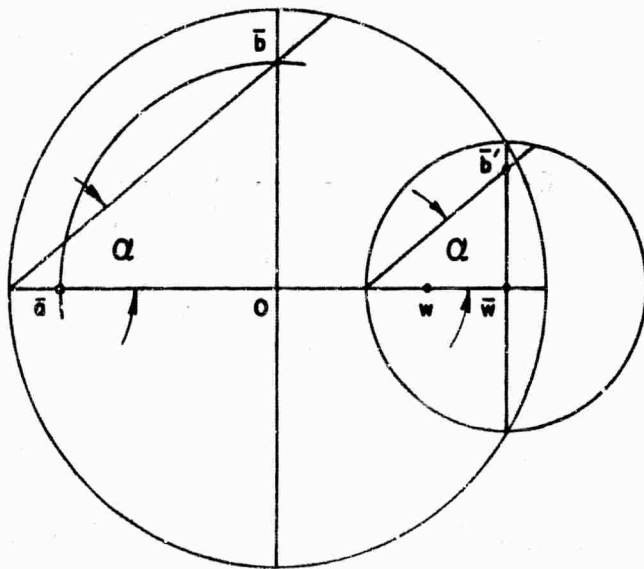


FIGURE-67 CONSTRUCTION FOR TRANSFORMING  
POINT  $b$  TO  $b'$

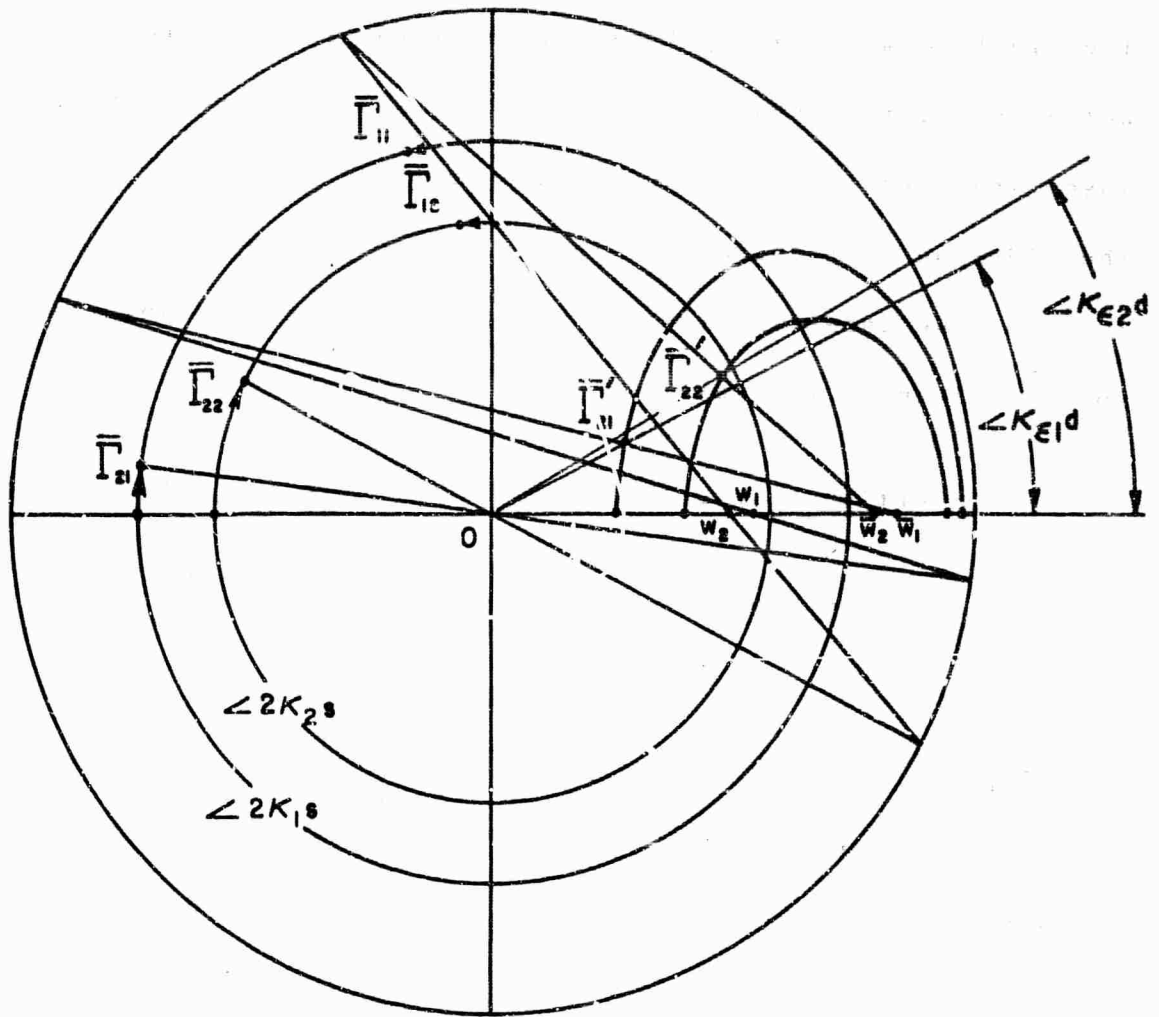


FIGURE B8 CONSTRUCTION SHOWING A SOLUTION YIELDING A COMPATIBLE SET OF DIMENSIONS  $\epsilon$  AND  $d$

shows the half of the assembly that lies on the output side of the midplane M. The input half (the mirror image of the output half) is not involved in the design, inasmuch as the overall insertion loss is determined by the real and imaginary parts of the midplane reflection coefficient. When the imaginary part is zero, the insertion loss is zero. Otherwise, the insertion loss is given by the relation:

$$\text{Insertion Loss} = 10 \text{ Log}_{10} \left[ 1 + \left( \frac{2 \text{ Im}(\Gamma_m)^2}{1 - |\Gamma_m|^2} \right) \right] \text{db} \quad (\text{B1})$$

where  $\Gamma_m$  is the midplane reflection coefficient, seen looking toward the load.

Typical reflection coefficient data derived from measurements on the output transducer are plotted in Figure B2. In this and the following figures, the first subscript indicates the plane of reference, and the second subscript indicates the frequency.

Figure B3 illustrates the construction for making a projective transformation of a point P on the reflection coefficient plane.\*

---

\*In the microwave literature, this transformation is referred to as the "g-transformation", a term apparently originated by Deschamps.<sup>52</sup> In texts on projective geometry, it is sometimes called the Darboux transformation.

By means of this transformation, reflection coefficients  $\Gamma_{11}$  and  $\Gamma_{12}$  are transformed to points  $\bar{\Gamma}_{11}$  and  $\bar{\Gamma}_{12}$ , plotted in Figure B4. The corresponding reflection coefficients at other reference planes throughout the distance  $s$  have the same magnitudes; therefore, their transformed values also lie on the circles  $C_1$  and  $C_2$ .

Upon crossing the interface at plane 2, a reflection coefficient is subjected to a bilinear transformation of the type produced by an ideal transformer. All impedance values are multiplied by the ratio  $\kappa_e/\kappa$  where  $\kappa_e$  is the propagation constant in the dielectric region, and  $\kappa$  is the propagation constant in the region  $s$ . For a typical window material, the ratio is about four; hence, all reflection coefficient values tend to move to the right. The center  $O$  moves to the point  $w$  on the real axis, at a radius (with respect to the new center) given by

$$w = \frac{\kappa_e - \kappa}{\kappa_e + \kappa} \quad (B2)$$

The circles  $C_1$  and  $C_2$  become smaller circles in the right half plane. When every point on the smaller circles is projected by the Darboux transformation, it is found that the projected points lie on ellipses, designated  $C_1'$  and  $C_2'$  in

Figure B5. Actually, it is not necessary to go through the transformation of the large circles to the small circles; the ellipses may be formed directly by using the concept of "invariance of the hyperbolic distance" described by Deschamps.<sup>52</sup> The constructions for transforming points  $\bar{a}$ ,  $\bar{b}$ , and  $\bar{c}$ , lying at the intersections of a circle with the axes to points  $\bar{a}'$ ,  $\bar{b}'$ , and  $\bar{c}'$ , lying on an ellipse, are illustrated in Figures B6 and B7.

The point  $\bar{w}$  is the Darboux projection of the point  $w$ . To find the point  $\bar{a}'$  such that the hyperbolic distance  $\langle \bar{w}\bar{a}' \rangle$  is equal to the hyperbolic distance  $\langle O\bar{a} \rangle$ , the point  $S$  is placed on the circumference in a position making the arc  $\widehat{SP}$  equal to the arc  $\widehat{PR}$ , where  $R$  is formed by the projection of  $\bar{a}$  on  $C$  from  $Q$ . The line  $ST$  is drawn through  $\bar{w}$ , and the point  $\bar{a}'$  is located at the intersection of the line  $TP$  with the real axis. It is an easily-proved theorem of Euclidean geometry that the angle  $\angle STP$  is independent of the location of the point  $T$ ; hence, it is invariant with the position of  $\bar{w}$ , and is designated  $\alpha$ . Likewise, the hyperbolic distance  $\langle \bar{w}\bar{c}' \rangle$  is made equal to the hyperbolic distance  $\langle O\bar{c} \rangle$  by finding the point  $V$  such that  $PV$  passes through  $\bar{w}$ , then drawing  $VS$ , which intersects the axis at  $\bar{c}'$ . As before, the angle  $\angle SVP$  is equal to  $\alpha$ .

To avoid confusion in Figure B6, the construction of point  $\bar{b}'$  is shown in Figure B7. The secondary circle is drawn with the chord through  $\bar{w}$  as a diameter, and the angle is constructed with respect to its axis. The hyperbolic distance  $\langle \bar{w}\bar{b}' \rangle$  is equal to the hyperbolic distance  $\langle 0\bar{b} \rangle$ . Other points on the ellipse can be found by constructions similar to that of Figure B7. Another chord through  $\bar{w}$  is selected as the diameter of a secondary circle, and the angle  $\alpha$  is constructed with respect to an orthogonal diameter. It can be proved, however, that the locus of all points derived in this way is an ellipse; therefore, it is simpler to construct the ellipse from its minor and major axes. The line length  $\bar{a}'/\bar{c}'$  forms the minor axis. The major axis is easily derived from the line length  $\bar{w}\bar{b}'$ , using the canonical equation for an ellipse.

According to Equation B2, the point  $w$  is frequency-sensitive. The propagation constant  $\kappa_e$  varies almost linearly with frequency, but the propagation constant  $\kappa$  varies somewhat more rapidly with frequency. Consequently, as the frequency increases, the point  $w$  and its projection  $\bar{w}$  move slowly toward the origin. This fact is taken into account in constructing the ellipses  $C_1'$  and  $C_2'$ .

A solution that yields a compatible set of dimensions is

shown in Figure B8. The angles  $\angle \kappa_{\epsilon_1} d$  and  $\angle \kappa_{\epsilon_2} d$  are the arguments of the dielectric-domain of reflection coefficients at plane 2. By construction, they are in the proportion of  $\kappa_{\epsilon_1} / \kappa_{\epsilon_2}$ ; hence, at both frequencies, the midplane reflection coefficients lie on the real axis, representing zero insertion losses. The hyperbolic "radii",  $\langle \bar{w}_1 \bar{\Gamma}'_{21} \rangle$  and  $\langle \bar{w}_2 \bar{\Gamma}'_{22} \rangle$  are transformed into the radii  $0\bar{\Gamma}_{21}$  and  $0\bar{\Gamma}_{22}$  by the constructions indicated. These constructions simply yield the angles; a point on either ellipse must transform to some point on the prototype circle. The constructions preserve the "elliptic angles" between the corresponding radii in the two domains.<sup>52</sup> That one of the construction lines happens to pass through the intersection of  $C_2$  with the imaginary axis is pure coincidence.

The points  $\bar{\Gamma}_{21}$  and  $\bar{\Gamma}_{22}$ , derived in this way, constitute a solution of the design problem if (and only if) they bear the proper angular relations with respect to the points  $\bar{\Gamma}_{11}$  and  $\bar{\Gamma}_{12}$ . That is, a length  $s$  can be found such that  $\bar{\Gamma}_{11}$  rotates into  $\bar{\Gamma}_{21}$  through the angle  $2\kappa_1 s$ , and  $\bar{\Gamma}_{12}$  rotates into  $\bar{\Gamma}_{22}$  through the angle  $2\kappa_2 s$ ; both relations being taken in the clockwise direction as shown. If no such length  $s$  can be found, a different trial value of window thickness  $d$  must be

chosen, yielding different positions for the points  $\bar{\Gamma}'_{21}$  and  $\bar{\Gamma}'_{22}$ . It will be noted that these points spread apart rapidly as  $\bar{\Gamma}'_{22}$  approaches the top of the ellipse  $C'_2$ ; hence, in this region the argument at  $\bar{\Gamma}'_{22}$  changes more rapidly with window thickness than does the argument of  $\bar{\Gamma}'_{21}$ . For this reason, successive trials can be made to converge rapidly on a compatible solution, if one exists.

## APPENDIX C

### ATTENUATION OF ELECTROMAGNETIC WAVES THROUGH THIN METALLIC FILME

Consider a wave incident on a thin metallic film of infinite lateral dimensions and located in the  $x - y$  plane, as shown in Figure C1. For reasons of simplicity, let the wave be a TEM wave, and assume a normal incidence on the plane. The thin film of Figure C1 can represent any metallic coating on the surface of a dielectric window. The mismatch due to the dielectric window is a window design problem and will be neglected here so that the space impedance and the propagation constant to both sides of the thin film element will be the same and equal to that of air.

The expression for the TEM wave incident upon the film in the positive  $z$ -direction can be written as

$$E = E_0 e^{-j\kappa_0 z} \quad (C1a)$$

$$H = \frac{E_0}{Z_0} e^{-j\kappa_0 z} \quad (C1b)$$

where  $\kappa_0$  is the propagation constant given by  $\omega/c$  (radian

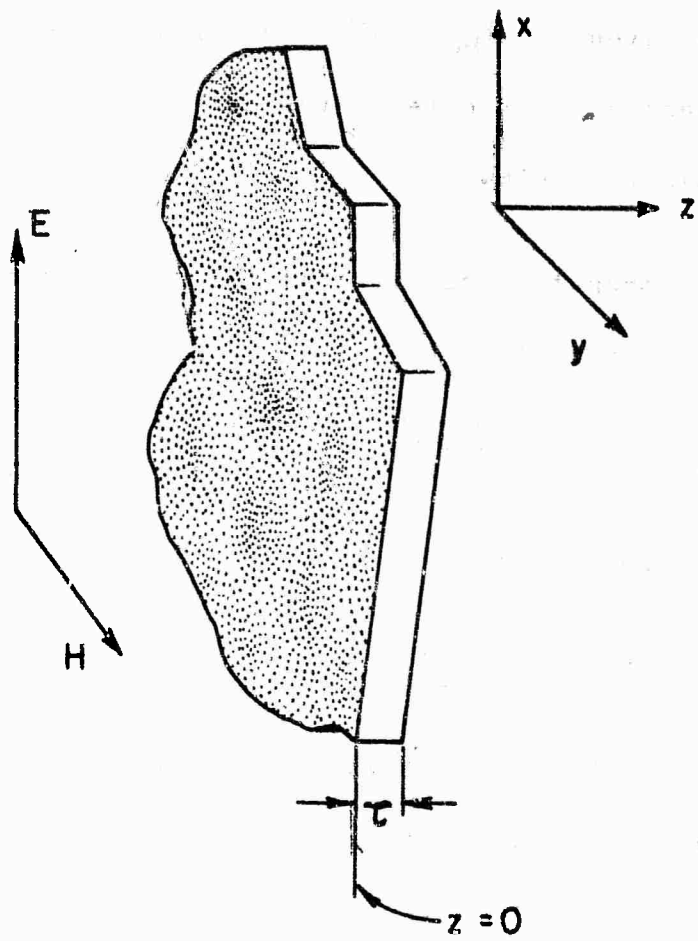


FIGURE - C1 A TEM WAVE INCIDENT ON A THIN METALLIC PLANE

frequency over velocity of light) and  $Z_0$  is the free space impedance given by  $(\mu_0/\epsilon_0)^{1/2} = 377$  ohms. Similar expressions for incident and reflected waves can be written for both surfaces of the thin film element.

The propagation constant within the conductor, when  $\sigma \gg \omega\epsilon$ , is given approximately by<sup>53</sup>

$$\gamma = (1 + j) \sqrt{\frac{\omega\mu\sigma}{2}} \quad (C2)$$

and the space impedance

$$Z = (1 + j) \sqrt{\frac{\omega\mu}{2\sigma}} \quad (C3)$$

where  $\sigma$  is the conductivity of the resistive material and  $\epsilon$  is the dielectric constant. The assumption of  $\sigma \gg \omega\epsilon$  is a valid one even in the case of imperfect conductors of the type used for window coatings. For example, it is reported that titanium films of  $10^6$  ohms/square resistivity suppress multipactor when deposited on the surface of the window.<sup>17</sup> The thickness of films of  $10^6$  ohms/square resistivity is smaller than 200 angstroms.<sup>18</sup> Using these values of resistivity and thickness, the bulk conductivity of the film comes out to be  $\sigma \approx 50$  mho/m. Thinner films produce higher conductivity. The product of  $\omega\epsilon$ , on the other hand, equals unity at a frequency of about 18 Gc.

When the expressions for the incident and reflected electric and magnetic fields are equated on both sides of the thin metallic element ( $z = 0$  and  $z = \tau$ ), a relationship between the wave amplitudes can be obtained. Each wave amplitude can be expressed as a function of the incident wave  $E_0$  and the thickness  $\tau$  of the conductive film. The resulting complex amplitude of the transmitted wave is found to be given by:

$$E_t = E_0 \left[ \cosh \gamma \tau + \frac{Z^2 + Z_0^2}{2ZZ_0} \sinh \gamma \tau \right]^{-1} \quad (C4)$$

where  $e^{j\kappa_0\tau}$  was set equal to one. This is a valid assumption since  $\kappa_0\tau$  is extremely small.

Assuming that  $\sigma$  is always greater than 50 mho/m, then the magnitude of the complex impedance of Eq. C3 is less than 1 for all frequencies less than 18 Gc. For all smaller frequencies and higher conductivities  $\sigma$  the impedance is even smaller. But, when  $Z \ll Z_0$ , Eq. C4 can be simplified to

$$E_t = E_0 \left[ \cosh \gamma \tau + \frac{Z_0}{2Z} \sinh \gamma \tau \right]^{-1} \quad (C5)$$

Eq. C5 can be simplified some more by considering only small values of thickness  $\tau$  as compared to skin depth  $\delta$ . Therefore, with

$$\tau \ll \delta = (2/\omega\mu\sigma)^{1/2}$$

$\gamma\tau$  becomes:

$$\gamma\tau \ll (1 + j)$$

With the magnitude of  $\gamma\tau$  smaller than one, the expression in the brackets of Eq. C5 can be expanded into power series and simplified by neglecting all higher order terms. Eq. C5 then becomes:

$$E_t = E_0 \left(1 + \frac{Z_0}{2Z} \gamma\tau\right)^{-1} \quad (C6)$$

When the expressions for the complex space impedance  $Z$  and the propagation constant  $\gamma$  (given by Eqs. C2 and C3) are introduced into Eq. C6, the magnitude of the transmitted wave is given by:

$$E_t = E_0 (1 + 188 \sigma\tau)^{-1} \quad (C7)$$

where  $Z_0$  was set equal to 377 ohms.

Eq. C7 gives the magnitude of the transmitted wave through a thin conductive film of thickness  $\tau$  and bulk conductivity  $\sigma$ . Knowing the values of  $\tau$  and  $\sigma$ , Eq. C7 can be used to determine a numerical value of  $E_t/E_0$ . However, it would be interesting to

relates the VSWR of the incident wave to the amplitude of the transmitted wave  $E_t$  and then to the surface resistivity  $R$  of the window coating. The VSWR of the incident wave is given by<sup>54</sup>

$$\left(\frac{E_t}{E_0}\right) = \frac{2\sqrt{\text{VSWR}}}{1 + \text{VSWR}} \quad (\text{C8})$$

Combining Eq. C7 and C8, it follows that the surface resistivity  $R$  in ohms per square is given by:

$$R = \frac{377\sqrt{\text{VSWR}}}{(\sqrt{\text{VSWR}} - 1)^2} \quad (\text{C9})$$

where  $R = 1/\sigma_T$ .

Figure C2 shows the dependence of surface resistivity  $R$  on VSWR for the input TEM wave. For other modes of propagation, the results will be very similar. It can be seen that in order not to have a higher VSWR than 1.05, the surface resistance of the coating should not be less than about 0.7 megohms/square. It is important to point out that the VSWR depends only on the surface resistivity and not on the film thickness or its conductivity. The thickness of the coating required is a function of the secondary emission property of the homogeneous coating.

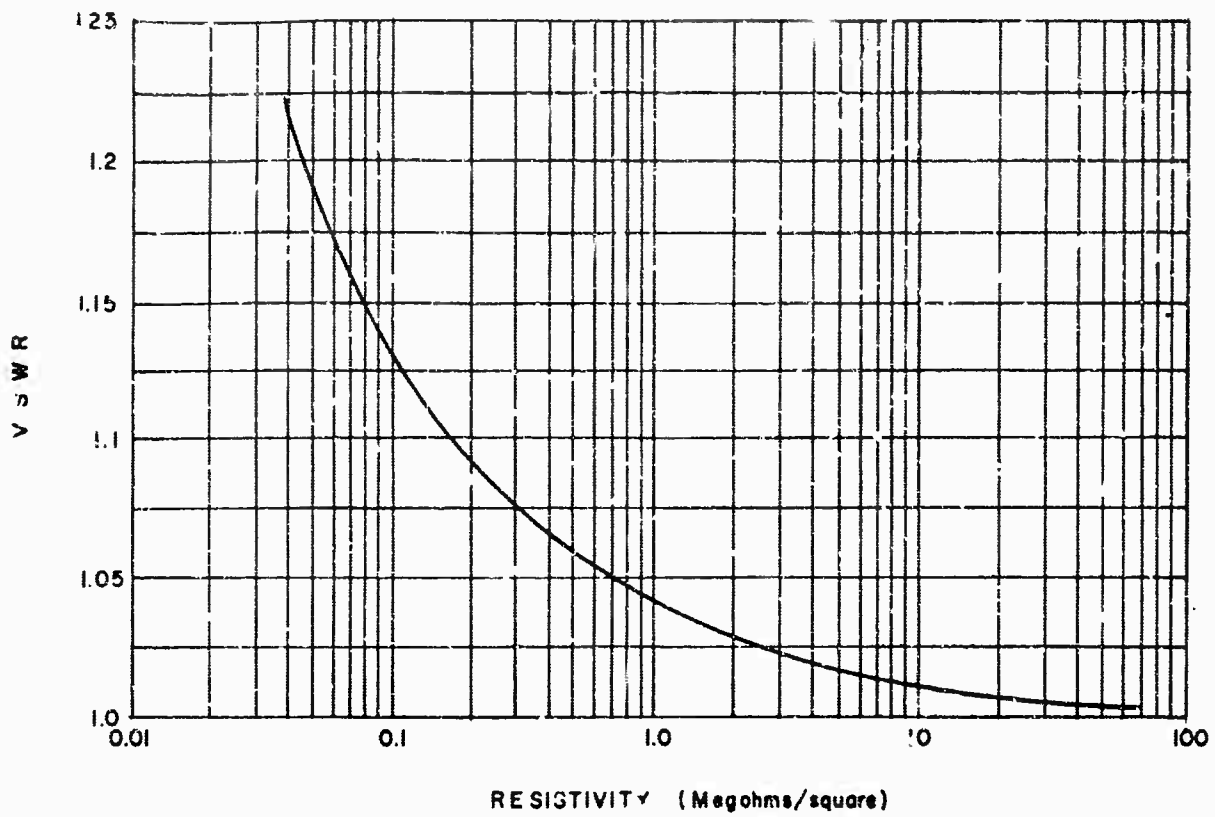


FIGURE-C2 CHANGE IN INCIDENT WAVE VSWR VS SURFACE RESISTIVITY OF THIN FILM

## APPENDIX D

### CALCULATION OF THICKNESS OF TITANIUM FILMS OF VERY HIGH RESISTIVITY

Experimental data shows that evaporated titanium films of  $10^6$  ohms per square, or an order or two magnitudes higher, suppress multipactor.<sup>17</sup> The bulk dc resistivity of titanium metal is about 50 microhm-cm. Assuming that the evaporated film of titanium is deposited in its pure metallic state, then the thickness of the film of  $10^8$  ohms/square is given by:

$$t = \frac{50 \times 10^{-6} \text{ cm}}{10^8} = 5 \times 10^{-3} \text{ angstroms}$$

For comparison, the diameter of one titanium atom is roughly two angstroms. Therefore, in order to obtain a film of titanium metal of only  $10^6$  ohms/square, the thickness of the uniform coating must be about three orders of magnitude less than one atomic layer. Usually, however, the tendency of thin films, assuming that they are deposited in their pure state, is to form discontinuous sections in form of islands, at least during the initial stages of their formation, so that no atom-splitting is actually necessary to obtain high resistivities.

APPENDIX E

SKETCHES OF SPUTTERING SETUPS  
USED IN THIS PROGRAM

- Figure E1                    Sketch of Sputtering Apparatus Used  
for Coating All Unmounted Windows.
- Figure E2                    Sketch of Sputtering Setup Used for  
Coating Brazed  $TE_{11}^0$ -Mode, S-Band  
Window Assemblies.
- Figure E3                    Sketch of Sputtering Setup Used for  
Coating Brazed  $TE_{11}^0$ -Mode, X-Band  
Window Assemblies.

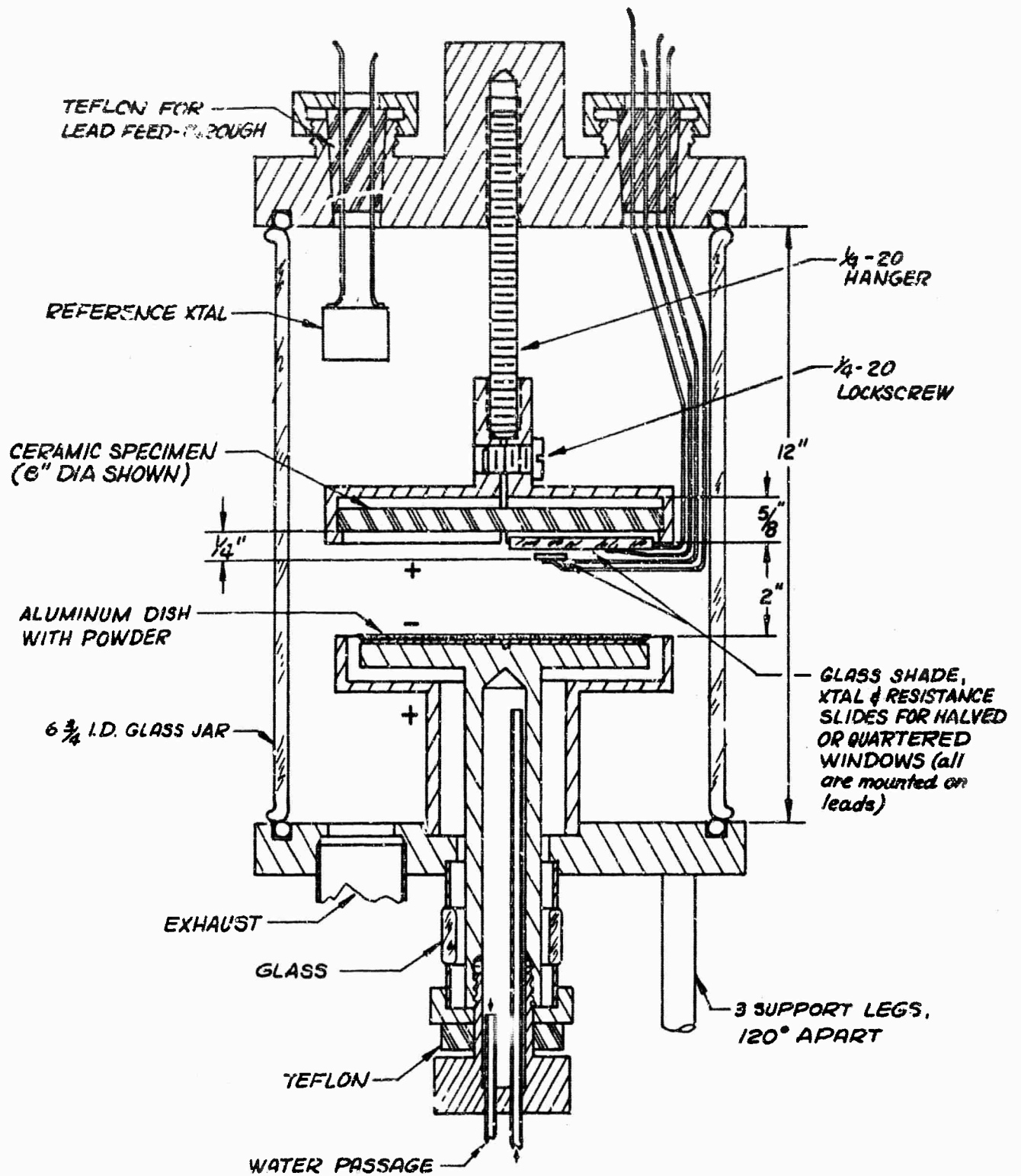


FIGURE - E1 SKETCH OF SPUTTERING APPARATUS USED FOR COATING ALL UNMOUNTED WINDOWS

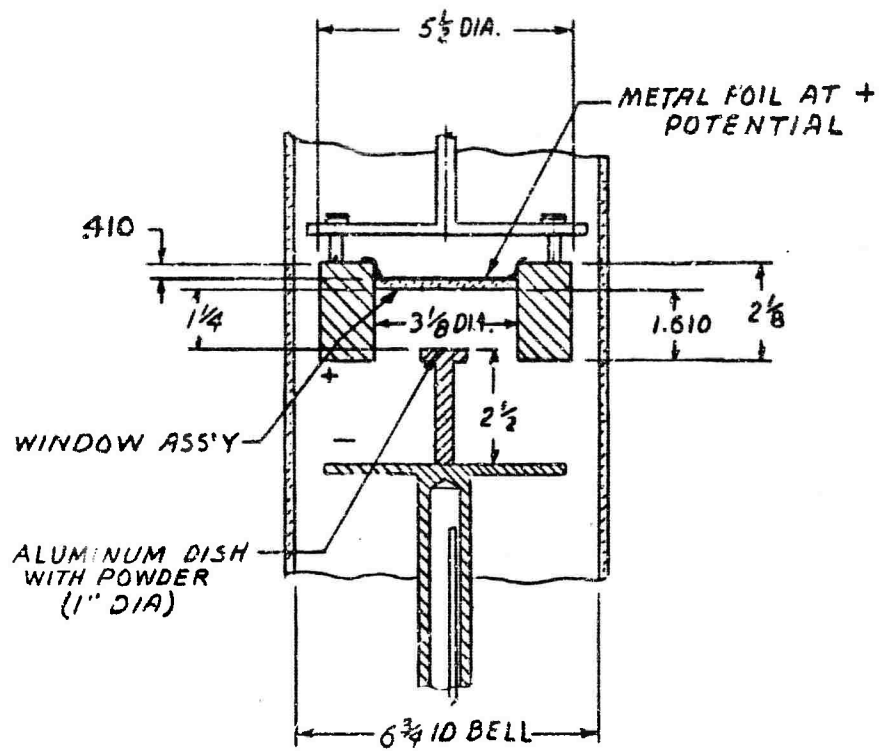


FIGURE -E2 SPUTTERING SET-UP FOR COATING BRAZED S-BAND WINDOW ASSEMBLIES

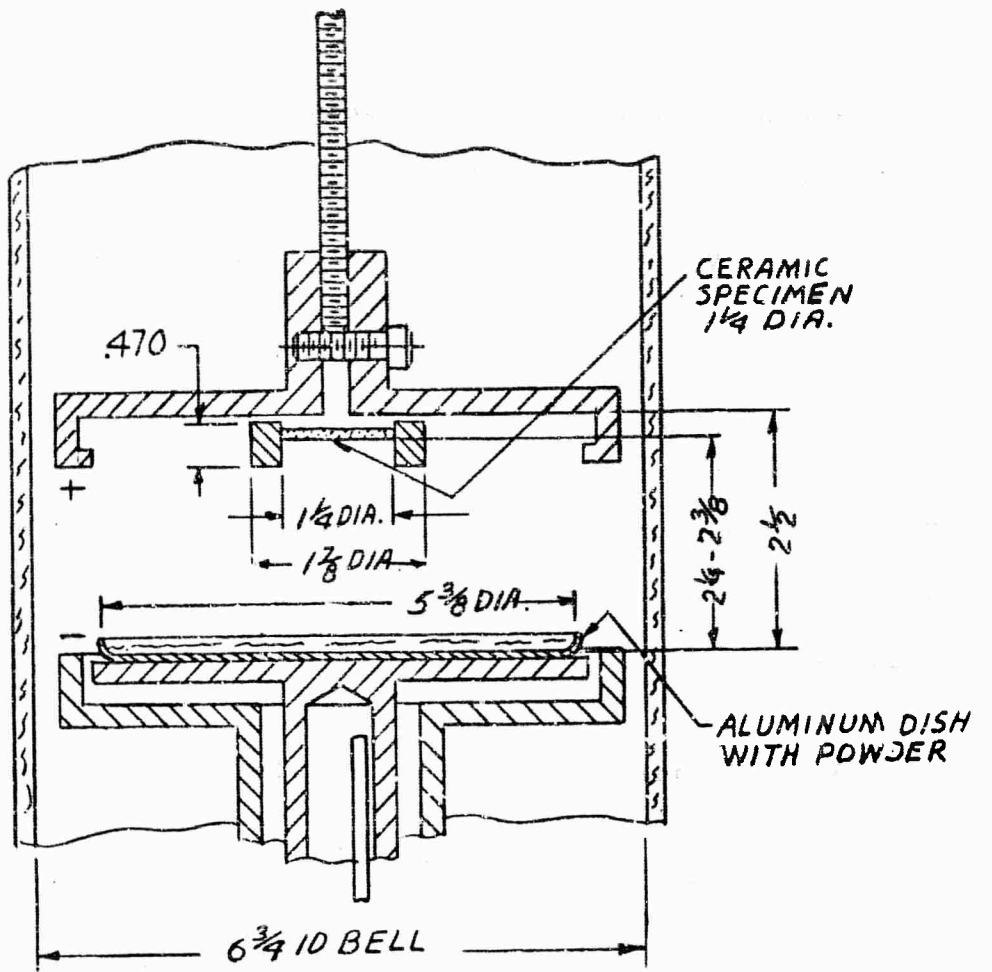


FIGURE-E3 SPUTTERING SET-UP FOR COATING BRAZED  
X-BAND WINDOW ASSEMBLIES

## APPENDIX F

### RESISTANCE BETWEEN TWO PROBES ON THE SURFACE OF A CONDUCTIVE SHEET

The potential anywhere between the two conductive cylinders of Figure F1 is given by:<sup>55</sup>

$$V = \frac{V_0}{2} \left\{ \frac{\ln [(x - p)^2 + y^2] - \ln [(x + p)^2 + y^2]}{\ln [q - r - p]^2 - \ln [q - r + p]^2} \right\} \quad (F1)$$

where  $p = \sqrt{q^2 - r^2}$

The potential function of Eq. F1 remains unchanged if the conductive cylinders of Figure F1 are imbedded in a conductive medium of conductivity  $\sigma$ .

By definition, the current density  $\vec{J}$  is given by:

$$\vec{J} = \sigma \vec{E} \quad (F2)$$

In Eq. F2, the current density  $\vec{J}$  and the electric field  $\vec{E}$  are vectors. The total current  $I$  flowing between the cylinders can be found by integration of Eq. F2 over any continuous surface separating the two cylinders. However, it is advantageous to

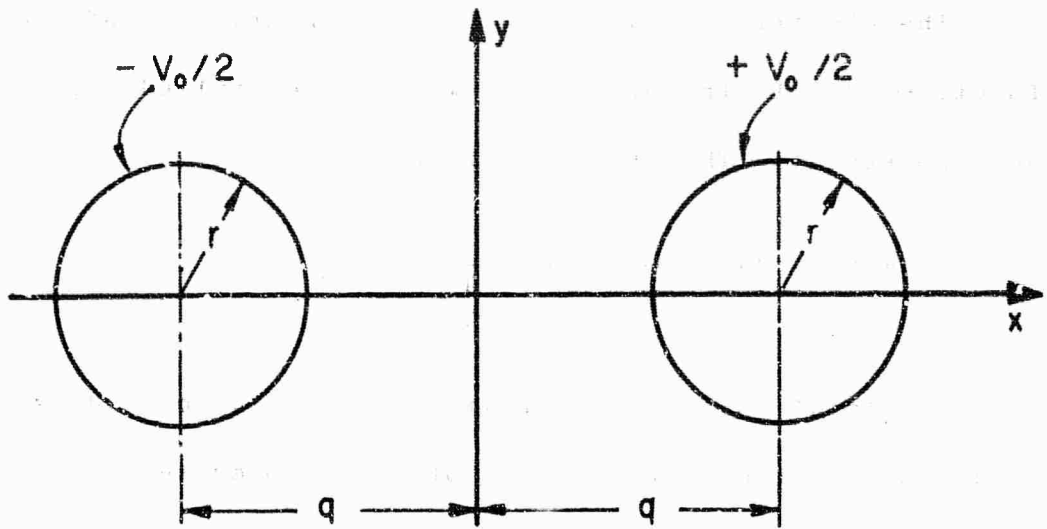


FIGURE F1 TWO PARALLEL CONDUCTING CYLINDERS

confine the integration over some specified plane which can simplify integration. A plane half-way between the cylinders and parallel to the y-axis is one such plane.

The electric field  $\bar{E}$ , defined as a gradient of the potential function  $V$ , in the plane half-way between cylinders, has only an x-component. Therefore, it is given by:

$$E_x(x = 0) = \frac{-pV_0}{(p + y) \ln \frac{q - r + p}{q - r - p}} \quad (F3)$$

The total current  $I$  flowing between the cylinders is equal to  $\sigma$  times the integral of Eq. F3 over the whole plane. Therefore,

$$I = 2\sigma\tau \int_0^{\infty} E_x(x = 0) dy \quad (F4)$$

where  $\tau$  is the thickness of the homogeneous film of conductivity  $\sigma$  (see Figure C1). In Eq. F4, the product  $\sigma\tau$  is equal to the reciprocal of the surface resistivity ( $R$ ) of the conductive film.

Integration of Eq. F4 gives an expression for the resistance between the conductive cylinders. This expression is:

$$\frac{V_0}{I} = \frac{2R}{\pi} \ln \frac{q - r + p}{q - r - p} \quad (F5)$$

With the definition of  $p$ , given in E. F1, Eq. F5 becomes:

$$\frac{V_o}{I} = \frac{R}{\pi} \ln \frac{1 + \sqrt{1 - r^2/q^2}}{1 - \sqrt{1 - r^2/q^2}} \quad (F6)$$

It can be seen that, except for a constant, the resistance measured between the two conductive cylinders is directly proportional to the surface resistivity of the film. For a particular choice of cylinder dimensions and their spacing, the resistance is exactly equal to the surface resistivity of the films. For smaller values of  $r/q$ , Eq. F6 can be simplified to

$$\frac{V_o}{I} = \frac{2k}{\pi} \ln \frac{2q}{r}$$

and the product  $(2/\pi) \ln(2q/r) = 1$  when  $q/r$  is approximately 2.4.

## APPENDIX G

### CALCULATION OF RF ELECTRIC FIELD DISTRIBUTION IN THE SPUTTERING SETUP

The variation in the magnitude of the rf field in the active region of the sputtering setup can be calculated provided two simplifying assumptions are made. First of all, it will be assumed that in the active region of the sputtering setup there is complete space charge neutralization. Second, it will be assumed that the rf coil used for sputtering and shown in Figure G1, is long so that the electromagnetic field induced by the coil within the sputtering region is independent of the longitudinal dimension  $z$ .

Using these assumptions, the two Maxwell curl equations can be simplified. From

$$\nabla \times \vec{H} = \vec{J} \quad (G1)$$

where the magnetic field  $\vec{H}$  and the current density  $\vec{J}$  are vectors, it follows that

$$-\frac{\partial H_z}{\partial r} = J_\theta \quad (G2)$$

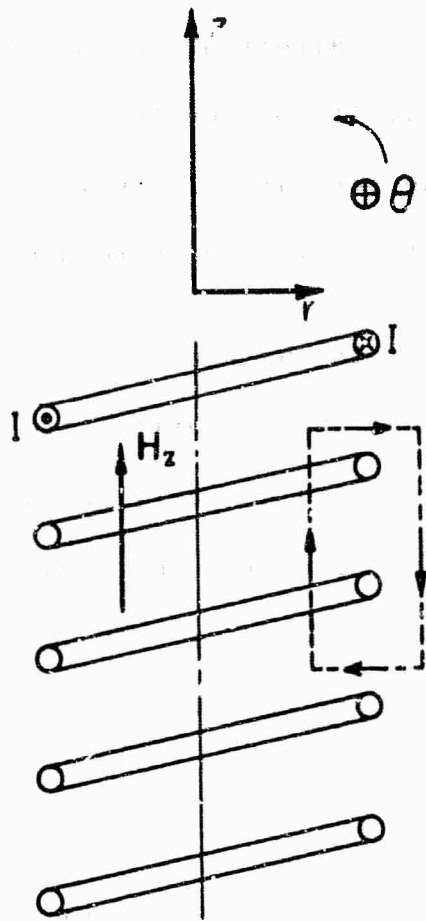


FIGURE 91 A CROSS SECTION VIEW OF THE rf COIL IN THE SPUTTERING APPARATUS

since  $\bar{J}$  is entirely  $\theta$ -directed. From the  $r$ -component of the curl equation (Eq. G1), it follows that  $H_z$  is circularly symmetric, so that the partial differential in Eq. G2 can be treated as a total differential with respect to  $r$ .

A line integral of Eq. G2 around a closed, rectangular loop of Figure G1, shows that the magnetic field induced inside the long rf coil is constant and directly proportional to the rf driving current  $I$  in the coil. The proportionality constant is a function of the coil geometry. The magnetic field within the rf coil can, therefore, be written in the complex form as:

$$H_z = A I e^{j\omega t} \quad (G3)$$

From the second Maxwell curl equation

$$\nabla \times \bar{E} = -\mu_0 \frac{\partial \bar{H}}{\partial t}$$

it follows that

$$\frac{1}{r} \left[ \frac{\partial}{\partial r} (r E_\theta) \right] = -\mu \frac{\partial H_z}{\partial t} = -j\omega \mu A I e^{j\omega t} \quad (G4)$$

where  $\mu$  is the permeability of space. Integration of Eq. G4 gives

$$E_\theta = \frac{j\omega \mu A I}{2} r e^{j\omega t} \quad (G5)$$

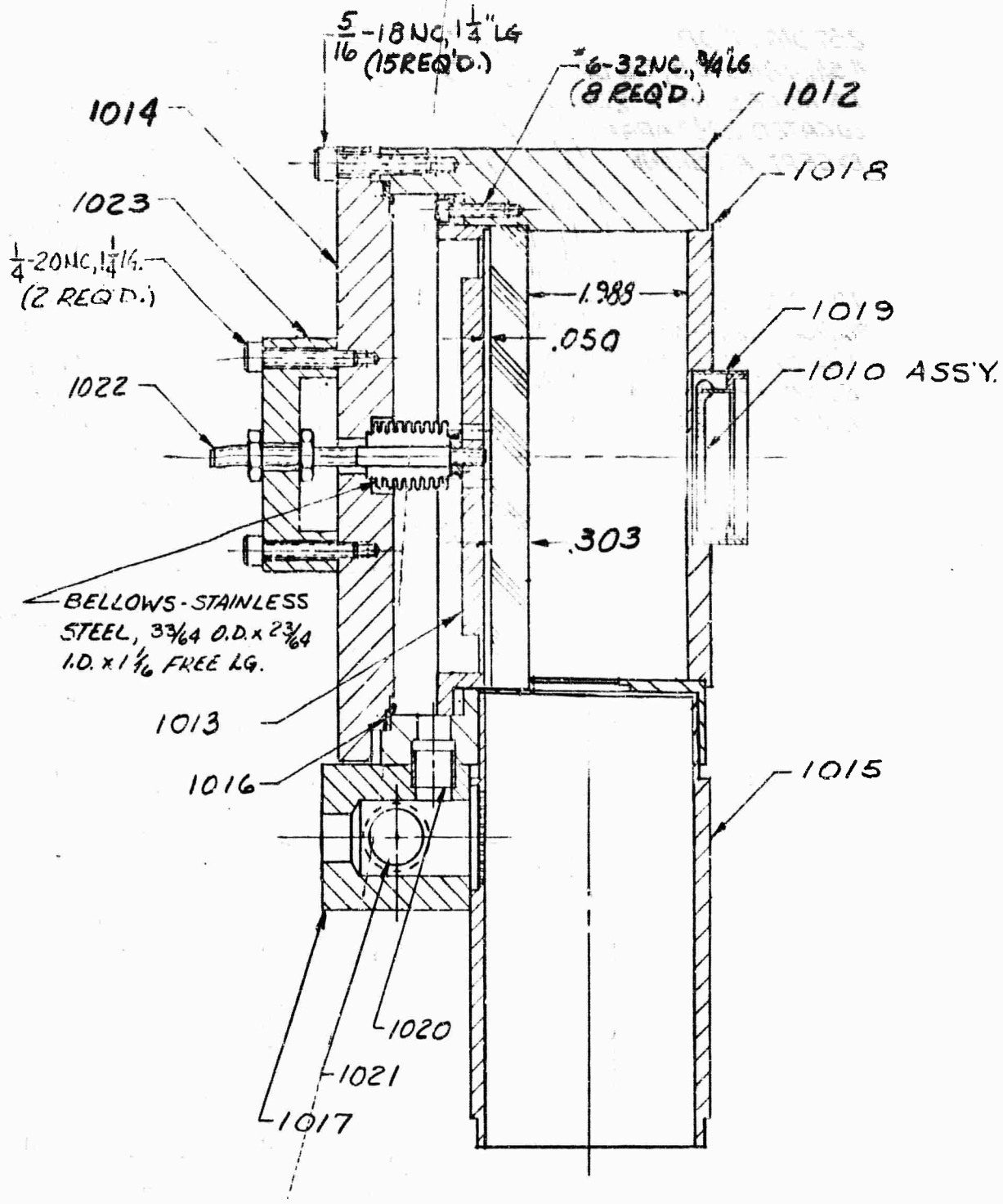
in Eq. G5, the singular solution resulting from the constant of integration was discarded. Eq. G5 shows that the induced rf electric field is directly proportional to radius  $r$ , and is zero at  $r = 0$ . It is also proportional to the applied rf current  $I$  in the coil.

APPENDIX H

DESIGN DRAWINGS FOR THE S-BAND  
MULTIPACTOR CAVITY,  $TE_{011}^o$ -MODE

1011	Final Assembly
1012	Body
1013	Cavity Wall
1014	Lid
1015	Waveguide
1016	Vacuum Gasket
1017	Exhaust Block
1018	Window Plate
1019	Window Frame
1020	Connector
1021	Exhaust Tube
1022	Tuner Screw
1023	Tuner Saddle

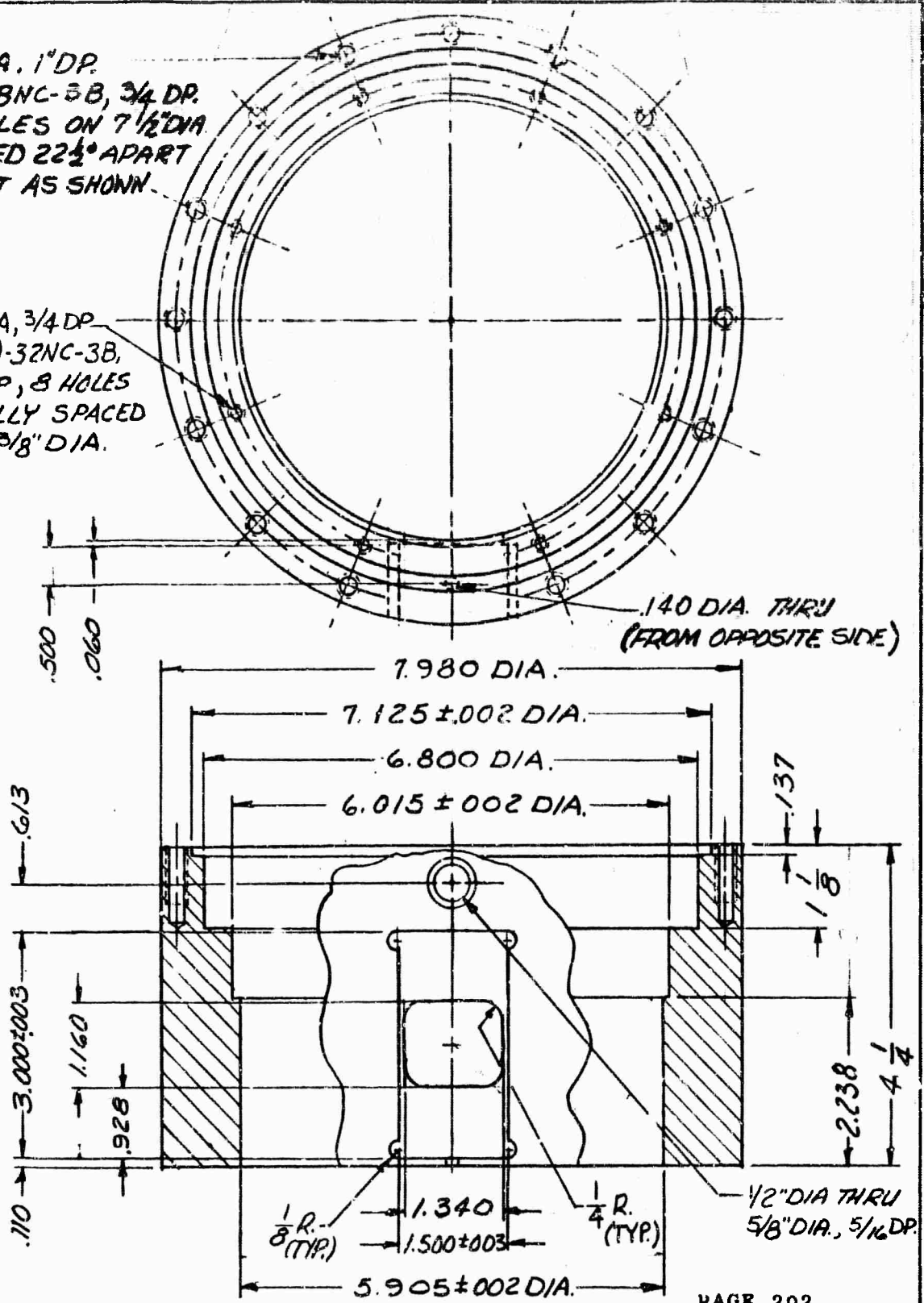
ALL BODY PARTS WERE NICKEL PLATED.



TOLERANCE ON DIMENSIONS NOT OTHERWISE SPECIFIED					SCALE	A. O.	ENGINEERING EXPERIMENTAL SKETCH	
DECI. DIM. $\pm .005$ PRAC. DIM. $\pm 1/64$ ANG. DIM. $\pm 1^\circ$					1/2	J. O.	FINAL ASSEMBLY	
REVISIONS					MAT. SIZE & CODE	USED ON D-SPEC. NO.		
REV. SUBL.	ITEM	CHANGED FROM	DATE	ENGINEER APPROVAL	LENGTH	REFERENCE DRAWING	SPERRY ELECTRONIC TUBE DIVISION OF	
							SPERRY RAND CORPORATION	
							GAINESVILLE, FLA.	
					FINISH		DRYAN BY	DATE
							R.M. CANN 10-4-65	APPROVED BY
							DEPT. NO.	DATE
							1011	
							CLASS "C" DRAWING OR SKETCH NO.	
							REV. SUB-LETTER	

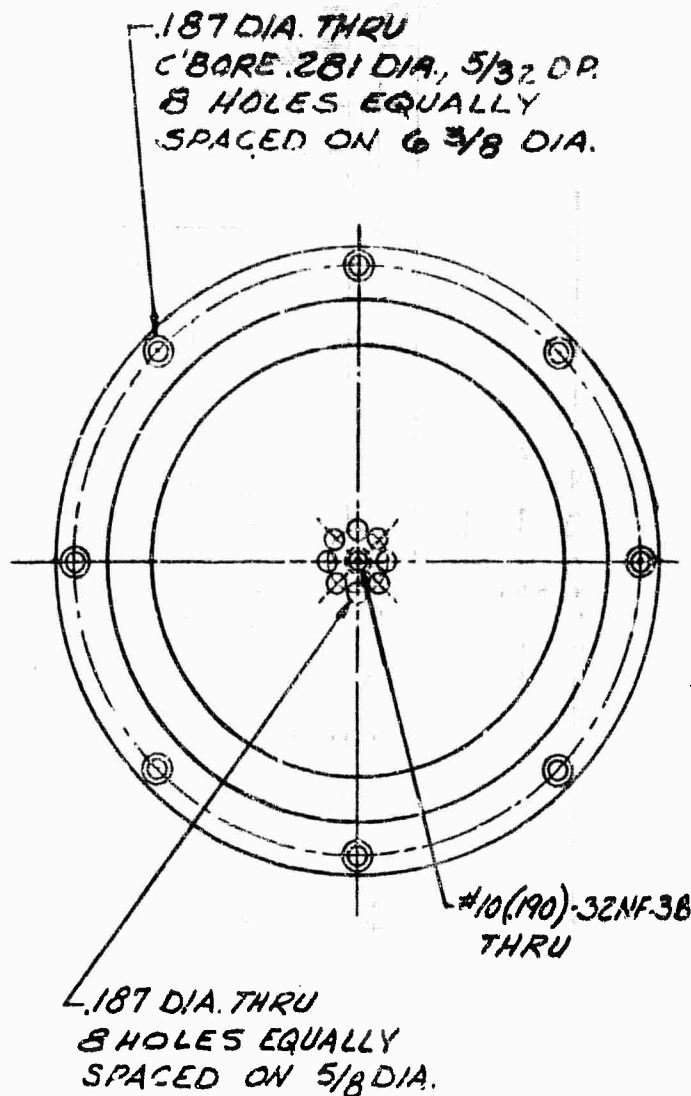
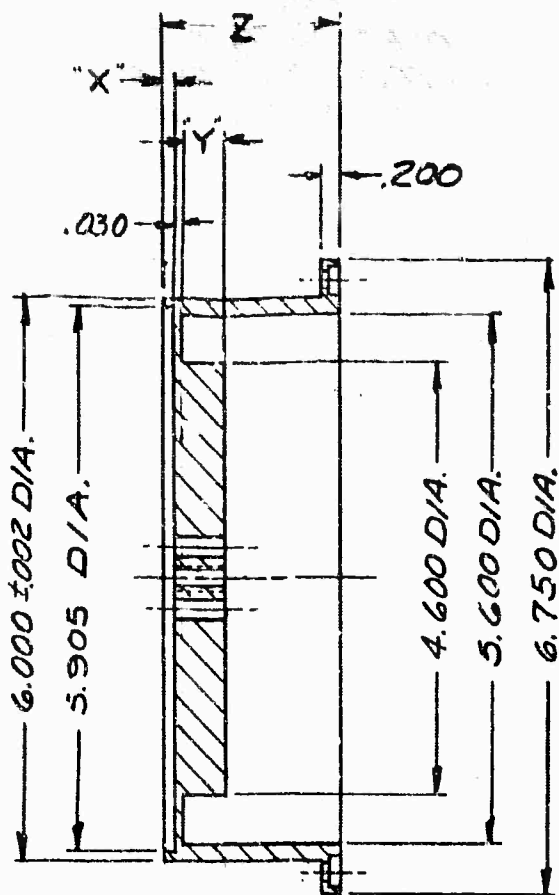
.257 DIA. 1" DP.  
 # 5/16-18NC-3B, 3/4 DP.  
 15 HOLES ON 7 1/2" DIA.  
 LOCATED 22 1/2° APART  
 EXCEPT AS SHOWN.

.106 DIA, 3/4 DP.  
 #6(138)-32NC-3B,  
 5/8 DP, 8 HOLES  
 EQUALLY SPACED  
 ON 6 3/8" DIA.



PAGE 202

TOLERANCE ON DIMENSIONS NOT OTHERWISE SPECIFIED					SCALE	A. O.	ENGINEERING EXPERIMENTAL SKETCH		
DECI. DIM. ± .005 FRACTIONAL DIM. ± 1/64 ANG. DIM. ± 1°					1/2	J. O.	BODY		
REVISONS					MAT. SIZE & COND.	USED ON E-RI EC. NO.			
PREV. SUB-L	ITEM	CHANGED FROM	DATE	ENGINEER APPROVAL	COLD FINISHED CARBON STEEL PER ASTM A108 GRADE 1018 1022 OR 1027	REFERENCE DRAWINGS	SPERRY ELECTRONIC TUBE DIVISION OF SPERRY RAND CORPORATION GAINESVILLE, FLA.		
					LENGTH	11230	P. MCCAIN 9-30-65		
					FINISH		DRAWN BY	DATE	APPROVED BY
							DEPT. NO.	10112	DATE
							CLASS "C" DRAWING OR SKETCH NO.		REV. SUB-LETTER



NOTES:

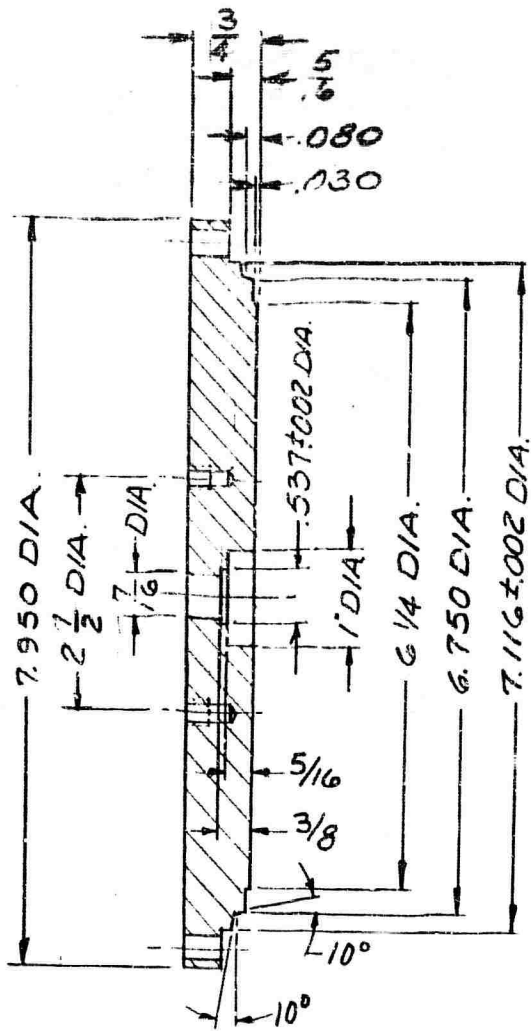
- 1- I DIMENSIONS ARE FOR .303 CERAMIC WINDOW
- 2- II DIMENSIONS ARE FOR .536 QUARTZ WINDOW

	I	II
X	.050	.080
Y	.530	.330
Z	.950	.750

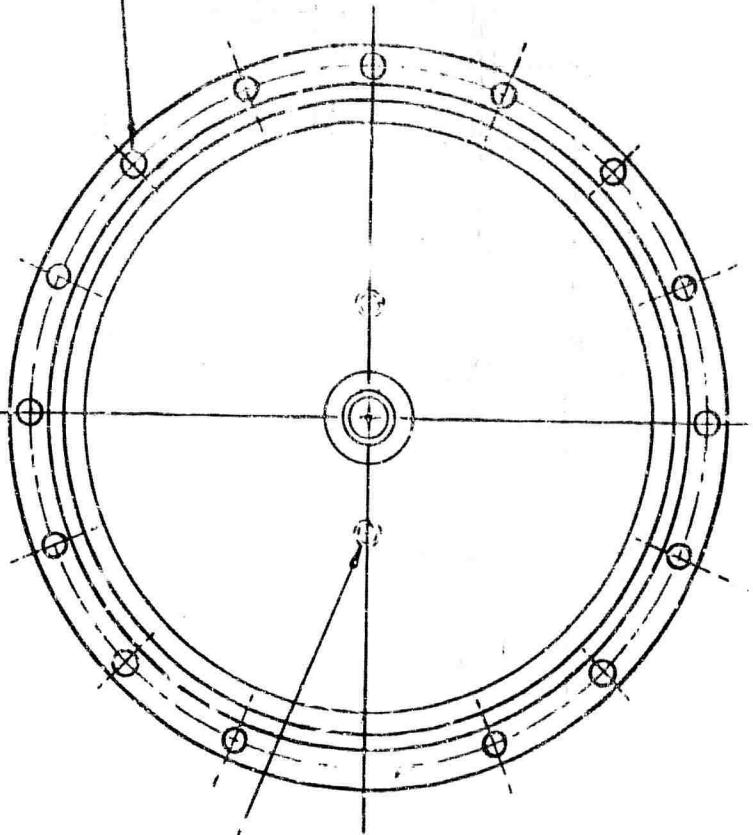
\*COLD FINISHED CARBON STEEL FLAT PER ASTM A108, GRADE 1018, 1020, OR 1022

TOLERANCE ON DIMENSIONS NOT OTHERWISE SPECIFIED				SCALE	A. O.	ENGINEERING EXPERIMENTAL SKETCH	
DEC. DIM. ±.005 PRAC. DIM. ± 1/64 ANG. DIM. ± 1°				N. T. S.	J. C.	CAVITY WALL	
REVISIONS				MAT. SIZE & CODE	USED ON D-SPEC. NO.		
REV.	ITEM	CHANGED FROM	DATE	ENGINEER APPROVAL	SPERRY ELECTRONIC TUBE DIVISION OF SPERRY RAND CORPORATION GAINESVILLE, FLA. RMC CAIN 9-30-65 <i>R. McCain</i> 10-5-65 DRAWN BY DATE APPROVED BY DATE DEPT. NO. 1013 CLASS "C" DRAWING OR SKETCH NO. REV. SUB-LETTER		
				LENGTH	REFERENCE DRAWINGS		
				FINISH	11244		

(10 TO INCH)



9/32 DIA. THRU  
15 HOLES ON 7 1/2" DIA  
LOCATED 22 1/2° APART  
EXCEPT AS SHOWN

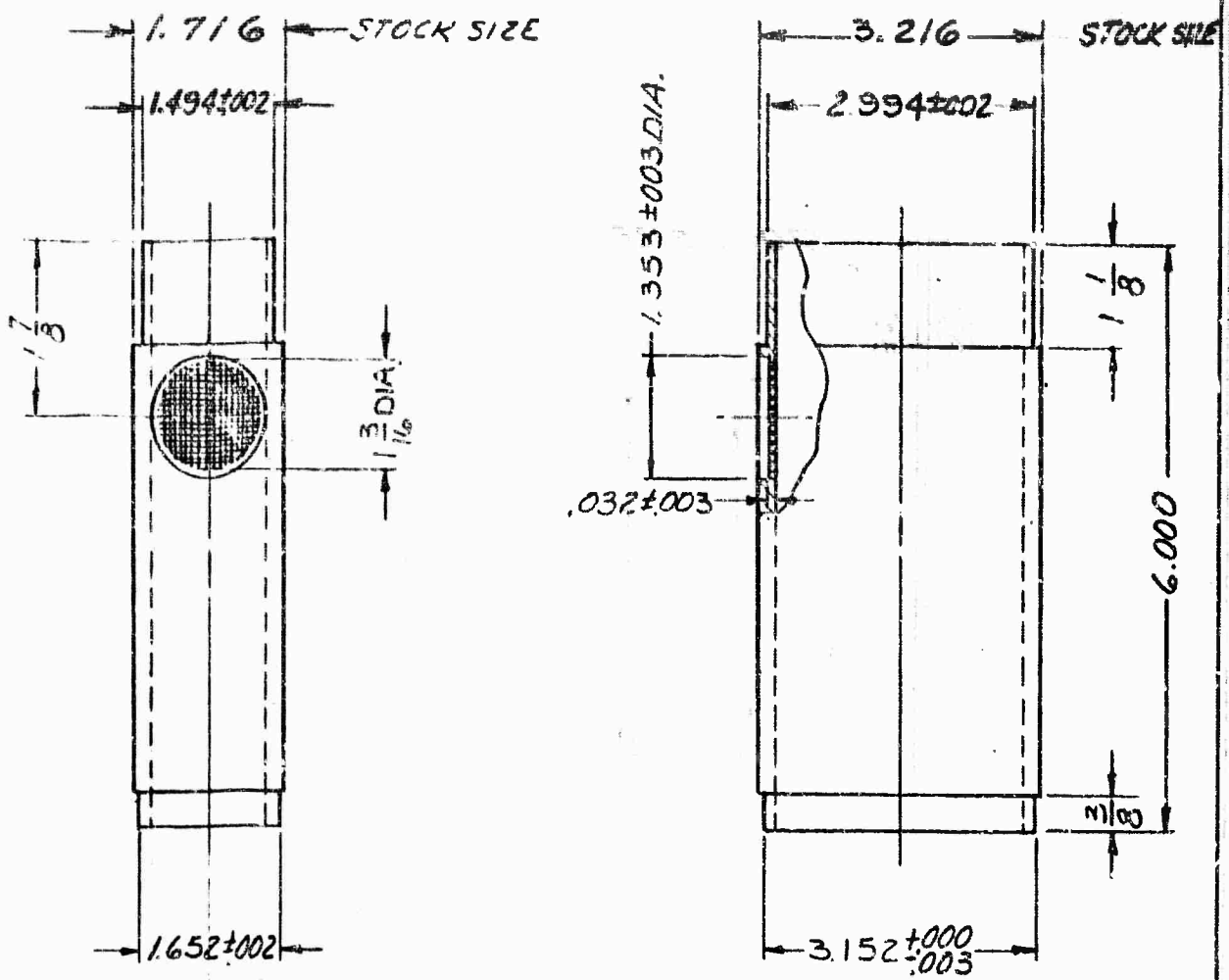


2.01 DIA., 1/2" DP.  
#14-20NC-3B, 3/8" DP  
2 HOLES LOCATED  
AS SHOWN.  
(OPPOSITE SIDE)

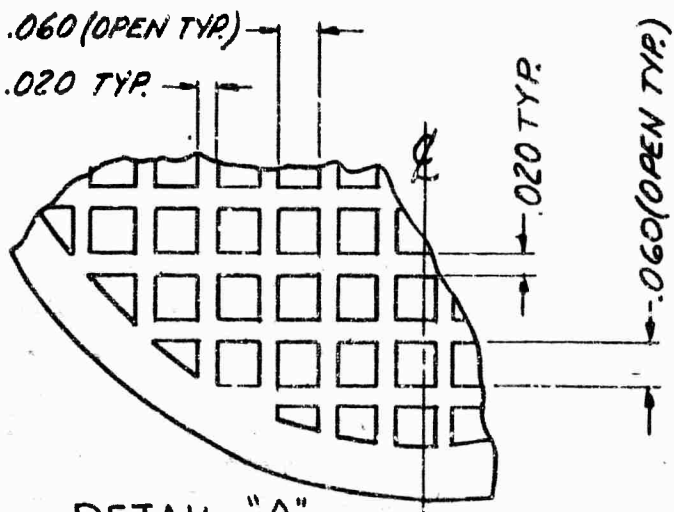
\* 3/4" TH x 8 1/8 x 8 1/8  
COLD FINISHED CARBON  
STEEL FLAT PER ASTM  
A 108, GRADE 1018, 1020  
OR 1022

TOLERANCE ON DIMENSIONS NOT OTHERWISE SPECIFIED DECI. DIM. ±.005 PRAC. DIM. ±1/64 ANG. DIM. ±1°					SCALE 1/2	A. O.	ENGINEERING EXPERIMENTAL SKETCH		
REVISIONS					MAT. SIZE & CODE *	J. O.	LID		
PREV. SUB-L.	ITEM	CHANGED FROM	DATE	ENGINEER APPROVAL	LENGTH	USED ON D-SPEC. NO.	SPERRY ELECTRONIC TUBE DIVISION OF SPERRY RAND CORPORATION GAINESVILLE, FLA.		
					FINISH	REFERENCE DRAWINGS 11243	DRAWN BY R.M.CANN 9-30-65		
							DATE 10-5-65		
							APPROVED BY		
							DEPT. NO. 1014		
							CLASS "C" DRAWING OR SKETCH NO.		
							REV. SUB-LETTER		

(10 TO INCH)

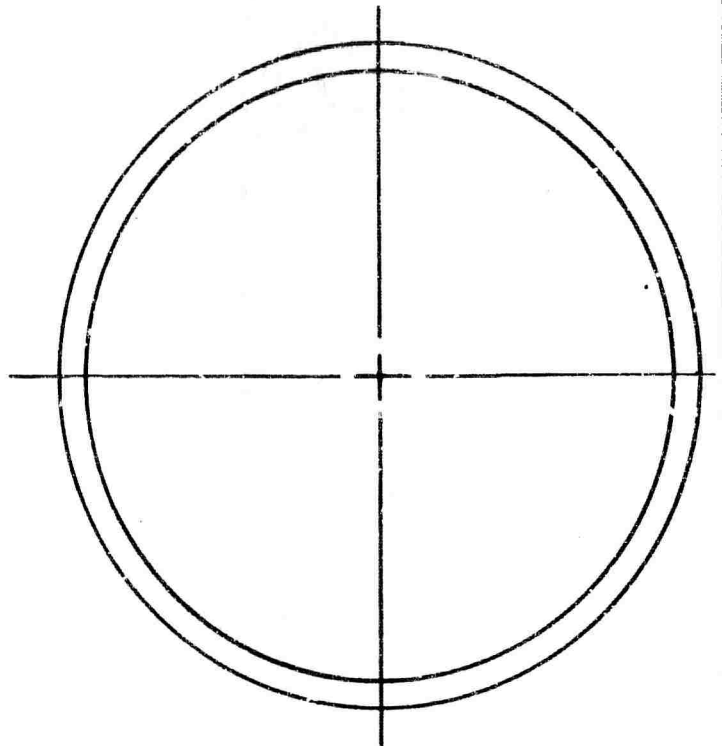
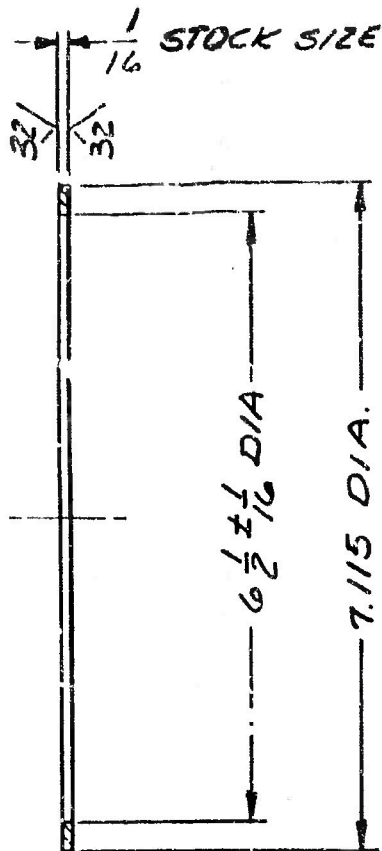


\* 3.216 x 1.716 O.D. x .188 WALL  
 OXYGEN-FREE COPPER  
 RECTANGULAR TUBING



DETAIL "A"  
 SCALE: 4/1 PAGE 205

TOLERANCE ON DIMENSIONS NOT OTHERWISE SPECIFIED					SCALE	A. O.	ENGINEERING EXPERIMENTAL SKETCH		
DECI. DIM. ±.005 FRAC. DIM. ±1/64 ANG. DIM. ~					1/2	J. O.	WAVEGUIDE		
REVISIONS					MAT. SIZE & CODE	USED ON D-SPEC. NO.			
PREV. SUB-L.	ITEM	CHANGED FROM	DATE	ENGINEER APPROVAL	*	REFERENCE DRAWINGS	SPERRY ELECTRONIC TUBE DIVISION OF		
					LENGTH	11231	SPERRY RAND CORPORATION		
					FINISH		GAINESVILLE, FLA.		
							DRAWN BY R. McCain 9-30-65 DATE 10-5-65		
							APPROVED BY DATE		
							DEPT. NO. 1015		
							CLASS "C" DRAWING OR SKETCH NO. REV. SUB-LETTER		

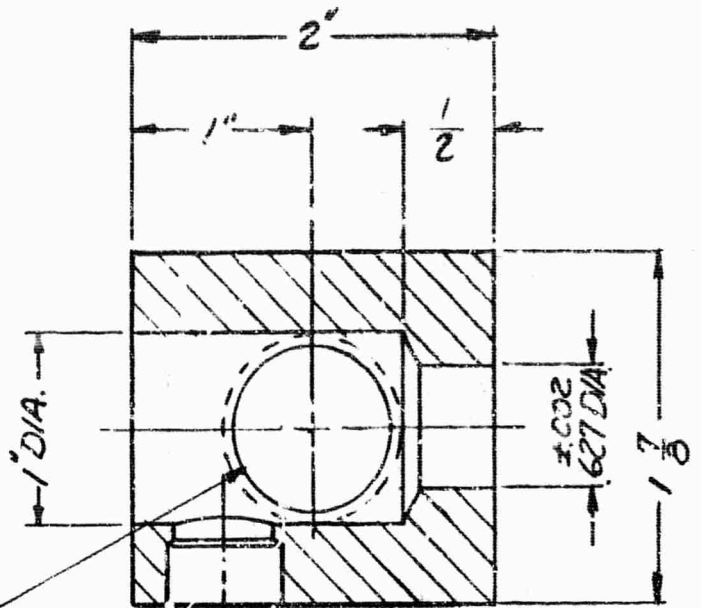
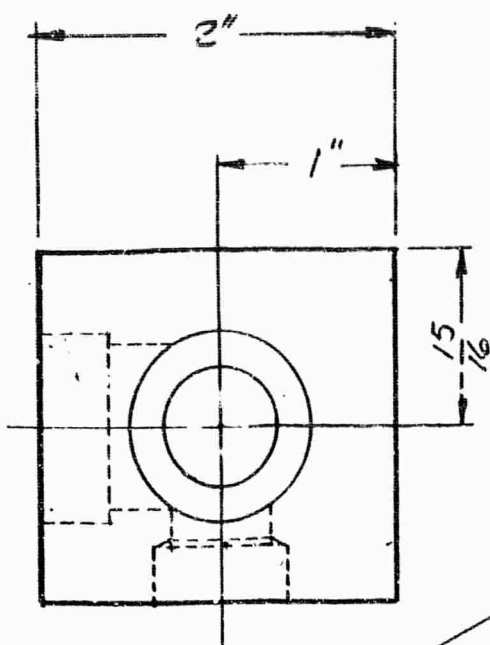


\*  $1/16$ " x  $7\ 3/8$  x  $7\ 3/8$   
 OXYGEN-FREE COPPER STRIP  
 HALF-HARD TEMPER PER  
 ASTM B 152, TYPE O.F.  
 EMBRITTLEMENT TEST (SEC. 12)  
 WILL APPLY. PHOSPHOROUS  
 CONTENT 0.0003% MAX.

PAGE 206

TOLERANCE ON DIMENSIONS NOT OTHERWISE SPECIFIED				SCALE	A. D.	ENGINEERING EXPERIMENTAL SKETCH	
DECI. DIG. $\pm 005$ FRAC. LIG. ~ ANG. DIM. ~				$1/2$		VACUUM GASKET	
REVISIONS				MAT. SIZE & QUOTE			
PREV. SUB-L.	ITEM	CHANGED FROM	DATE	ENGINEER APPROVAL			
						SPERRY ELECTRONIC TUBE DIVISION OF SPERRY RAND CORPORATION GAINESVILLE, FLA.	
					REFRESHED DRAWING	DATE	
					11238	DRAWN BY RALPHAIN 7-29-65 DATE 10-5-65	
					FINISH	DEPT. NO.	APPROVED BY
					VH <sub>2</sub> -900°	1016	B. Winters
						CLASS "C" DRAWING OR SKETCH NO.	REV. SUB-LETTER

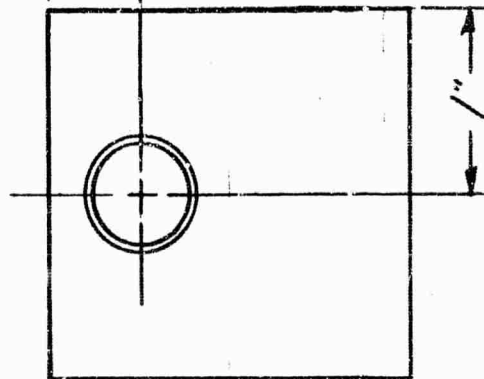
(10 TO INCH)



7/8" DIA. THRU  
1" DIA., 3/8" DP.

±.002  
502

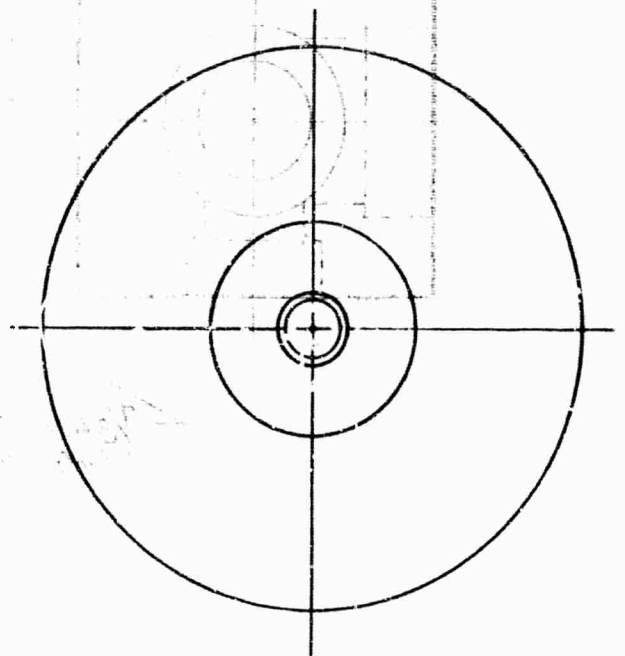
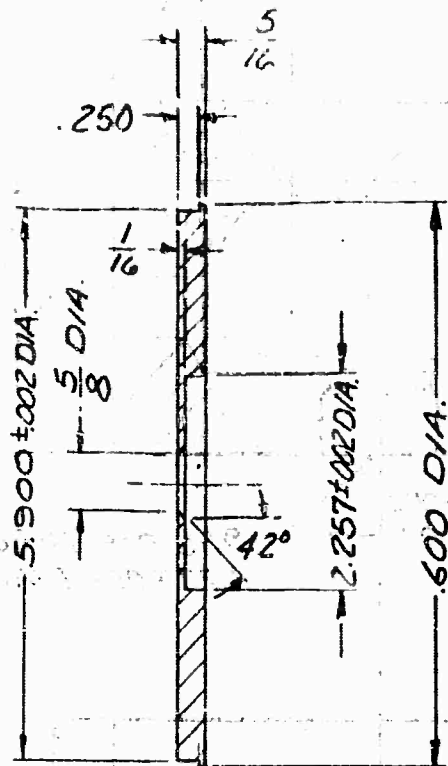
9/16 DIA. THRU  
.627 ±.002 D.A., 5/16 DP.



\* 2" SQUARE  
COLD FINISHED CARBON  
STEEL SQUARE PER  
ASTM A 108, GRADE 1018,  
1020 OR 1022

PAGE 207

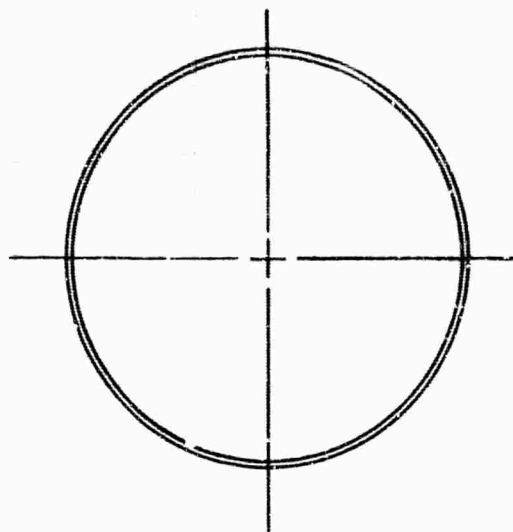
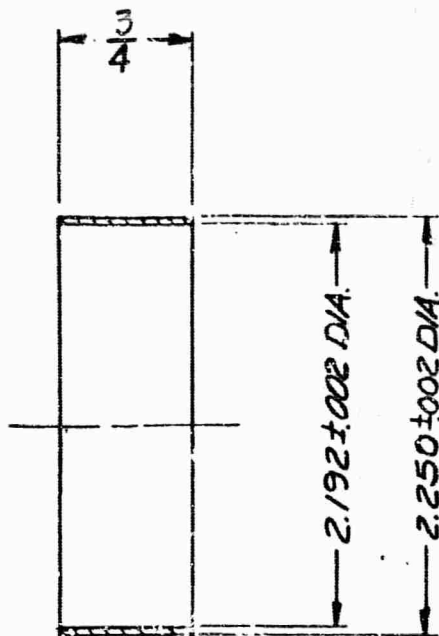
TOLERANCE ON DIMENSIONS NOT OTHERWISE SPECIFIED					SCALE	A. O.	ENGINEERING EXPERIMENTAL SKETCH			
DEC. DIM. ±.005 PRAC. DIM. ± 1/64 ANG. DIM. ~					1/1	J. G.	EXHAUST BLOCK			
REVISIONS					MAT. SIZE & CODE	USED ON D-SPEC. NO.				
PREV. SUB-L.	ITEM	CHANGED FROM	DATE	ENGINEER APPROVAL	*	SPERRY ELECTRONIC, USE DIVISION OF SPERRY RAND CORPORATION GAINESVILLE, FLA.				
					LENGTH	REFERENCE DRAWINGS	R. MCCAIN 9-30-65 B. HINTON 10-5-65			
					FINISH	11232	DRAWN BY	DATE	APPROVED BY	DATE
							DEPT. NO.	1.017		
							CLASS "E" DRAWING OR SKETCH NO.		REV. SUB-LETTER	



\* 5/16" TH x 6 1/4 x 6 1/4  
 COLD FINISHED CARBON  
 STEEL FLAT PER ASTM  
 A 108, GRADE 1018, 1020 OR  
 1022.

PAGE 208

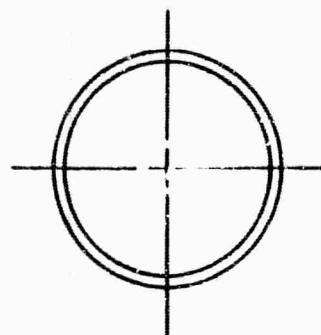
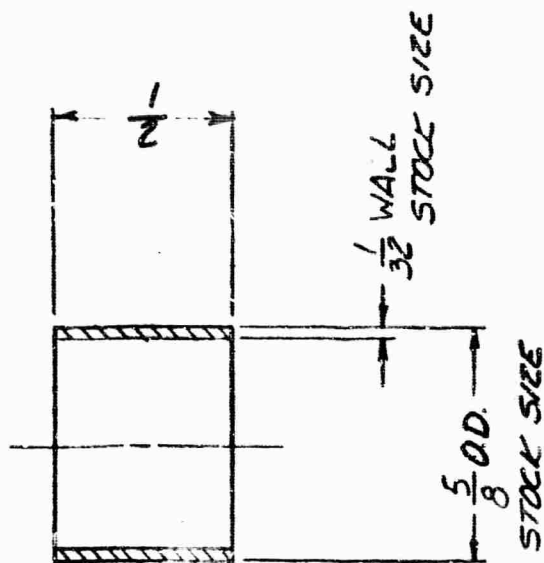
TOLERANCES ON DIMENSIONS NOT OTHERWISE SPECIFIED				SCALE	A. O.	ENGINEERING EXPERIMENTAL SKETCH	
DECI. DIM. ± .005				1/2	J. O.	WINDOW PLATE	
FRAC. DIM. ± 1/64				MAT. SIZE & CODE	USED ON D-SPEC. NO.		
ANG. DIM. ± 1°				* LENGTH FINISH	REFERENCE DRAWINGS		
REVISIONS					11242		
PREV. SUB-L.	ITEM	CHANGED FROM	DATE		ENGINEER APPROVAL	SPERRY ELECTRONIC TUBE DIVISION OF SPERRY RAND CORPORATION GAINESVILLE, FLA.	
					DRAWN BY R. McCain 9-29-65		
					DATE 10-5-65		
					DEPT. NO.	1018	REV. SUB-LETTER
CLASS OF DRAWING OR DETACH M.						REV. SUB-LETTER	



\* 2 1/4" O.D. x .065 WALL x 1' Lg.  
 COLD DRAWN & STRESS RELIEVED  
 LOW CARBON SEAMLESS STEEL  
 TUBING PER FED. SPEC. QQ-T-830A,  
 TYPE MT1015. HARDNESS TO BE  
 ROCKWELL "B" 65 TO 90

PAGE 209

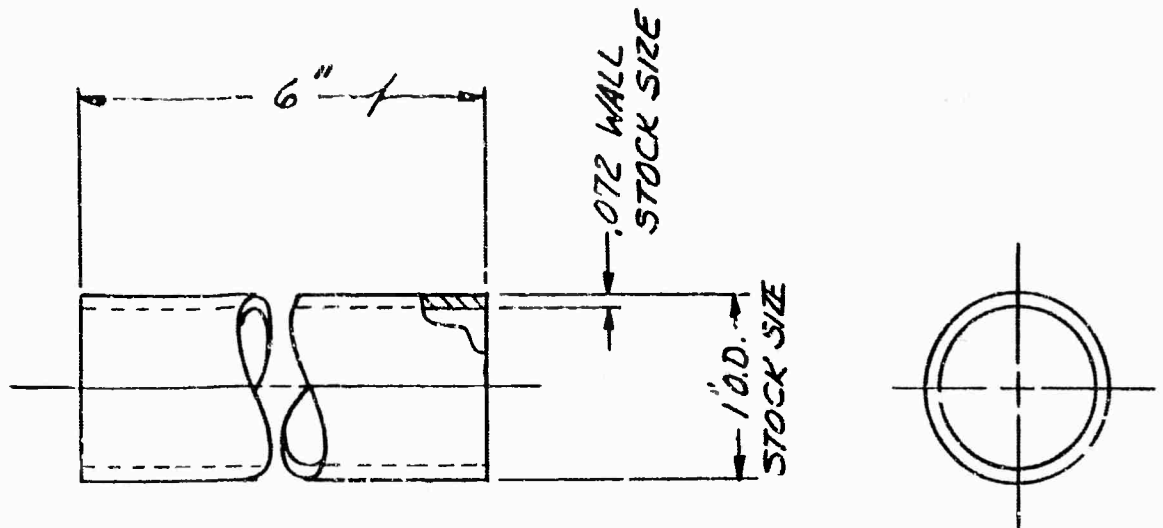
TOLERANCE ON DIMENSIONS NOT OTHERWISE SPECIFIED					SCALE	A. O.	ENGINEERING EXPERIMENTAL SKETCH	
DECI. DIM. ~		FRA. DIM. ± 1/64		ANG. DIM. ~		V/V		
REVISED					MAT. SIZE & CODE	J. O.	WINDOW FRAME	
PREV. SUB-1	ITEM	CHANGED FROM	DATE	ENGINEER APPROVAL	*	USED ON D-SPEC. NO.		
						REFERENCE DRAWINGS		
						11228		
					LENGTH	DRAWN BY		DATE
					FINISH	R. MCCAW 9-29-65		APPROVED BY
						B. Winters 10-5-65		DATE
						DEPT. NO.		DATE
						1019		DATE
					CLASS "C" DRAWING ON SKETCH NO.			REV. SUB-LETTER



\* 5/8" O.D. x 1/32" WALL x 3/4" L.  
 OXYGEN FREE COPPER SEAMLESS  
 TUBING, HARD DRAWN TEMPER PER  
 ASTM B 75, TYPE O.F. EMBRITTLEMENT  
 TEST (SEC. 13) WILL APPLY. PHOSPHOROUS  
 CONTENT 0.0003% MAX.

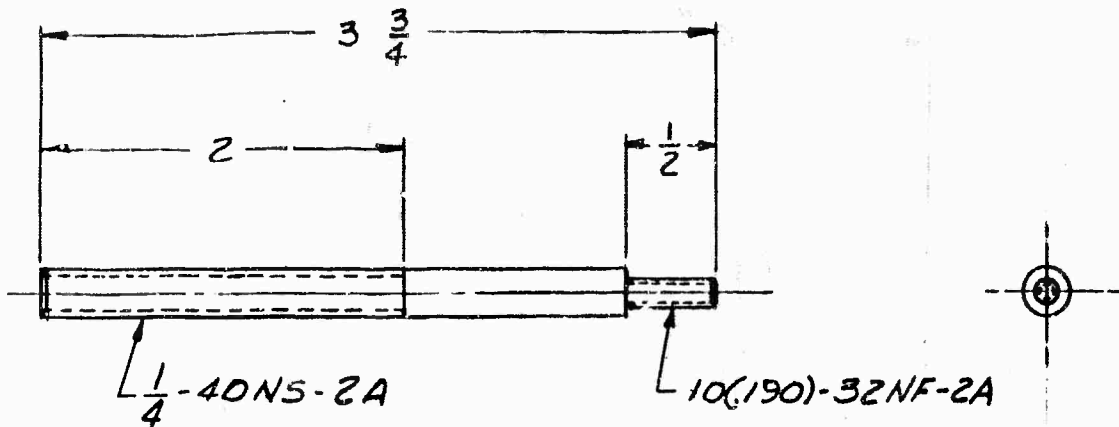
PAGE 210

TOLERANCE ON DIMENSIONS NOT OTHERWISE SPECIFIED				SCALE	A. O.	ENGINEERING EXPERIMENTAL SKETCH	
DE' L. DIM. ~		FRAC. DIM. ±1/64 ANG. DIM. ~		2/1	J. O.	CONNECTOR	
REVISIONS				MAT. SIZE & CODE	USED ON D-SPEC. NO.		
PREV. SUB-L.	ITEM	CHANGED FROM	DATE	ENGINEER APPROVAL	SPERRY ELECTRONIC TUBE DIVISION OF SPERRY RAND CORPORATION GAINESVILLE, FLA. R. McCain 9-29-65 B. Winters 10-5-65 DRAWN BY DATE APPROVED BY DATE DEPT. NO. 1020		
				*			
				LENGTH			
				FINISH			
				REFERENCE DRAWINGS	CLASS "C" DRAWING OR SKETCH NO. REV. SUB-LETTER		
				11245			



\* 1" O.D. x .072 WALL  
 COLD DRAWN & STRESS RELIEVED  
 LOW CARBON SEAMLESS STEEL  
 TUBING PER FED. SPEC. QQ-T-830A,  
 TYPE MT1015. HARDNESS TO BE  
 ROCKWELL "B" 65 TO 90.

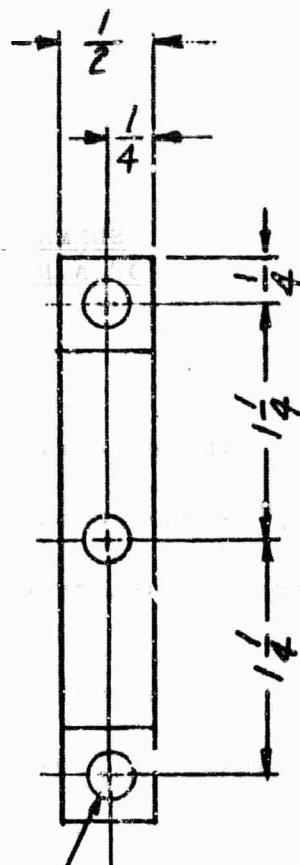
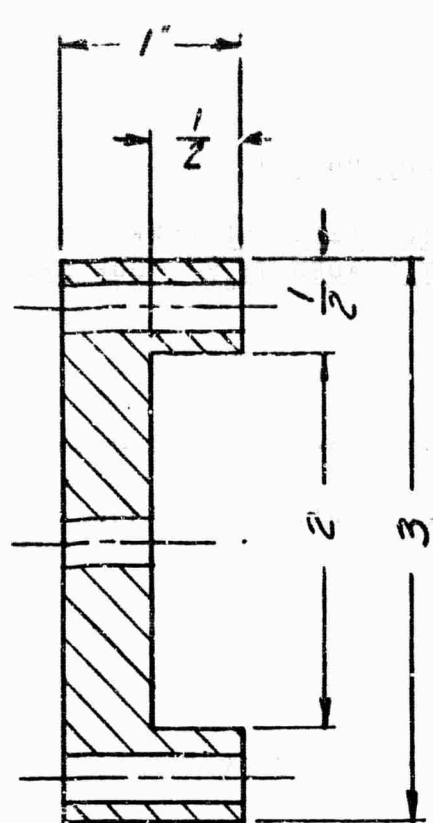
TOLERANCE ON DIMENSIONS NOT OTHERWISE SPECIFIED					SCALE	A. O.	ENGINEERING EXPERIMENTAL SKETCH	
DECI. DIM. ~		FRAC. DIM. ± 1/64		ANS. DIM. ~		1/1	EXHAUST TUBE	
REVISONS					MAT. SIZ. & CODE	USED ON D-SPEC. NO.		
PREV. SUB-L	ITEM	CHANGED FROM	DATE	ENGINEER APPROVAL	*	SPERRY ELECTRONIC TUBE DIVISION OF SPERRY RAND CORPORATION GAINESVILLE, FLA.		
					LEN. STR	REFERENCE DRAWINGS	K.McCANN 9-29-65 @ W. H. 10-5-65	
					FINISH	11241	DRAWN BY	DATE APPROVED BY
							DEPT. NO.	1021
							CLASS "C" DRAWING OR SKETCH NO.	
							REV. SUB-LETTER	



\* COLD-FINISHED AND ANNEALED  
 STAINLESS STEEL ROUND,  
 TYPE 416, PER ASTM A-276

PAGE 212

TOLERANCE ON DIMENSIONS NOT OTHERWISE SPECIFIED				SCALE	A. C.	ENGINEERING EXPERIMENTAL SKETCH		
DECI. DIM. ~ FRAS. DIM. ± 1/64 ANG. DIM. ~				1/1	J. C.	TUNER SCREW		
REVISIONS				MAT. SIZE & CODE	USED ON D-SPK. NO.		SPERRY ELECTRONIC TUBE DIVISION OF SPERRY RAND CORPORATION GAINESVILLE, FLA. RMCCAIN 9-29-65 <i>B. Winters</i> 10-5-65 DRAWN BY DATE APPROVED BY DATE	
PREV. SUB-L.	ITEM	CHANGED FROM	DATE	ENGINEER APPROVAL	REFERENCE DRAWINGS	DEPT. NO.		
					11234	1022		
					LENGTH	CLASS "C" DRAWING OR SKETCH NO.		
					FINISH	REV. SUB-LETTER		



.281 DIA. THRU  
3 HOLES

\* 1/2" TH. x 1 1/8 x 3 1/8  
COLD FINISHED CARBON  
STEEL FLAT PER ASTM A108,  
GRADE 1018, 1020 OR 1022

PAGE 213

TOLERANCE ON DIMENSIONS NOT OTHERWISE SPECIFIED				SCALE	A. O.	ENGINEERING EXPERIMENTAL SKETCH	
DEC. DIM. $\pm .005$ FRACTIONAL DIM. $\pm 1/64$ ANG. DIM. $\sim$				1/1	J. O.	TUNER SADDLE	
REVISIONS				MAT. SIZE & CODE	USED ON D-SPEC. NO.		
PREV. SUB.	ITEM	CHANGED FROM	DATE	ENGINEER APPROVAL	SPERRY ELECTRONIC TUBE DIVISION OF SPERRY RAND CORPORATION GAINESVILLE, FLA.		
				*	DRAWN BY <u>E. MCCAIN</u> 9-30-65 @ <u>Winters</u> 10-5-65		
				LENGTH	REFERENCE DRAWING	DATE	APPROVED BY
				FINISH		1023	
CLASS "C" DRAWING OR SKETCH NO.						REV. SUB-LETTER	

APPENDIX I

SUMMARY OF ELECTRIC FIELD AND POWER RELATIONS  
OF A DIELECTRICALLY LOADED TE<sub>011</sub><sup>0</sup>-MODE RESONATOR

The electric field expressions for an asymmetrically loaded TE<sub>011</sub><sup>0</sup>-mode resonator have been derived previously.<sup>56</sup> This Appendix gives a summary of these results.

In the multipactor test cavity, the schematic representation of which is shown in Figure 11, the electric field in the three regions of the cavity is:

$$E_{\theta s_1} = AJ'_0 \left( \frac{\chi'_{01} r}{r_c} \right) \sin \kappa z, \quad 0 \leq z \leq s_1 \quad (11)$$

$$E_{\theta d} = BJ'_0 \left( \frac{\chi'_{01} r}{r_0} \right) \cos \kappa_c (s_1 + d - z), \quad s_1 \leq z \leq (s_1 + d) \quad (12)$$

$$E_{\theta s_2} = CJ'_0 \left( \frac{\chi'_{01} r}{r_0} \right) \cos \kappa (z - s_1 - d), \quad (s_1 + d) \leq z \leq (s_1 + d + s_2) \quad (13)$$

For the definition of terms, see the list of symbols at the end of this report.

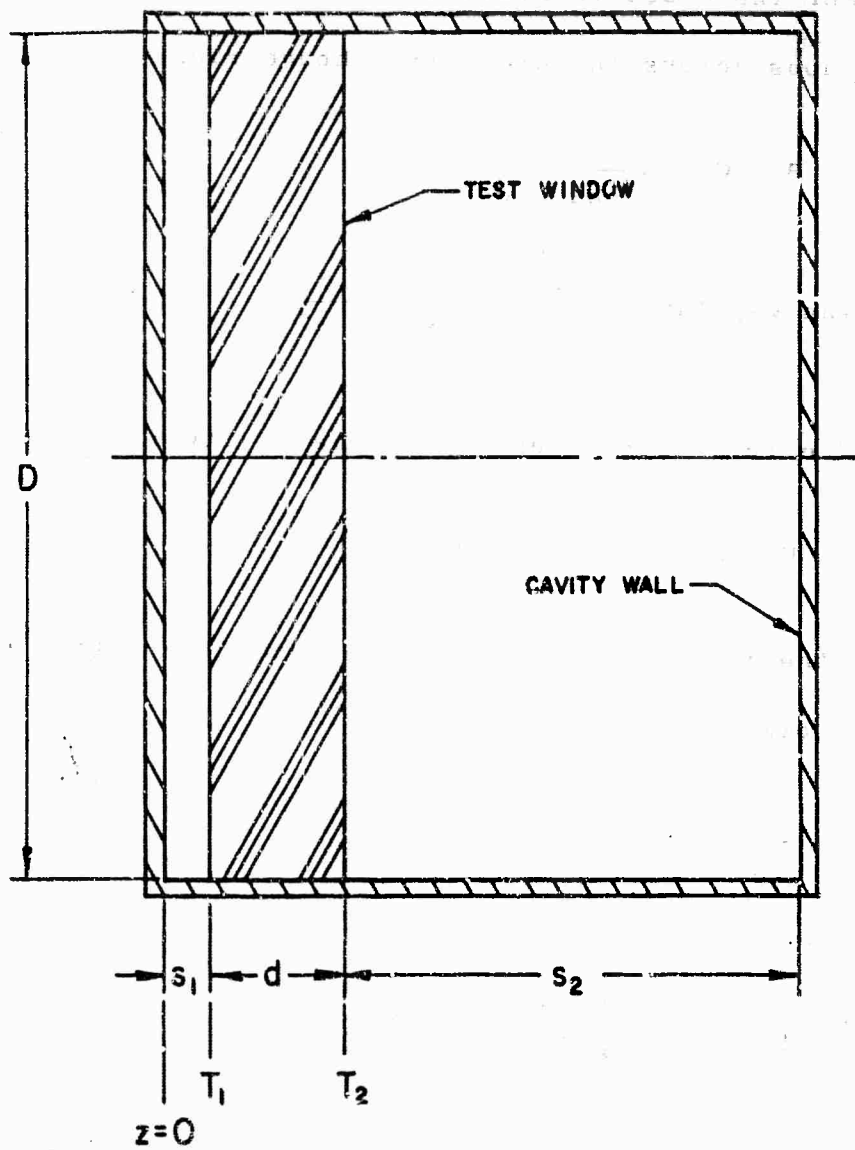


FIGURE 11 SCHEMATIC OF TEST CAVITY WITH AN OFF-CENTER DIELECTRIC DISC

For the electric field and its first derivatives to be continuous across the dielectric boundaries

$$E = C = A \frac{\sin \kappa s_1}{\cos \kappa_\epsilon d} \quad (14)$$

$$\text{and } \tan \kappa s_1 \tan \kappa_\epsilon d = \frac{\kappa}{\kappa_\epsilon} = \sqrt{\frac{1 - v^2}{\epsilon' - v^2}} \quad (15)$$

The total stored energy in the cavity is given by

$$U = \iiint \frac{\epsilon}{2} |E_\theta|^2 du, \quad (16)$$

where the integration is performed over the entire cavity volume.

It follows that

$$U = .0406 \pi \epsilon_0 r_0^2 B^2 F \quad (17)$$

where

$$F = \frac{\cos^2 \kappa_\epsilon d}{\sin^2 \kappa s_1} \left[ 1 - \frac{\sin 2\kappa s_1}{2\kappa s_1} \right] + \epsilon' d \left[ \frac{\sin 2\kappa_\epsilon d}{2\kappa_\epsilon d} \right] + s_2 \left[ 1 + \frac{\sin 2\kappa s_2}{2\kappa s_2} \right] \quad (18)$$

Using the definition of the internal Q of the cavity and the relationship

$$P_i = \frac{(1 + \beta)^2}{4\beta} P_d \quad (19)$$

the modulus of the electric field strength, given in Eq. 17, becomes:

$$B = \frac{86.8 \beta}{D(1 + \beta)} \sqrt{\frac{P_1 Q_e \lambda_0}{F}}$$

The maximum of the electric field on the surface of the window occurs at

$$r_{\max} = .4804 r_0$$

so that

$$J'_0 \left( \frac{\chi'_{01} r_{\max}}{r_0} \right) = .582 ,$$

and

$$E_{\theta \max} = \frac{50.51 \beta}{D(1 + \beta)} \sqrt{\frac{P_1 Q_e \lambda_0}{F}} \quad (110)$$

where  $F$  is given by Eq. 18.

In an experiment with an uncoated alumina window at S-band (Experiment #2, Table 1, p. 88), arcing at the window was observed when the incident power was 5.6 MW. The VSWR at this power level (shortly before arcing) was 5.0 to 1, and the cavity was still undercoupled. The initial change in VSWR for this run is given in Figure A1 of Appendix A. The cold-test loaded  $Q$  of the cavity was 1030 and a VSWR at resonance of 1.2 to 1 (undercoupled).

Therefore, the external Q in this experiment was 2270.

The diameter of the S-band multipactor cavity was 15 cm and the geometric factor F, given by Eq. 18, was found to be 13.4 cm. With this value of incident power and the cavity parameters,  $E_{\max}$  at 2858 Mc was found to be equal to:

$$E_{\theta} = \frac{50.51}{15 \times 6} 10^5 = 56 \text{ kv/cm}$$

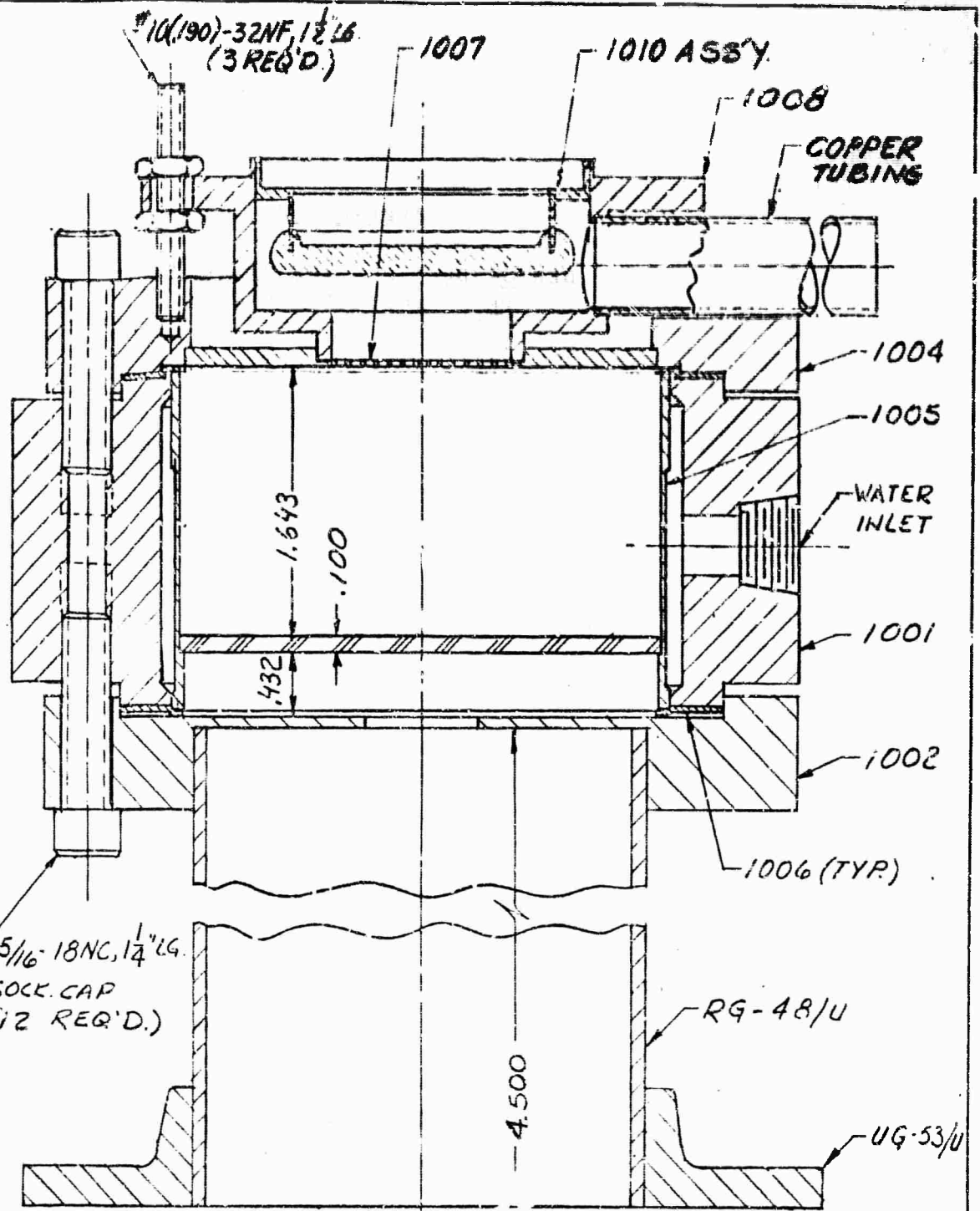
At X-band, the loaded Q of multipactor test cavities was about 500. The diameter of the test cavity was 5.07 cm. The geometric factor F, for the multipactor cavity loaded with an AL-995 alumina window, was 4.08 cm at 8915 Mc.

APPENDIX J

DESIGN DRAWINGS FOR THE S-BAND,  
TE<sub>101</sub>-MODE TEST CAVITY

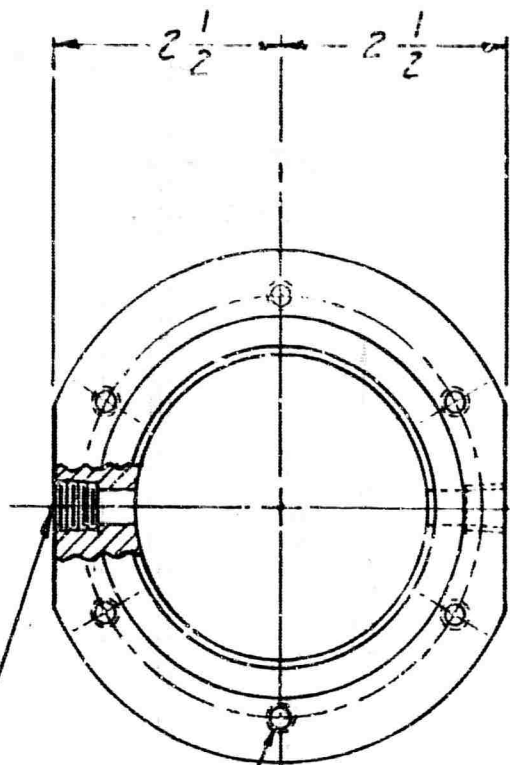
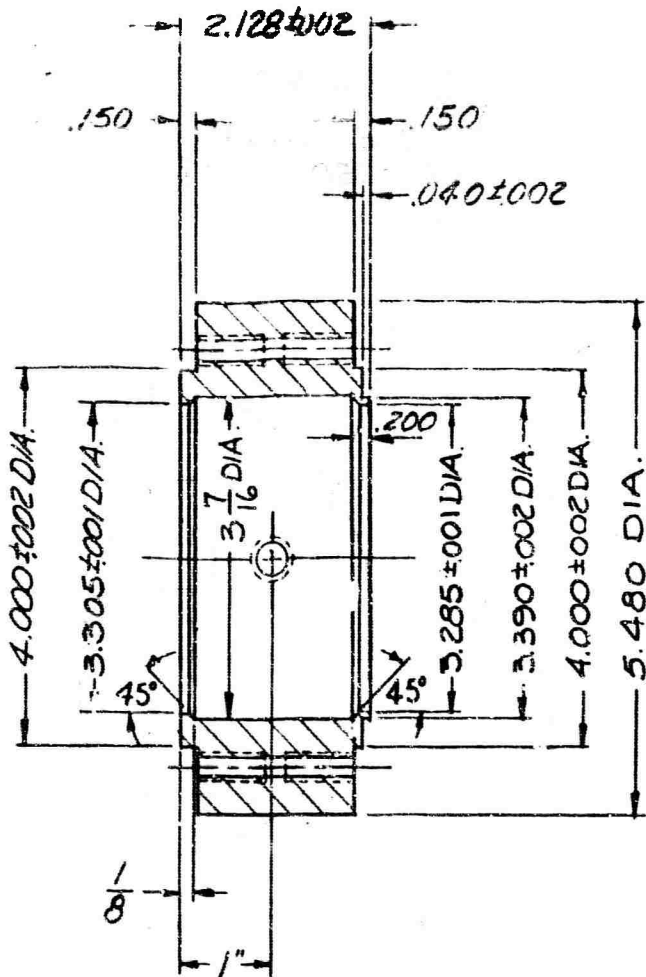
1000	Final Assembly
1001	Body
1002	Back Cover
1003	Flange, Window
1004	Flange, Tuner
1005	Window Sleeve
1006	Gasket
1007	Diaphragm
1008	Cup, Tuner
1009	Window Core
1010	Window Assembly

ALL BODY PARTS WERE NICKEL PLATED.



PAGE 220

TOLERANCE ON DIMENSIONS NOT OTHERWISE SPECIFIED					SCALE	A. O.	ENGINEERING EXPERIMENTAL SKETCH		
DECI. DIM. $\pm 1/64$ FRACTIONAL DIM. $\pm .005$ ANG. DIM. $\pm 1^\circ$					1/1	J. O.	FINAL ASSEMBLY		
REVISIONS					MAT. SIZE & CODE	USED ON D-SPEC. NO.			
REV. NO.	ITEM	CHANGED FROM	DATE	ENGINEER APPROVAL		REFERENCE DRAWINGS			
					LENGTH	12053			
					FINISH	DRAWN BY R. MCCAIN 9-29-45 DATE 10-5-45			
						DEPT. NO.	1000		
						CLASS "C" DRAWING OR SKETCH NO.			REV. SUB-LETTER

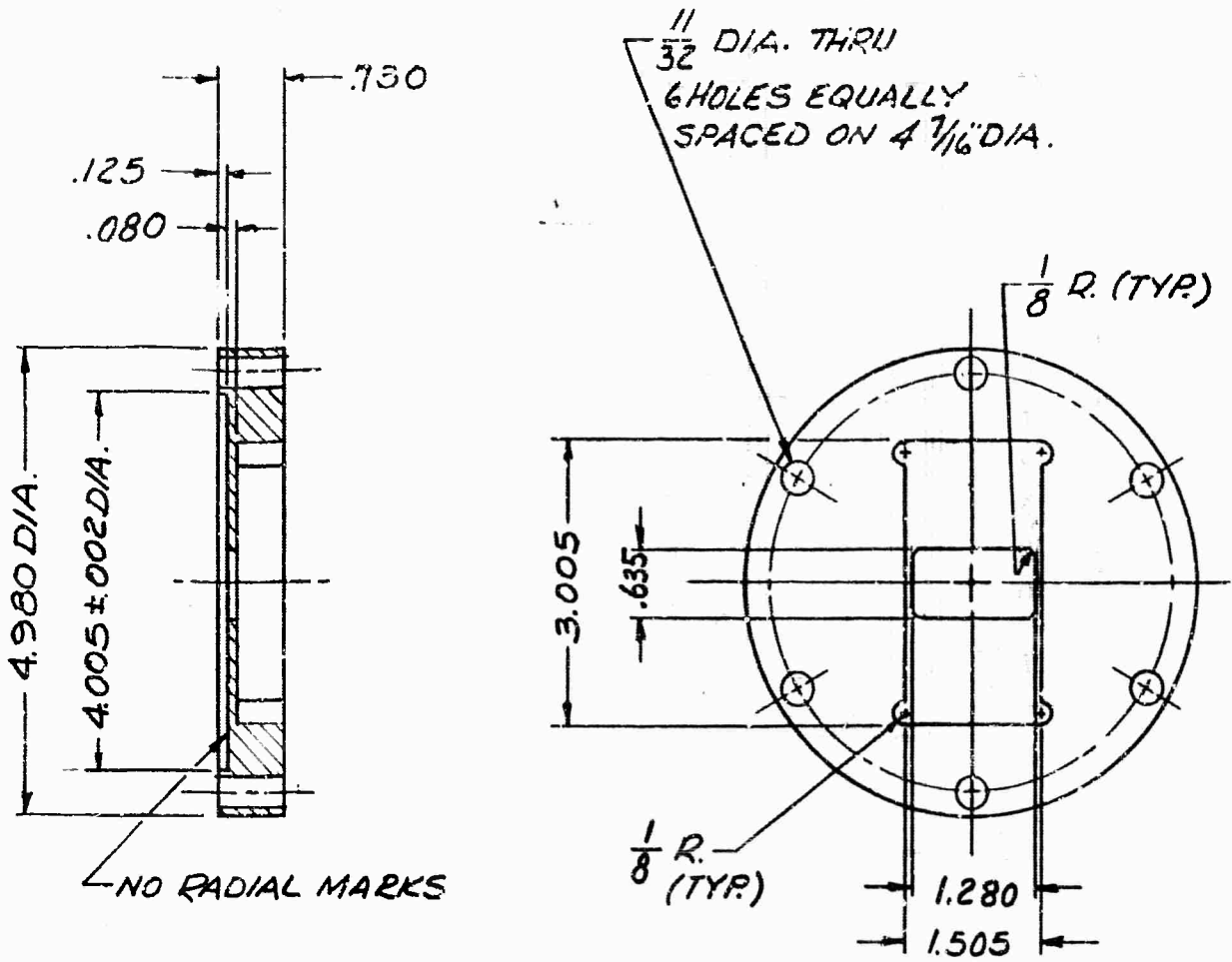


375 DIA. THRU  
1/4 ANPT TAP  
AS SHOWN  
(2 HOLES)

.257 DIA. THRU  
5/16 - 18NC-3B, 3/4 DP.  
FROM BOTH SIDES  
6 HOLES EQUALLY  
SPACED ON 4 7/16 DIA.

\* 5 1/2" O.D. x 1 1/4" WALL x 2 3/8" LG.  
COLD DRAWN & STRESS RELIEVED  
LOW CARBON SEAMLESS STEEL  
TUBING PER FED. SPEC. QQ-T-830A  
TYPE MT 1015. HARDNESS TO BE  
ROCKWELL "B" 65 TO 90.

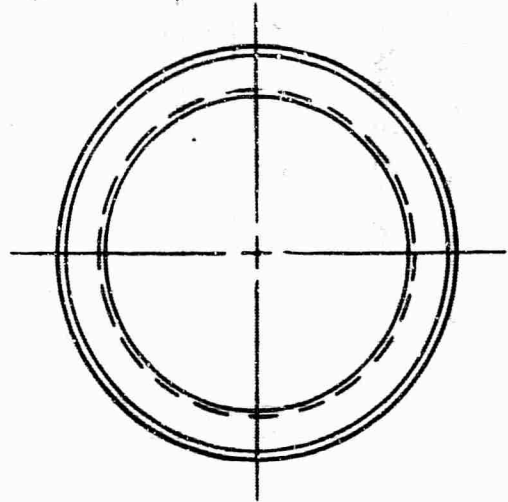
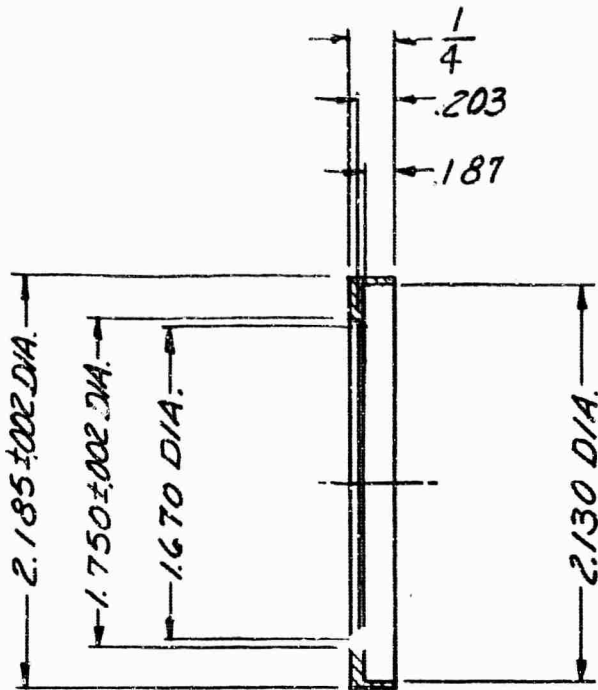
TOLERANCING ON DIMENSIONS NOT OTHERWISE SPECIFIED				SCALE		ENGINEERING EXPERIMENTAL SKETCH	
DECI. DIM. ± .005 FRAC. DIM. ± 1/64 ANG. DIM. ± 5°				1/2		BODY	
REVISIONS				MAT. SIZE & CODE		USED ON D-APPC. NO.	
REV.	ITEM	CHANGED FROM	DATE	ENGINEER		SPERRY ELECTRONIC TUBE DIVISION OF	
				APPROVAL		SPERRY RAND CORPORATION	
						GAINESVILLE, FLA.	
						D. McGAIN 9-29-65 R. Hunter 10-5-65	
					REFERENCE	DRAWN BY	DATE
					12054	APPROVED BY	DATE
						CEPT. NO.	
						1,001	
						CLASS "C" DRAWING OR SKETCH NO.	REV. SUB-LETTER



\* 3/4" D. x 5 1/4" x 5 1/4"  
 COLD FINISHED CARBON STEEL  
 FLAT PER ASTM A 108, GRADE  
 1018, 1020 OR 1022

TOLERANCE ON DIMENSIONS NOT OTHERWISE SPECIFIED					SCALE	A. O.	ENGINEERING EXPERIMENTAL SKETCH		
DECI. DIM. ± .005 FRACTIONAL DIM. ± 1/64 ANG. DIM. ± 1°					1/2	J. O.	BACK COVER		
REVISIONS					MAT. SIZE & CODE	USED ON I-SPEC. NO.			
DRY. SUB.	ITEM	CHANGED FROM	DATE	ENGINEER APPROVAL	*	SPERRY ELECTRONIC TUBE DIVISION OF SPERRY RAND CORPORATION GAINESVILLE, FLA.			
					LENGTH	REFERENCE DRAWINGS	R MCCAIN 9-29-65		
					FINISH	12055	DRAWN BY	DATE	APPROVED BY
							DEPT. NO.	1092	DATE
							CLASS "C" DRAWING OR SKETCH NO.		REV. OUB-LST'62

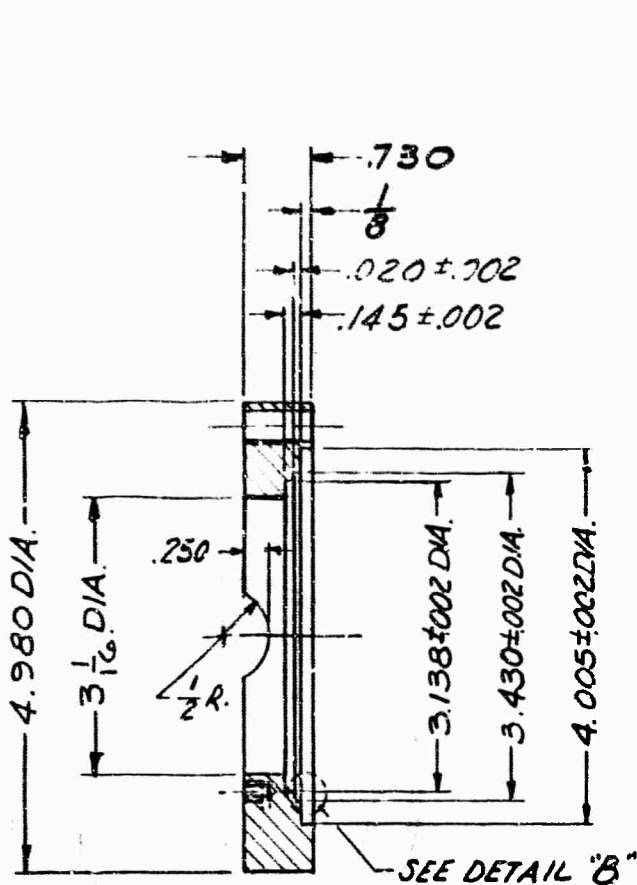
(10 TO INCH)



\* 2 1/4" O.D. x .625 WALL x 3/8" LG.  
 COLD DRAWN & STRESS RELIEVED  
 LOW CARBON SEAMLESS STEEL  
 TUBING PER FED. SPEC. QQ-T-830A,  
 TYPE MT1015. HARDNESS TO BE  
 ROCKWELL "B" 65 TO 90.

PAGE 223

TOLERANCE ON DIMENSIONS NOT OTHERWISE SPECIFIED					SCALE	A. O.	ENGINEERING EXPERIMENTAL SKETCH	
DECI. DIM. ± .005    PRAC. DIM. ± 1/64    ANG. DIM. ~					1/1	J. O.	FLANGE, WINDOW	
REVISIONS					MAT. SIZE & CODE	USED ON D-SPEC. . O.		
PREV. SUB-L.	ITEM	CHANGED FROM	DATE	ENGINEER APPROVAL	*	SPERRY ELECTRONIC TUBE DIVISION OF SPERRY RAND CORPORATION GAINESVILLE, FLA.		
					LENGTH	REFERENCE DRAWINGS	R. MC CAIN 9-28-65 @ Nintire 10-5-65	
					FINISH	11226	DRAWN BY	DATE
							DEPT. NO.	APPROVED BY
							1003	DATE
CLASS "G" DRAWING OR SKETCH NO.							REV. SUB-LETTER	

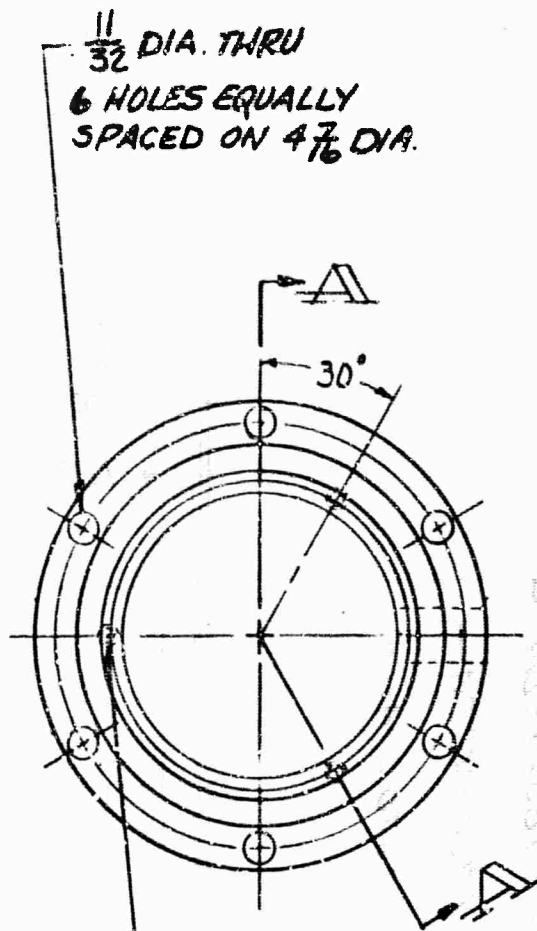


SECTION A-A



NO RADIAL MARKS

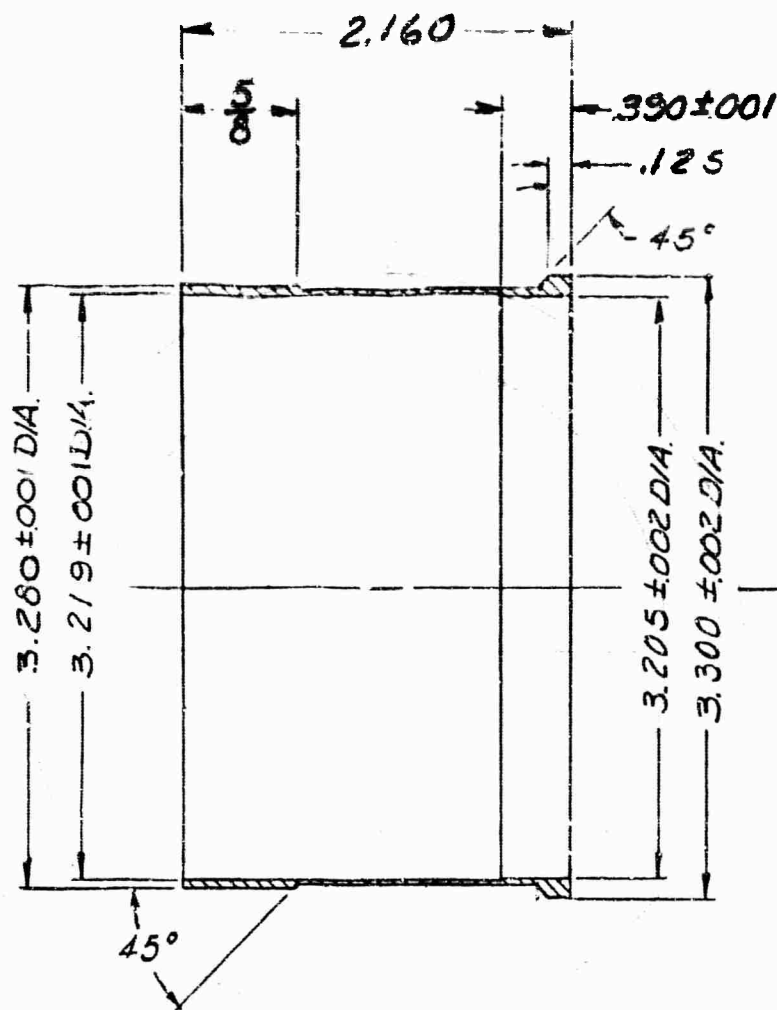
DETAIL "B"  
SCALE: 2/1



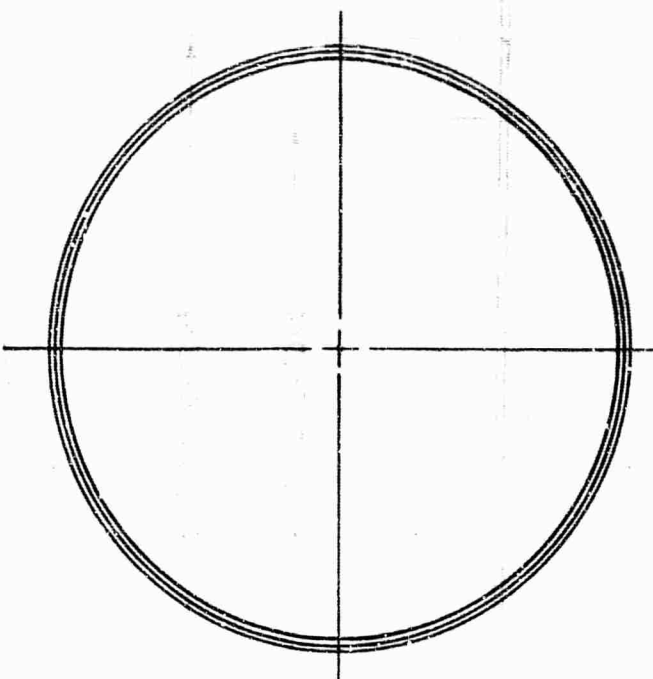
11/32 DIA. THRU  
6 HOLES EQUALLY  
SPACED ON 4 7/16 DIA.  
30°  
159 ± .003 DIA. x 1/4 DP.  
#10 (190) - 32NF - 38 x 3/16 DP.  
3 HOLES EQUALLY  
SPACED ON 3 5/16 DIA.  
(OPPOSITE SIDE)

\* 3/4" W. x 5 1/4 x 5 1/4  
COLD FINISHED CARBON STEEL  
FLAT PER ASTM A 108, GRADE  
1018, 1020 OR 1022

TOLERANCE ON DIMENSIONS NOT OTHERWISE SPECIFIED DECI. DIM. ± .005 FRACTIONAL DIM. ± 1/64 ANG. DIM. ± 1°					SCALE 1/2	A. O.	ENGINEERING EXPERIMENTAL SKETCH	
REVISIONS					MAT. SIZE & CODE	J. O.	FLANGE, TUNER	
REV. SUB-L.	ITEM	CHANGED FROM	DATE	ENGINEER APPROVAL	*	USED ON D-SPEC. NO.		
						REFERENCE DRAWINGS		
						12056		
					LENGTH		SPERRY ELECTRONIC TUBE DIVISION OF SPERRY RAND CORPORATION GAINESVILLE, FLA.	
					FINISH		R. McCairn 9-28-65 @ Winters 10-5-65	
							DRAWN BY DATE APPROVED BY DATE	
							DEPT. NO. 1,004	
							CLASS "C" DRAWING OR SKETCH NO. REV. SUB-LETTER	



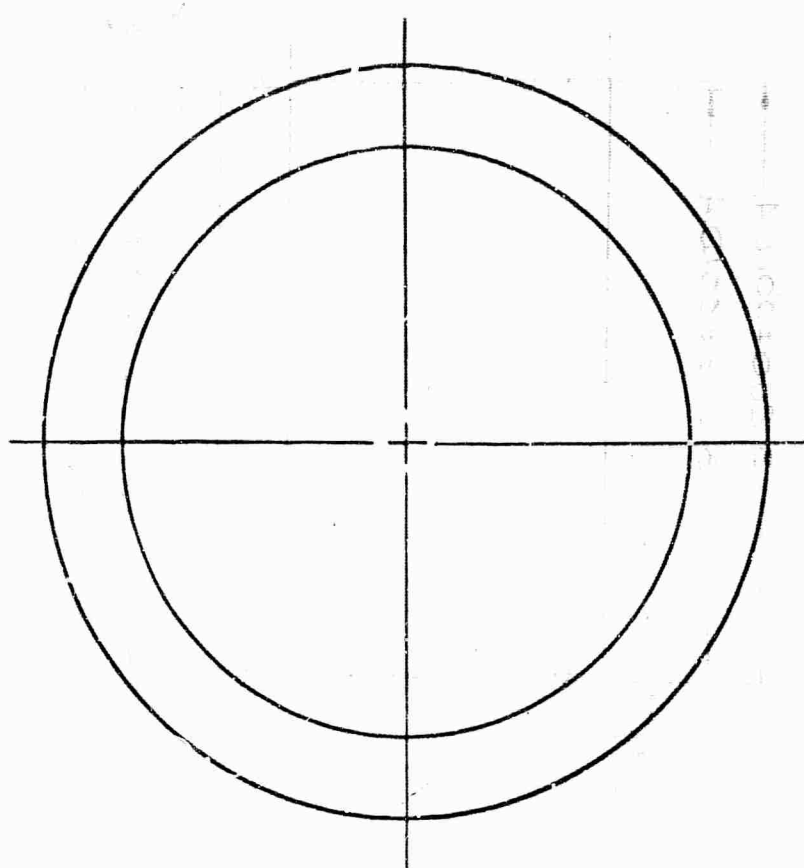
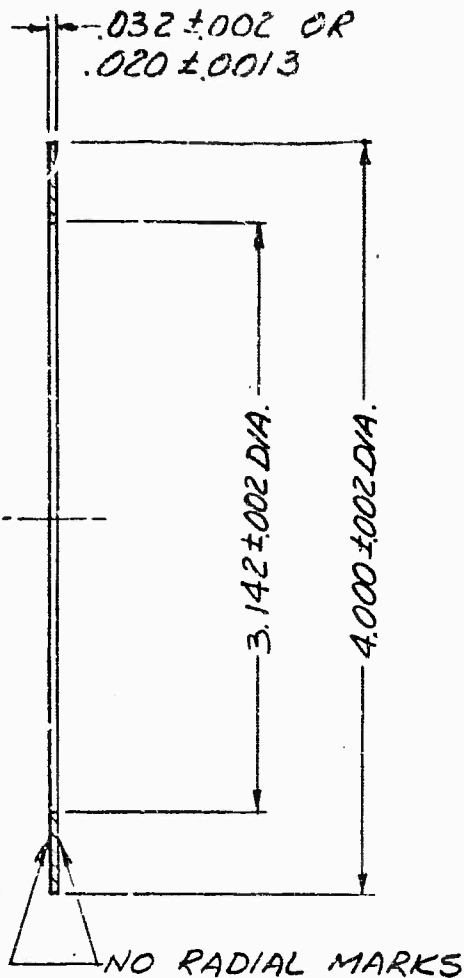
10-5-65  
10-5-65



\* IRON-NICKEL-COBALT SEALING ALLOY  
(KOVAR) ASTM F-15-61T

TOLERANCE ON DIMENSIONS NOT OTHERWISE SPECIFIED					SCALE	A. O.	ENGINEERING EXPERIMENTAL SKETCH		
DECI. DIM. ±0.005 FRACTIONAL DIM. ±1/64 ANG. DIM. ±1°					N.T.S.	J. O.	WINDOW SLEEVE		
REVISIONS					MAT. SIZE & CODE	USED ON D-EPEC. NO.			
PREV. SUB-L.	ITEM	CHANGED FROM	DATE	ENGINEER APPROVAL	*		SPERRY ELECTRONIC TUBE DIVISION OF SPERRY RAND CORPORATION GAINESVILLE, FLA.		
					LENGTH	REFERENCE DRAWING	R.M.CCA:V 9-28-65 10-5-65		
					FINISH	12060	DRAWN BY	DATE	APPROVED BY
							DEPT. NO.	1005	
CLASS "C" DRAWING OR SKETCH 1/2								REV. SUB-LETTER	

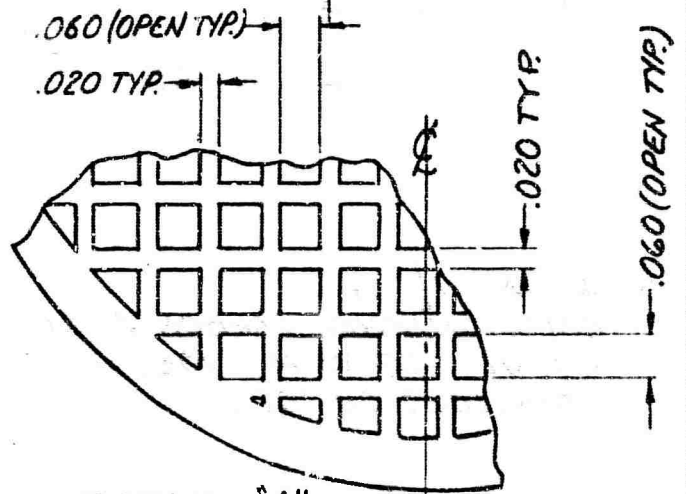
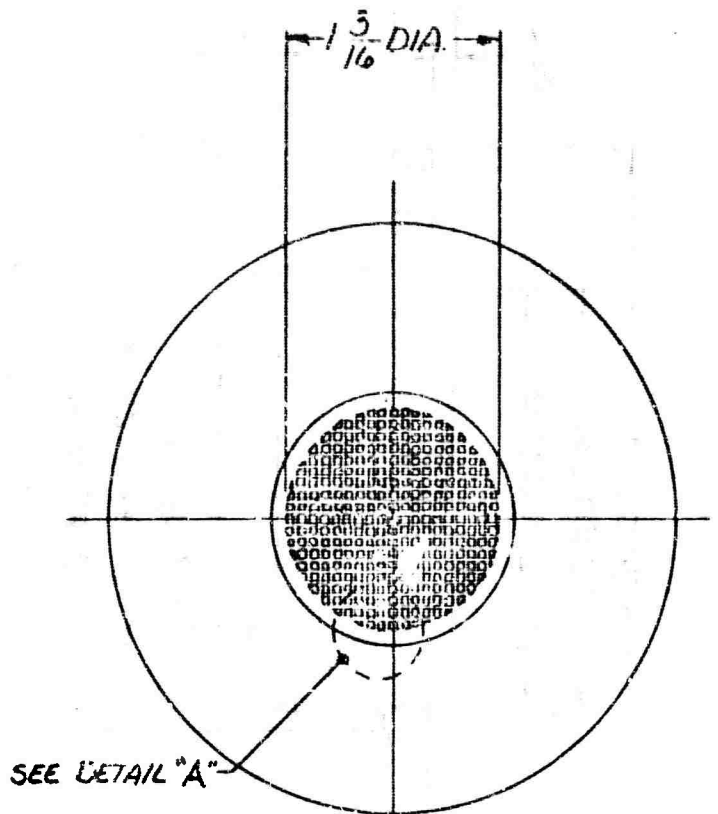
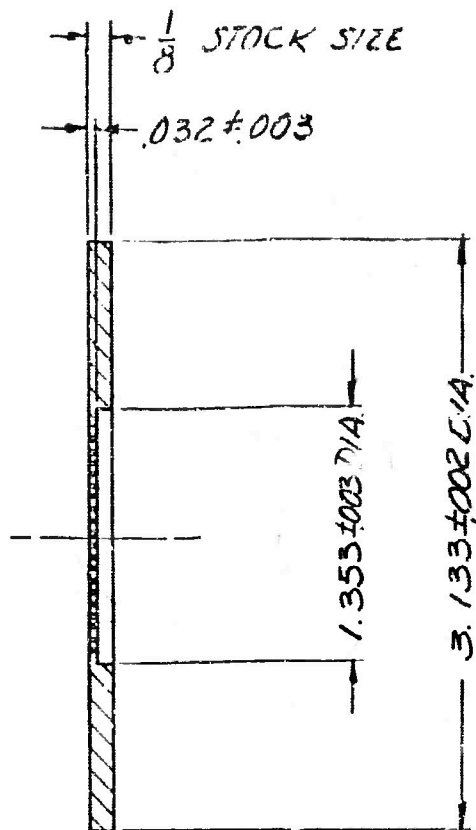
(10 TO 1/16")



$*.032^{TH} \pm .020^{TH} \times 4 \frac{1}{4} \times 4 \frac{1}{4}$   
 OXYGEN-FREE COPPER SHEET  
 HALF-HARD TEMPER PER  
 ASTM B 152, TYPE O.F.  
 EMBRITTLEMENT TEST (SEC. 12)  
 WILL APPLY. PHOSPHORUS CONTENT  
 $0.0003\%$  MAX.

PAGE 228

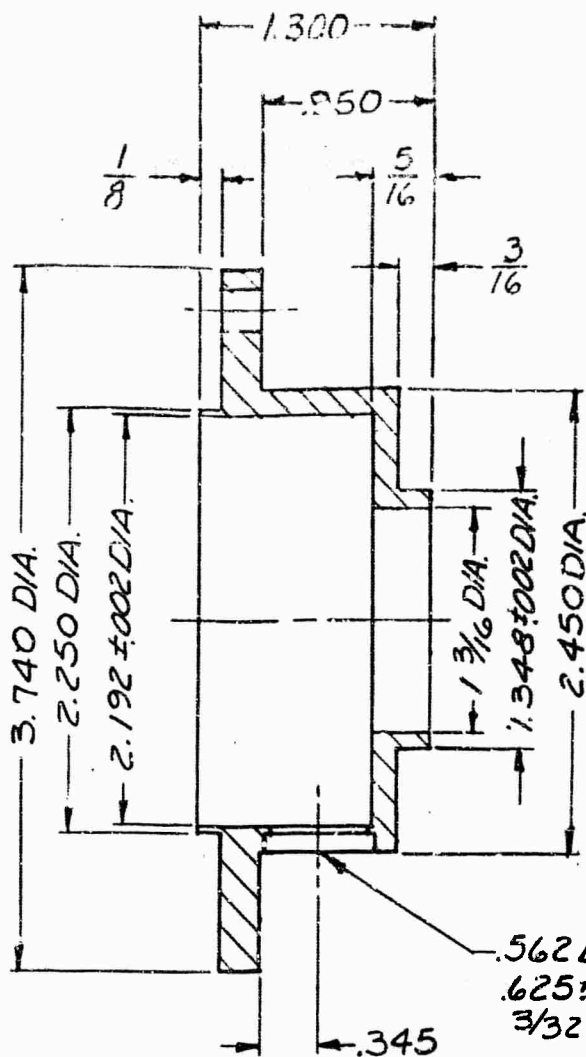
TOLERANCE IN DIMENSIONS NOT OTHERWISE SPECIFIED					SCALE	A. O.	ENGINEERING EXPERIMENTAL SKETCH		
DECI. DIM. ~ TRAC. DIM. ~ ANG. DIM. ~					1/1	J. O.	GASKET		
REV. SIONS					MAT. SIZE & CODE	USED ON D-SPEC. NO.			
PREV. SUB L.	ITEM	CHANGED FROM	DATE	ENGINEER APPROVAL	*	SPERRY ELECTRONIC TUBE DIVISION OF SPERRY RAND CORPORATION GAINESVILLE, FLA.			
					LENGTH	REFERENCE DRAWING	DRAWN BY DATE APPROVED BY DATE		
					FINISH	12059	RM-CAIN 9-28-65 DEPT. NO. 1,00,6 CLASS "C" DRAWING OR SKETCH NO. REV. LETTER		



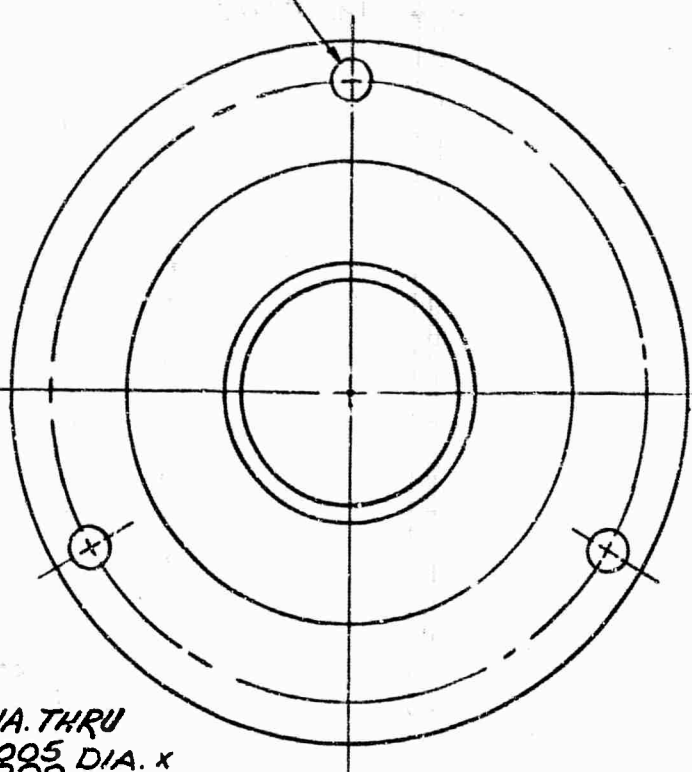
\*  $\frac{1}{8}$ "  $\times$   $3\frac{1}{2}$ "  $\times$   $3\frac{1}{2}$ "  
 OXYGEN-FREE COPPER  
 SHEET HALF-HARD  
 TEMPER PER ASTM B152,  
 TYPE O.F. EMBRITTLEMENT  
 TEST (SEC. 12) WILL APPLY.  
 PHOSPHOROUS CONTENT  
 0.0003% MAX.

DETAIL "A"  
 SCALE: 4/1

TOLERANCE ON DIMENSIONS NOT OTHERWISE SPECIFIED				SCALE	A. C.	ENGINEERING EXPERIMENTAL SKETCH	
DECI. DIM. $\pm 005$ FRAC. DIM. $\pm \frac{1}{64}$ ANG. DIM. $\sim$					J. O.	DIAPHRAGM	
REVISIONS				MAT. SIZE & CODE	USED ON B-SPEC. NO.		
PREV. SUB-L.	ITEM	CHANGED FROM	DATE	ENGINEER APPROVAL		SPERRY ELECTRONIC TUBE DIVISION OF SPERRY RAND CORPORATION GAINESVILLE, FLA.	
					REFERENCE DRAWINGS	P. McCain 9-28-65 <i>P. McCain</i> 10-5-65	
					12061	DRAWN BY	DATE
						DEPT. NO.	1007
						CLASS "C" DRAWING OR SKETCH NO.	
						REV. SUB-LETTER	



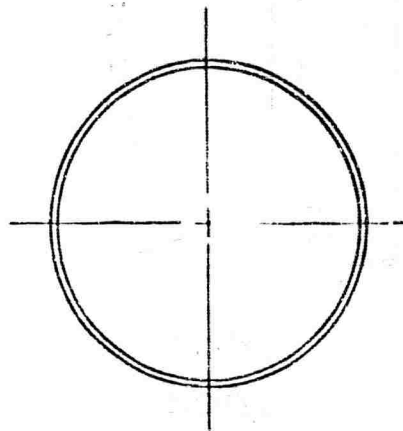
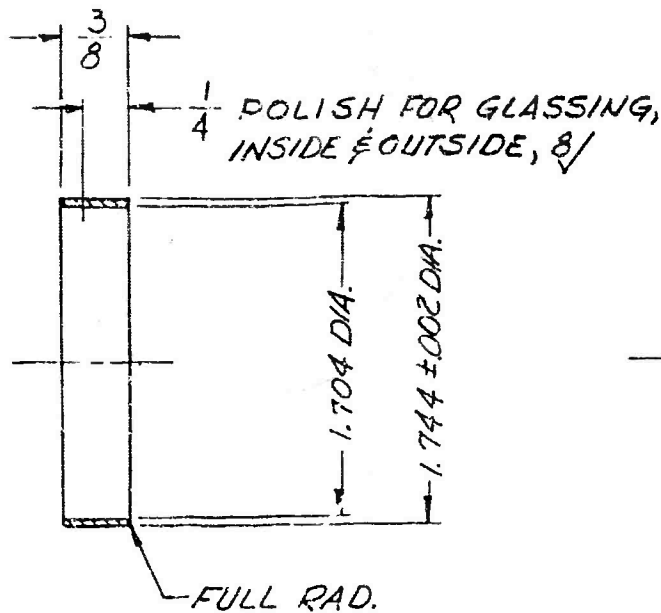
218 DIA. THRU  
LOCATED ON 3.312 DIA.  
3 HOLES EQUALLY  
SPACED.



562 DIA. THRU  
.625 ±.005 DIA. X  
3/32 DR. C'BORE

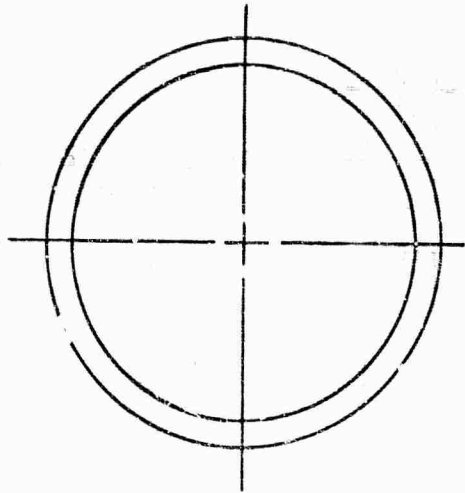
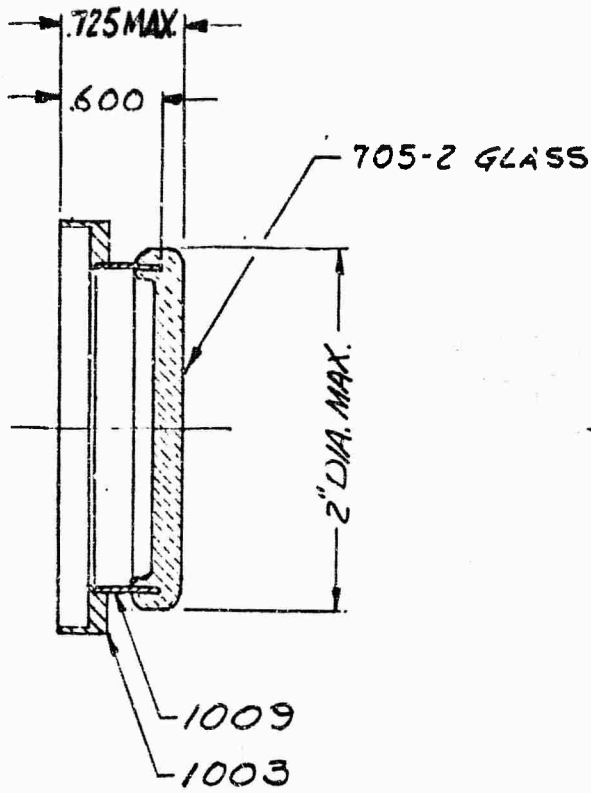
\* 4" DIA. x 1 1/2" LG.  
COLD FINISHED CARBON STEEL  
ROUND PER ASTM A 108, GRADE  
1018, 1020 OR 1022

TOLERANCE OF DIMENSIONS NOT OTHERWISE SPECIFIED				SCALE	A. O.	ENGINEERING EXPERIMENTAL SKETCH	
DECI. DIM. ±.005    PRAC. DIM. ± 1/64    ANG. DIM. ± 1°				1/1	J. O.	CUP, TUNER	
REVISIONS				MAT. SIZE & CODE	USED ON D-SPEC.		
PREV. SUB-L.	ITEM	CHANGED FROM	D. YR	ENGINEER APPROVAL	SPERRY ELECTRONIC TUBE DIVISION OF SPERRY RAND CORPORATION GAINESVILLE, FLA. R. MCCAIN 9-28-65    J.P.H. 10-5-65 DRAWN BY    DATE    APPROVED BY    DATE DEPT. NO.    1,008		
				LENGTH	REFERENCE DRAWINGS	CLASS "G" DRAWING OR SKETCH NO.	
				FINISH	12058	REV. SUB-LETTER	



\* IRON-NICKEL-COBALT SEALING ALLOY  
 (KOVAR CUP) ASTM F-15-61T  
 EXCEPT DIMENSIONAL TOLERANCES.  
 STUPAKOFF DIV. CAT. NO. 940033

TOLERANCES ON DIMENSIONS NOT OTHERWISE SPECIFIED					SCALE	A. O.	ENGINEERING EXPERIMENTAL SKETCH		
DECI. DIM.	FRAC. DIM.	ANG. DIM.	REVISIONS				MAT. SIZE & CODE	WINDOW CORE	
PREV. SUB-L.	REV.	CHANGED FROM	DATE	ENGINEER APPROVAL	*  LENGTH  FINISH	USED ON D-SPRC. NO.	SPERRY ELECTRONIC TUBE DIVISION OF SPERRY RAND CORPORATION GAINESVILLE, FLA.		
							REFERENCE DRAWINGS 11227	R. McCain 9-28-65 DRAWN BY DATE APPROVED BY DATE B. Winters 10-5-65	
								DEPT. NO. 1009	
CLASS "C" DRAWING OR SKETCH NO.							REV. SUB-LETTER		



PAGE 230

TOLERANCE ON DIMENSIONS NOT OTHERWISE SPECIFIED					SCALE	A. C.	ENGINEERING EXPERIMENTAL SKETCH		
DECI. DIM. $\pm 005$		FRAC. DIM. $\sim$		ANG. DIM. $\sim$		J. O.	WINDOW ASS'Y.		
REVISIONS					MAT. SIZE & CODE	USED ON S-SPEC. NO.			
PREV. PUB-L.	ITEM	CHANGED FROM	DATE	ENGINEER APPROVAL	LENGTH	REFERENCE DRAWINGS	SPERRY ELECTRONIC TUBE DIVISION OF		
						11279	SPERRY RAND CORPORATION		
							GAINESVILLE, FLA.		
					FINISH	DRAWN BY	DATE	APPROVED BY	DATE
						DIPT. NO.	1010		
						CLASS "C" DRAWING OR SKETCH NO			REV. SUB-LETTER

APPENDIX K

SUMMARY OF ELECTRIC FIELD AND POWER RELATIONS OF A  
DIELECTRICALLY LOADED TE<sub>111</sub><sup>0</sup>-MODE RESONATOR

The electric field expressions for an asymmetrically loaded TE<sub>111</sub><sup>0</sup>-mode resonator have been derived previously. This Appendix gives a summary of these results.

The schematic diagram of the high-power test cavity is given in Figure 11 of Appendix I. The electric field in the three regions of Figure 11 is given by:

$$E_{\theta} = \chi_{11} J_1' \left( \frac{\chi_{11} r}{r_0} \right) \cos \theta Z(z) \quad (K1)$$

and

$$E_r = \frac{r_0}{r} J_1 \left( \frac{\chi_{11} r}{r_0} \right) \sin \theta Z(z) \quad (K2)$$

where

$$Z(z) = \begin{cases} A \sin \kappa z, & 0 \leq z \leq s_1 \\ B \cos \kappa_e (s_1 + d - z), & s_1 \leq z \leq (s_1 + d) \\ C \cos \kappa (z - s_1 - d), & (s_1 + d) \leq z \leq (s_1 + d + s_2) \end{cases} \quad (K3)$$

For the definition of terms, see a list of symbols at the end of the report.

For the electric field and its first derivatives to be continuous across the dielectric boundaries:

$$B = C = A \frac{\sin \kappa_s d}{\cos \kappa_e d} \quad (\text{K4})$$

and

$$\tan \kappa_s d \tan \kappa_e d = \frac{\kappa_s}{\kappa_e} = \sqrt{\frac{1 - v^2}{\epsilon' - v^2}} \quad (\text{K4})$$

The total stored energy in the cavity is given by

$$U = \iiint \frac{c}{2} | \bar{E}_T \cdot \bar{E}_T | d\tau \quad (\text{K5})$$

where the integration is performed over the entire cavity volume.

Integration of Eq. K5 gives:

$$U = .101 \pi \epsilon_0 r_0^3 H^2 F, \quad (\text{K6})$$

where  $F$  is given in Eq. 18 of Appendix I. Using the definition of internal  $Q$  of the cavity and the expression of Eq. 19, the modulus of electric field given in Eq. K6 becomes:

$$B = \frac{55.0 \beta}{D(1 + \beta)} \sqrt{\frac{P_i Q_e \lambda_0}{F}} \quad (\text{K7})$$

With the maximum value of electric field of the  $TE_{01}^0$ -mode occurring at  $r = 0$ , it follows from Eq. K1 or K2:

$$E_{\max} = \frac{50.7 \beta}{D(1 + \beta)} \sqrt{\frac{P_1 Q_e \lambda_0}{F}} \quad (K8)$$

where  $F$  is given in Eq. 18. The evaluation of the maximum field of the  $TE_{111}^0$ -mode is identical with the procedure described in Appendix I for the multipactor test cavity.

11 7 5

APPENDIX L

RELATIONSHIP BETWEEN TRANSMITTED POWER  
AND MAXIMUM ELECTRIC FIELD IN CIRCULAR WAVEGUIDES

The maximum electric field intensity in a round waveguide propagating an electromagnetic wave in the  $TE_{1,1}$  circular dominant mode is given by:<sup>58</sup>

$$E_{\max} = \frac{22.3}{a} \left( P \frac{\lambda_g}{\lambda_0} \right)^{1/2} \frac{\text{volts}}{\text{unit length}} \quad (L1)$$

For the definition of terms, see the list of symbols at the end of this report.

It can be seen that the maximum value of the electric field in a waveguide transmitting a given amount of rf power depends on the transverse dimension of the waveguide. There is a large number of waveguide diameters suitable for window design. At S-band, a logical choice would be a window with a diameter equal to the inside diagonal of a WR-284 rectangular waveguide. This would correspond to a window diameter of 3.14 inches. The cut-off frequency of the  $TM_{0,1}^0$ -mode for this diameter guide is 2880 Mc. From Eq. L1, it follows that for a window of 3.14 inches diameter,

a wave propagating 100 MW of S-band power at 2856 Mc would produce a maximum electric field at the center of the guide of 70.1 kv/cm. Figure L1 gives a relationship between the transmitted power and the different values of maximum electric field at a window of 3.14-inches diameter.\*

An S-band window of 3.14-inches diameter can be utilized for high-power applications. For example, it is being used in a Sperry SAS-159 klystron, a tube with a nominal power output of 21 MW peak and 20 kw average. However, for high-power windows, windows capable of transmitting a peak of 100 MW of rf power, a logical thing to do would be to increase the diameter of the window. The danger of producing undesirable window modes must be considered individually.

A logical choice for the diameter of a high-power window is the internal diagonal of WR-340 rectangular guide. This corresponds to a circular window diameter of 3.80 inches, and the maximum electric field of a 100 MW wave in this size guide is only 52.8 kv/cm. This particular value of the electric field was used in this program for the computation of the equivalent

---

\* Figures L1 and L2 were submitted by Gunther Wurthmann of U. S. Army Electronics Command, Fort Monmouth, New Jersey.

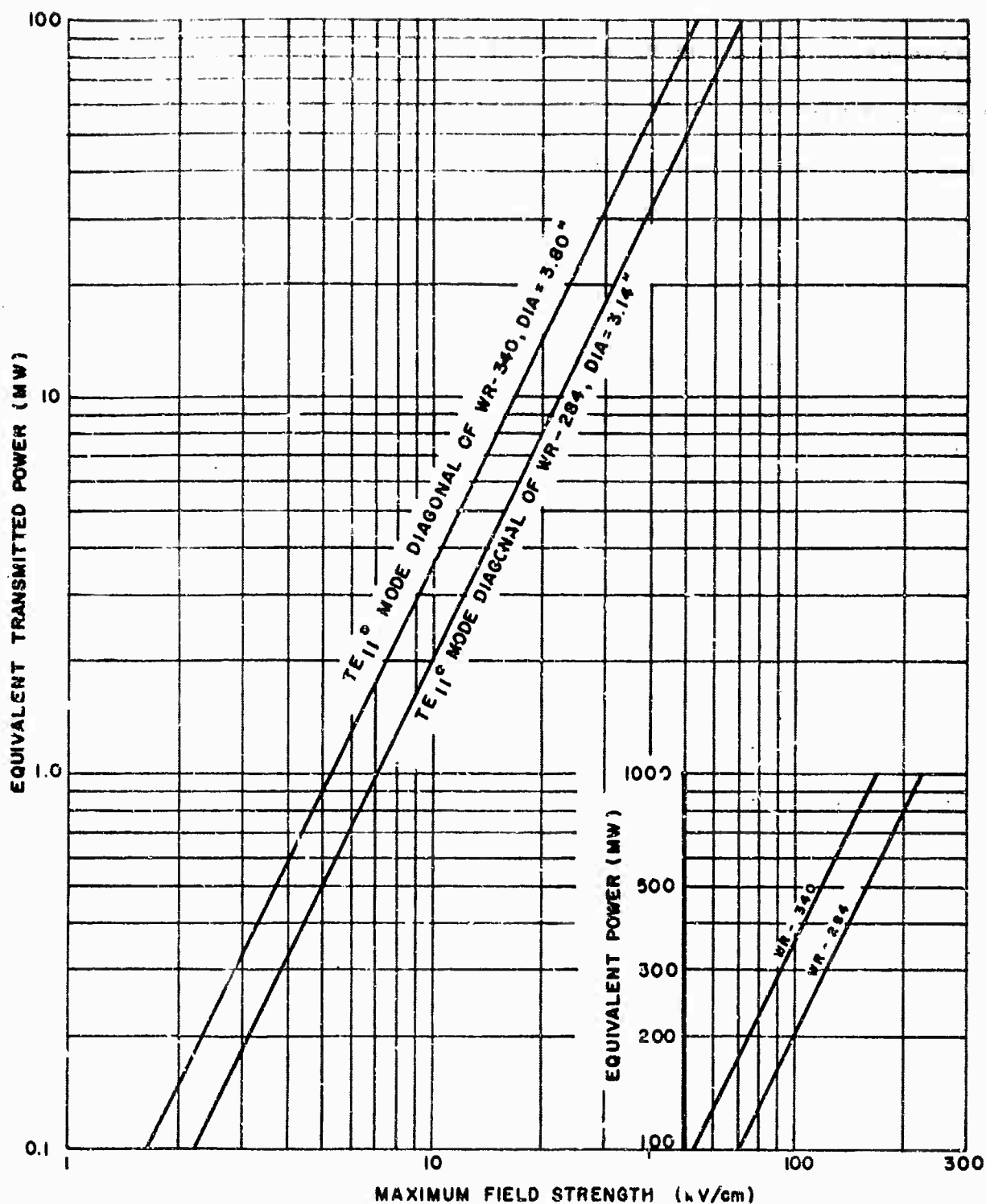


FIGURE -L1 PLOT OF EQUIVALENT TRANSMITTED POWER VS MAXIMUM FIELD STRENGTH IN A CIRCULAR S-BAND WAVEGUIDE AT 2856 Mc

transmitted power at S-band. For example, if an observation in the multipactor cavity was made at an electric field of 16 kv/cm, then 16 over 52.8 squared times 100 was the equivalent transmitted power through the window at that time.

The relationship between the transmitted power and the maximum electric field for the S-band window of 3.80-inches diameter is given in Figure L1. Note that for this diameter guide, the cut-off frequency of the second higher order mode ( $TE_{21}^0$ ) is 3020 Mc. The cut-off frequency of  $TM_{01}^0$ -mode is 2380 Mc.

In Figure L2, a similar power-electric field relationship was plotted for two different diameters of X-band windows, and the diameter of the window equal to the inside diagonal of WR-112 waveguide (1.225 inches) was used for the computation of the equivalent transmitted power at X-band. For this size window, 51.3 kv/cm corresponds to 10 MW of transmitted power at 8900 Mc. Actually, in high-power experiments at X-band, a window diameter of 1.250 inches was used so that the reported values of the equivalent transmitted power were slightly smaller than experienced during the test.

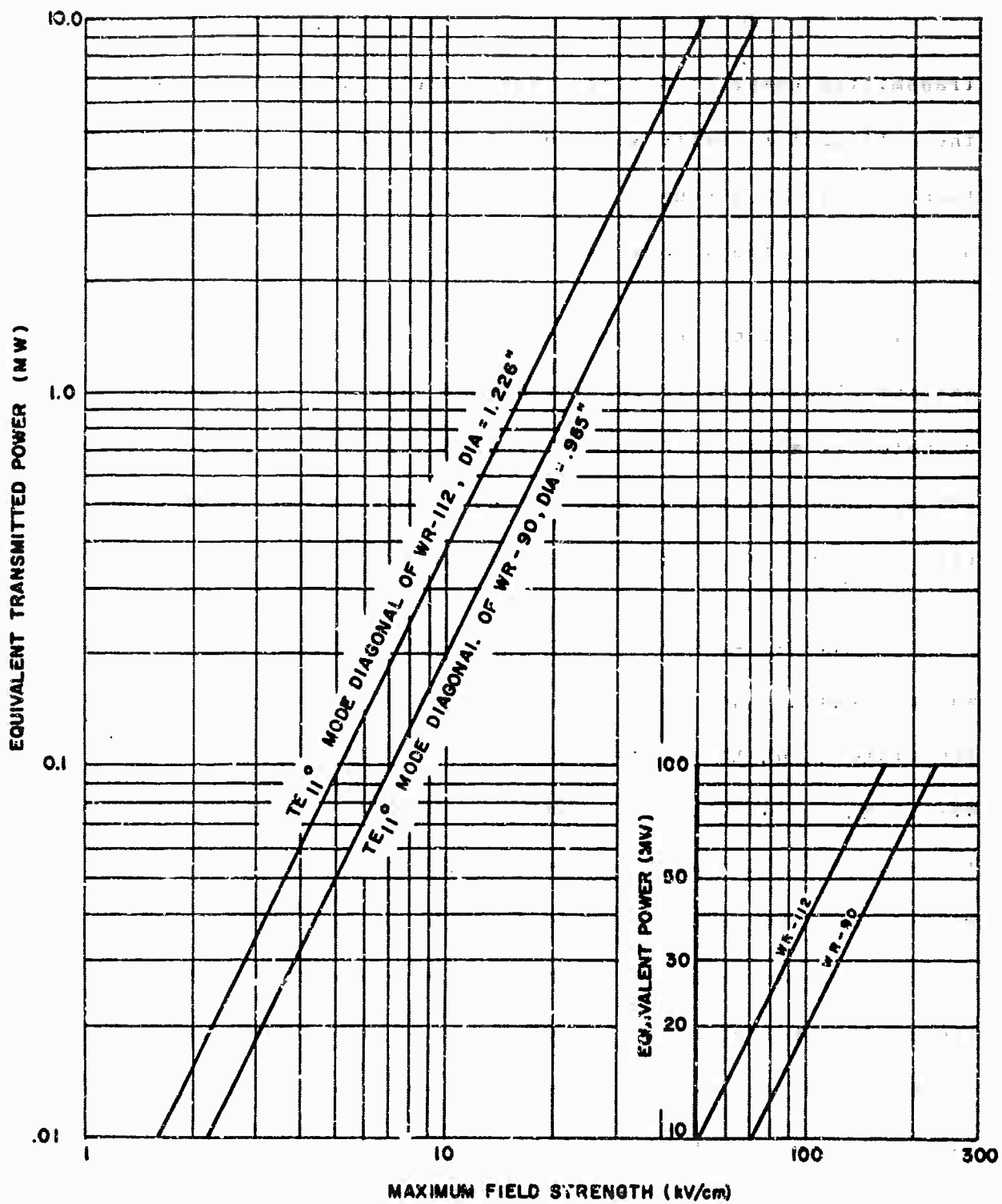


FIGURE -1.2 PLOT OF EQUIVALENT TRANSMITTED POWER VS MAXIMUM FIELD STRENGTH IN A CIRCULAR X-BAND WAVEGUIDE AT 8.00 Mc

APPENDIX M

PREPARATION OF DIFFERENT METALIZING PAINTS  
AND APPLICATION PROCEDURES

The following is the list of some of the metalizing paints which were used on the window-study program.

1. Preparation of Binder S-400

To every 750 ml of equal volumes of butyl acetate and butyl alcohol, add the following:

Nophthenic Acids - 25 ml  
Pyroxylin (Dupont No. 5511) - 25 gm

Mix in glass container for at least three to four hours before use.

2. Conventional (Mo-Mn) Paint - S-100

S-100 paint shall be made up in the following proportions:

Molybdenum Powder - 80 parts by weight  
Manganese Powder - 20 parts by weight

To every 100 grams of the above, add 50 ml of S-400 binder.

Mill powders in ball mill to fineness of 7 - 7.5 grind

(Hegmen Fineness Gage), density 2.30 - 2.45 (Gardener No. 5070-W-3) and viscosity 16 ± Sec (Zahn No. 2).

3. MoO<sub>3</sub> - MnO<sub>2</sub> Metalizing Paint S-200

Molybdenum Trioxide	- 600 gms
Manganese Dioxide	- 32 gms
Cuprous Oxide	- 0.60 gms
S-400 Binder	- 360 ml

Mix the above mixture in a ball mill jar for thirty hours.

4. Solution Metalizing

Solution a

Ammonium Molybdate	- 300 gm
Deionized Water	- 1000 ml

Solution b

Manganous Nitrate (50%) solution

Metalizing solution: To every 100 ml of Solution a, add 0.5 ml of Solution b. (Metalizing solution should be prepared immediately prior to using.)

5. Nickel Paint S-58

Nickeleous Oxide	- 50 gm
S-400 Binder	- 50 ml

This mixture was ball milled 24 hours before using.

During the process of metalizing, all test specimens were brush coated (two coats) with a hydrogen firing at the specified temperature after each coat. The MoO<sub>3</sub>-MnO<sub>2</sub> and solution metalizing

specimens were burnished with a steel wire brush to remove excess metal powders after firing operation. The test pieces used for solution metalizing experiments were heated in an air oven to a temperature of 90 - 100°C prior to painting in order to obtain a high concentration of Mo and Mn and to facilitate drying. All test pieces with the exception of the conventionally metalized specimens were given a brush coat of nickel oxide and reduced in a hydrogen furnace at 900° - 1000°C. The conventionally metalized (Mo-Mn) test pieces were nickel plated (.0002 - .0003) and hydrogen fired at 900° - 1000°C. Test pieces were measured for coating thickness after each firing step. The test pieces were then copper brazed and tensile tested. A test specimen from each group was then selected for micrographic inspection. The metalizing data obtained from 35 tests performed with 99.5 percent alumina bodies is given in the following table.

TABLE M1

METALIZING DATA ON 99.5% ALUMINA

Metalizing Technique	Firing Temperature	No. of Coats	Coating Thickness Inches	Ni Plate Inches	Tensile Strength (psi)
A Mo-Mn	1475°C	2	0.0012	0.0003	8,240
B MoO <sub>3</sub> -MnO <sub>2</sub>	1475°C	2	0.00033	0.0006	11,740
C MoO <sub>3</sub> -MnO <sub>2</sub>	1100°C	2	0.00013	0.0007	8,290
D Solution Metalizing	1475°C	2	0.00012	0.0005	7,830
E Solution Metalizing	1100°C	2	0.0001	0.0006	8,410

#### REFERENCES

1. Churchill, D. B., Waveguide Windows for High Power Microwave Tubes, Paper presented at Session 43, Microwave High Power, IEEE International Convention, New York, 27 March 1963.
2. Final Technical Report, High Power RF Window Study Program, Furnished by Varian Associates to Rome Air Development Center under Contract No. AF30(602)-2844, November, 1963.
3. Churchill, D. B., Waveguide Window Structure Having Three Resonant Sections Giving Broadband Transmission with Means to Fluid Cool Center Section, Patent No. 3,110,000 Granted 5 November 1963.
4. Final Report, "Superpower Microwave Windows," Furnished by Sperry Gyroscope Co., to U. S. Army Electronics Laboratories Under Contract No. DA-36-039 AMC-02161(E), p. 5, January, 1964.
5. Batelle Memorial Institute, Technical Summary Report on a Survey of the High-Power Microwave-Tube Window Problem, Furnished to Advanced Research Projects Agency of the Department of Defense under Contract SB-80, ARPA Order 197, pp. 18-20. Since this survey was published (November, 1962) the following additional programs have been initiated: High Power RF Window Study Program, conducted by Varian Associates for Rome Air Development Center, Air Force Systems Command, under Contract No. AF 30(602)-2344; Research on Dielectrics for Microwave Electron Devices, conducted by Stanford Research Institute for U. S. Army Electronics Research and Development Laboratories, under Contract No. DA 36-039 SC-90856; Research on Microwave Window Multipactor and its Inhibition, conducted by Eitel-McCullough, Inc., for U. S. Army Electronics Research and Development Laboratories, under Contract DA 36-039 SC-90818; Metallurgical Research and Development for Ceramic Electron Devices, conducted by Eitel-McCullough, Inc., for U. S. Army Electronics Research and Development Laboratories, under Contract No. DA 36-039 SC-90903.

6. Praist, D. and Talcott, R., "On the Heating of Output Windows of Microwave Tubes by Electron Bombardment," IRE Trans. ED-8, p. 243, July, 1961.
7. Final Report, "Research on Microwave Window Multipactor and Its Inhibition," Furnished by Eitel-McCullough, Inc., to U. S. Army Electronics Command under Contract No. DA 36-039 SC-90818, p. 9, June, 1964.
8. Reference 7, p. 40b.
9. Bruining, H., Physics and Applications of Secondary Electron Emission, Pergamon Press, New York, p. 37, 1954.
10. Talcott, E. C., "The Effects of Titanium Films on Secondary Electron Emission Phenomena in Resonant Cavities and at Dielectric Surfaces," IRE Trans. E. D. 1, p. 405, September, 1962.
11. Reference 7, p. 24.
12. Reference 7, p. 50.
13. Reference 7, p. 77.
14. Reference 7, p. 35.
15. Reference 9, p. 3.
16. Kanicheva, I. R. and Burtsev, V. V., "Investigation of Transmission of 0.5 - 16 kev Electrons Through Collodian and Gold Films," Soviet Physics Solid State, 1, #8, p. 1146, February, 1960.
17. Reference 7, p. 38a.
18. Reference 7, p. 34a.
19. Reference 10 and Reference 7, p. 30, and 46.
20. Vierstra, A. and Butman, R. C., "Secondary Emission Characteristics of High-Power Microwave Tube Surfaces," MIT, Lincoln Laboratory Technical Report #257, p. 11, 20 February 1962.

21. Reference 7, p. 43.
22. "High-Power Microwave Tube Window Investigations," Furnished by Sperry Electronic Tube Division of Sperry Rand Corp., to U. S. Army Electronics Command under Contract No. DA 28-043-AMC-00373(E), Third Quarterly Report, p. 10, June, 1965.
23. Hall, W. J., "A Study of Thin Films in Electron Tubes," Prepared by General Electric Co. in Owensboro, Ky., under Contract No. NObsr 81225.
24. "High-Power Microwave Tube Window Investigations," Furnished by Sperry Electronic Tube Division of Sperry Rand Corp., to U. S. Army Electronics Laboratories under U. S. Contract No. DA 28-043-AMC-00373(E), Second Quarterly Progress Report, p. 13, March, 1965.
25. Gerstenberg, P. and Mayer, E. H., Proc. Electronic Comp. Conf., p. 57, 1962.
26. Reference 7, p. 33.
27. Holland, L., Vacuum Deposition of Thin Films, Chapman & Hall Ltd., p. 423, 1963. Also discussed by Blevis, E. H., "Glow Discharge Sputtering - Theory and Practice," February, 1964, an article distributed by R. D. Mathis Co., Long Beach, California.
28. Reference 24, p. 43.
29. "High-Power Microwave Tube Window Investigation," Furnished by Sperry Electronic Tube Division of Sperry Rand Corp. to U. S. Army Electronics Laboratories under U. S. Contract No. DA 28-043-AMC-00373(E), First Quarterly Progress Report, p. 63, December, 1964.
30. Harrison, J. R., "Design Considerations for Directional Couplers," Rad. Lab. Rpt. #724, Mass. Inst. of Tech., December, 1945.
31. Reference 29, pp. 37 and 60.
32. Final Report, "Superpower Microwave Windows," Furnished by Sperry Gyroscope Co. to U. S. Army Electronics Laboratories under Contract No. DA-36-039 AMC-02161(E), p. 73, January, 1964.

33. D. B. Churchill, "Tangent Relation for Determining Impedance Inverter Parameters." IEEE, Trans. MTT, Vol. MTT-12, p. 551, September, 1964.
34. "Handbook on High-Power Capabilities of Waveguide Systems," Furnished by Microwave Associates, Inc., to the Dept. of Navy, Bureau of Ships, Electronic Division under Contract No. NObsr-85190, p. 14, June, 1963.
35. Long, E. B., Carbon Products Division of Union Carbide Corp., New York City, New York, private communication.
36. Reference 7, p. 27.
37. Reference 7, p. 29.
38. Reference 7, p. 30.
39. Klopter, A., et al., Vacuum Technology Transactions, Pergammon Press, p. 302, 1960, and Ames, I. and Chritenson, R., Vacuum Technology Transactions, Pergammon Press, p. 311, 1960.
40. Vaughan, J. R. M., "Some High-Power Window Failures," PGED Trans. IRE, ED-8, #4, pp. 302-308, July, 1961.
41. Reference 40, also Howie, J., "Radiation Damage in Ceramics," Nuclear Engineering, Vol. 6, No. 62, pp. 299-304, 1961, and Mike, T., et al., "Effects of Electron Bombardment on Properties of Various Glasses," J. Am. Ceramic Soc., Vol. 43, No. 8, pp. 405-407, 1960.
42. Cullity, B. B., Elements of X-Ray Diffraction, Addison Wesley Co., Inc., p. 11, 1956.
43. Reference 29, p. 19.
44. "Low Temperature Refractory Metal-to-Ceramic Seals," prepared by Sperry Electronic Tube Division for the U. S. Army Electronics Research and Development Laboratory, Contract No. DA-36-039-AMC-03734(2).
45. References 17 and 18.

46. Reference 7, p. 66.
47. Ginzton, E. L., Microwave Measurements, McGraw Hill Co., Inc., New York, pp. 397 and 407, 1957.
48. Reference 47, p. 396.
49. Moreno, T., Microwave Transmission Design Data, Dover Publication, Inc., New York, p. 235, 1958.
50. Solyman, L. and Eaglesfield, C. C., "Design of Mode Transducers," IRE Trans. MTT-8, pp. 61-65, January, 1960, and Churchill, D. B., "An Additional Relation for Design of Mode Transducers," IRE Trans. MTT-12, No. 5, p. 547, September, 1964.
51. Reference 47, Chapter 5.
52. Deschamps, G. A., "A New Chart for the Solution of Transmission Line and Polarization Problems," IRE Trans. MTT-1, No. 1, p. 5, March, 1953.
53. Montgomery, C. G., et al., Principles of Microwave Circuits, McGraw Hill, New York, pp. 46 and 47, 1948.
54. The Microwave Engineers' Handbook, Horizon House Publishing Company, p. 8, 1965.
55. Ramo, S. and Whinnery, J. R., Fields and Waves in Modern Radio, John Wiley & Sons, New York, p. 110, 1946.
56. Reference 29, p. 57.
57. Reference 24, p. 91.
58. Reference 49, p. 124.
59. Reference 9, p. 49.

### LIST OF SYMBOLS

- $\beta$  = Cavity coupling coefficient (ratio of the unloaded Q to the external Q)
- $\gamma$  = Propagation constant in a conductive film
- $\Gamma$  = Voltage reflection coefficient
- $\Gamma_m$  = Midplane voltage reflection coefficient
- $\delta$  = Skin Depth
- $\epsilon$  = Dielectric constant
- $\epsilon_0$  = Dielectric constant of vacuum
- $\epsilon'$  = Relative dielectric constant (referred to vacuum)
- $\eta$  = Electronic charge to mass ratio
- $\theta$  = Angular coordinate variable
- $\kappa = \kappa_0 \sqrt{1 - v^2}$  , waveguide propagation constant
- $\kappa_\epsilon = \kappa_0 \sqrt{\epsilon' - v^2}$  , waveguide propagation constant in dielectric medium, dielectric constant  $\epsilon'$ .
- $\kappa_0 = \omega/c$  , free space propagation constant
- $\lambda_0$  = Wavelength in free space
- $\lambda_g$  = Guide wavelength
- $\mu$  = Permeability constant
- $\mu_0$  = Permeability of vacuum
- $v = \frac{fc}{f} = \frac{2\sqrt{nc}}{\omega_0 D}$  , dispersion constant

- $\sigma$  = Electric conductivity of material  
 $\tau$  = Coating thickness  
 $\chi'$  = Bessel function argument  
 $\chi'_{01}$  = 3.832, first real root of equation  $J'_0(\chi') = 0$   
 $\chi'_{11}$  = 1.841, first real root of equation  $J'_1(\chi') = 0$   
 $\omega$  = Angular frequency  
 $\omega_0$  = Resonant angular frequency  
 $a$  = Radius of a circular waveguide propagating  $TE_{11}$  dominant mode or the inside width dimension of a rectangular waveguide when applicable  
A, B, C = Moduli of field strength equations  
 $b$  = The inside height dimension of rectangular waveguide  
 $c$  = Velocity of light in vacuum  
 $D$  = Cavity diameter  
 $d$  = Thickness of dielectric disc  
 $dV$  = Differential element of volume  
 $E_\theta$  = Angular component of the electric field  
 $E_0$  = Maximum amplitude of the electric field  
 $\bar{E}_T$  = Tangential electric field  
 $F$  = Geometric parameter of the dielectrically loaded cavity  
 $f$  = Frequency  
 $f_c$  = Cutoff frequency  
 $f_0$  = Resonant frequency

$J$  = Current density  
 $J_n$  = Bessel function of nth order  
 $J_n'$  = First derivative of Bessel function with respect to its argument  
 $P$  = Power propagating through a guide window  
 $P_d$  = Dissipated power in the cavity  
 $P_1$  = Incident-wave power in waveguide  
 $Q_e$  = Cavity external Q  
 $Q_L$  = Cavity loaded Q  
 $Q_0$  = Cavity unloaded (internal) Q  
 $r$  = Radial coordinate variable  
 $r_m$  = Value of  $r$  for maximum field strength  
 $r_0$  = Cavity radius, also VSWR at resonance when applicable  
 $R$  = Surface resistivity of coating  
 $s_1, s_2$  = Longitudinal cavity spacing parameters  
 $t$  = Time variable  
 $U$  = Stored energy  
 $x$  = Rectangular coordinate variable  
 $y$  = Rectangular coordinate variable  
 $z$  = Axial coordinate variable, also rectangular coordinate variable  
 $Z$  = Space impedance  
 $Z_0$  = Free space impedance

DOCUMENT CONTROL DATA - R&D

(Security classification of title, body of abstract and indexing annotation must be entered when the overall report is classified)

1. ORIGINATING ACTIVITY (Corporate author) <b>Sperry Rand Corporation Gainesville, Florida</b>		2a. REPORT SECURITY CLASSIFICATION <b>UNCLASSIFIED</b>	
		2b. GROUP <b>N/A</b>	
3. REPORT TITLE <b>HIGH-POWER MICROWAVE TUBE WINDOW INVESTIGATIONS</b>			
4. DESCRIPTIVE NOTES (Type of report and inclusive dates) <b>Final Report - 15 September 64 - 15 September 65</b>			
5. AUTHOR(S) (Last name, first name, initial) <b>Saharian, A., Kiefer, A., Lally, P.</b>			
6. REPORT DATE <b>September 1965</b>		7a. TOTAL NO. OF PAGES <b>253</b>	7b. NO. OF REFS <b>89</b>
8. CONTRACT OR GRANT NO. <b>DA 28-043 AMC-00373(E)</b>		9a. ORIGINATOR'S REPORT NUMBER(S)	
b. PROJECT NO. <b>7900-21-223-15-00</b>		9b. OTHER REPORT NO(S) (Any other numbers that may be assigned this report)	
c.			
d.			
10. AVAILABILITY/LIMITATION NOTICES <b>Qualified requesters may obtain copies of this report from DDC. DDC release to CFSTI not authorized.</b>			
11. SUPPLEMENTARY NOTES		12. SPONSORING MILITARY ACTIVITY <b>U. S. Army Electronics Command Ft. Monmouth, N. J., AMSEL-KL-TM</b>	
13. ABSTRACT <p>This report gives a brief description of high-power microwave tube window problems. The emphasis in the discussion is placed on problems associated with the single-surface multipactor phenomenon. Window coating criteria and means of eliminating multipactor and multipactor-related problems are presented.</p> <p>Sputtering equipment and new coating and control procedures developed in this program are described in greater detail. Problems associated with the changes in the resistivities of coatings, including the effects of tube processing techniques, are discussed. Work performed on coating identification and problems associated with producing a uniform coating are described.</p> <p>A wide variety of coating materials were evaluated in specially-designed <math>TE_{011}</math> cavities at S-band and X-band. The most promising coatings were evaluated at S- and X-band in <math>TE_{211}^0</math> cavities. The geometry of these cavities was such as to closely simulate practical high-power window configurations. The report includes a description of all of these cavities and the procedures followed in the test work.</p> <p style="text-align: right;">(Continued)</p>			

CONTRACT DA 28-043 AMC-00373(E)

ABSTRACT (Continued)

Results of some thirty-seven experiments performed in this program are presented. Physical changes in window materials arising from multipactor are described. In the  $TE_{11}^0$ -mode experiments, windows have been tested at S-band up to 120 MW with no multipactor or seal area arcing. At X-band a power level of 13 MW has been obtained without multipactor or arcing.

Finally, a new, improved metalizing-window-brazing technique, which produces a strong metal-to-dielectric bond with thin metalizing layer and a minimum of penetration of metalizing constituents into the dielectric, is given, and pertinent fabrication procedures described.

KEY WORDS	LINK A		LINK B		LINK C	
	ROLE	WT	ROLE	WT	ROLE	WT
Sputtering, Arcing, Multipactor, Alumina, Beryllia, Quartz, Boron Nitride, High-Power Microwave Tube Windows, Metalizing Ceramics, Ring Resonator, Secondary Emission Ration, Cavity, Gas Evolution, Window Design, X-Ray Damage to Alumina, Titanium Nitride, Titanium, Vanadium Carbide.						

INSTRUCTIONS

1. **ORIGINATING ACTIVITY:** Enter the name and address of the contractor, subcontractor, grantee, Department of Defense activity or other organization (*corporate author*) issuing the report.
- 2a. **REPORT SECURITY CLASSIFICATION:** Enter the overall security classification of the report. Indicate whether "Restricted Data" is included. Marking is to be in accordance with appropriate security regulations.
- 2b. **GROUP:** Automatic downgrading is specified in DoD Directive 5200.10 and Armed Forces Industrial Manual. Enter the group number. Also, when applicable, show that optional markings have been used for Group 3 and Group 4 as authorized.
3. **REPORT TITLE:** Enter the complete report title in all capital letters. Titles in all cases should be unclassified. If a meaningful title cannot be selected without classification, show title classification in all capitals in parentheses immediately following the title.
4. **DESCRIPTIVE NOTES:** If appropriate, enter the type of report, e.g., interim, progress, summary, annual, or final. Give the inclusive dates when a specific reporting period is covered.
5. **AUTHOR(S):** Enter the name(s) of author(s) as shown on or in the report. Enter last name, first name, middle initial. If military, show rank and branch of service. The name of the principal author is an absolute minimum requirement.
6. **REPORT DATE:** Enter the date of the report as day, month, year; or month, year. If more than one date appears on the report, use date of publication.
- 7a. **TOTAL NUMBER OF PAGES:** The total page count should follow normal pagination procedures, i.e., enter the number of pages containing information.
- 7b. **NUMBER OF REFERENCES:** Enter the total number of references cited in the report.
- 8a. **CONTRACT OR GRANT NUMBER:** If appropriate, enter the applicable number of the contract or grant under which the report was written.
- 8b, 8c, & 8d. **PROJECT NUMBER:** Enter the appropriate military department identification, such as project number, subproject number, system numbers, task number, etc.
- 9a. **ORIGINATOR'S REPORT NUMBER(S):** Enter the official report number by which the document will be identified and controlled by the originating activity. This number must be unique to this report.
- 9b. **OTHER REPORT NUMBER(S):** If the report has been assigned any other report numbers (*either by the originator or by the sponsor*), also enter this number(s).

10. **AVAILABILITY/LIMITATION NOTICES:** Enter any limitations on: further dissemination of the report, other than those imposed by security classification, using standard statements such as:

- (1) "Qualified requesters may obtain copies of this report from DDC."
- (2) "Foreign announcement and dissemination of this report by DDC is not authorized."
- (3) "U. S. Government agencies may obtain copies of this report directly from DDC. Other qualified DDC users shall request through \_\_\_\_\_."
- (4) "U. S. military agencies may obtain copies of this report directly from DDC. Other qualified users shall request through \_\_\_\_\_."
- (5) "All distribution of this report is controlled. Qualified DDC users shall request through \_\_\_\_\_."

If the report has been furnished to the Office of Technical Services, Department of Commerce, for sale to the public, indicate this fact and enter the price, if known.

11. **SUPPLEMENTARY NOTES:** Use for additional explanatory notes.
12. **SPONSORING MILITARY ACTIVITY:** Enter the name of the departmental project office or laboratory sponsoring (paying for) the research and development. Include address.
13. **ABSTRACT:** Enter an abstract giving a brief and factual summary of the document indicative of the report, even though it may also appear elsewhere in the body of the technical report. If additional space is required, a continuation sheet shall be attached.

It is highly desirable that the abstract of classified reports be unclassified. Each paragraph of the abstract shall end with an indication of the military security classification of the information in the paragraph, represented as (TS), (S), (C), or (U).

There is no limitation on the length of the abstract. However, the suggested length is from 150 to 225 words.

14. **KEY WORDS:** Key words are technically meaningful terms or short phrases that characterize a report and may be used as index entries for cataloging the report. Key words must be selected so that no security classification is required. Identifiers, such as equipment model designation, trade name, military project code name, geographic location, may be used as key words but will be followed by an indication of technical context. The assignment of links, rules, and weights is optional.